DISSERTATION

FREQUENCY ANALYSIS AND TWO-DIMENSIONAL SIMULATIONS

OF EXTREME FLOODS ON A LARGE WATERSHED

Submitted by

John Fredrick England, Jr.

Department of Civil Engineering

In partial fulfillment of the requirements

For the Degree of Doctor of Philosophy

Colorado State University

Spring 2006

COLORADO STATE UNIVERSITY

December 1, 2005

WE HEREBY RECOMMEND THAT THE DISSERTATION PREPARED UNDER

OUR SUPERVISION BY JOHN FREDRICK ENGLAND, JR. ENTITLED FREQUENCY

ANALYSIS AND TWO-DIMENSIONAL SIMULATIONS OF EXTREME FLOODS ON A

LARGE WATERSHED BE ACCEPTED AS FULFILLING IN PART REQUIREMENTS

FOR THE DEGREE OF DOCTOR OF PHILOSOPHY.

<u>Committee on Graduate Work</u>

_____

_____

_____

_____
Adviser

_____
Department Head

ABSTRACT OF DISSERTATION

FREQUENCY ANALYSIS AND TWO-DIMENSIONAL SIMULATIONS

OF EXTREME FLOODS ON A LARGE WATERSHED

Estimates of extreme floods and probabilities are needed in hydrologic engineering

and in risk analysis to assess the safety of dams. This research focuses on developing a two-

dimensional, distributed model to simulate extreme floods with return periods up to 10,000

years. The four objectives of this dissertation are to: (1) develop a two-dimensional model

suitable for large watersheds (area greater than 2,500 km^2); (2) calibrate and validate the

model to the June 1921 and May 1894 extreme floods on the Arkansas River; (3) develop a

flood frequency curve with the model using the stochastic storm transposition technique; and

(4) conduct a sensitivity analysis for initial soil saturation, storm duration and area, and

compare the flood frequency curve with gage and paleoflood data.

A new channel mesh generator was developed to provide spatially-distributed channel

geometry inputs to the TREX model. The channel geometry was defined using power

functions for bank heights and channel widths based on field data collected at 20 sites. An

improved channel topology algorithm was implemented to allow channels to be connected in

eight directions. The TREX model was then applied to the 12,000 km^2 Arkansas River basin

above Pueblo, Colorado. The model was successfully calibrated to the record June 1921 flood. This flood peak discharge exceeded 100,000 ft^3/s and had a return period greater than 200 years. The May 1894 flood was used to validate the model. Based on the calibration and validation, the model is suitable for simulating extreme floods on large watersheds.

Basin-average rainfall depths and probabilities were estimated using depth-area-duration data and a stochastic storm transposition technique with elliptical storms. From these extreme rainstorms, the TREX model was used to estimate a flood frequency curve for this large watershed. Model-generated peak flows were as large as 90,000 to 282,000 ft^3/s at Pueblo for 100- to 10,000-year return periods.

The sensitivity analysis showed that initial soil moisture was important and affected peak flows by a factor of 1.18 to 2.15. The temporal distribution of rainstorms did not significantly affect flood frequency predictions. By reducing storm areas, basin-average depths and estimated peak-flow probabilities were reduced. Model-generated frequency curves were generally comparable to peak flow and paleoflood data-based frequency curves. This model provides a unique physically-based method for determining flood frequency curves under varied scenarios of antecedent moisture conditions, space and time variability of rainfall and watershed characteristics, and storm center locations.

John Fredrick England, Jr.
Civil Engineering Department
Colorado State University
Fort Collins, CO 80523
Spring 2006

ACKNOWLEDGMENTS

TABLE OF CONTENTS

CHAPTER 8: CONCLUSIONS AND RECOMMENDATIONS

LIST OF TABLES

LIST OF FIGURES

LIST OF SYMBOLS

Symbol	Description
a	storm ellipse major axis
A_c	catchment area
$A_{eff,j}$	effective area of the jth storm
A_s	storm area
A_{tr}	storm transposition area
b	storm ellipse minor axis
$b_g(t)$	rainfall interpolation intercept for gage g
c	storm ellipse major to minor axis ratio
$\bar{d}_c$	maximum areally-averaged storm rainfall depth over catchment
d_{oj}	spatial rainfall interpolation distance for gage j
E	storm severity criterion
f	infiltration rate
$f(x)$	probability density function
F	total infiltration depth
$F(x)$	cumulative distribution function
$F_{\bar{d}_c(\Delta t)}$	cumulative probability distribution function (cdf) of the basin-average depth
$G^a_{\bar{d}_c(\Delta t)}$	maximum average total storm depth annual exceedance probability
$G(q)$	peak flow exceedance probability
h	surface flow depth
i	net rainfall intensity
K_s	hydraulic conductivity
$m_g(t)$	rainfall interpolation slope for gage g
M_d	soil moisture deficit
n_{ov}, n_{ch}	Manning coefficients for overland and channel flow transport
N_s	number of extreme storms
N	number of years of record
P_r	probability of occurrence of a storm with depth that exceeds some minimum
P_t	probability of a storm center falling within or near the watershed
q_x, q_y	unit flows in the x- and y-directions
Q_p	peak flow

r	rainfall intensity
S_e	initial soil moisture saturation fraction
S_{fx}, S_{ox}	friction and bed slopes in x-direction
t_r	total storm duration
w	grid cell size
w_j	interpolation weight of rainfall gage j
x_s, y_s	storm center cartesian coordinates
$Z(1)$	random number of extreme storms per year
θ	storm orientation angle
θ_e	effective porosity
θ_r	residual saturation
θ_i	soil initial moisture content
λ	pore size distribution index
$\mathbf{\Lambda}_p$	two-dimensional vector which describes the storm position
$\mathbf{\Lambda}_s$	random vector of storm characteristics
ϕ	total soil porosity
ψ_b	bubbling pressure
ψ_f	capillary pressure (suction) head
ψ_w	water entry pressure

Chapter I

INTRODUCTION

"As the great American philosopher Yogi Berra is reputed to have said, 'In theory, there is no difference between theory and practice. In practice, there is.'" Brian Kernighan, 2003, http://www.linuxjournal.com/article/7035

Estimates of extreme floods and probabilities are needed for hydrologic engineering and dam safety risk analysis. Extreme flood estimates are needed for situations where the reservoir inflow peak discharge is greater than the maximum spillway capacity, the reservoir has a large, carry-over storage, and/or the reservoir has dedicated flood control space. Typical extreme flood estimates include peak flow, volume, timing, and reservoir levels. Flood hydrographs include peak, volume and timing, and integrate the drainage basin and channel response to precipitation, given some initial, variable state of moisture throughout the watershed. To conduct risk analyses and dam safety evaluations, extreme floods and probability estimates are required (Reclamation, 1999, 2003).

Estimation of extreme flood probabilities is a long-standing problem in hydrology. Over ninety years ago, Allen Hazen recognized the practical value of this problem (Hazen,

1914) when commenting on a paper by one of his workers (Fuller, 1914):

> "This is a most important paper, because, as far as the writer knows, it is the first attempt to apply the principles of probabilities to the flood problem. The writer has followed the author's work in detail, and believes that his methods are sound. As time goes on, data covering longer periods and more streams may change some of the numerical values; but the underlying idea of treating the recurrence of floods as a matter of probabilities, to be determined by an examination of the records of many streams, will stand. ... One of the most important matters developed by the paper is that there is no such thing as a maximum flood. There is an annual flood which must be expected every year. There is a 10-year flood which is much greater. There is a 100-year flood much greater than the 10-year flood; and, although no records are at hand to demonstrate it adequately, there is every reason to believe that there is a 1,000-year flood, which will prove to be much greater than the 100-year flood."

In contrast to widely used deterministic design procedures for large dams, such as the Probable Maximum Flood (PMF), methods to estimate extreme floods and their probabilities are not mature (NRC, 1988), and flood frequencies are not well understood (Pielke, 1999). Burges (1998) notes that assessing the adequacy of existing spillways for extreme floods is a major hydrometeorological issue and that critical factors include the complete spatial and temporal descriptions of extreme storms and the associated complete flood hydrograph.

1.1   BACKGROUND

Since 1902, the Bureau of Reclamation has continually been involved in developing and applying different flood hydrology methods to estimate extreme floods for spillway design and analysis and dam safety. These methods have traditionally focused on

deterministic and design-centered methods such as using Probable Maximum Precipitation

(PMP) to estimate a Probable Maximum Flood (PMF) (Cudworth, 1989). Reclamation

currently uses risk analysis to assess the safety of dams and prioritize expenditures

(Reclamation, 1999, 2003). The ideal flood inputs required for risk analysis are frequency

distributions of peak flows, volumes, and peak reservoir stages which, for dams with

potentially high loss of life, might extend to very low probabilities.

For Reclamation dam safety risk assessments, flood estimates are needed for Annual

Exceedance Probabilities (AEPs) of 1 in 10,000 (1 x 10^{-4}) and ranging down to 1 in

100,000,000 (1 x 10^{-8}). However, in practice, there are few tools available for one to make

these estimates. In contrast to developing PMP and PMF estimation methods, the research

and development efforts to estimate extreme flood probabilities have been modest. Current

procedures used by Reclamation to estimate these floods and associated probabilities are

described in Swain et al. (2004), and are generally simple. The initial Reclamation approach

is to extrapolate a peak-flow frequency curve assuming a two-parameter log Normal

distribution fit through the 100-year peak flow and paleoflood data.

This research focuses on new methods to estimate extreme floods for dam safety and

hydrologic engineering. Physically-based, distributed watershed models are used as an

avenue to estimate extreme floods, and as a basis to derive flood frequency curves. Ramirez

et al. (1994) state that the distributed approach provides a better insight into flood processes

within the catchment. The main elements of this research include improving and using a

physically-based rainfall-runoff model with a stochastic storm model to estimate extreme

floods and probabilities for dam safety on a large watershed, the Arkansas River above

Pueblo, Colorado.

1.2   OBJECTIVES

There were four objectives of this research.

1. Develop a suite of new tools for input data processing, including a channel mesh

    generator, so that a two-dimensional, physically-based, rainfall-runoff model can be

    applied on large watersheds, with areas greater than $1,000 \text{ mi}^2$ ($2,500 \text{ km}^2$).

2. Calibrate the two-dimensional model to the June 1921 flood and validate this model

    to the May 1894 flood on the Arkansas River above Pueblo, Colorado, thereby

    demonstrating that the model can be used to simulate extreme floods on a large

    watershed.

3. Develop new components, including space-time extreme storms, extreme storm

    probabilities, and initial conditions, for the two-dimensional watershed model.

    Develop a flood frequency curve with this model by combining it with the stochastic

    storm transposition technique.

4. Perform a series of sensitivity analyses with the two-dimensional watershed model in

    simulating extreme floods. These include examining: the spatial distribution of storm

    rainfall with location and area; storm duration and temporal distribution; and initial

soil saturation. Show the effects of these factors on the model flood frequency curve. Compare the model predictions with flood frequency curves estimated from gage (peak flow), historical and paleoflood data.

1.3   APPROACH AND METHODOLOGY

The general approach and methods used in this work are data analysis and numerical modeling. The major tool that is used is computer-based simulation experiments with a storm rainfall model and a distributed runoff model. The research entails a new linking of three concepts to estimate extreme floods and probabilities on large watersheds: stochastic storm transposition, the CASC2D rainfall-runoff model, and streamflow/paleoflood data. Two of three principles for estimating the probabilities of extreme floods (NRC, 1988) are implemented: space for time substitution (storm rainfall); and focusing on extreme tails of the storm and flood distributions.

The approach that was used in this research included the following main elements. The two-dimensional, physically-based, rainfall-runoff model CASC2D (Julien and Saghafian, 1991; Julien et al., 1995; Ogden and Julien, 2002; Rojas-Sanchez, 2002) was selected. Computer code was written to implement new preprocessing tools for channel geometry and network topology. For simulating extreme floods, an elliptical spatial storm model (Hansen et al., 1982) that uses depth-area duration (DAD) data was implemented within CASC2D. The initial soil saturation scheme for CASC2D was reparameterized to

5

explicitly specify the initial soil moisture for this event model. A stochastic storm transposition (SST) approach (Foufoula-Georgiou, 1989) was implemented in an orographic region to estimate extreme basin-average rainfall depths probabilities for application to a large watershed. The model was applied to the 4,660 mi^2 (12,000 km^2) Arkansas River basin above Pueblo, Colorado, and calibrated and validated with the largest storms and floods in the watershed. The SST model and CASC2D were then applied to the Arkansas River to estimate a flood frequency curve and conduct sensitivity analyses. Flood frequency analysis was conducted using peak-flow, historical and paleoflood data within the watershed using the Expected Moments Algorithm (Cohn et al., 1997) and log-Pearson Type III distribution, to compare with rainfall-runoff model predictions.

The overall goal is to improve a two-dimensional, spatially distributed watershed model that includes physically-based and relevant hydrologic and hydraulic processes to simulate extreme floods on large watersheds. The model can be tested and used for understanding the behavior of extreme floods and estimating flood frequency curves when coupled with a stochastic storm model.

Chapter II

LITERATURE REVIEW

This chapter presents a literature review that is limited to topics in two specific areas: simulating extreme floods on large watersheds; and estimating flood frequency curves with rainfall-runoff models. The focus of the literature review is on extreme floods and salient factors and models that can be used for dam safety hydrologic risk analysis.

2.1 SIMULATING EXTREME FLOODS ON LARGE WATERSHEDS

Mathematical watershed models are used to describe or simulate extreme floods. These models usually have two purposes in hydrology: the first is to explore the implications of making certain assumptions about the nature of the real world system; the second is to predict the behavior of the real world system under a set of naturally-occurring circumstances (Beven, 1989). One main reason to use a rainfall-runoff model is because we have not measured the variable of interest, and need a way to extrapolate those measurements (Beven, 2001).

The estimation and prediction of extreme floods is a central theme in hydrology and hydrologic engineering. I define an extreme flood by magnitude and probability, as one that

is typically the largest magnitude at a site or region, and/or with an annual exceedance

probability (AEP) of 1 in 2,000 or less (Figure 2.1). In most cases, these extreme floods are

seldom, if ever, directly measured.
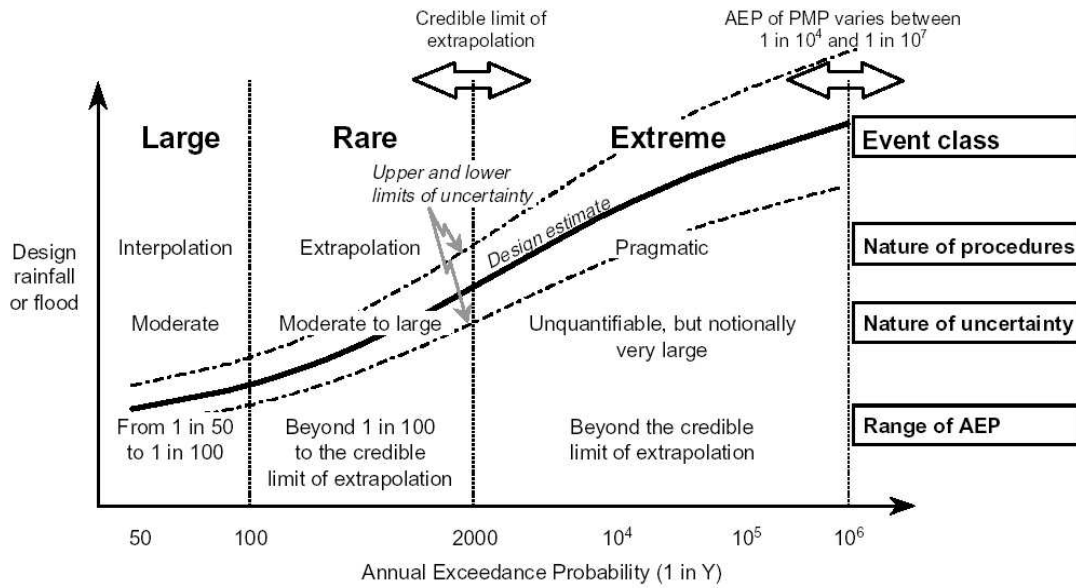
Figure 2.1. Design flood class descriptions (adapted from Nathan and Weinmann, 1999).

2.1.1   Large Watersheds, Scale and Runoff Processes

In order to effectively simulate extreme floods on large watersheds, one must first

define areas, lengths, and scales of processes. A large watershed is defined in this research as

one with a drainage area that exceeds 386 mi^2 (1,000 km^2). Ponce (1989) defined watershed

scales in the context of rainfall-runoff models, and suggested that values ranging between

100 to 5,000 km^2 have been variously used to define the limit between midsize and large

catchments. Singh (1995, p. 9) states that usually watersheds with areas 100 km^2 or less can

be called small, those with areas of 100 to 1,000 km^2 medium, and those with an area greater

than 1,000 km^2 large. Investigators conducting watershed modeling on different catchments

have used a variety of descriptors for watershed scales. Frenette and Julien (1987) described

a model for soil erosion and sediment yield for large watersheds and demonstrated its

application on a 6,684 km^2 watershed in Quebec. Molnar (1997) described a large watershed

as one with an area between about 100 km^2 and 1,000 km^2 in the context of applying

CASC2D. Feyen et al. (2000) described a 600 km^2 catchment in Belgium as a medium sized

catchment. Lange et al. (1999) describe a model for large, arid catchments and apply it to a

1,400 km^2 watershed. Sloan et al. (1997) present a water balance model for very large river

basins, with suggested applications on the River Tyne, UK and the Arkansas-Red River basin

(570,000 km^2). Guntner and Bronstert (2004) considered large-scale modeling for a 148,000

km^2 state in Brazil. Boston et al. (2004) applied TOPMODEL to a 730 km^2 subcatchment of

the Malianhe watershed in China, and termed this watershed as a large semi-arid region.

Skøien et al. (2003) divided catchments in Austria into three groups based on area: small (3-

70 km^2), medium (70-250 km^2), and large (250-130,000 km^2). Based on this limited review,

it is clear that there is no universal definition of scale that defines a "large" watershed.

Two issues for modeling extreme floods on large watersheds are scales and process

identification. In terms of scales of processes, Blöschl and Sivapalan (1995) and Skøien et

al. (2003) clearly illustrate the length and time scales for major processes in hydrology

(Figure 2.2). The temporal scales of interest for large watershed runoff are much longer than

one day (Figure 2.2). Skøien et al. (2003) suggest that the temporal pattern of flow in large

9

catchments is dominated by the temporal behavior of precipitation forcing and runoff

generation processes at daily and longer timescales, not by the routing of surface runoff.

Grayson and Blöschl (2000) and Blöschl (2001) suggest that a "Dominant Process Concept"

(DPC) is a way to handle scale issues. The DPC suggests to: (1) develop methods to identify

the dominant processes that control hydrologic response in different environments; and (2)

develop models that focus on these dominant processes. Sivakumar (2004) notes that the

DPC is not totally new, but there is not currently a consensus on how to implement the DPC.

Woods and Sivapalan (1999) used an analytical method to identify the dominant processes in

a humid temperate catchment. They noted that the multitude of interactions make it difficult

to identify the dominant controls on catchment response and on catchment-to-catchment

variability within any particular river basin.
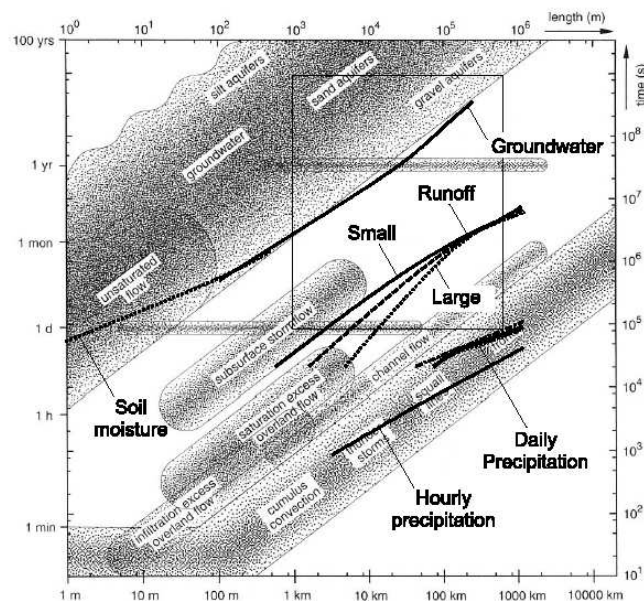
Figure 2.2. Schematic relationship between spatial and temporal process scales in hydrology (modified from Skøien et al., 2003).

In addition to scale, it is important to understand and describe physical processes on large watersheds. Nearly 100 years ago, Edward Charles Murphy described what he thought were the six salient flood physical processes (Murphy and others, 1906 pp. 55-56):

> "Primarily the flood flow of a stream depends on (1) The extent, duration, and intensity of precipitation, especially the intensity in the case of small drainage basins. (2) The direction of motion of the storm causing the flood. If the storm moves in the direction of the flow of the stream the flow will be greater than if it moves in the opposite direction or across it. (3) The amount of snow on the ground and the temperature during the storm. The large floods on northern streams are due almost entirely to the rapid melting of snow. When the ground is frozen the measured run-off is occasionally more than three times the precipitation during the month. (4) The storage, both natural and artificial, in the drainage basin. In some basins ground storage may take up to 9 inches of precipitation. Storage extends the flood period and reduces the maximum flow. (5) The size of the drainage basin. Most great rainstorms cover comparatively small areas, so that a big storm is likely to cover a larger part of a small drainage basin than of a large one. The maximum rate of discharge per square mile will therefore increase as the size of the drainage basin decreases. (6) The physiography of the drainage basin. The maximum rate of flow from a comparatively long and narrow basin with tributaries entering a considerable distance apart will be less than from a basin of nearly circular shape of the same size but with tributaries entering the main stream in close proximity. Steep, impervious, deforested slopes of basin and steep slope of stream bed cause rapid run-off. Narrow, deep, crooked channels of small slope cause sluggish flow, great variations in stage, and frequent overflow."

Since that time, these flood-causing factors have been listed by many others. However, the challenge remains to provide quantitative estimates of these processes on large watersheds. Dunne (1998) notes that on drainage areas greater than about 10^4 km^2, physical theory in flood hydrology seems to be abandoned in favor of statistical analysis of floods as random variates. He suggests that a focus is needed on the processes that actually generate floods, including extreme runoff generation, large rainstorms and snowmelt timing (Dunne, 1998 p. 25). The focus of this research is on processes in arid and semi-arid regions within the mountainous western United States. Pilgrim et al. (1988) describe the major problems with

11

rainfall-runoff modeling and briefly describe hydrologic processes in semi-arid and arid

regions. Klemeš (1990) indicates the modeling difficulties in mountainous areas.

Weingartner et al. (2003) describe flood characteristics in mountains. Beven (2002) suggests

that hydrological systems are sufficiently complex that each hydrologist will have his or her

own impression or perceptual model of what is most important in the rainfall-runoff process.

I summarize the important processes and factors that contribute to extreme floods and

extreme flood variability in semi-arid regions (Table 2.1). The processes can be placed in

various general categories, such as forcing functions (inputs), losses (subtractions), and

movement (transfer of mass in space and time). Alternately, they may be described using

hydrologic and hydraulic descriptors. Singh (1995) describes these different classification

methods in the context of watershed models.

Some processes mentioned by Pilgrim et al. (1988), such as evaporation and

transpiration, are not included here; they and others may be important for general rainfall-

runoff modeling, but are deemed not to be dominant factors in extreme floods. Two

elements that are common to all important extreme flood factors and processes on large

watersheds are high spatial and temporal variability. In addition to processes and scale, it is

also necessary to include variability for particular processes. It is important in physically

based modeling that sources of variability be identified and assumptions made concerning the

nature of variability be described explicitly because they may have a large effect on the

degree of modeling success (Seyfried and Wilcox, 1995).

Table 2.1: Important Extreme Flood Processes and Factors in Western U.S. Semi-Arid and Mountainous Regions

Process/Factor	Aspect(s)
Rainfall	high spatial and temporal variability; storm intensity, extreme rainfall rates (Smith et al., 1996), storm duration, direction and movement (Singh, 1997, 2002; de Lima and Singh, 2002), storm areal extent, storm type and circulation (Maddox et al., 1980; Hirschboeck, 1987) and spatial patterns (Obled et al., 1994)
Interception	significantly reduces lower intensity rainfall amounts (Pilgrim et al., 1988), improves hourly streamflow (Atkinson et al., 2003)
Infiltration	significantly affects surface runoff (Horton, 1933), very important physical process in the hydrologic cycle (Smith, 2002); high spatial variability of topography, soils properties and infiltration on large watersheds
Snowmelt	significant portion of runoff in western U.S., affects flood runoff and volume, especially in mountainous regions (USACE, 1998; Singh and Singh, 2001; Verbunt et al., 2003), high spatial variability
Hillslope Runoff and Routing	infiltration excess overland flow, partial area infiltration excess overland flow, saturation excess overland flow, subsurface stormflow (Beven, 2001); overland flow routing is significant (Troch et al., 1994); runoff, runon and infiltration important (Smith, 2002)
Partial Area Rainfall and Runoff	significant factor on large watersheds (Horton, 1937a); storm duration and movement (Singh, in press); affects flood runoff, volume, hydrograph shape (Woolhiser, 1996; Goodrich et al., 1997) and flood frequency (Marco and Valdés, 1998; Moon et al., 2004)
Upland Storage	depression storage on hillslopes and overland planes affects surface runoff
Channel and Floodplain Storage	can have a significant affect on flood hydrographs (Horton, 1936, 1937b), and reduce peaks on small and large watersheds (Horton, 1941; Woltemade and Potter, 1994, Turner-Gillespie et al., 2003), and flood frequency (Wolff and Burges, 1994)
Channel Network and Routing	streamflow delivery system: network morphology, connectivity and cross sections (Garbrecht, 1984); network definition (Giannoni et al., 2003)
Channel Transmission Losses	important factor in southwestern U.S., and ephemeral channels (Pilgrim et al., 1988; Woolhiser et al., 1990; Goodrich et al., 1997)
Antecedent Conditions	exhibits seasonal dependence (Horton, 1933); affects infiltration rate, surface runoff rate, and volume (Woolhiser et al., 1996; Heggen, 2001; Zehe and Blöschl, 2004)
Physiography	elevation, slope, aspect, orography; affects spatial distributions (Weingartner et al., 2003)

Singh and Woolhiser (2002) note that the spatial variability of hydraulic roughness,

infiltration, and rainfall are important considerations in watershed modeling.

A watershed can be conceptualized as being comprised of a hillslope phase and a channel phase. Singh (1995, p. 9) notes that large watersheds have well-developed channel networks and channel phase, thus channel storage is a dominant factor at this scale. In order to model extreme floods on a large watershed, it is hypothesized that the basin response is dominated by the following major factors:

- infiltration excess (Hortonian) overland flow;

- storm precipitation: spatial, temporal, duration, movement/direction;

- drainage and channel network;

- snowmelt during storm; and

- antecedent conditions/wetness.

Some of these factors have been explored recently and have been highlighted by various investigators. Researchers have been active in three areas over the last several years: spatial variability of rainfall with radar data; hillslopes, channels and drainage network with watershed response; and initial soil moisture.

In order to understand extreme floods on large watersheds, it is important to describe the temporal and spatial aspects of rainfall. Much work has been done in improving radar data and using radar data in runoff models. Krajewski and Smith (2002) review the state of the art in using radar for rainfall estimation, and highlight one most important area for radar hydrology is the diffusion of radar-rainfall products into a diverse array of hydrologic applications, such as engineering design of flood control structures and precipitation

frequency analysis. Radar data have great utility for understanding extreme floods (e.g., Smith et al., 1996; Borga et al., 2000; Ogden et al., 2000; Zhang et al., 2001; Giannoni et al., 2003). Creutin and Borga (2003) suggest that radar hydrology has revolutionized the estimation of flash flood risk. Radar has been used to understand rainfall in mountainous areas by interpreting measurements (Andrieu et al., 1997), and validating measurements (Creutin et al., 1997). Much work has been done in error estimation, bias correction and accuracy (e.g., Sharif et al., 2002; Borga et al., 2002; Borga, 2002). An important application of radar data is to directly improve rainfall depth-area relations; Durrans et al. (2002) show some preliminary results for a region in the central United States. A new radar-based rainfall simulation model that incorporates some physics and dynamics is presented by Andrieu et al. (2003). Zhang et al. (2004) and Neary et al. (2004) demonstrate use of radar with the National Weather Service model in Oklahoma and the HEC-HMS model in Tennessee, respectively. It is anticipated that this radar work will help improve extreme flood understanding and support existing elevation limits to rainfall flooding hypotheses in semi-arid, mountainous areas in the western U.S. (Jarrett, 1987, 1993; NRC, 1999).

A second area in which researchers have been active that is relevant for extreme flood modeling is flood processes, spatial variability and similarity. Merz and Blöschl (2003) focus on classifying the causative mechanisms of floods and describe five major types: long-rain floods, short-rain floods, flash floods, rain-on-snow floods, and snowmelt floods. Kandel et al. (2004) demonstrate that finer time scales (less than daily) need to be used to

effectively simulate runoff and erosion processes. Zhang et al. (2001) and Turner-Gillespie et al. (2003) highlight the role of valley bottom storage in extreme floods and that hydrographs attenuate. Their results in Nebraska and North Carolina support similar conclusions by Woltemade and Potter (1994) in Wisconsin and Archer (1989) in the U.K. Osterkamp and Friedman (2000) suggest that vegetation and soils affect infiltration rates in semi-arid areas and are major factors in causing extreme floods. Hydrologic similarity and scale in catchment processes has been an active area since Wood et al. (1988) defined the Representative Elementary Area. Their work related to storm response is summarized by Wood et al. (1990), and has been continued extensively by Robinson and Sivapalan (1997a,b), Woods and Sivapalan (1999) and Jothityangkoon and Sivapalan (2001), among others. In terms of improving our understanding of hillslope processes, Weiler and McDonnell (2004) outline a new computation-based approach they call "virtual experiments", that includes an experimental design between experimentalists and modelers, and use animated simulations to visualize the results. D'Odorico and Rignon (2003) show that representation of hillslopes and channels clearly affect travel times and hydrologic response, and that saturated portions of hillslopes are important to runoff contribution. Jothityangkoon and Sivapalan (2003) demonstrate that hillslopes, saturation excess runoff, and overbank floodplain flows play important roles in estimating extreme floods. However, Sivapalan (2003) suggests that if the focus is the watershed, some of the detailed process descriptions such as hillslopes might be less important, and it is important to find linkages

between hillslope and watershed scales.

There has been some recent work on the role of hillslopes, drainage networks and hydrograph response. Garbrecht (1984) includes the rainfall phase, the overland flow phase, the channel flow phase, and the channel network phase for describing watershed runoff, and suggests that each are recognized as important and distinct in transforming rainfall to basin runoff. Garbrecht and Shen (1988) show that these five phases affect runoff, peak and timing, and that peak flow in a channel is a function of the overland and channel flow processes and the drainage network. Saco and Kumar (2002a) show that spatially varying parameters in the drainage network and channel geometry affect the peak flow, time to peak, and hydrograph duration, and that these parameters change across scales (Saco and Kumar, 2002b). White et al. (2004) investigated network response on a large (26,000 km^2) watershed and suggest that hydrodynamic dispersion effects (akin to diffusion) are important, and that geomorphological dispersion (due to river network) cannot be ignored. Saco and Kumar (2004) suggest that even on large basins it is crucial to simulate hillslope dynamics. Paik and Kumar (2004) suggest that spatially-varying channel properties and velocities are one explanation for the observed nonlinear response in watersheds.

One area that is important to the event watershed model considered in this research is the role of initial conditions. Several investigators have recently pointed out the importance of initial soil moisture in runoff modeling, and that spatial variability of infiltration parameters is an important consideration. Entekhabi and Rodriguez-Iturbe (1994) developed

a space-time model to describe the spatial variability of surface soil moisture. Goodrich et al.

(1994) demonstrate that initial soil moisture can be estimated from remote-sensed

instruments on aircraft and satellites. Including the spatial distribution of saturated hydraulic

conductivity has a dramatic effect on predicted surface runoff (Woolhiser et al., 1996). Spah

(2000) showed that a watershed with higher initial soil moisture had higher peak flows and

generally decreased time to peak. Ashby (2001) showed that initial soil moisture played a

role in storm evolution and rain rates for the July 28, 1997 Fort Collins, CO storm. Instead

of using a mean or median initial soil saturation level or loss prior to a storm, Rahman et al.

(2002) recommend to estimate a random initial loss using a four-parameter beta probability

distribution for design floods and derived frequency curves. Castillo et al. (2003) suggested

that the antecedent soil water content is an important factor in controlling runoff from

medium and low intensity storms, but runoff from high intensity storms appeared to be

independent of initial moisture. However, their results were based on three very small

catchments ranging from 0.08 to 0.24 km^2. In contrast, Zehe and Blöschl (2004) investigated

initial conditions at the plot (1 m^2) and catchment (3.6 km^2) scales and showed that at both

scales the runoff predictions depend on the initial soil moisture state. They also showed the

difficulties of conducting repeated field experiments on watersheds and recommended that a

better strategy in watershed modeling would be to allow for uncertainty in the initial state

(Zehe and Blöschl, 2004).

2.1.2   Rainfall-Runoff Models for Large Watersheds

There are many rainfall-runoff models that have been developed for a variety of

purposes (understanding, investigation, prediction) and/or to be applied at particular

locations. The models include a wide assortment of conceptualizations, physical process

representations, and simplifications. Recent reviews of models that are applicable to large

watersheds and flood prediction are by Singh (1995), Singh and Woolhiser (2002) and Singh

and Frevert (2002). Hornberger and Boyer (1995) provide a summary of current research on

data advances (hydrologic units, tracers, and DEMs) and approaches to use the data in

watershed modeling. They also note that defining effective parameters at one scale and

linking them across another scale is an unsolved problem (Hornberger and Boyer, 1995).

Beven (2001) also summarizes some watershed models that he has helped develop, notably

the distribution function TOPMODEL.

The main interest here is on reviewing rainfall-runoff models that can be potentially

used to simulate extreme floods and be applied on large watersheds. A sample of the most

popular models in watershed hydrology spanned two pages in Singh and Woolhiser (2002).

Many of the models are classified according to processes or space and time. Common terms

to discriminate models are: lumped or distributed; continuous or event; deterministic or

stochastic (Singh, 1995). Ponce (1989, p. 8) has an interesting classification of model

approaches for flood hydrology. His classification (Figure 2.3) is relevant here as it suggests

one should use routing-based methods (e.g., CASC2D) rather than unit hydrograph

approaches for large watersheds.

Figure 2.3. Relationship between catchment scale and flood hydrology model (modified from Ponce, 1989).

When one uses a watershed model to represent the physical processes outlined above,

it is important to recall basics of models. Woolhiser (1996) states the issues clearly:

> "We must keep in mind that all models are simplifications or abstractions of reality and all
> models are to some extent wrong. In fact, if they aren't simpler in some sense than the real-
> world object, they aren't useful! For this reason we neglect certain aspects of the problem
> because they are considered to be unimportant. These simplifications should be based on
> sound physical reasoning or strong empirical evidence obtained from field studies or
> appropriate material models." (Woolhiser, 1996 p. 123)

It is also important to know that there are lots and lots of models, and that they may give the

right results for the wrong reason (Loague and VanderKwaak, 2004). There are many

disagreements on research modeling strategies to best represent watershed response between

simpler approaches (e.g., Beven, 1989, 2000, 2001) and distributed modeling methods

(Woolhiser, 1996; Loague and VanderKwaak, 2004). There are conflicting opinions in

modeling extreme floods and prediction as well. NRC (1988, p. 78) suggested that models

that are more physically based should perform better than empirical models for floods much

larger than those used in calibration. However, NRC (2002, p. 17) cautions that, in terms of

watershed rainfall-runoff transformation, "we cannot currently predict the spatial pattern of

watershed response to precipitation and cannot quantitatively describe the surface and

subsurface contributions to streamflow with enough accuracy and consistency to be

operationally useful." With this in mind, I first summarize flood models used extensively in

practice. Then some research models that have been used to simulate floods are discussed.

Finally, I close with a summary of recent work that focused on comparing several distributed

models.

The watershed models that are extensively used to simulate extreme floods and

Probable Maximum Floods (PMFs) are, in most cases, unit hydrograph or storage routing

models. In the United States, the HEC-1 model (HEC, 1998) is used by the Corps of

Engineers, and Flood Hydrograph and Runoff (FHAR) (Reclamation, 1990) is used by the

Reclamation. These two models are unit hydrograph approaches and are used nearly

exclusively for dam safety. On occasion other models, such as variants to the Stanford

Watershed model, have been used for PMF estimation (Cecilio et al., 1974). In the United

Kingdom, the national flood guidelines that were published in 1975 and called the Flood

Studies Report, have recently been updated as the Flood Estimation Handbook (IH, 1999).

These guidelines specify the use of a unit hydrograph model for extreme flood runoff and

PMF calculations (IH, 1999). In a similar vein, the Australian Rainfall-Runoff guidelines for

extreme flood estimation, published in 1987, have been revised (ARR, 2001). They

recommend using unit hydrograph or storage routing models such as RORB (Laurenson and

Mein, 1995). Nathan and Weinmann (1999) provide guidance on choosing between unit

hydrograph or storage models in Australia. Pilgrim and Cordery (1993) summarize these

unit hydrographs and flood hydrograph models in current practice.

In contrast to "design" flood models, there have been several recent models developed

and applied to estimate floods and flash floods in various locations. These models are

typically existing models that have been less utilized for "routine" flood prediction, or are

newer research models that have not made their way into engineering practice. Many of

these models are distributed in some sense. Some of these have been used for hydrologic

risk analysis, but have not yet been used routinely in engineering practice. The National

Weather Service model (Burnash, 1995) has been extensively used for flood forecasting on

large river basins. The Stochastic Event Flood Model (SEFM) (MGS, 2001; Schaefer and

Barker, 2002) has recently been developed to simulate extreme floods for hydrologic risk

analysis based on general storms and the HEC-1 runoff model. Sivapalan et al. (1990)

demonstrated the use of a variant of TOPMODEL to estimate extreme floods. WATFLOOD

has been used for flood forecasting in Canada (Kouwen and Mousavi, 2002). There have

been several newer models that have been used to simulate extreme floods; these and others

are described in Singh and Frevert (2002). Yu (2002) presents a new physically-based

watershed model (HMS) coupled with an atmospheric model; it uses kinematic wave for

overland flow and Muskingum-Cunge for channel routing. The model has been applied to a

14,710 km^2 portion of the Susquehanna River basin in Pennsylvania (Yu, 2002). The ARNO

model, a continuous semidistributed rainfall-runoff model, has been applied on many rivers

in Italy for analyzing floods and flood forecasting, including the 17,000 km^2 Tiber River

(Todini, 2002). Todini and Ciarapica (2002) describe a relatively new semidistributed model

called TOPKAPI that combines some of the concepts from TOPMODEL and the ARNO

model. It has been used to simulate a large flood in November 1990 on the 1,051 km^2 Upper

Reno watershed (Todini and Ciarapica, 2002). Yates et al. (2001) used PRMS (Leavesley et

al., 1983) with radar data to evaluate flash flood forecasting strategies for the July 1996

Buffalo Creek, Colorado flash flood. Ferraris et al. (2002) used a semidistributed rainfall-

runoff model to reproduce observed flash floods in November 1994 in northwestern Italy.

Gaume et al. (2004) used a lumped kinematic wave overland flow model with the SCS curve

number to compute rainfall excess for several small watersheds. A geomorphological

instantaneous unit hydrograph (GIUH) network model has been used to understand extreme

storm, flood and watershed dynamics for flash floods in Texas (Smith et al., 2000), Virginia

(Sturdevant-Rees et al., 2001), Nebraska (Zhang et al, 2001), and North Carolina (Smith et

al., 2002). A DEM-based Muskingum routing model with the SCS curve number for losses

was used by Montaldo et al. (2004) to reproduce a large flood in September 1993 in the

1,534 km^2 Toce watershed in Italy.

Some exciting collaborative research has recently been completed on distributed watershed models. The NWS sponsored a project called the Distributed Model Intercomparison Project (DMIP). The main goals of DMIP were: to identify and help develop models and modeling systems that best utilize NEXRAD and other spatial data sets to improve River Forecast Center (RFC)-scale river simulations; and to help guide NWS distributed modeling research, science and applications (Smith et al., 2004). A special issue of the Journal of Hydrology, volume 298 (1-4) published in 2004, describes DMIP and highlights the results in 14 papers. Smith et al. (2004) describe the motivation for the project and the three watersheds used (Elk, Illinois and Blue in Missouri, Arkansas and Oklahoma), list the 12 participating groups, and summarize model comparison metrics. The aim was to examine a multitude of distributed models versus an existing lumped model (Burnash, 1995) for operational river forecasting. Reed et al. (2004) summarize results from twelve different models compared against observed streamflow and a lumped model. Overall, the lumped model outperformed distributed models in most cases, but some calibrated distributed models performed comparable to or better than a lumped calibrated model (Reed et al., 2004). Based on the DMIP results, it is suggested that factors such as model formulation, parameterization, and the skill of the modeler can have a bigger impact on simulation accuracy than simply whether or not the model is lumped or distributed (Reed et al., 2004). Some of the models demonstrated as part of DMIP appear to be suitable for extreme flood modeling (Ivanov et al., 2004; Vieux et al., 2004; Bandaragoda et al., 2004).

2.1.3   Recent CASC2D Developments

CASC2D is a fully-unsteady, physically-based, distributed-parameter, raster (square-grid), two-dimensional, infiltration-excess (Hortonian) hydrologic model for simulating the runoff response of a watershed subject to an input rainfall field for a particular storm event (Julien and Saghafian, 1991; Julien et al., 1995; Ogden and Julien, 2002). Major components of the model include: rainfall interception, infiltration, surface and channel runoff routing using the diffusive wave method, soil erosion and sediment transport. CASC2D is appropriate for simulating extreme floods and physically-based extrapolations of frequency relationships, combined with a derived distribution approach. CASC2D is a fully distributed model and uses hydraulic principles for runoff generation and routing precipitation excess. CASC2D is also a somewhat experimental model that has not been used in extreme flood applications for dam safety, or for many applications outside academic research. Ogden and Julien (2002, p. 108) note that the appropriate and acceptable range of application of the model has not been established.

There has been much research work conducted with CASC2D. Most of this work is briefly described in Ogden and Julien (2002). One of the major focus areas with CASC2D has been in understanding effects of spatial and temporal variability in rainfall and watershed characteristics, space-time rainfall effects on runoff, and time to equilibrium (Ogden and Julien, 1993; Saghafian et al., 1995; Ogden et al., 1995; Saghafian and Julien, 1995). The model has been used with radar data (Ogden, 1992; Ogden and Julien, 1994; Julien et al.,

1995; Jorgeson, 1999; Ogden et al., 2000), for extreme floods (Ogden et al., 2000) and for

flash flood forecasting (Julien et al., 1998; Jorgeson, 1999). Grid size effects on runoff

(Molnar, 1997; Molnar and Julien, 2000) and sediment transport response (Rojas-Sanchez,

2002) have been explored as well. The most recent development and applications with

CASC2D have been in two areas: upland and watershed erosion and sediment transport

(Molnar and Julien, 1998; Johnson et al., 2000; Rojas-Sanchez, 2002; Julien and Rojas,

2002); and in adding unsaturated and groundwater flow options (Downer et al., 2002;

Downer and Ogden, 2003, 2004). I summarize prior CASC2D applications and watershed

sites in Table 2.2. The CASC2D model has not yet been applied on watersheds exceeding

about 1,000 km^2, and has not yet been applied to estimating flood frequency curves.

Applications for flash floods have been limited to smaller basins (Table 2.2) such as Spring

Creek in Fort Collins, CO (Ogden et al., 2000).

Table 2.2: CASC2D Applications and Watershed Sites

River/Watershed	Drainage Area (km^2)	Main Purpose	Reference
Goodwin Creek, MS	20.7	Hydrology and Sediment Transport Calibration/Prediction	Johnson et al. (2000); Senarath et al. (2000); Julien and Rojas (2002)
Hickahala/Senatobia, MS	560	Hydrology and Grid Cell Size	Molnar (1997); Molnar and Julien (2000)
Taylor Arroyo, CO	120	Effects of Military Maneuvers	Ogden and Julien (1993); Doe et al. (1996)
Spring Creek, CO	25	Flash Flood Modeling	Ogden et al. (2000)
Hassayampa Creek, AZ	1,111	Flash Flood Forecasting	Jorgeson (1999)
Cave Creek, AZ	349	Flash Flood Forecasting	Jorgeson (1999)
Macks Creek, ID	32	Hydrology/Model Demonstration and Testing	Julien and Saghafian (1991); Saghafian (1992)
Little Washita, OK	535.5	Initial Soil Moisture, Infiltration	Spah (2000)

2.2   ESTIMATING FLOOD FREQUENCY CURVES WITH RAINFALL-RUNOFF MODELS

There has been a fairly long history of using rainfall-runoff models to estimate peak flow probabilities. These models are typically used to estimate more common probabilities (1 in 25, 1 in 50 year) for designing culverts, cross-drainage facilities and bridge openings, where one typically assumes the 1 in Y rainfall depth causes the 1 in Y peak flow (Pilgrim and Cordery, 1993). Linsley (1986) demonstrates how this is not correct and the probability of estimated runoff is usually much lower than that of the rainfall. An example of using a rainfall-runoff model to improve peak flow frequency is given by Lichty and Liscum (1978). However, this work, as with much other practical work in this area, is focused on small basins and more frequent floods. There has been a dichotomy between probabilistic approaches using rainfall-runoff models and estimating extreme flood probabilities. Most probabilistic rainfall-runoff approaches focus on more common floods, such as 1 in 50 (NRC, 1988). Extreme flood probability estimates are typically made by either extrapolation of some statistical function (e.g., Stedinger et al., 1993), or abandoning making a probability statement and calculating some practical design maximum such as the PMF (Pilgrim and Cordery, 1993; NRC, 1988), and assuming the PMF cannot be exceeded (e.g., Nathan and Weinmann, 1999). In contrast to PMF calculations developed over the past 60 years, the use of rainfall-runoff models to estimate probabilities of extreme floods is a research area that is not yet mature and has not yet been embraced by practitioners (e.g., Burges, 1998). This

situation is improving, as extreme flood and probability estimation techniques using rainfall-runoff models are being advocated within Australia (Nathan and Weinmann, 1999; ARR, 2001), the United Kingdom (IH, 1999) and the United States (Swain et al., 2004).

The current approaches to utilize rainfall-runoff models for flood frequency estimation focus on two avenues: derived distributions via analytical or numerical techniques, and hydrologic simulation (Loukas, 2002). Bocchiola et al. (2003) call these techniques "indirect methods", and use the term "direct methods" to describe peak-flow frequency using statistical techniques. Curiously, they do not describe how one estimates a hydrograph or volume using direct techniques. Regardless of classification, most investigators use a variant of the method proposed by Eagleson (1972). The general concepts are outlined in Figure 2.4, and consist of a rainfall model, some other initiating conditions, a runoff and routing model, and model output analysis and calibration. Possible repetition for Monte-Carlo simulation is also included.

The idea and basis to use CASC2D for extreme flood modeling and prediction is centered on two concepts: a derived distribution approach (e.g., Eagleson, 1972) can be used to estimate the extreme flood peak and volume probability distributions; and physically-based methods for flood runoff and routing provide a suitable and improved physical basis for the extrapolations of derived flood probability distributions. Ramirez (2000) summarizes the theory behind the derived distribution approach. In the disciplines of science and engineering, relationships that predict the value of a dependent variable in terms of one or

28

many basic (independent) variables are commonly developed.
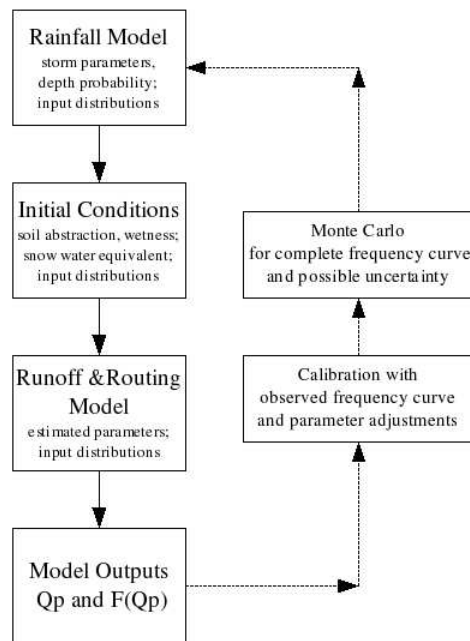
Figure 2.4. General derived flood frequency distribution method, with event model (modified from Eagleson, 1972; Bocchiola et al., 2003).

Physical systems are naturally complex. The functional form of the relationship between independent and dependent quantities, or values of the independent variables (or both) is not usually known with certainty. Techniques based on probabilistic assumptions can be used to account for this uncertainty. When the uncertainty derives from uncertainty in the independent variables, but not from uncertainty in the functional dependence, a derived distribution approach leads to the probability density function (PDF) of the dependent variable. In this case, the functional form relating independent and dependent variables is assumed known with certainty. In such instances, it is possible to derive the PDF of the dependent variable(s) from that of the independent variable(s) (Ang and Tang, 1975).

There are several research applications using the derived distribution approach to estimate flood frequency curves; these show much promise. The pioneering study for flood frequency is Eagleson (1972). Bras (1990) discusses some of the potential applications of derived distributions in hydrology. Table 2.3 summarizes some of the flood frequency work using derived distributions that generally followed Eagleson's (1972) approach. Notice that nearly all the sites are smaller basins ($< 1,000$ km^2) and only four out of 23 studies make probability estimates of 1 in 10,000 or less. From this work, some of the key questions that still remain are data availability (e.g., Hornberger and Boyer, 1995), calibration, and how far one can extrapolate the derived distributions. Dooge (1986) suggests that paleohydrologic data are an extremely valuable adjunct to instrument data for the calibration of existing methods in flood hydrology.

There has been a resurgence in derived flood frequency methods over the past several years, as shown by some recent publications (Table 2.3). Gottschalk and Weingartner (1998) derived peak flows from rainfall and unit hydrographs. Hashemi et al. (2000), using a Monte Carlo derived distribution approach, show some major factors, such as the probability distribution of initial soil moisture at the storm arrival time, affect flood frequency curves. Menabde and Sivapalan (2001) explored scaling issues and the flood frequency curve, and showed that storm duration, time of concentration, rainfall spatial variability and relative contribution of direct runoff were important. Rulli and Rosso (2002) used a space-time stochastic rainfall model and a distributed runoff model to predict flood frequency curves.

Table 2.3: Recent flood frequency studies using rainfall-runoff models and derived distributions (modified from Beven, 2001).

Study	Catchment	Watershed Area (km^2)	Rainstorm Model	Runoff Generation	Routing	Exceedance Prob. Limit
Eagleson (1972)	3 US catchments	5.7 - 991	Eagleson Exponential I,D	Variable Contrib. Area	Analytical KW	1/10
Hebson and Wood (1982)	Bald Eagle Cr., Davidson R., US	105 – 992	Eagleson Exponential I,D	Hortonian Infiltration Excess	GUH	1/100
Cordova and Rodriguez-Iturbe (1983)	Quercual, Venezuela	250	Observed	Hortonian Infiltration Excess	GUH	1/1,000
Diaz-Granados et al. (1984)	Santa Paula Cr. and Nashua, US	104 – 277	Observed	Hortonian Infiltration Excess	GUH	1/100
Shen et al. (1990)	hypothetical	7.8	Eagleson Exponential I,D	Hortonian Infiltration Excess	KW	1/100
Sivapalan et al. (1990)	hypothetical	-	Eagleson Exponential	Saturation excess and infiltration excess	GUH	1/500
Cadavid et al. (1991)	Ralston Cr., Santa Anita, US	7.8 – 25.1	Eagleson Exponential I,D	Hortonian Infiltration Excess	KW	1/80
Troch et al. (1994)	Mahatango Cr., US	420	Observed	TOPMODEL	linear NWF	1/30
Calver and Lamb (1996)	10 UK catchments	1 – 225	Observed	PDM & TATE models	NWF and parallel TF	1/500
Franchini et al. (1996)	hypothetical midwest US	-	Stochastic Storm Transposition	ARNO	parabolic	1/100,000
Robinson and Sivapalan (1997b)	Salmon Cr., AU	0.81	Seasonal Exponential/power law	Saturation excess/subsurface	linear TF	1/100
Lamb (1999)	40 UK catchments	0.9 – 523	Observed (hourly)	PDM	linear TF	1/30
Cameron et al. (1999)	Wye, UK	10.6	GPD extension to observed	TOPMODEL	linear NWF	1/1,000
Steel et al. (1999)	11 Scotland catchments	69 – 4,407	Observed (daily)	IHACRES	linear TF	1/400
Hashemi et al. (2000)	hypothetical	100	Modified Neyman-Scott	ARNO	parabolic	1/10,000
Cameron et al. (2000)	4 gaged UK catchments	0.9 – 415.6	GPD extension to observed	TOPMODEL	linear NWF	1/1,000
Goel et al. (2000)	4 India catchments; Davidson, US	42 – 151	Bivariate Exponential	phi-index	GCIUH	1/100
Arnaud and Lavabre (2002)	15 Mediterranean catchments	17.2 – 216	Direct hyetograph sampling	GR3H UH	linear reservoir	1/100
Blazkova and Beven (2002)	Joseful Dul, Czech Rep.	25.8	Modified Eagleson	TOPMODEL	linear NWF	1/10,000
De Michele and Salvadori (2002)	3 Italy catchments	34.2 – 206	Generalized Pareto DDF	Hortonian infiltration excess	none	1/100

Table 2.3 (continued): Recent flood frequency studies using rainfall-runoff models and derived distributions (modified from Beven, 2001).

Study	Catchment	Watershed Area (km^2)	Rainstorm Model	Runoff Generation	Routing	Exceedance Prob. Limit
Rulli and Rosso (2002)	Bisagno, Italy	92	Generalized Neyman-Scott	FEST	Muskingum-Cunge	1/100
Rahman et al. (2002)	3 Victoria, AU catchments	78 – 127	Design IDF	Hortonian infiltration excess	nonlinear storage	1/100
Blazkova and Beven (2004)	Zelivka, Czech Rep.	1,186	Modified Eagleson	TOPMODEL	network constant velocity	1/10,000
I, intensity; D, storm duration; F, frequency; GPD, Generalized Pareto Distribution; KW, kinematic wave, GUH, geomorphological instantaneous unit hydrograph NWF, network width function; TF, transfer function; see Beven (2001) for runoff generation model descriptions						

Loukas (2002) described recent research on derived distributions and flood frequency, and demonstrated a method to estimate flood frequency curves for ungaged small to medium watersheds in British Columbia. Jothityangkoon and Sivapalan (2003) demonstrated the importance of channels and floodplain processes when deriving flood frequency curves.

One interesting area that some researchers have recently focused on is the partial storm area/partial runoff generation problem. This is an important consideration when understanding and modeling large watersheds. Seo and Smith (1996) show the effects of partial rainfall field coverage from radar data on the mean areal precipitation estimates. Their analysis could be used to convert rainfall at one spatial scale to another under fractional conditions. Marco and Valdés (1995, 1998) demonstrate the effects of partial area storms on flood frequency for regular storm and watershed geometries (circles). Iacobellis and Fiorento (2000) investigated partial contributing areas to floods and suggested that climate and physical factors, including the runoff generation mechanism, play significant roles in

determining flood frequency. They later interpreted their results for dry and humid climates (Fiorento and Iacobellis, 2001). Moon et al. (2004) adopted the Marco and Valdés (1998) storm coverage model and demonstrated that the storm coverage effect was significant for flood frequency analysis in the Pyungchang River basin in Korea.

It is known that storm rainfall is the most important factor in estimating extreme floods with rainfall-runoff models (NRC, 1988; 1994). One method to estimate extreme rainfalls is to use stochastic storm transposition. Stochastic storm transposition (SST) is an alternative method to station-based rainfall analyses. NRC (1994) reviewed approaches to estimating Probable Maximum Precipitation (PMP) in the United States. They noted the conflict between storm-based and station-based analyses, and that current PMP techniques are based on storm analyses. In looking at alternatives to PMP, NRC (1994) recommended pursuing the stochastic storm transposition procedures (e.g., Fontaine and Potter, 1989; Foufoula-Georgiou, 1989). They noted that these techniques are not mature. There has been some limited progress and applications in this area over the past 10 years. Bradley and Potter (1992) utilized the technique to expand storm samples for flood frequency simulation in the Midwest. Franchini et al. (1996) extended the technique to focus on design flood estimation, by including stochastic descriptions of antecedent moisture and storm temporal distributions. Fontaine and Potter (1989) and Wilson and Foufoula-Georgiou (1990) demonstrate average catchment depth probability curves with AEPs that range from 10^{-3} to 10^{-9}. Agho et al. (2000) focused on the problem of regional homogeneity for SST, and developed a

nondimensionalized approach to overcome statistical nonhomogeneity of depth exceedance probabilities. However, there are many unresolved questions with developing SST concepts and applying the method. Little research and virtually no practical work has been done with SST since recommendations made by NRC (1994). There has not been a published case of using SST to estimate extreme storms and resultant floods for a real watershed, and demonstrating the subsequent impacts to dam safety. The only storm data that have been analyzed and probability estimates made are for a nine state midwestern U.S. region (Foufoula-Georgiou and Wilson, 1990; Wilson and Foufoula-Georgiou, 1990). Fontaine (1989) and Fontaine and Potter (1993) did briefly demonstrate the task of computing flood probabilities for a 570 km^2 site in Wisconsin, and note there is much work to be done prior to routine application.

A different approach that has been used for simulating extreme floods and estimating probabilities is to use a continuous watershed model such as the Stanford Model (Crawford and Linsley, 1966), combined with a multivariate hourly stochastic rainfall model (Ott, 1971). Ott and Linsley (1972) describe efforts to estimate peak-flow frequency curves to a 1,000-year return period on Dry Creek in the Russian River basin, California and Fisher River in North Carolina. The rainfall model was a multivariate normal hourly model based on rain gage data within the watershed. Franz et al. (1989, 1991) and Kraeger and Franz (1992) extended this work by applying the rainfall generator and Stanford Model to the Russian River in California, the Sulphur River in Texas and the Altamaha River in Georgia.

34

The frequency curve at the Russian River was based on rainfall data from two rain gages (20 years each) and was extrapolated to 100,000 years. There were 26 years of raingage data at three sites on the Sulphur River; data were generated and flood frequency extrapolated to 100,000 years. Nine gages (30-year period) were used on the Altamaha River to extrapolate the frequency curve to 10,000 years (Franz et al., 1991). The limitations of this work are related to the rainfall model (NRC, 1988 p. 62) and sampling variability of short records.

Chapter III

CASC2D MODEL ENHANCEMENTS AND TREX

This chapter presents the main hydrologic and hydraulic process components within CASC2D and describes enhancements made to particular model features as part of this dissertation. Improvements are made in two main areas: pre-processing and channel network; and storm rainfall modeling. As noted in Chapter 2, CASC2D is primarily a research model. The applications have been limited to relatively "small" watersheds and have been completed by researchers at universities. It has not been used outside these environs except for limited small-watershed research applications by the U.S. Army. The new enhancements expand the capabilities of the model to simulate extreme floods and flood frequency on large watersheds. The goal is to have a practical and tested alternative to the current lumped-parameter unit hydrograph watershed models (Cudworth, 1989) used to simulate extreme floods in the western United States. Based on improvements made as part of this work and by Velleux (2005), the name of the model is changed from CASC2D to TREX. TREX is the Two-dimensional Runoff, Erosion, and eXport model, and is a generalized watershed rainfall-runoff, sediment transport and contaminant transport model. The CASC2D name is used in this chapter for comparisons with prior work.

3.1   CASC2D OVERVIEW

The model that is utilized in this research and improved is CASC2D. CASC2D is a

fully-unsteady, physically-based, distributed-parameter, raster (square-grid), two-

dimensional, infiltration-excess hydrologic model for simulating the runoff response of a

watershed subject to an input rainfall field for a particular storm event (Julien and Saghafian,

1991; Julien et al., 1995; Ogden and Julien, 2002). The CSU version of CASC2D, recently

updated by Rojas-Sanchez (2002), was used as the basis to develop the new features to

CASC2D (and the TREX model) that are described here. It is classified as an event model as

it simulates the Hortonian (overland flow) surface watershed response from a single storm

with no soil infiltration capacity recovery between events.

The major components of the model include: rainfall interception, infiltration, surface

and channel runoff routing using the diffusive wave method, soil erosion and sediment

transport, and chemical transport. The Green and Ampt (1911) equation is used to represent

infiltration:

$$f = K_s (1 + \frac{\psi_f M_d}{F}) \quad (3.1)$$

where f is the infiltration rate, K_s is the hydraulic conductivity at normal saturation, ψ_f is the

capillary pressure head at the wetting front, M_d is the soil moisture deficit equal to ($\theta_e - \theta_i$),

θ_e is the effective porosity equal to ($\phi - \theta_r$), ϕ is the total soil porosity, θ_r is the residual

saturation, θ_i is the soil initial moisture content, and F is the total infiltration depth. Overland

flow is estimated in two dimensions via the continuity equation:

$$\frac{\partial h}{dt} + \frac{\partial q_x}{dx} + \frac{\partial q_y}{dy} = i \quad (3.2)$$

where h is the surface flow depth, q_x and q_y are unit flows in the x- and y-directions, and i is the net rainfall intensity. The momentum equation for the x-direction, using the diffusive wave approximation, is:

$$S_{fx} = S_{ox} - \frac{\partial h}{\partial x} \quad (3.3)$$

where S_{fx} and S_{ox} are the friction and bed slopes, respectively. A general depth-discharge relationship is used, assuming Manning equation holds:

$$q_x = \alpha_x h^\beta \quad ; \quad \alpha_x = \frac{S_{fx}^{1/2}}{n} \quad ; \quad \beta = 5/3 \quad (3.4)$$

where n is the Manning coefficient. Channel flow is estimated in one dimension using the diffusive wave approximation:

$$\frac{\partial A}{\partial t} + \frac{\partial Q}{\partial x} = q_l \quad (3.5)$$

where A is the channel flow cross-sectional area, Q is the total channel discharge, and q_l is the lateral inflow rate to the channel. Q is estimated using the Manning equation with the friction slope S_f.

CASC2D is appropriate for simulating extreme floods and physically-based extrapolations of frequency relationships, combined with a derived distribution approach.

CASC2D is a fully distributed model and uses hydraulic principles for runoff generation and routing precipitation excess. CASC2D is also a somewhat experimental model that has not been used in extreme flood applications for dam safety, or for many applications outside academic research. Ogden and Julien (2002, p. 108) note that the appropriate and acceptable range of application of the model has not been established.

The basic components of CASC2D are described in Julien and Saghafian (1991), Julien et al. (1995) and Ogden and Julien (2002). The major model components of interest for this research are rainfall, infiltration, overland flow routing, and channel flow routing, and are summarized in Table 3.1. The model requires four main parameters for each grid cell, and one parameter for each channel segment (Table 3.1).

Table 3.1: A Summary of Major CASC2D Model Processes Considered

Process Name	Process Description/Mechanism	Parameters
Rainfall	Single or multiple rain gages; constant temporal interpolation; spatially uniform or inverse-distance squared spatial interpolation	none
Infiltration (Overland Plane)	Green and Ampt (1911) equation, explicit formulation (Li et al., 1976)	soil saturated hydraulic conductivity Ks capillary pressure head at wetting front Hf soil moisture deficit Md
Overland Flow Routing	Diffusive wave equation (Julien, 2002) in two dimensions (x,y) for each grid cell, explicit finite difference formulation	Manning n_{ov} (geometry estimate includes cell size W and depression storage depth)
Channel Flow Routing	Diffusive wave equation (Julien, 2002) in one dimension (defined along channel segment path), explicit finite difference formulation	Manning n_{ch} (geometry estimates includes width, bank height, slope, length, sinuosity, and dead storage depth)

The CASC2D components that are modified, tested and enhanced as part of this research are summarized in Table 3.2. Each component is then discussed in detail below. Data pre-processing tools that are developed as part of this research consist of an automated channel mesh generator. The components that make up the pre-processing tools are briefly described.

Table 3.2: New Features and Improvements to Existing CASC2D Model Processes

Process/Model Component	Existing CASC2D Model	New Features, Improvements and Testing
Rainfall	Single or multiple rain gages; constant temporal interpolation; spatially uniform or inverse-distance squared spatial interpolation	Temporal interpolation for all rainfall inputs and options: linear. Spatial interpolation for rain gages: generalized inverse distance with radius of influence. New Design Storm (PMP) input: spatially uniform within user-defined sub-areas. Re-implement radar input: rainfall rates defined from radar file; nearest neighbor spatial interpolation. New Observed Extreme Storm Estimate: input as average depth and distribute in time using data-based hyetograph and in space with user-entered elliptical parameters.
River Channels	Channel segments connect in x or y direction. Floodplain option (Julien et al., 1995) not in current software version and has not been tested with extreme floods.	New topology to allow channel connectivity in eight directions (includes diagonals). Re-implement floodplain connectivity, new definition for floodplain interactions. New semi-automated processing routines for developing: channel connectivity model input information (links and nodes); spatially-varying channel geometry for each node; channel grid cell checking and optional modification of elevations at flat nodes.
Initial Conditions	Initial water depth in overland plane.	New explicit declaration and input of: initial water depths in both overland plane and channel segments; initial soil moisture content.

3.2   RAINFALL MODELING

In order to successfully model large watersheds using CASC2D, and within a practical hydrologic engineering framework, additional rainfall techniques are added to the model as part of this research. These include replacing the temporal interpolation method, modifying the rain gage spatial interpolation algorithm, re-implementing use of radar data, and including design storm and space-time depth-area duration (DAD) storm techniques.

The rainfall input to CASC2D consists of a time series of rainfall intensity and time "pairs" for each rain gage that is specified. The original temporal interpolation scheme that was used for CASC2D model time steps between rainfall intensity observations was to use a constant value equal to the previous rainfall intensity observation for each gage. This concept has been replaced with a piecewise linear interpolation scheme between observation pairs i and $i+1$. For each rain gage g ($g = 1, nrg$) the rainfall intensity r [L/T] at time increment t_j (function of model time step Δt) is:

$$r_g(t_j) = b_g(t) + m_g(t) \cdot \left(t_i + \sum_{j=1}^{n} \Delta t \right) \qquad for \quad \left(t_i + \sum_{j=1}^{n} \Delta t \right) \leq t_{i+1} \quad (3.6)$$

where $b_g(t)$ is the intercept estimated by

$$b_g(t) = r_g(t)_{i+1} \quad (3.7)$$

$m_g(t)$ is the slope estimated by

$$m_g(t) = \frac{r_g(t)_{i+1} - r_g(t)_i}{t_{i+1} - t_i} \quad (3.8)$$

and n is an integer number of time steps between t_i and t_{i+1} with any remainder time added as a last step. This temporal interpolation scheme is used for all the rainfall options.

Four main spatial rainfall options are now operational in the model as part of this research: inverse-distance weighting (IDW) with rain gages; constant in space over user-specified areas for design storms; restricted nearest neighbor with radar data; and elliptical storms with depth-area duration (DAD) data.

The existing CASC2D inverse-distance squared spatial interpolation algorithm is modified to a more flexible inverse-distance weighting (IDW) approach. Two changes are made: introducing a user-defined exponent (or power) parameter instead of a strict value equal to 2, and adding a radius of influence parameter. The general spatial interpolation problem described here is based on Tabios and Salas (1985) and Salas et al. (2002). We define rainfall gage coordinates in a regular square grid as x_j and y_j. The rainfall process at this gage j is defined as h_j, where the number of rain gages (nrg) is defined by $j=1, 2, \ldots , nrg$. An estimate of the rainfall process (rate or depth) is defined as h_o at any point in space (x_o, y_o). This process h_o can be estimated by a weighted linear combination of the observations via:

$$h_o = \sum_{j=1}^{nrg} w_j h_j \quad (3.9)$$

where w_j is the weight of rainfall gage j. This weight is a function of the distance d_{oj} between h_o and h_j. CASC2D uses a straight-line distance estimator:

$$d_{oj} = \sqrt{(x_o - x_j)^2 + (y_0 - y_j)^2} \quad j=1, \dots , nrg \quad (3.10)$$

The weight w_j for station h_j is (Tabios and Salas, 1985):

$$w_j = \frac{f(d_{oj})}{\sum\limits_{i=1}^{nrg} f(d_{oi})} \quad (3.11)$$

where $f(d_{oj})$ represents a function of the distance d_{oj} between the estimation point h_o and the

gage point h_j. The new power function that is implemented in CASC2D is:

$$f(d_{oj}) = \frac{1}{d_{oj}^{\alpha}} \quad (3.12).$$

Common values for α are 1, 1.5 and 2. Simanton and Osborn (1980) tested α values from 0

to 4.0 for summer thunderstorm rainfall and recommended using 1.0 in areas where air-mass

thunderstorms dominate. If α is 1, the function is known as reciprocal distance, and if α is

2 it is called the inverse distance squared method. If higher values of this exponent are used,

less weight is given to gages at increasing distance from the estimate point h_o. A restriction

is placed on d_{oj}. A radius of influence parameter r_{max} is defined to be the maximum distance

between the point of interest (x_o, y_o) and the gage location (x_j, y_j). If d_{oj} is less than r_{max}, this

gage is considered in the weighting calculations. Otherwise, the gage is excluded as w_j is

zero. This parameter allows one to model partial-area rain storm cases directly with one or

more rainfall gages covering discrete areas of a watershed.

A related approach is implemented for spatial interpolation of radar data. Instead of

the inverse distance, a restricted nearest neighbor approach is implemented. As a point

interpolator, the Theissen method is essentially a proximal or nearest distance neighbor

technique (Salas et al., 2002). To interpolate radar data, the simple technique is to search

over all radar grid locations and map the rainfall process value from the nearest distance

location to the CASC2D grid cell center. First, equation 3.10 is used to obtain the distance

d_{oi} from each radar pixel (x_j, y_j) to the grid cell location (x_o, y_o). We then determine the

distance $d_{oi} = min(d_{o1}, \ldots, d_{on})$, and subject it to the following restriction:

$$d_{oi} = d_{o1} \quad for \, d_{o1} \leq r_{max}$$
$$(3.13).$$
$$d_{oi} = 0 \quad otherwise$$

The weights in (3.9) are estimated for the case where $d_{oi} < r_{max}$ from:

$$w_j = 1 \quad for \, j = i$$
$$(3.14).$$
$$w_j = 0 \quad for \, j \neq 1$$

This technique is used because the radar data are specified as an intensity or depth over a

fixed area (typically a square grid cell). The radar cell geometry (size and orientation) can be

different than the CASC2D model grid. A restricted nearest neighbor interpolator allows one

to easily handle these geometric discrepancies in a straightforward manner, and handle cases

when the input radar grid does not cover the entire watershed (Figure 3.1), or when

individual storm cells cover small areas.
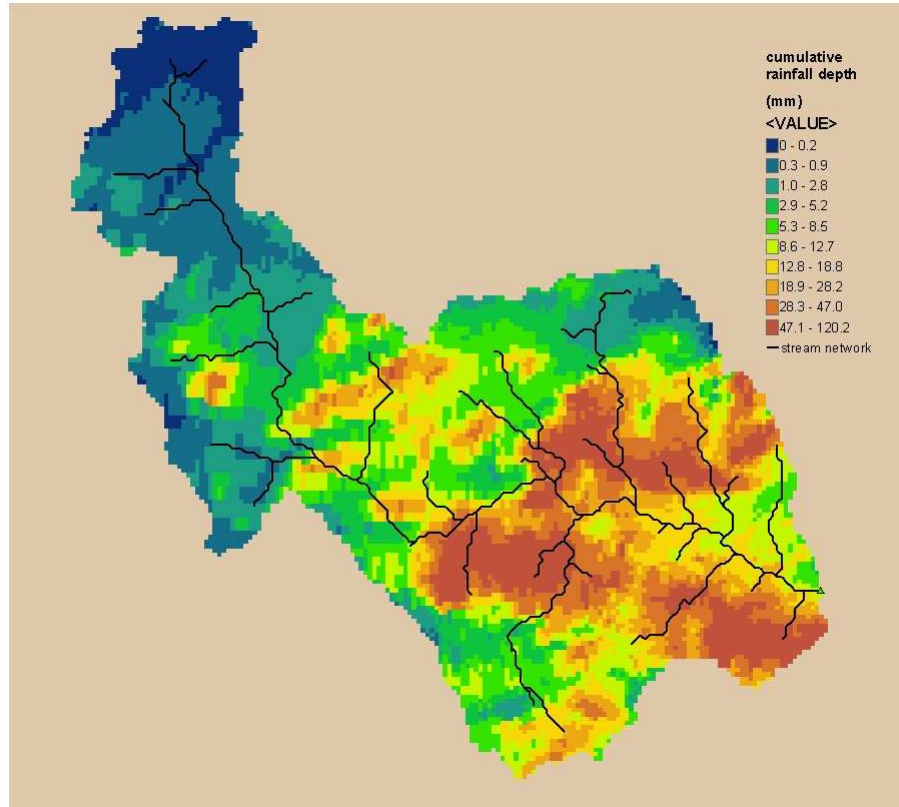
Figure 3.1. Total 24-hour rainfall (mm) over the Pueblo watershed for the July 13, 2001 storm; 1 km^2 radar data interpolated to 960 m model grid cells. Radar rainfall data provided by Jim Smith and Julie Javier, Princeton University.

A new design storm method is added to CASC2D in order to effectively simulate PMP design storms. When estimating PMP for a particular watershed, the standard procedure is to determine an average rainfall depth for a specified duration over the entire watershed. A design storm is then estimated by distributing this depth in time using alternating blocks with the maximum at the 2/3 point, and in space using successive subtractions for subbasins (Cudworth, 1989). The PMP storm is entered into CASC2D using an index grid map of subbasins and a rainfall time series for each subbasin. A subbasin index grid map consists of integer values denoting the location of each subbasin ($i = 1, ..., nsubbasins$) in the watershed. A rainfall time series is entered for each subbasin i and the

45

rainfall rate is applied uniformly over that subbasin (Figure 3.2). In this way, we can mimic a simpler, spatially uniform interpolator that has been used for modeling extreme storms in the western United States, termed the "method of successive subtraction of subbasin PMP volumes" (Cudworth, 1989 p. 59).
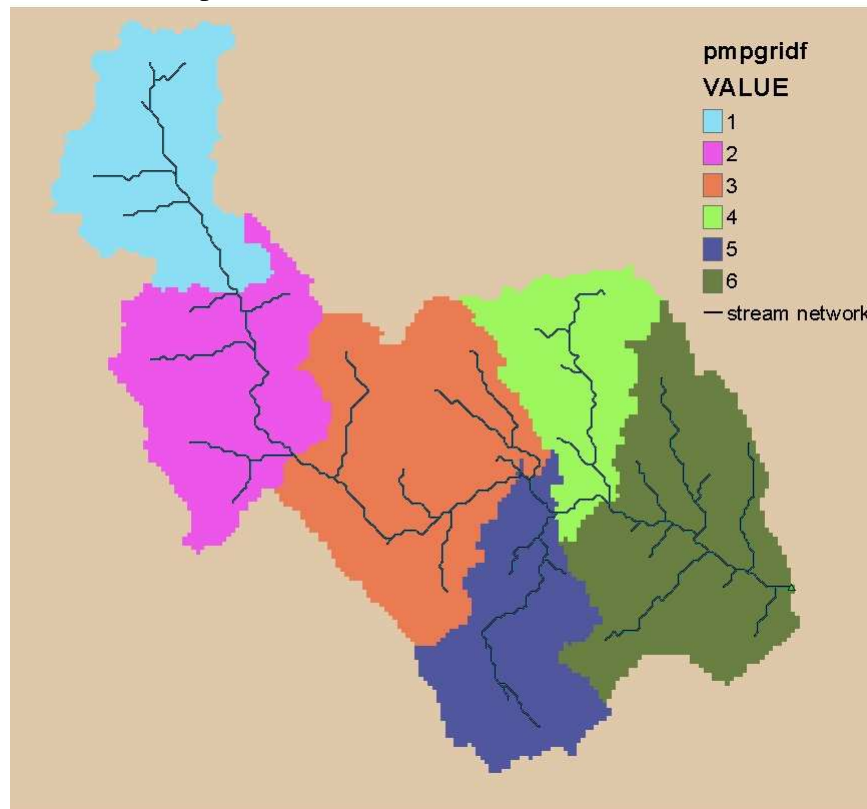
Figure 3.2. Spatially-uniform subareas (one through 6) for PMP design storm application over Pueblo watershed. Areas determined from Bullard and Leverson (1991).

A stochastic design storm method is added to CASC2D in order to use depth-area-duration (DAD) data from an existing extreme storm catalog (USACE, 1945-) and to simulate extreme storms. The standard DAD information is shown in Chapter 4, and includes cumulative rainfall depths for specific durations and area sizes. Rain rates r [L/T] are determined by simple difference from each successive cumulative depth d:

$$r(t) = \frac{d(t)_{i+1} - d(t)_i}{t_{i+1} - t_i} \quad (3.15).$$

There are several approaches to develop a spatial distribution of an extreme storm. The approach that is implemented here is a simple, parsimonious model based on DAD data. It is assumed that the storm is single-centered, and isohyets are geometrically similar in the form of an ellipse (e.g., Hansen et al., 1982). The equation for the ellipse geometry is (Grossman, 1984):

$$\frac{(x - x_s)^2}{a^2} + \frac{(y - y_s)^2}{b^2} = 1 \quad (3.16)$$

where (x_s, y_s) is the storm center and a and b are major and minor axes, respectively. This assumed storm shape describes both within-storm amounts and storm totals, and can be an adequate spatial representation based on the DAD data (Foufoula-Georgiou and Wilson, 1990). Although storm shapes are generally very complex, Hansen et al. (1982) recommended using a standardized elliptical pattern to represent the storm isohyets. The storm spatial pattern that is adopted has geometrically similar ellipses with a major (a) to minor (b) axis ratio c, where $c = a/b$ (Figure 3.3).
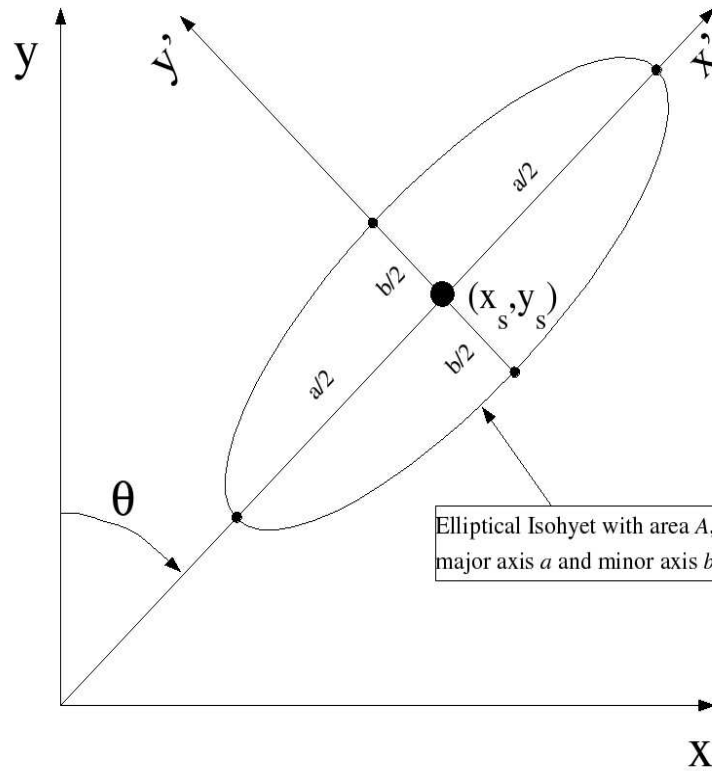
Figure 3.3. Storm spatial representation with storm center location (x_s, y_s), orientation θ, and cartesian coordinate system.

The storm orientation θ is defined clockwise in degrees from North (y) in the half-plane (0, 180), following Hansen et al. (1982). The (x',y') coordinates of the ellipse after rotation are (Grossman, 1984):

$$x' = \left(x - x_s\right)\cdot\cos\theta + \left(y - y_s\right)\cdot\sin\theta \quad \text{(3.17a)}$$

$$y' = -\left(x - x_s\right)\cdot\sin\theta + \left(y - y_s\right)\cdot\cos\theta \quad \text{(3.17b)}$$

Using this geometry to represent a complete storm, the parameters are c and θ, and user-defined storm center (x_s, y_s). The ellipse parameter c is limited to [1.0, 8.0] where 1.0 represents a circle. Typical c values for extreme storms range between 1.0 and 3.0 (Hansen

48

et al., 1982; Foufoula-Georgiou and Wilson, 1990). The storm orientation angle θ is limited

to 180° in the half plane. An example spatial distribution with an elliptical storm pattern is

shown in Figure 3.4.
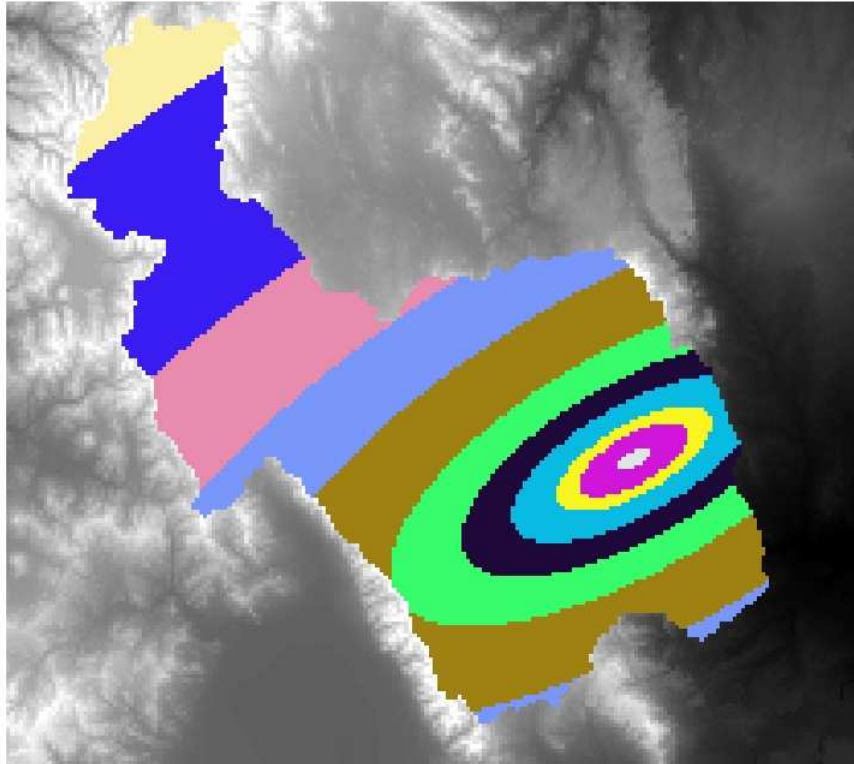
Figure 3.4. Example storm spatial distribution over the Arkansas River watershed with CASC2D. Rainfall is uniform within the area shown by each color. The storm orientation angle is 60 degrees (clockwise) from North.

3.3   CHANNEL INPUTS AND FLOODPLAIN INTERACTIONS

Several improvements are made to CASC2D to enable the modeling of channels on

large watersheds. These include modifications to topology, new data processing and grid

generation techniques, and enhanced floodplain modeling. Channels are segments that

connect from overland grid cell center to grid cell center, and represent rivers or creeks in a

watershed. The location of channel cells within the DEM is typically determined from stream network generation techniques within a GIS. The tools of choice to estimate locations of channel cells and the stream channel network in this research are ArcGIS/ArcInfo 8.3 (ESRI, 2003) and TauDEM (Tarboton, 2002).

The new topology feature that is required for modeling large watersheds is the ability for channel segments to be connected in eight directions, known as the D8 approach (Tarboton, 1997). The current version of CASC2D only supports channels connected in north-south or east-west directions. The CASC2D topology routine is modified to directly use information from a flow direction grid. The flow direction grid is defined by TauDEM (Tarboton, 2002). Flow directions (1-8) are defined counter-clockwise from the east: 1: East, 2: Northeast; 3: North, 4: Northwest; 5: West, 6: Southwest, 7: South, 8: Southeast (see Figure 3.5). The channel connectivity for this new topology routine is shown in Figure 3.6. This hypothetical case shows channels segments connecting four cells, with the first segment on a diagonal.
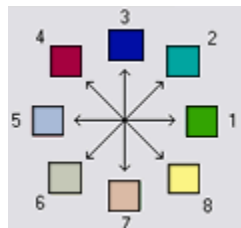
Figure 3.5. D8 flow directions as defined by Tarboton (2002) in TauDEM.
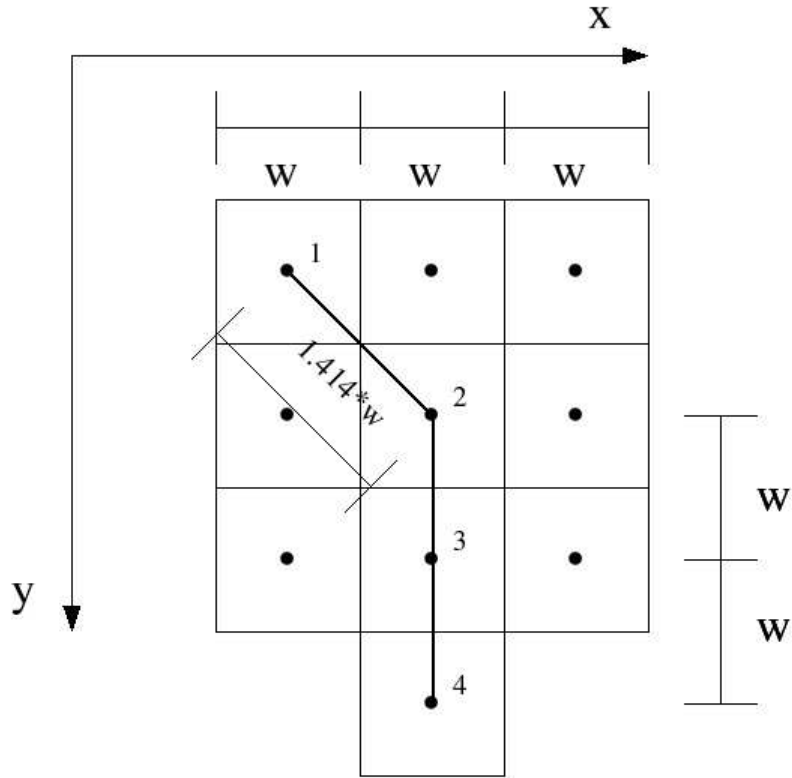
Figure 3.6. Hypothetical channel connections for a link with four nodes (numbered 1 to 4). The channel lengths are defined from grid cell center to grid cell center. Connections between nodes are either orthogonal (distance is equal to grid cell resolution) or diagonal (distance is equal to grid cell size sqrt(2)*W).

One of the most difficult aspects of using CASC2D on large watersheds is the development of connectivity relationships required for modeling channels. New input pre-processing routines that automate development of channel connectivity model input information for CASC2D have been developed as part of this research. In order to model channels, the user first specifies a stream network that defines the location of cells that contain channel segments. The topology of this network is then used to specify two maps to CASC2D that contain the connectivity information. The first map is called a "link" map and contains a grid of integers that denote channel locations for each grid cell within the

51

watershed, and how each channel segment or "river reach" is connected to another. Link

segments now follow current GIS connectivity rules for flow modeling in eight directions

(D8) from a grid (Tarboton, 2002). A "node" map is derived from a link map and contains

integer numbers that designate the connectivity between each grid cell (and thus flow

direction) within an individual link. For example, if a link contains five grid cells, these cells

are numbered 1, 2, 3, 4, and 5 for that link. Example link and node maps that have been

developed with the new preprocessing routine are shown in Figure 3.7. One can readily

observe that many channel cells are connected on diagonals within the Arkansas River basin;

thus a new topology routine was required in order to properly model this watershed.

A new channel bed elevation checking and smoothing routine was developed to

handle potentially flat slopes in channel cells. The basic problem considered here is zero

(flat) slopes in channel (stream network) cells within the watershed. The result is the model

grid will not properly drain. This can be an important issue on large watersheds (> 1,000

km^2) when using "larger" (> 150m) grid cell sizes or due to problems with DEM quality in

complex terrain. With larger grid cells, there can be many contiguous locations within the

defined stream channel that have zero slopes (Figure 3.8). Several other researchers have

noted the problems with flat slopes in DEMs and their effects on hydrologic modeling.

Ogden et al. (1994) recognized adverse slopes and errors in channel slopes derived from

DEMs. They proposed smoothing of the channel network using an ordered search and
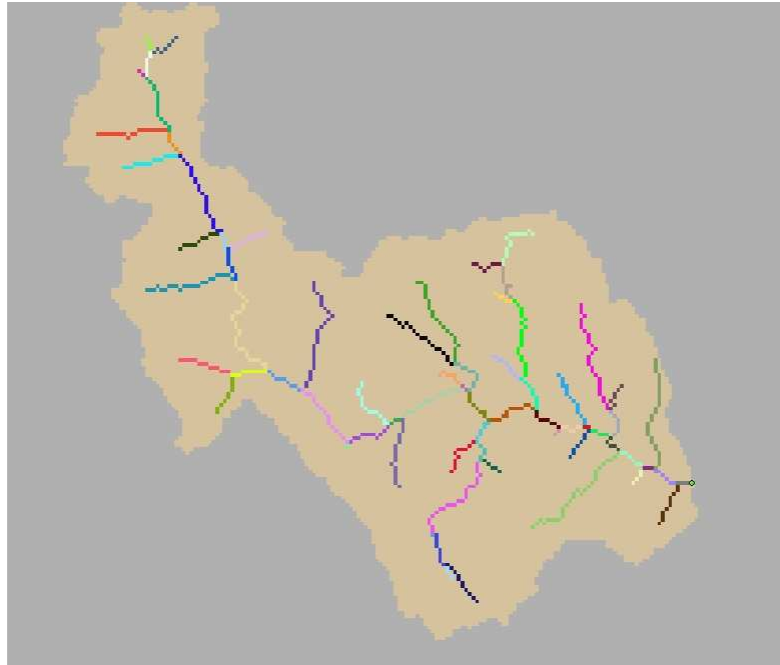
(a)
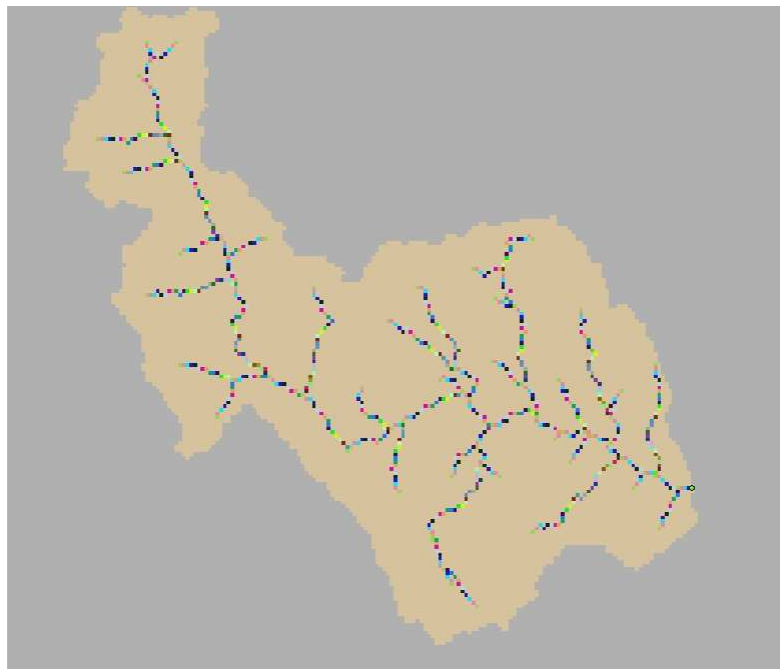
(b)

Figure 3.7. Example link map (a) and node map (b) for modeling channels in the Arkansas River basin. Colors represent different links and nodes. Grid cell size is 960m; there are 69 links and 764 nodes.
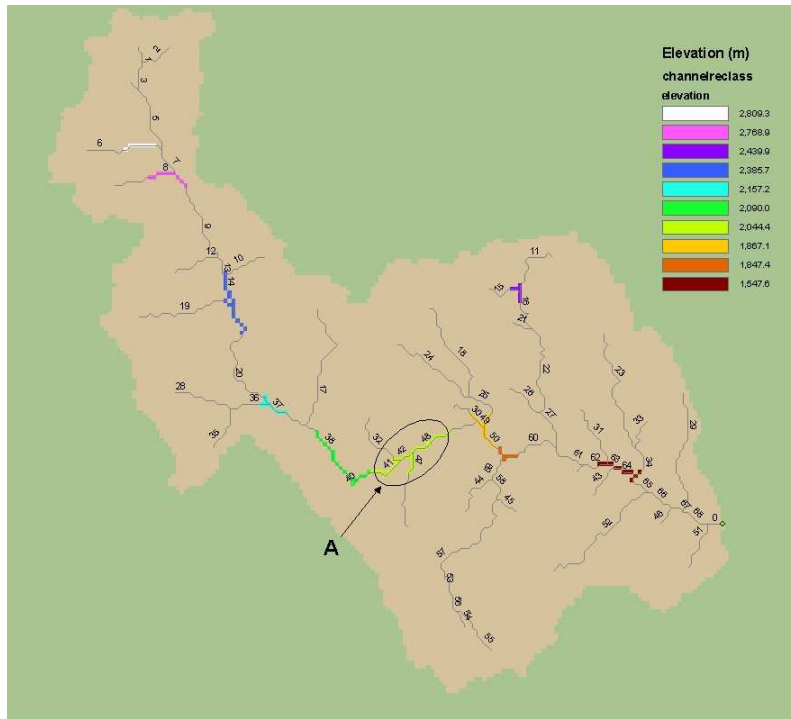
Figure 3.8. Arkansas River stream channel network, estimated using a constant-area threshold equal to 100 cells, at 960 m cell size with link numbers from TauDEM. Ten channel segments, with at least seven contiguous equal elevation (zero slope) cells in each, are shown. Segment labeled "A" has 27 cells that span five links (32, 41, 42, 47 and 48) and two junctions.

estimating the local slope from node to node using the slope from a previous node or by

reducing the elevation of the cell by an arbitrary 25 cm amount. They used a 3-point moving

average filter to smooth the final channel profiles (Ogden et al., 1994). Liu et al. (2003)

recognized the problem with zero slopes along river corridors in the context of GIUH grid-

based modeling for a watershed. They recommended modifying elevations to achieve some

minimum slope in the floodplain and channel areas, and complete a sensitivity analysis to

determine if the assumed slope has much effect on the GIUH runoff model results. Slope

values used were 0.01%, 0.05% and 0.1% (Liu et al., 2003). In the context of TOPMODEL,

Wolock and McCabe (1995) and Pan et al. (2004) recognized that zero slopes from DEMs cause problems calculating the $\ln(a/\tan\beta)$ index. They both provided simple solutions to flat areas. For areas with flat slopes, Wolock and McCabe (1995) redefined the local slope to be equal to (0.5 * vertical resolution)/(horizontal resolution). Pan et al. (2004) used Wolock and McCabe's assumption, called it 0.5VR/HR, and also tested an option where they flagged all cells in the watershed with flat slopes to be undefined, then reset slopes of all undefined cells to the minimum of all defined cell slopes.

Based on the research cited above, one simple solution to the zero slope problem is implemented based on assuming a minimum slope between channel segments (nodes). The user enters this minimum slope value as a constant value; it is then used to modify elevations of every node within a channel link where a zero slope is found between two nodes. The minimum slope estimate can be made using several different approaches: (1) Wolock and McCabe's vertical to horizontal resolution criterion; (2) a minimum value based on precision of the data and floating-point storage limits; (3) some minimum value based on minimum channel slope estimates from topographic maps, vector data, or other data source; or (4) some arbitrary minimum value.

Another difficult aspect of modeling channels in large watersheds with CASC2D is estimation of channel geometric properties and parameters. The geometric properties can include base width, bank height, sideslope, dead storage depth, and channel sinuosity; parameters include Manning *n*. Bed slope is determined from the DEM elevation at each

grid cell and subtracting the bank height. Channel length is determined by multiplying the

channel segment length (w or *1.414*$^*w$, where w is the grid cell size) times the sinuosity. A

cross section of an example channel cell and required geometry is shown in Figure 3.9. The

current version of CASC2D allows trapezoidal cross sections; these can include regular

trapezoids, rectangles, or triangles.
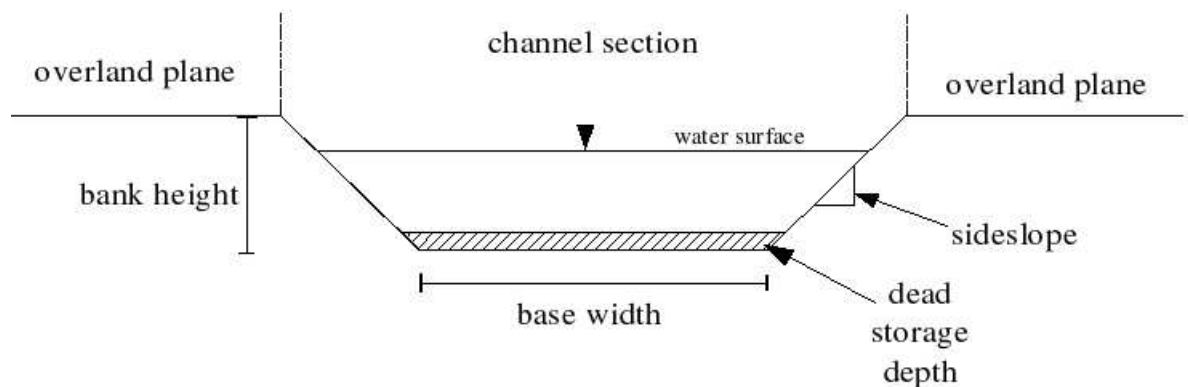
Figure 3.9. CASC2D channel cross section with user-input dimensions: base width, bank height, sideslope, and dead storage depth.

When one models large watersheds, it is a challenge to define these properties for

every channel link and node. A new tool has been developed to estimate channel properties,

including spatially uniform, uniform within a link, and spatially varying properties from node

to node options. In order to model the Arkansas River watershed using 960m grid cell sizes

(Chapter 7), there are 764 cells that have channel segments in them out of the 12,879 total

cells within the watershed. Semi-automated techniques are needed to define channel

properties on this many channel nodes; it is infeasible to do this without developing semi-

automated tools. Channel parameters can be estimated as uniform over the watershed, or

spatially varying between links using downstream hydraulic geometry concepts. Widths and

depths are estimated using power functions based on drainage area (e.g., Orlandini and

Rosso, 1998) and data from the watershed. An example width distribution is shown in

Figure 3.10.
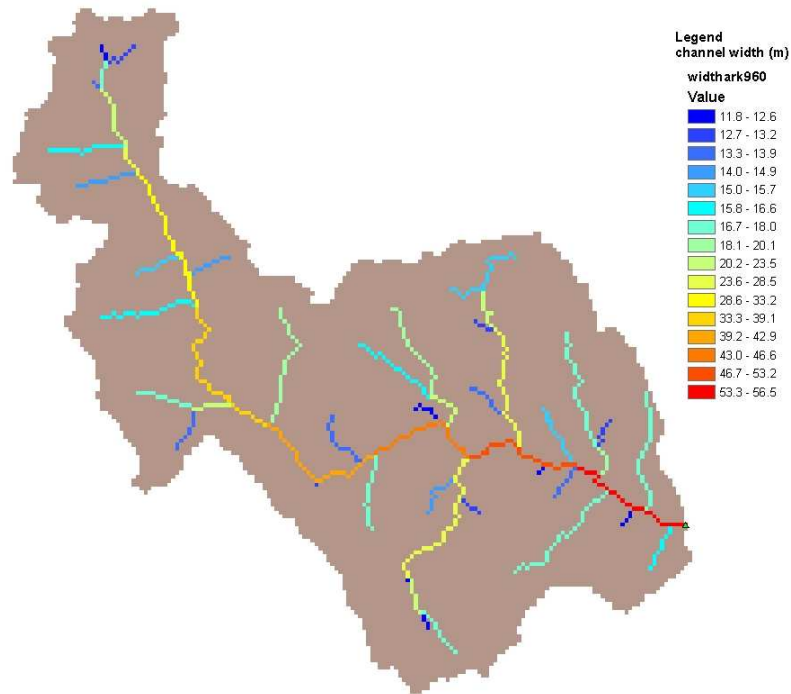
Figure 3.10. Spatially-varying channel widths in the Arkansas River watershed for CASC2D input.

One important process in modeling large watersheds is the floodplain connection

between overland cells and channel sections. CASC2D originally had the ability to model

floodplains (Julien et al., 1995). This process has been reimplemented in the current version

of the model with additional modifications and improvements, so that this process could be

represented. Here, we now handle three cases:

   1. overland water surface elevation > channel water surface elevation

      a. channel water depth < bank height

b. channel water depth >= bank height

2. channel water surface elevation > overland water surface elevation (channel flow
depth always greater than bank height)

3. overland water surface elevation = channel water surface elevation (no water
transfer)

These cases are handled by first comparing water surface elevations, then computing water volumes in the overland and channel portions, respectively, to determine the appropriate volume to transfer. For example, in the case where the channel is dry and water is on the overland plane, the volume in the overland plane is computed. If this volume is less than or equal to the available volume in the channel section, all flow is transferred to the channel. If there is insufficient volume available in the channel to hold the entire overland flow volume, the volume is then proportioned between the overland and channel segments. The major boundary assumption in modeling floodplain connectivity with the adjacent overland portion of the grid cell is the enforcement of an equal water surface elevation in the channel and overland plane sections of the grid cell (Julien et al., 1995). The original floodplain process code only redistributed water from the channel back onto the overland portion of the cell for case 2, and performed the calculation based on flow depth.

3.4   <u>INITIAL CONDITIONS SPECIFICATION AND INFILTRATION PARAMETERS</u>

One crucial feature for simulating extreme floods with an event model such as

CASC2D is the estimation and specification of initial conditions. Differing initial conditions can sometimes have a dramatic effect on model predictions. One new feature that has been added to CASC2D as part of this research is the explicit capability to specify three important initial states: (1) the initial depth of water on the overland plane cells within the watershed; (2) the initial depth of water in channels; and (3) the initial soil moisture.

The initial soil moisture is now entered as spatially-varying values for each soils type and expressed as a saturation fraction S_e, where $0 \leq S_e \leq 1$ (e.g., Saghafian, 1992; Rawls et al., 1993). The Green-Ampt soil moisture deficit M_d is then determined by:

$$M_d = \theta_e (1 - S_e) \quad (3.18).$$

The program now requires the user to input values for these three states prior to running CASC2D. Initial water depths on the overland plane and in the channel are entered directly. Initial soil moisture is also a direct user input. The initial soil moisture and the initial water depths in overland planes can play an important role in predicted runoff volume and peak for extreme floods (e.g., Goldman, 1987; Goldman et al., 1990; Fontaine and Potter, 1993; Franchini et al., 1996; De Michele and Salvadori, 2002).

The estimation procedures for determining the Green-Ampt infiltration parameters K_s (hydraulic conductivity), ψ_f (capillary pressure head), and θ_e (effective saturation) are based on using data obtained from the STATSGO database (NRCS, 1994). The parameter estimation procedure follows the approach used by Goldman et al. (1990) and Rawls et al.

(1993). The saturated hydraulic conductivity [cm/s] is estimated from:

$$K_s = \frac{a\,\theta_e^2\,\lambda^2}{\psi_b^2(\lambda+1)(\lambda+2)} \quad (3.19)$$

where the constant $a = 21.0$, λ is the pore size distribution index, and ψ_b is the bubbling

pressure. We estimate the effective saturation by:

$$\theta_e = \phi - \theta_r \quad (3.20)$$

where ϕ is the porosity and θ_r is the residual saturation. The capillary suction head is

estimated by:

$$\psi_f = \frac{n}{n-1}\,\psi_w \quad (3.21)$$

where $n = (3\lambda + 2)$ and the water entry pressure $\psi_w = (\psi_b/2)$. The Brooks-Corey parameters

residual saturation θ_r, pore size distribution index λ and bubbling pressure ψ_b are estimated

from soils texture regression equations (Rawls and Brakensiek, 1985; Rawls et al., 1993) that

are functions of porosity, percent sand and percent clay. These values are determined for

each soils series in the watershed from the STATSGO data base.

3.5   DERIVED FLOOD FREQUENCY FRAMEWORK

        The framework to estimate flood frequency with CASC2D for a watershed is based

on four main criteria:

1. the CASC2D (TREX) model is used to compute runoff;

2. the Annual Exceedance Probabilities (AEPs) of interest range from about 1/1,000 to

   1/10,000, and may extend perhaps even to 1/500,000;

3. storm characteristics, including duration, timing and areal distribution can be included;

   and

4. rainfall-runoff results can be compared with a data-based peak-flow frequency curve.

These considerations are based on the large watershed research issues that have been

identified in Chapter 2 and Arkansas River basin data analysis described in Chapter 4. As

CASC2D is an event model, initial conditions are also included in the criteria.

The procedure that is used is a hydrologic simulation method (e.g., Bocchiola et al.,

2003) coupled with the stochastic storm transposition (SST) technique (Foufoula-Georgiou,

1989) to estimate extreme rainfall probabilities. The procedure is based on the stochastic

storm transposition and runoff approach used by Franchini et al. (1996) with some

modifications. This approach is outlined by NRC (1988, p. 5), in their "Method III":

1. construct a stochastic mathematical model of extreme rainfall (in space and time);

2. generate several large synthetic storms from model;

3. model deterministic rainfall-runoff transformation; and

4. produce approximate probability statements for resultant large flood hydrographs.

Stedinger et al. (1993, p. 18.52) note that the SST methodology has been developed

for very low frequency rainfall (exceedance probabilities less than 1/1,000). Wilson and

Foufoula-Georgiou (1990) demonstrate average catchment depth probability curves with

AEPs that range from 10^{-3} to 10^{-9}.

The essential elements of the approach that are implemented here are as follows. The stochastic model of extreme rainfall is the SST method described in Foufoula-Georgiou (1989) and Wilson and Foufoula-Georgiou (1990). and is described in Chapter 6. The maximum areally averaged depth that can occur over a catchment of area A_c during a time period Δt is estimated via:

$$\bar{d}_c = \frac{1}{|A_c|} \int_{Ac} \int \left[d(x,y,t_s+\Delta t) - d(x,y,t_s) \right] dxdy \quad (3.22)$$

where d_c is the maximum areally-averaged depth, (x,y) are spatial coordinates and t_s is related to the storm duration. The annual probability of exceedance of the maximum average depth is:

$$G^a(d) = 1 - \sum_{v=0}^{\infty} \left[F_{d\bar{c}(\Delta t)}(d) \right]^v \cdot pr\left[Z(1) = v \right] \quad (3.23)$$

where $Z(1)$ is the random number of extreme storms per year. Further details of the rainfall model are presented in Chapter 6. The exceedance probability of peak flow Q_p can be derived numerically via (Franchini et al., 1996):

$$G(q) = 1 - \int_{\Omega} \int_{Wo} \int_{\Psi} \int_{T(t)} pr\left[Q_p \leq q | \omega, w_o, \psi, \tau(t) \right] \\ \times f_{\Omega}(\omega) f_{Wo}(wo) f_{\Psi}(\psi) f_{T(t)}(\tau(t)) d\omega d\omega_o d\psi d\tau(t) \quad (3.24).$$

In order to fully develop the derived distribution concept for a particular site, the hydrologist must first determine what variables may be held fixed (deterministic), and what

variables may be considered as random. Goldman (1987, p. 228) notes this as:

$$Y_i = h(x_i, c) \quad (3.25)$$

where x_i is a vector of stochastic parameters, c is a vector of deterministic parameters, and h *(.)* is the transformation of input rainfall to output flows that the watershed model represents. These correspond to the vectors in equation (3.24): Ω is the vector of storm characteristics and locations, W_o is the initial storage condition, Ψ is the vector of runoff model properties, and *T(t)* is the temporal distribution of storm depths. The vector of storm characteristics has six variables: D_o^*, K^*, *N*, *C*, Φ and *(X,Y)*, where D_o^* is the maximum *d*-hour storm center depth, K^* and *N* are the depth-area parameters, *C* is the major-to-minor axis ratio, Φ is the orientation of major axis, and *(X,Y)* is the random vector of spatial coordinates of the storm. The initial storage condition has three parameters: S_e, the initial soil saturation; h_{ov}, the initial water depth on overland flow planes; and h_{ch}, the initial water depth in channels. The vector of model parameters consists of: n_{ov} and n_{ch} Manning coefficients for overland and channel flow transport; and saturated hydraulic conductivity and wetting front suction head for infiltration. Note that the third parameter for infiltration is described under the initial storage condition vector. Also, the overland cell dimensions and channel geometry (width, bank height, etc.) are considered to be fixed. The vector *T(t)* is user-entered probability distribution function (pdf) for the temporal distribution during the storm; it is typically four probability groups, as in Huff (1967).

After the random components are selected from each vector, the distributions of random input variables are determined based on available data. For example, Franchini et al. (1996) chose Ψ to be represented by one parameter (average storage capacity) out of 14 ARNO model parameters. One challenge with CASC2D is to represent the few number of parameters in a spatially-distributed context. For example, overland flow Manning n is a vector that depends on the number of land use classes for a particular watershed (see Chapter 7). The random parameters for each vector are considered as fixed for this research. Data and model parameters for the stochastic storm transposition and runoff are discussed in Chapters 6 and 7.

The model-generated peak flows are then compared to a peak-flow frequency curve estimated directly from gage, historical and paleoflood data (Chapter 5). Rainfall-runoff model parameters, storm parameters, and the factors that affect estimated probabilities can then be investigated for potential adjustment. Because the SST method provides a probability associated with a basin average rainfall depth, the results of storm modeling (Chapter 6) might have a large effect on estimated peak flows and probabilities from the runoff model.

3.6   <u>SUMMARY</u>

The existing CASC2D model was enhanced in several areas. New components were added to improve the ability to model extreme storms. Design storms such as PMP and

elliptical storm patterns can now be used with the model. The storm ellipse model consists of a DAD table, storm center, orientation and major-to-minor axis ratio. A new channel mesh generator was devised to enable the estimation of channel width and bank height properties in space for large watersheds. An improved channel topology algorithm allows channels to be connected in eight directions; CASC2D can be applied on large watersheds with an improved representation of channel and their connectivity. The methods to estimate infiltration parameters were documented and the initial soil moisture is parameterized using a saturation fraction. After these improvements, the name of the model was changed from CASC2D to TREX, the Two-dimensional Runoff, Erosion, and eXport model.

Following general concepts in NRC (1988), a derived flood frequency framework was outlined that couples TREX with stochastic storm transposition to develop a flood frequency curve. This pairing is a new application for the CASC2D model. In addition, the stochastic storm transposition approach has not previously been used with a distributed rainfall-runoff model.

Chapter IV

FLOOD HYDROLOGY AND HYDROMETEOROLOGY

This chapter presents flood hydrology and hydrometeorology data within the Arkansas River basin and surrounding region. The main purpose is to gain a direct, data-based physical understanding of extreme flood hydrology and hydrometeorology in order to develop predictive models for extrapolation. Three main areas are explored: (1) review and documentation of extreme floods, flood typology and seasonality within the Arkansas River and surrounding region; (2) documentation of historical information that includes known floods prior to establishment of gaging stations; and (3) review and documentation of an extreme storm catalog and meteorology, that are supplemented by radar data. The focus is to describe the data and flood mechanisms that will form the basis to estimate peak discharge probability relationships and perform rainfall-runoff modeling of extreme floods at several scales within the Arkansas River watershed. An extreme storm database is developed that is subsequently used for extreme storm modeling (Chapter 6).

4.1   ARKANSAS RIVER BASIN OVERVIEW

The Arkansas River basin is a main tributary to the Mississippi River and covers

approximately 160,000 mi^2 (414,400 km^2) in Colorado, Kansas, Oklahoma, and Arkansas (Iseri and Langbein, 1974). The study watershed within this basin is an approximately 4,660 mi^2 (12,000 km^2) portion located in the Arkansas Headwaters (11020001) and Upper Arkansas (11020002) hydrologic units (Seaber et al., 1987) within Colorado. A general outline of the watershed, including major tributaries, towns, and gage locations is shown in Figure 4.1.
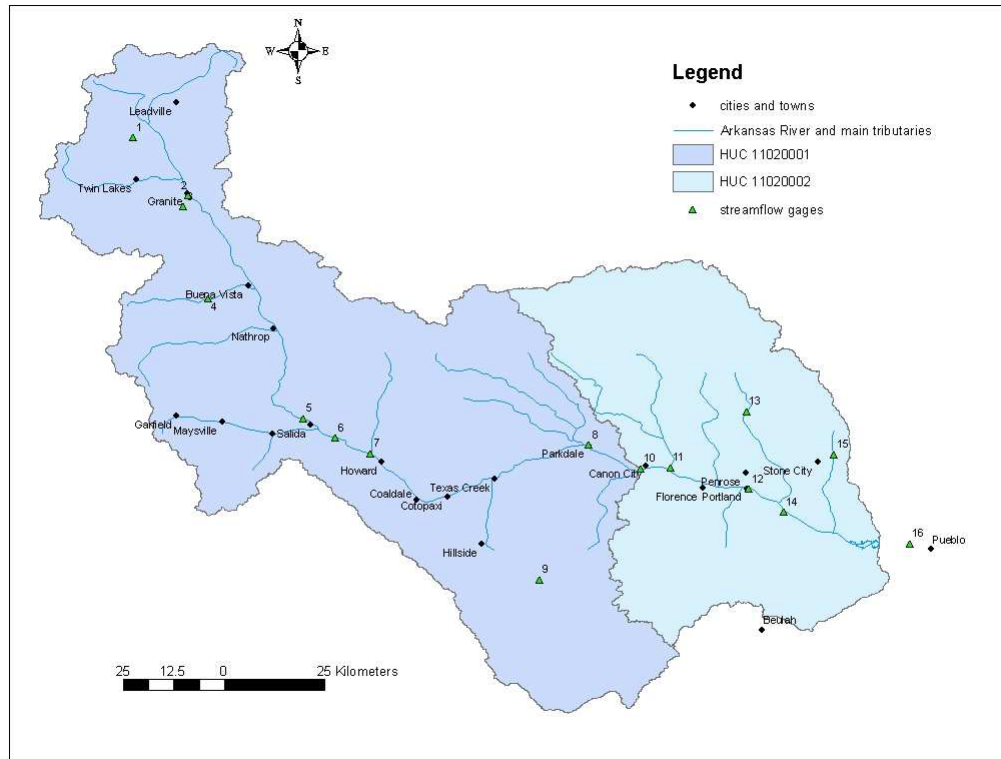
Figure 4.1. Arkansas River Basin study watershed. Major towns and tributaries to the Arkansas River, and streamflow gages within the watershed that are analyzed as part of this study (Table 4.1), are shown.

The Arkansas River study watershed is located in the south-central and southeastern portions of Colorado. The Arkansas River originates at the confluence of the East Fork Arkansas River and Tennessee Creeks, high in the Colorado Rocky Mountains near Malta,

Colorado. The main river travels in a general southerly direction from Malta toward Salida.

The upper watershed in this section consists of narrow valleys and short, steep canyon

reaches. Numerous small tributary creeks flow into the main river in this section. Just

upstream of Salida, the Arkansas River flows in a southeasterly direction to Coaldale. Two

majors tributaries enter the Arkansas River within this section and include the South

Arkansas River and Badger Creek. The river then flows in a general northeasterly direction

to Parkdale. From Salida to Parkdale the river also flows through a canyon environment

with relatively narrow valleys connecting short, narrow canyon reaches. Main tributaries

within this section include Bernard, Texas, Currant, Tallahassee, and Cottonwood Creeks.

The river then flows southeasterly through the Royal Gorge (originally called the Grand

Canyon of the Arkansas) to Cañon City. At Cañon City, Grape and Fourmile Creeks enter

the river. At Cañon City, the topography and river corridor change from steep canyons and

narrow valleys to rolling terrain and an ever-widening river valley. Main tributaries between

Cañon City and Pueblo include Eightmile, Beaver, Oak, Hardscrabble, and Turkey Creeks.

Elevations in the Arkansas River watershed range from 14,433 ft (4,400 m) (Mt.

Elbert) to about 4,700 ft (1,430 m) (Arkansas River downstream of Pueblo Reservoir). The

river cuts through the Colorado Front Range between about Cotopaxi and Cañon City.

Upstream of Cañon City, the mean elevation is 9,550 ft (2,911 m) and the mean basin slope

is 20.5%. Downstream of Cañon City, the basin is generally lower and flatter; the mean

elevation is 6,152 ft (1,875 m) and the mean slope is 9.9% within the watershed between

Cañon City and Pueblo. For the entire watershed, the mean basin elevation is 8,655 ft (2,638 m) and the mean basin slope is 18.1%. The straight-line distance from Leadville to Pueblo is about 115 mi (185 km). Approximate distances along the main-stem Arkansas River are 35 mi (57 km) from Leadville to Buena Vista, 27 mi (43 km) from Buena Vista to Salida, 17 mi (27 km) from Salida to Coaldale, 23 mi (37 km) from Coaldale to Parkdale, 9 mi (14 km) from Parkdale to Cañon City, and 41 mi (66 km) from Cañon City to Pueblo.

The TREX rainfall-runoff model is used to estimate extreme flood peaks and hydrographs. The available data within the watershed for TREX model parameter estimation and calibration consists of three main types: GIS data, physical data, and hydrographic and atmospheric measurement data from gages. The GIS data that are used include: a Digital Elevation Model (DEM) of elevations in the watershed (Figure 4.2a); a map of land use and land cover (Figure 4.2b); a surficial soils map (Figure 4.2c); a bedrock map; hydrography (rivers and lakes); and snow cover information. Physical data consists of river channel dimensions (thalweg elevations, widths, bank heights, sideslopes, lengths, sinuosity). The measurement data includes precipitation (rainfall rates and total accumulations), streamflow (peaks, daily flows, unit values), snow depth and water equivalent at SNOTEL sites, and radar data from Pueblo and Denver. There are six main land use classes present in the watershed based on the USGS National Land Cover Data (NLCD): evergreen forest (35%), grasslands/herbaceous (29%), shrubland (23%), deciduous forest (7%), bare rock/sand/clay (3%) and pasture/hay (2%). A description of each class is in Anderson et al. (1976). Areas

of the watershed with elevations greater than 9,840 ft (3,000 m) are usually snow-covered

from November through mid-April. Snowmelt is the dominant runoff mechanism in much of

the watershed.
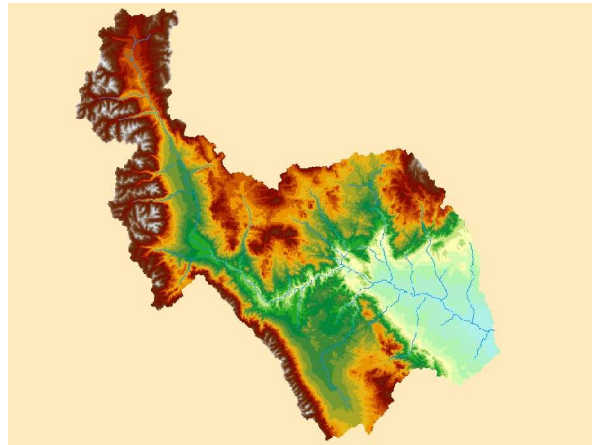
(a)
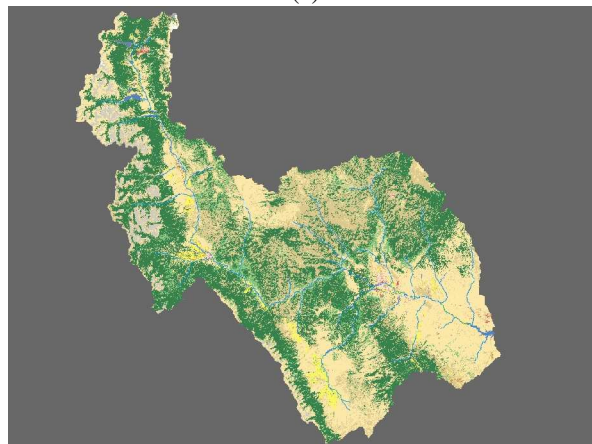
(b)
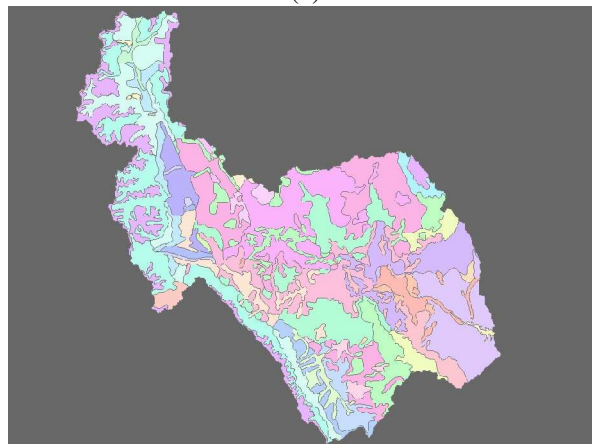
(c)

Figure 4.2. Arkansas River study watershed main GIS data layers: (a) DEM; (b) landuse; and (c) soils.

4.2   EXTREME FLOODS IN THE ARKANSAS RIVER BASIN AND REGION

The Arkansas River basin study watershed falls within two flood peak discharge

hydrologic regions (Vaill, 2000): the Mountain region and the Plains region. The Arkansas

River watershed upstream of Wellsville (1,486 mi^2; 3,850 km^2) is in the mountain region; the

remaining downstream portion of the watershed (3,174 mi^2; 8,150 km^2) is in the plains

region. The mountain region consists of the high topographic relief of the Rocky Mountains

north of the continental Divide and north of the Rio Grande drainage basin and is defined by

the 7,500 ft (2,290 m) elevation contour along the eastern and western slopes of the Rocky

Mountains. The western boundary of the plains region coincides with a line along an

elevation of 7,500 ft in the South Platte River basin, south to a transition zone near the

Chaffee-Fremont County line, to a line along an elevation of about 9,000 ft (2,740 m) in the

Arkansas River basin (Vaill, 2000). These hydrologic region boundaries described by Vaill

were determined by McCain and Jarrett (1976) and Kircher et al. (1985). The regions do not

correspond to hydrologic units; rather, they are determined by examining residuals from

peak-flow regression equations and grouping similar areas. The spatial distribution of

elevations relative to 2,290 m within the watershed is shown in Figure 4.3.

Streamflow data are used to understand and quantify floods and flood magnitude.

Three data sources from the U.S. Geological Survey and Colorado Division of Water

Resources were used to characterize streamflow in the Arkansas River basin: (1) annual peak

discharge estimates at gaging stations and miscellaneous sites; (2) daily mean discharge

estimates and unit (hourly or 15-minute) values at gaging stations; and (3) qualitative and

quantitative information from USGS Water-Supply Papers and other reports.
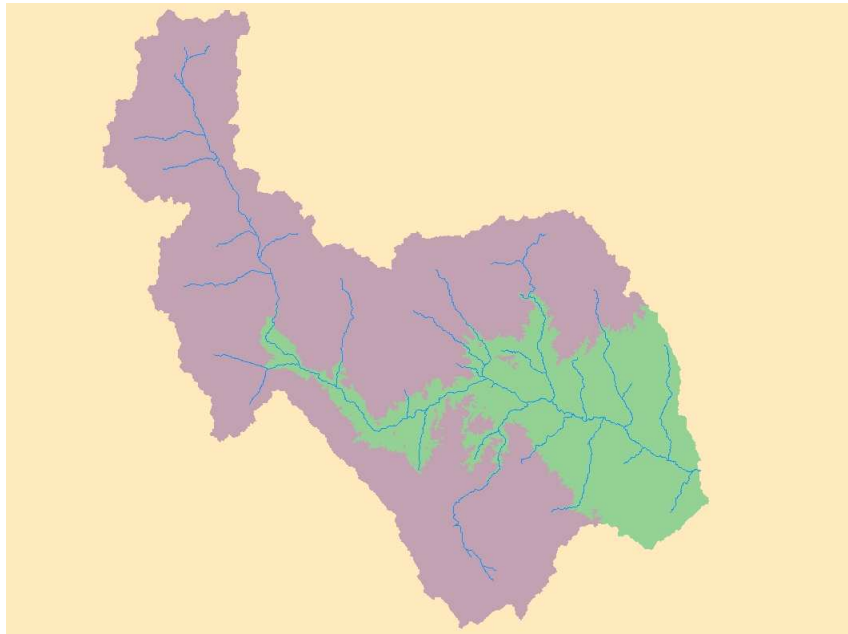
Figure 4.3. Locations of elevations greater than (magenta) and less than or equal to (green) 7,500 ft (2,290 m) within the Arkansas River watershed, based on a DEM with 150 m cell size. Approximately 74% of the watershed area is greater than 7,500 ft.

The USGS and the Colorado Division of Water Resources have been measuring and

publishing streamflow records in Colorado since the late 1800s. The first regular

streamflow-gaging station was established by the State Engineer in 1883 on the Cache la

Poudre River and operated by L.G. Carpenter of the Colorado State Agricultural College

(Colorado State Engineer, 1885; Fellows, 1902). The USGS established many stations in

Colorado in 1888 (Fellows, 1902; Frazier and Heckler, 1972). There are many long-term

gaging stations located in the Arkansas River basin upstream from the city of Pueblo,

Colorado (Crowfoot et al., 2004). The stations with the longest records are all located on the

Arkansas River main stem and include: at Granite (1895); at Salida (1895); at Canon City

(1888); and at Pueblo (1885). Including tunnels, seepage locations, and dams, there are

approximately 25 active gaging stations in the Upper Arkansas River basin upstream of

Pueblo (Crowfoot et al., 2004). This study focuses on using data from 16 active and

discontinued gaging stations located within the Arkansas River basin upstream from Pueblo

Dam (Figure 4.1). Streamflow data from these gaging stations were used for peak discharge

frequency and understanding flood hydrometeorology. The station names, location,

elevation and period of record at each site are summarized in Table 4.1.

Streamflow data were obtained directly from the USGS National Water Information

System (NWIS) Database. These data were cross-checked with those published in USGS

Water-Data Reports and Water-Supply Papers, including: Fellows (1902), USGS (1923),

Follansbee and Jones (1922), Jarvis and others (1936), Follansbee and Sawyer (1948), USGS

(1955), USGS (1964), Patterson (1964), USGS (1969), and Crowfoot et al. (2004). The

records were supplemented by Colorado Division of Water Resources data published at

selected locations. These sources indicate that there are relatively very long stream gaging

records that are essentially complete at certain scales (predominantly along the main stem).

In addition to data at gaging stations, historical information (discussed below) is used to

supplement peak discharge estimates and extend record lengths for peak flow frequency

estimation.

Table 4.1: Streamflow Gaging Stations Analyzed

No. (Fig. 4.1)	USGS Gaging Station No.	Station Name	Drainage Area (mi^2)	Lat.	Long.	Gage Elevation (feet, NGVD)	Hydrologic Unit Code	Period of Record (Water Years)
1	07083000	Halfmoon Creek near Malta	23.6	39.1722	-106.3886	9,830	11020001	1947-2003
2	07086000	Arkansas River at Granite	427	39.0428	-106.2653	8,914.86	11020001	1895-2003
3	07086500	Clear Creek above Clear Creek Reservoir	67.1	39.0181	-106.2772	8,885	11020001	1946-1995
4	07089000	Cottonwood Cr. bl Hot Springs, near Buena Vista	65	38.8128	-106.2217	8,532	11020001	1912-1986
5	07091500	Arkansas River at Salida	1,218	38.5458	-106.0100	7,050.45	11020001	1895-1979
6	07093700	Arkansas River near Wellsville,	1,485	38.5028	-105.9392	6,883.40	11020001	1961-2003
7	07093775	Badger Creek, lower station, near Howard	211	38.4672	-105.8594	6,780	11020001	1981-2003
8	07094500	Arkansas River at Parkdale	2,548	38.4872	-105.3731	5,720	11020001	1946-2003
9	07095000	Grape Creek near Westcliffe	320	38.1861	-105.4831	7,690	11020001	1925-1995
10	07096000	Arkansas River at Canon City	3,117	38.4339	-105.2567	5,342.13	11020002	1889-2003
11	07096500	Fourmile Creek near Canon City	434	38.4364	-105.1908	5,254	11020002	1949-1997
12	07097000	Arkansas River at Portland	4,024	38.3883	-105.0156	5,021.59	11020002	1939-2003
13	07099050	Beaver Cr above Upper Beaver cemetery near Penrose	122	38.5617	-105.0214	6,020	11020002	1991-2003
14	07099200	Arkansas River near Portland	4,280	38.3372	-104.9383	4,940	11020002	1965-1974
15	07099230	Turkey Creek above Teller Res near Stone City	62.3	38.4650	-104.8258	5,520	11020002	1978-2003
16	07099500	Arkansas River near Pueblo	4,686	38.2672	-104.6572	4,689.74	11020002	1885-1975

4.2.1   Flood Process Typology

In order to understand and predict extreme floods within a particular watershed, it is imperative to understand the causative mechanisms of floods. Meyer (1917) outlined three mechanisms: floods due to rainfall on small and large basins; floods due primarily to snowfall; and fall floods. Foster (1948) suggested three general classes for the causes of natural floods: excessive rainfall; rapid melting of deep snow cover; and ground conditions

(frozen or saturated). Hoyt and Langbein (1955) describe five broad causative mechanisms of floods: rainstorms; thunderstorms; hurricanes; snow; and ice jams. Jarrett and Costa (1988, p. 4) summarized three types of floods that occur in the Colorado Front Range: snowmelt, rainfall; and rain falling on snow or mixed-population. Cudworth (1989, p. 177-179) presents four primary meteorologic classes of floods: thunderstorms; general rain type events; snowmelt floods; and rain-on-snow events. He defined these classes as follows: (1) thunderstorm events where the resulting flood is caused by high-intensity, short duration rainfall that produces high peak discharges and relatively low volumes; (2) general rain type events where the resulting flood is caused by moderate intensity, long duration rainfall; (3) snowmelt floods resulting from the melting of an accumulated snowpack; and (4) floods resulting from a combination of rain falling on a melting snowpack.

Doesken (1991) suggested that floods occur primarily from April through October in Colorado from three principal causes: intense local thunderstorms; intense widespread rainfall; and snowmelt. Loukas et al. (2000) classified peak flows in British Columbia into five types: rainfall events; snowmelt events; winter rain-on-snow events; spring rain and snowmelt events; and summer runoff events with contribution of glacier melt. Merz and Blöschl (2003) recently classified the causative mechanisms of floods for Austria into five major types: long-rain floods, short-rain floods, flash floods, rain-on-snow floods, and snowmelt floods. Based on the past work summarized above, we use the four class flood process typology from Cudworth (1989) to describe floods within the Arkansas River basin

75

and region. We also review prior work on extreme floods in the Colorado Front Range.

Hydrometeorologic mechanisms for the observed floods and storms are described in Section

4.3. The types of extreme floods in Colorado are described by Follansbee and Hodges (1925,

p. 105):

> "Floods in the Rocky Mountain region are of two types – the floods in the larger streams due
> to the general rains of several days' duration over large areas and the so-called cloudburst
> floods due to intense rains of short duration covering well-defined small areas. Floods of the
> first type are relatively infrequent, and, as they are well understood, their characteristics will
> not be discussed. Only the severe floods of this type that occurred in 1923 are described in
> this report. Cloudburst floods cause the streams to rise and fall suddenly."

Matthes (1922) discusses cloudburst mechanisms and major flood observations in the United

States; he suggests that cloudbursts in the foothills of the Rocky Mountains are common, at

higher elevations they are rare, and that the relation between topography and cloudburst

frequency needs to be studied.

The flood hydrology of the foothills and mountain streams in the Colorado Front

Range is characterized by mixed-population flooding from snowmelt and rainfall (Elliott et

al., 1982; Jarrett, 1987). Rain-on-snow floods do occur infrequently, but have been observed

primarily in the Rio Grande, Gunnison River, and Colorado River basins (Follansbee and

Sawyer, 1948). Short-duration, high-intensity local convective thunderstorms are the

dominant mechanism for causing flash floods and the largest instantaneous peak discharges

on foothills streams (e.g,. McCain et al., 1979). Follansbee and Sawyer (1948, p. 22) term

these events cloudbursts, which they define as follows.

> "A type of storm confined chiefly to the eastern foothills region below an altitude of about

7,500 feet and extending eastward from the mountains about 50 miles, is the so-called cloudburst, which is a rainfall of great intensity confined to a very small area and lasting usually a very short time. ... Cloudbursts occur only where there is a marked range in temperature within a relatively small area. This condition exists chiefly within the foothills, where warm air from the plains drifts toward the mountains, is deflected upward, and cools rapidly at the higher altitudes near the heads of canyons. For this reason cloudbursts generally occur in the afternoon or early evening of an unusually warm day. ... At the higher altitudes the differences in temperature are usually insufficient and the mass of air too small to cause cloudbursts, although on rare occasions they have occurred at high altitudes during unusually warm weather."

The Arkansas River watershed is subject to extreme flooding in the warm season (April through August) from cloudburst rainfalls, snowmelt runoff, and spring general rainstorms. Topography is the major influence on extreme precipitation. The largest recorded floods at streamflow-gaging stations on the Arkansas River main stem upstream of Cañon City have been from snowmelt. At Cañon City and downstream, the largest peak flows have been from rainfall-runoff. Within the Arkansas River Basin, there are some mixed-population (rainfall-runoff and snowmelt runoff) flooding on small tributaries at higher elevations. Follansbee and Hodges (1925, p. 107) note the following, relevant to extreme floods at high elevations.

"The east side of the Arkansas valley between Granite and Buena Vista, embracing the western slope of the Park Range, is also subject to occasional cloudbursts, which, however, are not so severe as those in the foothills region. Cloudbursts have also been recorded near the mouth of Texas Creek above the Royal Gorge. ... Most cloudbursts occur at altitudes between 6,000 and 7,000 feet, although those near Ouray are between 8,000 and 9,000 feet, those near Granite about 9,500 feet, and the one series of cloudbursts recorded on the North Fork Shoshone River in northern Wyoming at 10,000 feet. ... It is readily seen that they can seldom occur at higher altitudes in the mountains, as there the differences in temperature are usually insufficient and the mass of warm air in the high valleys is not great enough to cause any decided drift toward adjacent mountains."

Twenty-three years later, Follansbee and Sawyer (1948, p. 73) clearly state their opinion on

the spatial distribution of extreme floods in the Arkansas River Basin:

> "Above the Royal Gorge, the Arkansas River is not subject to heavy floods. A few of its
> upper tributaries are subject to cloudburst floods, but the volume of these floods is too small
> to affect seriously the Arkansas River itself."

Hoyt and Langbein (1955, p. 272) also suggest that floods on the Arkansas River in Colorado

upstream of John Martin Reservoir are generally of the summer cloudburst type. Streamflow

and storm data are summarized below that show thunderstorms and general storms can cause

extreme floods within the Arkansas River basin east of Parkdale.

4.2.2   Largest Recorded Peak Discharges

Peak flow data are one of the most important measures of extreme floods (e.g.,

Dalrymple, 1964). The largest peak flows recorded within the Arkansas River watershed

upstream from Avondale are listed in Table 4.2; the flood season is typically from late April

through mid-September. Peak flows for rainfall-dominant portions of the watershed

downstream of Parkdale are from general storms in May and June, and local thunderstorms

in July and August. Snowmelt causes the largest flood peaks within the upper basin

upstream of Parkdale, and occurs from late May through mid July. The most important of

the largest floods recorded at these gaging stations were: June 3, 1921 at Pueblo; August 2,

1921 at Canon City; June 17-18, 1965 on the Arkansas River east of Pueblo; and April 30,

1999 on Fountain Creek. The largest flood on the Arkansas River upstream of Pueblo, in

terms of peak discharge and stage, occurred on June 3, 1921 (Follansbee and Jones, 1922).

Table 4.2: Largest Peak Discharge Estimates in the Arkansas River Basin Upstream of Avondale

USGS Gaging Station No.	Station Name	Drainage Area (mi²)*	Period of Record	Date	Peak Discharge (ft³/s)	Flood Type
07086000	Arkansas River at Granite, CO	427	1897 - 2002	06/28/1957	5,360	snowmelt
07091200	Arkansas River near Nathrop, CO	1,060	1965 - 2002	07/14/1995	5,540	snowmelt
07091500	Arkansas River at Salida, CO	1,218	1895 - 1979	06/29/1957	9,220	snowmelt
07093700	Arkansas River near Wellsville, CO	1,485	1961 - 2002	06/12/1980	6,240	snowmelt
07094500	Arkansas River at Parkdale, CO	2,548	1946 - 2002	06/18/1995	6,830	snowmelt
07095000	Grape Creek near Westcliffe, CO	320	1925 - 1995	08/02/1966	7,460	thunderstorm
misc.	Grape Creek in Canyon above Cañon City, CO	(32)	1925	07/21/1925	14,500	thunderstorm
07096000	Arkansas River at Cañon City, CO	3,117	1889 - 2002	08/02/1921	19,000	thunderstorm
misc.	Wilson Creek near Mouth	61.3	1941	07/04/1944	16,800	thunderstorm
07096500	Fourmile Creek near Cañon City, CO	434	1949 - 1997	07/11/1951	4,260	thunderstorm
07097000	Arkansas River at Portland, CO	4,024	1939 - 2002	06/05/1949	21,100	thunderstorm
07099100	Beaver Creek near Portland, CO	214	1971 - 1981	09/09/1973	4,800	thunderstorm
07099200	Arkansas River near Portland, CO	4,280	1965 - 1974	08/21/1965	23,900	thunderstorm
07099400	Arkansas River Above Pueblo, CO	4,670	1966 - 2002	08/01/1966	10,100	thunderstorm
07099500	Arkansas River near Pueblo, CO	4,686	1895 - 1975	06/03/1921	103,000	general storm
misc.	Monument Creek at Colorado Springs	75		05/30/1935	50,000	general storm
07105500	Fountain Creek at Colorado Springs, CO	392	1976 - 2002	09/02/1994	10,100	thunderstorm
07105530	Fountain Cr Bl Janitell Rd Bl Colo. Springs, CO	413	1990 - 2002	04/30/1999	13,800	general storm
07105800	Fountain Creek at Security, CO	495	1965 - 2002	07/24/1965	25,000	thunderstorm
misc.	Jimmy Camp Creek near Fountain, CO	54.3		06/17/1965	124,000	general storm
07106000	Fountain Creek near Fountain, CO	681	1939 - 2002	05/28/1940	22,100	general storm
07106300	Fountain Creek near Pinon, CO	849	1973 - 2002	04/30/1999	19,100	general storm
07106500	Fountain Creek at Pueblo, CO	926	1921 - 2002	06/17/1965	47,000	general storm
07109500	Arkansas River near Avondale, CO	6327	1939 - 2002	06/18/1965	50,000	general storm
07110500	Chico Creek near North Avondale, CO	864	1921 - 1946	06/04/1921	28,600	general storm

* values in parentheses (.) are contributing drainage area estimates from Follansbee and Sawyer (1948)

Regional flood peak discharge data from U.S. Geological Survey and Colorado

Division of Water Resources gaging stations and miscellaneous sites were examined to gain

an understanding of maximum flood experience to date in an area near and adjacent to the

Arkansas River basin. A regional envelope curve was prepared from these data, based on

techniques presented in Cudworth (1989). Regional peak discharge envelope curves are

useful to: (1) expand the flood data base for the watershed of interest with data from nearby

streams; (2) portray extreme flood potential in the area being studied; (3) gain an

understanding of the regional hydrometeorology based on the largest floods; and (4) as a

base to compare probabilistic estimates of peak discharge and/or design floods. Envelope

curves do not typically have any probability or frequency associated with them (Crippen and

Bue, 1977; Crippen, 1982). Some investigators have proposed various methods to estimate

probabilities for the largest observed regional floods, such as those used to develop envelope

curves (Fuller, 1914; Carrigan, 1971; Wahl, 1982; Jarrett and Tomlinson, 2000 Figure 13;

Vogel et al. 2001; Troutman and Karlinger, 2003), but these techniques need further

development and testing prior to implementation.

The hydrologic region for the peak discharge envelope curve was selected based on

the eight Arkansas River hydrologic regions in Colorado (Patterson, 1964), the nine South

Platte hydrologic regions in Colorado (Matthai, 1968), the transition zone/South Platte region

used by Jarrett and Costa (1988), the Mountain region (east of Continental Divide) from

Kircher et al. (1985), and the Mountain (east of the Continental Divide) and Plains regions

presented in Vaill (2000). Peak discharge data from east of the Continental Divide within

Colorado, excluding the Rio Grande, were used. This mixes data from the Mountain and

Plains regions. The area encompasses eastern Colorado at the Continental Divide

(headwaters of the Arkansas and South Platte Rivers), north to the Wyoming border, east to

the Kansas and Nebraska borders, and south to the Rio Grande and New Mexico. Data from

the Arkansas and South Platte drainage basins in Colorado, that are subsets of the Missouri

River basin, were utilized. This region is a subset of Region 12 presented by Crippen and

Bue (1977, Figure 1). Crippen and Bue included southwestern Nebraska, eastern New

Mexico and west Texas (including the Canadian, Devils and Pecos Rivers).

The Mountain and Plains hydrologic regions from Vaill (2000) were combined in

order to obtain a larger sample of peak discharge data potentially applicable to the Arkansas

River basin. These regions were also combined in order to address one of the issues raised

when developing the current PMF using generalized procedures for Pueblo Dam (Bullard

and Leverson, 1991). This issue was the fact that record peak flows from June 1965 in the

Colorado Front Range were significantly larger than the inflow design flood peak for Pueblo

Dam. Peak-flow data within this region were segregated into three main groups: South Platte

data, upper Arkansas data (upstream from Pueblo), and lower Arkansas data. The peak flows

were further segregated by type: indirect measurement or estimate at a gaging station. Peak

discharge data from areas outside Colorado were not considered applicable to the Arkansas

River basin.

Data from the Mountain and Plains regions include data from mixed populations. As

discussed below, and shown in Table 4.2, peak discharge estimates in the mountain region

(upper Arkansas and South Platte) are significantly lower than peak discharge estimates from

the Plains. The drainage area to Pueblo Dam spans both the Mountain and Plains Regions.

McCain and Ebling (1979), Jarrett (1987) and Jarrett and Costa (1988) describe a "transition

zone" that encompasses the area with elevations below about 7,500 to 8,000 feet in the

canyons of the Colorado Front Range, and is a transition between the two regions. There is

clear evidence that rainfalls have caused large magnitude flood peaks in the immediate area

upstream and downstream of Pueblo Reservoir. These floods are similar to those that have

occurred on other Front Range streams such as the South Platte River, but are distinctly

different than the snowmelt floods in upstream sections of the Arkansas basin.

A regional peak discharge envelope curve for Colorado, including areas east of the

Continental Divide within the Arkansas and South Platte basins, is shown in Figure 4.4. The

largest peak discharge estimates used to construct the curve are listed in Table 4.3 for this

area. The maximum, instantaneous peak discharge observed for a basin in eastern Colorado

with a comparably-sized drainage area to Pueblo Dam (4,560 mi^2) is subject to large

uncertainties. A regional value is approximately 188,000 ft^3/s for rainfall-dominated events,

based on a relation for drainage areas between 1,000 and 20,000 mi^2 (Figure 4.4). However,

there is a distinct scale-dependent feature to the data. It appears that rainfall over partial

areas and/or watersheds less than about 1,000 mi^2 follow a relation that has a higher slope

and intercept than data from larger watersheds. This relation would suggest a maximum

observed peak flow of about 560,000 ft^3/s for a watershed with contributing drainage area of

1,000 mi^2. Thus, the simple notion that flood magnitude increases in some fashion with a

concomitant increase in drainage basin scale is rejected for this area in Colorado.

Considering that the contributing rainfall area for the June 1921 Penrose storm (discussed

below) is about 550 mi^2 (Follansbee and Jones, 1922), an estimated peak for this storm and

watershed scale is 428,000 ft^3/s. These data indicate approximate, maximum peak flood

experience to date in the region, and are in general greater than the existing design spillway

capacity (191,500 ft^3/s) at Pueblo Dam.
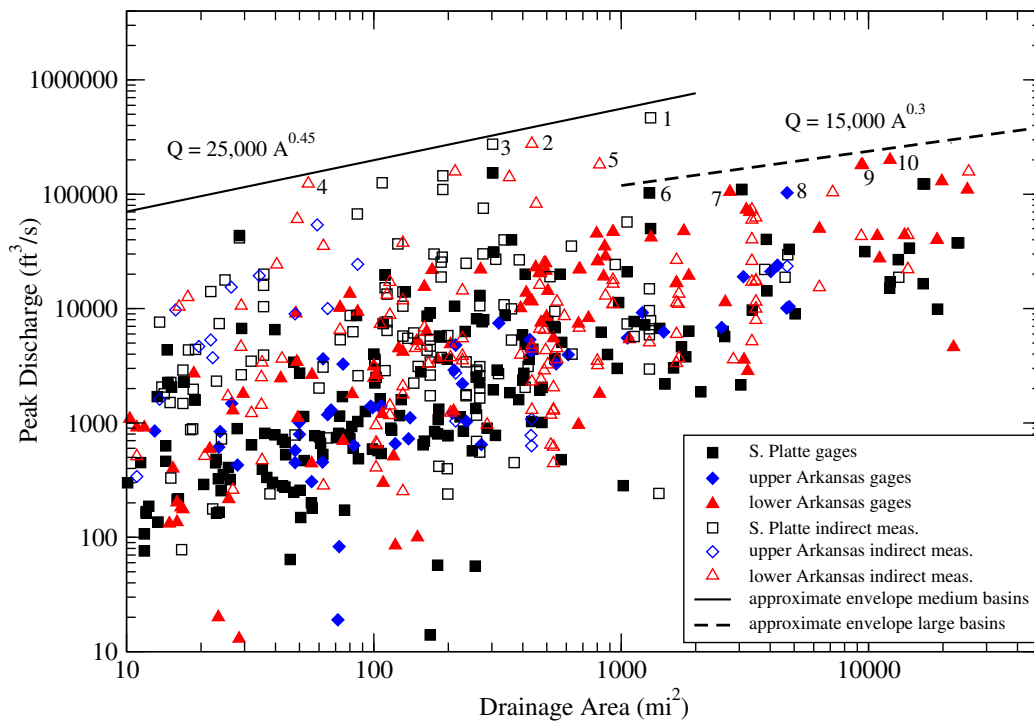
Figure 4.4. Maximum peak discharge data and drainage-area envelope curve for observations within the Arkansas and South Platte River Basins in Colorado.

The regional relations shown in Figure 4.4 follow a typical Myers-type envelope curve formula (Jarvis and others, 1936; Creagher et al., 1945):

$$Q = CA^n \quad (4.1)$$

where Q is peak discharge (ft^3/s); C is a constant; A is the drainage area (mi^2); and n is a slope. This equation is empirical and has no theoretical basis. Based on data shown in Figure 4.4, it appears that the parameters C and n are not constant and change with scale. Matthai (1969) demonstrates a similar scale dependence with a change in parameters at 200 mi^2. The curves are considerably higher than Follansbee and Sawyer (1948), due to the addition of 1965 flood data. The curves are similar in shape to that shown by Matthai (1969), but his equation was limited to drainage basins less than 200 mi^2. He used the same curve for larger areas as Hoyt and Langbein (1955). However, the Hoyt and Langbein curve, as well as curves shown by most others (e.g. O'Connor and Costa, 2004), includes data from most of the United States, such as Seco Creek and the West Nueces River in Texas and the Eel River in California. The relation shown in Figure 4.4 is considerably lower for drainage basins greater than 1,000 mi^2 than that depicted by Crippen and Bue (1977) for their Region 12, as they also relied on data from Texas to define the envelope curve for drainage basins greater than 1,500 mi^2. The relation is also lower than the Hoyt and Langbein (1955) and O'Connor and Costa (2004) curves because they also use data from Texas and other locations within the United States. Those data are not considered applicable to the Arkansas River basin in Colorado.

Table 4.3: Largest Observed Peak Discharge Estimates that Define a Drainage Area-Peak Discharge Relation for the Arkansas and South Platte River Basins

Point No. (Fig. 4.4)	Station Name	Drainage Area (mi^2)	Date	Peak Discharge (ft^3/s)	Measurement Type	Meas. Rating	Flood Type
1	Bijou Creek near Wiggins, CO	1,314.0	06/18/1965	466,000	slope-area at misc. site	poor	general storm
2	Rule Creek nr Toonerville, CO	435.0	06/18/1965	276,000	slope-area at misc. site	fair	general storm
3	East Bijou Creek at Deer Trail, CO	302.0	06/17/1965	274,000	slope-area at misc. site	fair	general storm
4	Jimmy Camp Creek near Fountain, CO	54.3	06/17/1965	124,000	slope-area at misc. site	fair	general storm
5	Two Buttes Creek near Holly, CO	817.0	06/17/1965	182,000	slope-area at misc. site	good	general storm
6	South Fork Republican River near Idalia, CO	1,300.0	05/31/1935	103,000	slope-area at gage	unknown	general storm
7	Purgatoire River at Ninemile Dam, near Higbee, CO	2,752.0	06/18/1965	105,000	estimated based on flow over dam at gage	unknown	general storm
8	Arkansas River near Pueblo, CO	4,686.0	06/03/1921	103,000	slope-area at gage	unknown	general storm
9	Arkansas River near Nepesta, CO	9,345.0	06/04/1921	180,000	slope-area at gage	unknown	general storm
10	Arkansas River at La Junta, CO	12,210.0	06/04/1921	200,000	slope-area at gage	unknown	general storm

Four peak discharge estimates control the position of the envelope curve for scales less than 1,000 mi^2 (Figure 4.4; Table 4.3): Bijou Creek near Wiggins (point 1), Rule Creek near Toonerville (point 2), East Bijou Creek (point 3) at Deer Trail, and Jimmy Camp Creek near Fountain (point 4). The June 1965 flood data (points 1, 3 and 4) were listed by Crippen and Bue (1977) as the largest floods in Colorado for their respective drainage areas. The Jimmy Camp Creek flood was also a point that defined the United States envelope curve (O'Connor and Costa, 2004). England (2004) suggested that the Jimmy Camp Creek peak may be overestimated and that it be further reviewed. The USGS has agreed that the measurement rating be changed from fair to poor.

Four peak discharge estimates control the position of the envelope curve for scales

greater than 1,000 mi^2: South Fork Republican River (point 6), Purgatoire River (point 7),

Arkansas River at Nepesta (point 9), and the Arkansas River at La Junta (point 10). These

points are associated with the June 1921, May 1935 and June 1965 storms and floods. The

largest peak flow on the Arkansas River upstream of Fountain Creek (at Pueblo) is the June

1921 flood, shown as point 8. It is slightly below the envelope curve relation.

There are three noteworthy features of the envelope curve. The first is that the nine

points that define the envelope curve all are observations that occurred east of the Front

Range - east of Pueblo, Colorado Springs and Denver. Orographics and topography appear

to play a significant role in extreme flood generation in the Colorado Front Range, and

record flood peaks have not been observed upstream of Pueblo other than the June 1921

flood. The second feature is that three storms caused the extreme floods: June 1921 (three

peaks), May 1935 (one peak), and June 1965 (six peaks). The third feature is that all of the

flood peaks that define the envelope curve are classified as being caused by general storms.

Storm classifications are further discussed in Section 4.3.

There are four limitations to the current, regional envelope: (1) adequate sampling in

space and time for known, observed events; (2) scaling issues (changes in relationships at

basins greater than 1,000 mi^2); (3) progressive regulation of flood peaks over time for these

larger basins; and (4) accuracy of the floods that define the envelope curve. Floods that are

recorded at multiple sources for the same rain-dominated flood (e.g. 1921, 1935, 1965, and

1976) limit space-for-time substitutions and potentially determining an approximate

exceedance probability (return period) for the curve. Flood peaks for observed events are sometimes not well sampled in space. There are extreme flood sampling and regulation problems for large basins. Crippen and Bue (1977, p. 13) limit their analyses to basins less than 7,000 mi^2 because "maximum floods for larger basins in this region cannot be defined from data presently available". One major problem is that the peak discharge estimates that define the envelope curves are uncertain; their accuracy is either poor, fair or unknown (Table 4.3). Matthai (1990) describes several other major problems with envelope curves, including data quality problems, partial area, and that the curve may not be representative of the geologic and climatic conditions at one's point of interest.

There is an additional, informative way to examine maximum peak discharge data in orographic regions by including elevation. A relation combining peak flows, drainage area and elevation, based on data in Jarrett (1987), England (1996), and updated through Water Year 2003, is shown in Figure 4.5. Data that control the location of the unit discharge-elevation envelope are listed in Table 4.4. This relationship shows several distinct features. The most important feature is the dramatic decrease in unit discharge with elevation. Jarrett (1987, 1990) described this very same feature in terms of the South Platte River basin; here we expand the focus to include the Arkansas River basin. The highest unit discharges are associated with very high runoff from small watersheds less than about 50 mi^2 (Table 4.4). Most of the largest events are associated with the July 1976 Big Thompson flood. The relation in Figure 4.5 supports Follansbee and Sawyer's (1948) views on extreme floods

within the Arkansas River basin upstream from Parkdale. It is also nearly identical to that

previously shown by Jarrett (1990). Recent extreme floods (including those from July 1997)

have not had higher unit discharges than those from 1976. What one can also infer from this

relationship is that extreme flooding on large watersheds that include the foothills transition

zone can be caused from partial-area runoff. Thus, one needs to carefully consider the

contributing drainage area above about 8,000 feet for these watersheds (Jarrett and Costa,

1988). Two of the largest events that occurred within the Arkansas watershed upstream from

Pueblo are shown on Figure 4.5: Orman's Gulch (point 6) and Arkansas tributary near

Parkdale (point 8). However, these points, while relatively extreme for the Colorado Front

Range, do not define the unit discharge envelope curve. The peak-flow and unit discharge

data show that topography and physiography appear to play a dominant role in extreme flood

hydrology for the Arkansas River basin upstream of Pueblo. O'Connor and Costa (2004)

concluded that topography and basin physiography were important factors in understanding

and predicting high unit discharges.

4.2.3   Seasonality and Process Relationships

Understanding flood seasonality and rainfall/snowmelt processes (mixed populations)

are crucial to predicting extreme floods in Colorado Front Range watersheds. Here we focus

on annual peak flow and annual maximum mean daily flow data sets from selected gaging

stations within the Arkansas River basin to demonstrate flood seasonality and process

relationships within the watershed upstream from Pueblo.

88
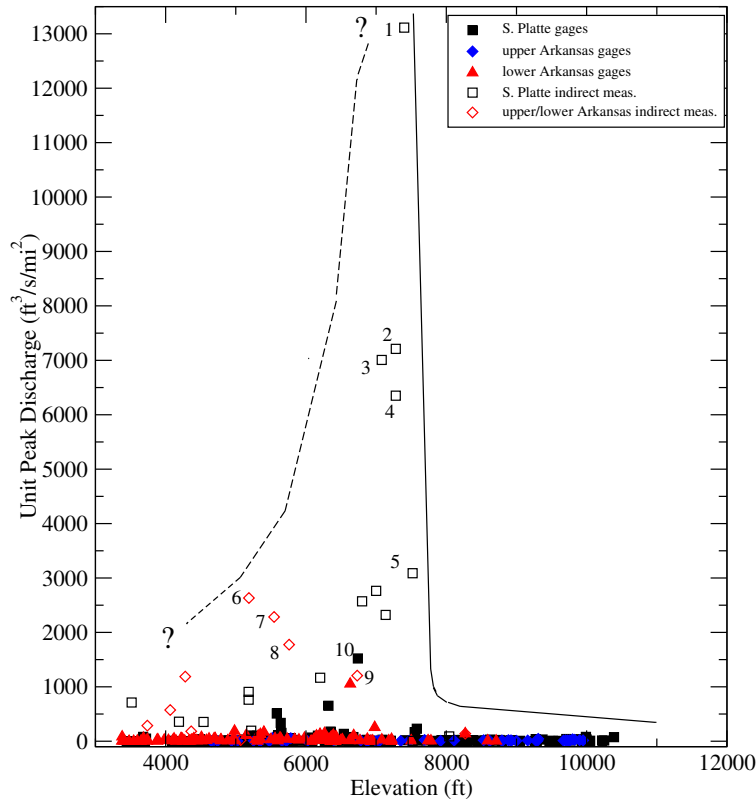
Figure 4.5. Maximum unit peak discharge data and elevation envelope curve for observations within the Arkansas and South Platte River Basins in Colorado.

Table 4.4: Largest Observed Unit Discharge Estimates that Define an Elevation-Unit Discharge Relation

Point No. (Fig. 4.5)	Station Name	Drainage Area (mi²)	Date	Peak Discharge (ft³/s)	Unit Peak (ft³/s/mi²)	Elev. (ft)	Measurement Type	Meas. Rating	Flood Type
1	Big Thompson River trib. blw. Glen Comfort	0.5	07/31/1976	6,950	13,113	7,400	SA (misc. site)	poor	thunderstorm
2	Dark Gulch at Glen Comfort	1.0	07/31/1976	7,210	7,210	7,280	SA (misc. site)	poor	thunderstorm
3	North Fork Big Thompson trib. nr. Glen Haven	1.4	07/31/1976	9,670	7,007	7,080	SA (misc. site)	poor	thunderstorm
4	Big Thompson River trib. blw. Loveland Heights	1.4	07/31/1976	8,700	6,350	7,280	SA (misc. site)	poor	thunderstorm
5	Devils Gulch nr. Glen Haven	0.9	07/31/1976	2,810	3,088	7,520	SA (misc. site)	poor	thunderstorm
6	Orman's Gulch nr. Swallows,	2.7	07/19/1965	7,000	2,632	5,187	SA (misc. site)	fair	thunderstorm
7	Jimmy Camp Creek near Fountain	54.3	06/17/1965	124,000	2,284	5,546	SA (misc. site)	fair	general storm
8	Arkansas River trib. no. 2 at Parkdale	0.2	07/27/1961	284	1,775	5,760	SA (misc. site)	good	thunderstorm
9	Molino Canyon nr. Weston	4.2	08/10/1981	5,100	1,206	6,730	culvert flow (misc. site)	poor	thunderstorm
10	Kiowa Creek at Elbert	28.6	05/30/1935	43,500	1,521	6,740	SA (gage)	unknown	general storm

Extreme floods in the Colorado Front Range typically occur from mid-April to late August. Hoyt and Langbein (1955, p. 51) present a very generalized map of flood seasons for the United States, and suggest that floods in Colorado and much of the Rocky Mountain west occur in late spring. Hirschboeck (1991, p. 84) also suggested that late spring is the typical season for which the largest flood peaks of the year occur in Colorado and much of the western United States. Doesken (1991) simply states that floods occur primarily from April through October in Colorado. The largest flood peaks in the Arkansas and South Platte River basins can be used to determine flood seasonality. Based on the data shown in Tables 4.2 through 4.4, the flood season for this region is late April through early September. General storms typically occur in late April through mid-June, snowmelt floods occur in mid-June through mid-July, and thunderstorms occur from early June through early September (Table 4.2). The most extreme floods in terms of peak discharge (Table 4.3) and unit discharge (Table 4.4) confirm this seasonality in the region.

Flood seasonality was explored using annual peak flow and maximum mean daily flow data from six gaging stations on the Arkansas River main stem: Granite, Salida, Wellsville, Parkdale, Canon City, and Pueblo (Figure 4.6). Runoff seasonality is very strong in the upper watershed from Granite to Parkdale, and limited to May through August. Monthly distributions of peak and maximum mean daily flows are unimodal, peak strongly in June, and daily and peak frequencies are nearly identical. These data indicate that snowmelt runoff processes are the dominant flood runoff mechanism in the upper watershed

90

upstream of Parkdale. There is a fairly consistent shape to the distributions from Granite to

Parkdale (site a through d). At Canon City and Pueblo, the distributions clearly change by

having more spread, and indicate the general storm rainfall-runoff process. Peaks at Canon

become relatively more frequent in July and August than at upstream sites. The peak

distribution for Pueblo is nearly uniform for June through August, and demonstrates that

there are even differences between these two lower elevation sites.

Snowmelt runoff within the basin shows a strong spatial coherence. The largest

snowmelt flood, in terms of peak discharge and volume, was the June 1957 runoff that lasted

approximately 21 days (Figure 4.7). Flow estimates are available at four locations for this

snowmelt flood: Granite, Salida, Canon City and Pueblo. The data from these locations

show that daily flows are remarkably similar at Salida, Canon City and Pueblo for the

maximum snowmelt runoff period. The data between the sites are highly correlated.

However, there is some variability and differences in runoff from Salida to Pueblo for

several days. A rainfall-runoff daily flow on May 17 at Pueblo was not observed at upstream

locations. Likewise, there are numerous small peaks on the falling limb of the snowmelt

runoff hydrograph at Pueblo that are not observed at upstream locations.

The maximum snowmelt runoff periods can also be substantially varying in shape,

volume and timing, but there is marked regularity within the basin. A recent very high

snowmelt runoff year was 1995; the record peak discharge at the Parkdale gage was

observed for this snowmelt runoff. Streamflow data for this runoff season were recorded at
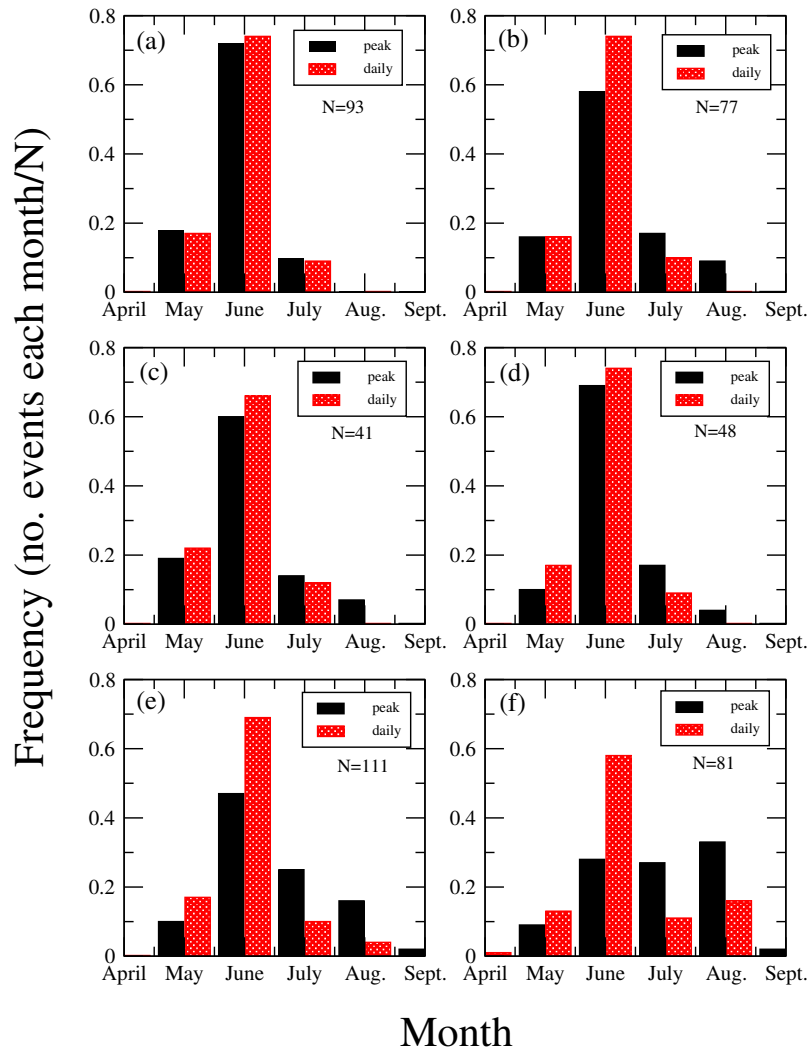
Figure 4.6. Histograms of annual peaks and 1-day maxima versus month for six locations within the Arkansas River basin upstream of Pueblo. Sites are listed from upstream (snowmelt) to downstream (general storms): (a) Granite; (b) Salida; (c) Wellsville; (d) Parkdale; (e) Canon City; and (f) Pueblo.

five locations: Granite, Wellsville, Parkdale, Canon City, and Portland (Figure 4.8). The

maximum runoff during a 30-day period was nearly the same at locations within the basin

from Wellsville to Portland. As in 1957, there is some higher variability in runoff at the

most downstream location. In late May and early June 1995, there were several days from

May 15 through about June 12 with slightly higher peaks and flows at Portland than at

upstream locations. Overall, the data for the highest snowmelt runoff periods demonstrate

that there is similar response at various locations within the watershed.
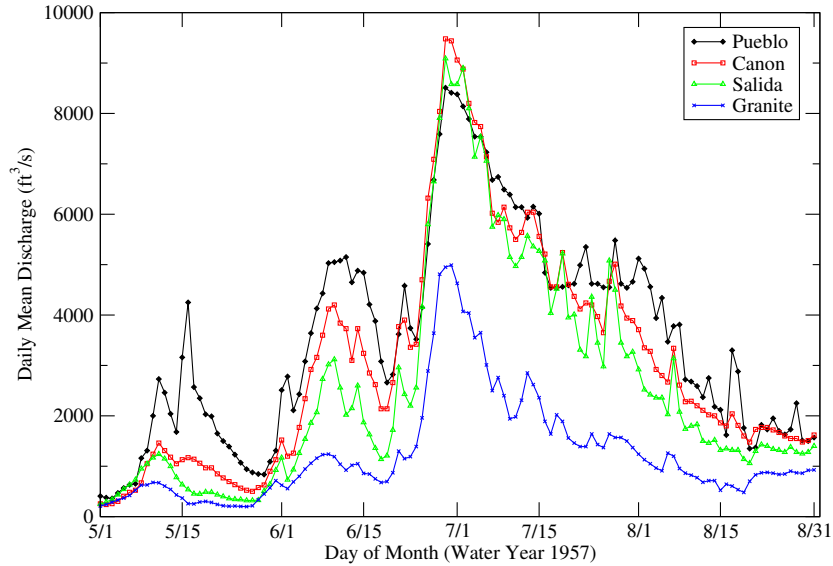
Figure 4.7. Record snowmelt flood within the Arkansas River basin during June 1957.
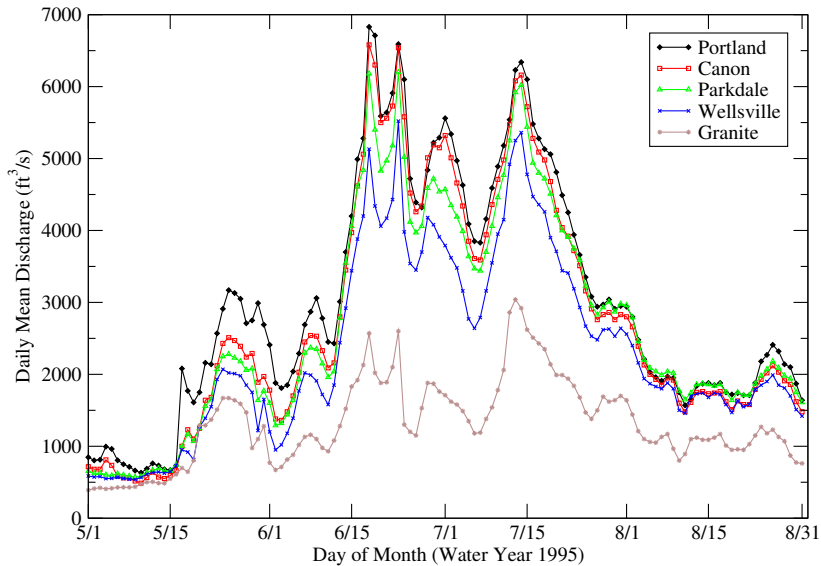
Figure 4.8. Recent snowmelt flood within the Arkansas River basin during June 1995.

In contrast to maximum snowmelt runoff, there are distinct differences in peak flow behavior within the watershed. The location of the mixed-population transition zone between snowmelt-dominant peak flows and rainfall-runoff dominant peak flows within the basin is explored with peak flow and daily flow data. It is clear that the extreme flood mechanism at Salida is snowmelt and the mechanism at Pueblo is from spring general storms and summer thunderstorms. The upper snowmelt and lower general storm flood hydrographs for these locations are shown in Figure 4.9. The flood at Salida in 1957 was the largest peak and was due to snowmelt. In contrast, the June 1921 flood at Pueblo was the largest recorded rainfall-generated flood.
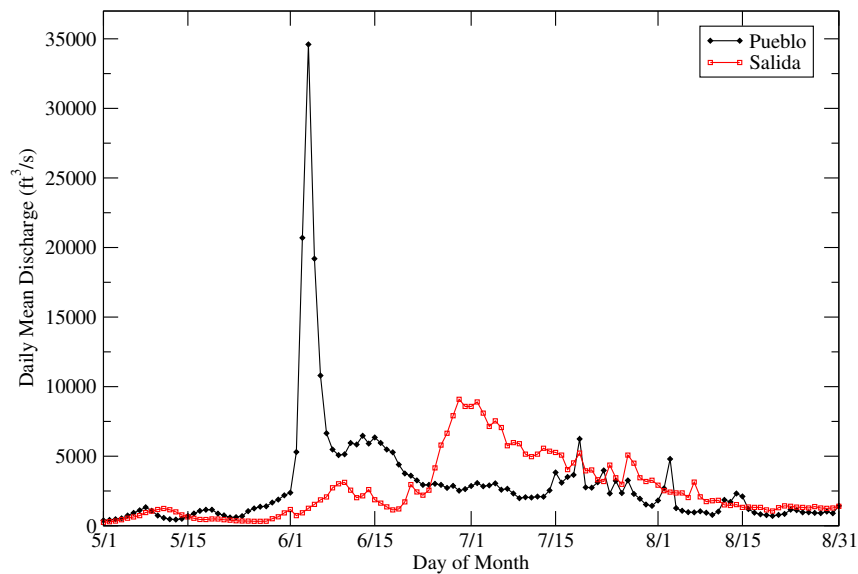
Figure 4.9. Largest recorded snowmelt (June 1957) and rainfall-generated flood (June 1921) hydrographs in the Arkansas River Basin upstream of Pueblo.

Peak-flow relationships between the gaging stations at various locations in the watershed clearly show that the transition between snowmelt-dominant runoff and rainfall

94

runoff is between Canon City and Parkdale (Figure 4.10). There is a relatively strong

relationship between Wellsville and Parkdale, indicating similar peak snowmelt runoff

behavior. The overlapping records between Salida and Canon City are the longest (77 years)

for comparison between snowmelt and snowmelt-rainfall flood peaks. These records show

that there are clear differences between snowmelt peak flows at Salida and the mixture of

snowmelt and rainfall-runoff dominant peaks at Canon City (Figure 4.10). Likewise,

overlapping records at Canon and Pueblo are relatively long (80 years). The peak-flow

comparison shows essentially no correlation between these two sites, indicating that the

largest peak flows are caused by partial-area rainstorms or storms with much higher rain

rates closer to Pueblo. The concept of flood processes can be further explored by

comparison of peak flows and maximum mean daily flows at a particular gaging station.

Typically, for snowmelt-dominant systems, peak flows are not that much larger than the

daily mean flows, and there is a strong relationship between annual peaks and maximum

mean daily flows. Relationships for Parkdale, Canon City, and Pueblo (Figure 4.11) clearly

show that there is a strong snowmelt-dominant relation at Parkdale. The snowmelt

relationship is inferred when the data depict a near-linear function between peak and

maximum one day. Weak relationships at Canon and Pueblo indicate a mixture of snowmelt

and rainfall-runoff flood processes, where there are very large peak flows compared to

maximum mean flows. There is definitely snowmelt runoff at both locations; however, at

Canon the near-linear relationship is stronger than at Pueblo.
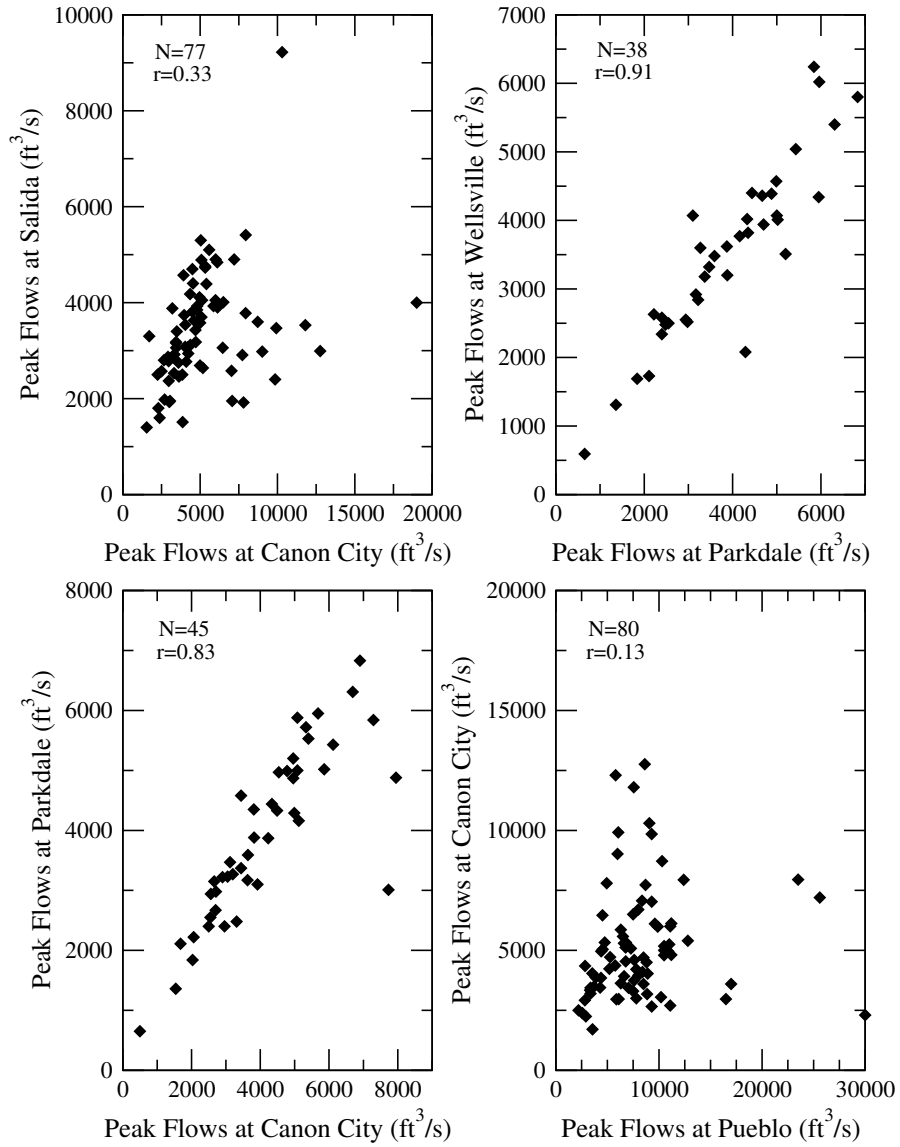
Figure 4.10. Peak-flow correlation relationships between upstream and downstream locations: Salida and Canon City; Wellsville and Parkdale; Parkdale and Canon City, and Canon City and Pueblo.
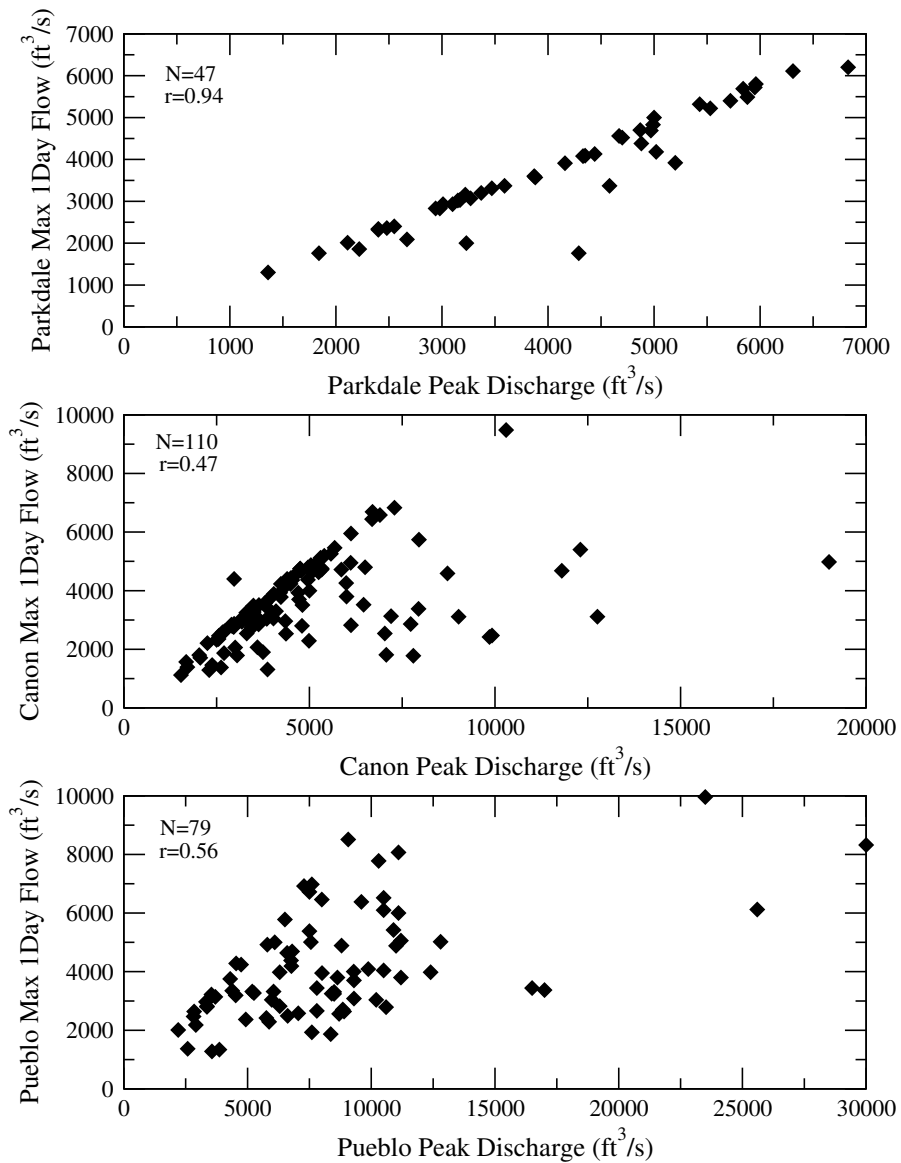
Figure 4.11. Peak discharge-maximum mean daily flow relationships at Parkdale, Canon City, and Pueblo.

4.2.4 Historical Information and Floods

Historical information is valuable to extend peak flow estimates from gaging stations

in time. Historical information is defined, for the purpose of this study, as broad categories

of data collected by humans prior to establishing systematic protocols such as streamflow and precipitation gaging stations. It generally consists of diaries, written accounts of settlements, folklore, and descriptions that may document periods where no extreme weather and/or floods have occurred. These accounts may also document historical floods. Historical floods are defined as flood events which were directly observed by humans, generally in a non-systematic manner by non-hydrologists (Baker, 1987). These events usually occurred and were described in some qualitative and/or quantitative fashion prior to the peak flow gaging station (systematic) record. Thomson et al. (1964), Gerard and Karpuk (1979) and England (1998) discuss historical data that are useful for flood frequency analysis.

Historical information is typically utilized in flood frequency analysis for three main purposes: (1) to extend the peak flow gaging station record length; (2) to provide estimates of extreme storms and floods that may have occurred prior to the establishment of gaging stations; and (3) to document potential limits on peak discharge magnitudes over time. The basic data that are needed for flood frequency include: (1) a peak discharge time series; (2) some historical period; (3) a discharge (stage) threshold for the historical period; and (4) knowledge of any floods that exceeded the discharge threshold, or that no floods exceeded the threshold. Historical information is used to estimate these last three elements. The time of people arriving in an area and establishing settlements is used as a base time to extend the extreme peak flow observation record. Likewise, human observation and documentation of large storms and floods, and development of floodplains during this period, allow one to

estimate discharge exceedance and/or nonexceedance thresholds and the number of historical floods (possibly zero) that exceeded the threshold.

Four main sources were used to document the time of human settlement, travel routes, population distribution, observations, and historical records along the upper Arkansas River in Colorado: (1) a history of Colorado (Baker and Hafen, 1927); (2) a history of Colorado and people (Hafen, 1948); (3) railroad history and development of the Denver and Rio Grande (Campbell, 1922); and (4) railroad guide of the Royal Gorge (Osterwald, 2003). The goal of reviewing information from these sources was to estimate the year to start the historical period at each gaging station site. The focus was on five locations within the Arkansas River basin where flood frequency estimates are made: Pueblo, Canon City, Parkdale, Wellsville, and Salida.

The earliest accounts of humans (other than native Americans) visiting the Arkansas River basin was in November 1806 by Zebulon Pike, who camped near the confluence of Fountain Creek and the Arkansas River (Campbell, 1922). Many people came to Colorado in search of gold and silver. The town of Fountain City (site of Pueblo) was begun in November 1858 (Baker and Hafen, 1927; Hafen, 1948). Gold was soon discovered in South Park and on the Blue River, and Canon City and Colorado City were formed in 1859 (Hafen, 1948). In the same year (1859), Pueblo expanded and the village consisted of some thirty cabins in June (Hafen, 1948). Most of the cities and towns along the Arkansas River valley were settled and subsequently grew in response to mining and railroads. The Canon City

Times, the first newspaper in Canon City, was established on September 8, 1860, and the

town had a population of 800 with 40 business houses (Hafen, 1948). By 1868 Canon City

had achieved some prominence and the state penitentiary was located there (Campbell,

1922). The Denver and Rio Grande Railroad completed its line to Leadville in 1880; the

towns that grew up along the line to the south of Leadville were Salida in 1880 and Buena

Vista in 1879 (Baker and Hafen, 1927). The largest town in the mountains west of Canon

City is Salida; it was settled in 1880 at the time the railroad was built up the Arkansas valley

(Campbell, 1922).

Historical information within the Arkansas River basin, which includes large floods

outside the streamflow gaging station period of record, helps to extend the record length, and

place extreme floods within the record in their proper context. A longer record provides

more assurance for peak discharge probability model selection and reduced variance of

estimated extreme flood quantiles. In addition to the historical sources listed above, data and

information were gathered that documents the positive evidence of historical (pre-gaging

station) flooding, and periods of no flooding, in the upper Arkansas River basin upstream

from Pueblo, Colorado. The major sources of historical flood information and data used in

this research were obtained from Follansbee and Jones (1922), Munn and Savage (1922),

Follansbee and Sawyer (1948), Patterson (1964), and Crowfoot et al. (2004).

The historical information and data indicate large floods might have occurred in the

Upper Arkansas River basin in the vicinity of the city of Pueblo in water years 1826, 1864,

1884, 1889, 1893, 1894 and 1921 (Follansbee and Jones, 1922; Follansbee and Sawyer,

1948; Hafen, 1948). The most disastrous flood in the Upper Arkansas was the Pueblo flood

of June 1921 (Hafen, 1948; Follansbee and Sawyer, 1948). However, there is only sufficient

quantitative information to determine approximate magnitudes for the 1864, 1893, 1894 and

1921 flood peaks. Based on the information in these reports, the start of the historical period

and the historical flood years with quantitative estimates at each site are summarized in Table

4.5. Estimates for these floods are discussed in Chapter 5.

Table 4.5: Historical Record Start Date and Floods at Select Locations Within the Arkansas River Basin

Flood Frequency Site	Start of Historical Record	Historical Flood Years (Outside Gage Record)	Source(s)
Arkansas River near Pueblo	1859	(1864), (1893), (1894) June 1921	Campbell (1922); Follansbee and Jones (1922); Baker and Hafen (1927); Hafen (1948)
Arkansas River at Canon City	1868	August 1921	Campbell (1922); Baker and Hafen (1927); Hafen (1948)
Arkansas River at Parkdale	1868	---	Campbell (1922); Baker and Hafen (1927); Hafen (1948)
Arkansas River near Wellsville	1880	---	Campbell (1922); (Baker and Hafen, 1927)
Arkansas River at Salida	1880	1957	Campbell (1922); (Baker and Hafen, 1927); Crowfoot et al. (2004)

4.3   REGIONAL EXTREME STORMS AND HYDROMETEOROLOGY

The precipitation source for the Arkansas River basin and vicinity is predominantly

Gulf of Mexico and subtropical Atlantic moisture from the southeast, and some Pacific

moisture from the west for the headwaters (Doesken, 1991). The majority of precipitation

falls as snow during the winter months. The snowmelt period is typically during the months

of May and June, with little snowpack remaining in the basin in the summer months. Two

major precipitation patterns affect the Arkansas River watershed in spring and summer and can result in significant rainfalls and large floods. From March through June, midlatitude systems cross the region, strengthen on the leeward side of the Rockies and draw moisture into eastern Colorado. This moisture and increased convective activity result in periodic, widespread rainfall and occasionally severe thunderstorms eat of the mountains (Doesken, 1991). Subtropical moisture from the Atlantic drifts northward to eastern Colorado starting in early July. This monsoon moisture peaks near the beginning of August, then gradually weakens and moves out of the region in late summer. The monsoon is responsible for the frequent summer thunderstorms in the southern Rocky Mountains.

4.3.1   Extreme Storm Database

An electronic database of extreme storms and pertinent characteristics was developed from existing data sets. The database was developed to provide quantitative estimates of extreme storm rainfall in space and time for estimating extreme storm probabilities (Chapter 6) and subsequent runoff modeling (Chapter 7). Two main sources of extreme storm data were used to develop the database. The first is depth-area duration (DAD) data from the Corps of Engineers storm catalog (USACE, 1945-) and Bureau of Reclamation cooperative storm studies. The DAD data are used nearly exclusively in developing regionalized hydrometeorological reports that provide Probable Maximum Precipitation (PMP) estimates (e.g., Hansen et al., 1988). The second source is a recently developed extreme storm catalog for Colorado (McKee and Doesken, 1997).

An initial geographic region was used to select storms from the DAD catalog for consideration in developing extreme storm probability estimates. This region covers the United States from the Canada to Mexico borders, and between about longitude 99° and the Continental Divide. This region is nearly the same as that used by Hansen et al. (1988). About 110 storms with some DAD data (not all complete) are located in the region. Most of these storms correspond to the "major" and "supplemental" storms listed in Hansen et al. (1988). An electronic database was developed of these 110 storms and includes the following components: DAD data; storm start and end dates; assignment number; total duration; maximum center location (nearest town and state); latitude and longitude of storm center; storm period; and storm start and end times. The DAD data are given for specific durations (typically six-hour increments) and area sizes. An example of a portion of DAD data for a storm is shown in Table 4.6. The storm orientation and major-to-minor axis ratio were estimated from the DAD summary for each of the 110 storms and included in the database.

Table 4.6: Example depth-area duration data table

Area (mi^2)	Rainfall Depth (in) for Duration (hours)				
	6	12	18	24	30
10	10.4	11.3	12.0	12.0	12.0
100	8.8	10.4	11.0	11.1	11.1
200	7.9	9.7	10.3	10.4	10.4
500	6.5	8.4	9.0	9.1	9.1
1,000	5.4	7.1	7.8	7.8	7.8
2,000	4.2	5.4	6.1	6.2	6.2

The Colorado Climate Center (CCC) storm catalog (McKee and Doesken, 1997) is a

listing of 328 storms in the Rocky Mountain region, including 14 states in the intermountain west and Great Plains. It consists of a simple table with the following elements: storm number; storm name; state; storm date; region; storm type; latitude and longitude of storm center; maximum precipitation; remarks; and notes if there are Reclamation storm files and DAD studies available. The CCC catalog is a comprehensive index to storms in Colorado and parts of the Rocky Mountain region. It is used to define the most important extreme storms that should be considered in the Colorado Front Range. However, it has limited utility as there are no detailed, quantitative storm data with depths, durations, areal distributions, etc. available for each storm. Summaries do exist for all the storms, and the information in the CCC files for each storm is of varying quality. The most useful information is for extending the DAD storm catalog by determining locations of extreme storms, seasonality, approximate frequency of storm center locations, and approximate duration. The July 1997 Fort Collins (Doesken and McKee, 1998) and July 1997 Pawnee Creek (Doesken, 1998) storms were included in the electronic database after manual processing of isohyet maps to DAD tables.

A review of the combined USACE/Reclamation DAD and CCC extreme storm catalog for the Colorado and Rocky Mountain region indicates that there are several observed, extreme flood-producing rainstorms in the lower elevation portions of the study watershed. There are 23 storms with DAD data and 154 storms from the CCC catalog that have been observed within Colorado east of the Continental Divide (Figure 4.12). The

104

majority of observed Colorado Front Range flood-producing storms are shorter duration

(generally less than 24 hours), high-intensity convective (cloudburst) events. In some cases

these are embedded in longer-duration storms that produce somewhat heavy rainfall over

several days. Large magnitude rainfall from these storms is typically limited in areal extent,

from tens to several hundreds of square kilometers. There is a lack of evidence of longer

duration, cyclonic storms that cause flooding in the Colorado Front Range, especially at

higher elevations (above about El. 7,500 ft). Based on an examination of regional rainfall

and streamflow records, Jarrett (1987, 1993) hypothesized that an elevation limit exists for

extreme floods caused predominately by rainfall in this region. The elevation limits are

approximately between 7,500 ft (2,290 m) and 8,000 ft (2,440 m) in the South Platte and

Arkansas River basins. However, Jarrett (1987) recommended that further work was needed

to document physical evidence of flooding (or lack of flooding) in the Arkansas River basin.

There are few observed flood-producing storms in the Upper Arkansas headwaters region

upstream of Wellsville (Figure 4.12); storm and streamflow data indicate that these storms

are very localized and cover small areas (several kilometers). The largest flood-producing

storm that occurred within the watershed is the June 1921 "Penrose" storm. The second-

largest storm and flood was the May 1894 "Ward District" storm. Other storms within the

region are also considered for transposition.

In order to estimate extreme storm and flood probabilities for the Arkansas River

basin above Pueblo, storm transposition is used in order to increase the data base for
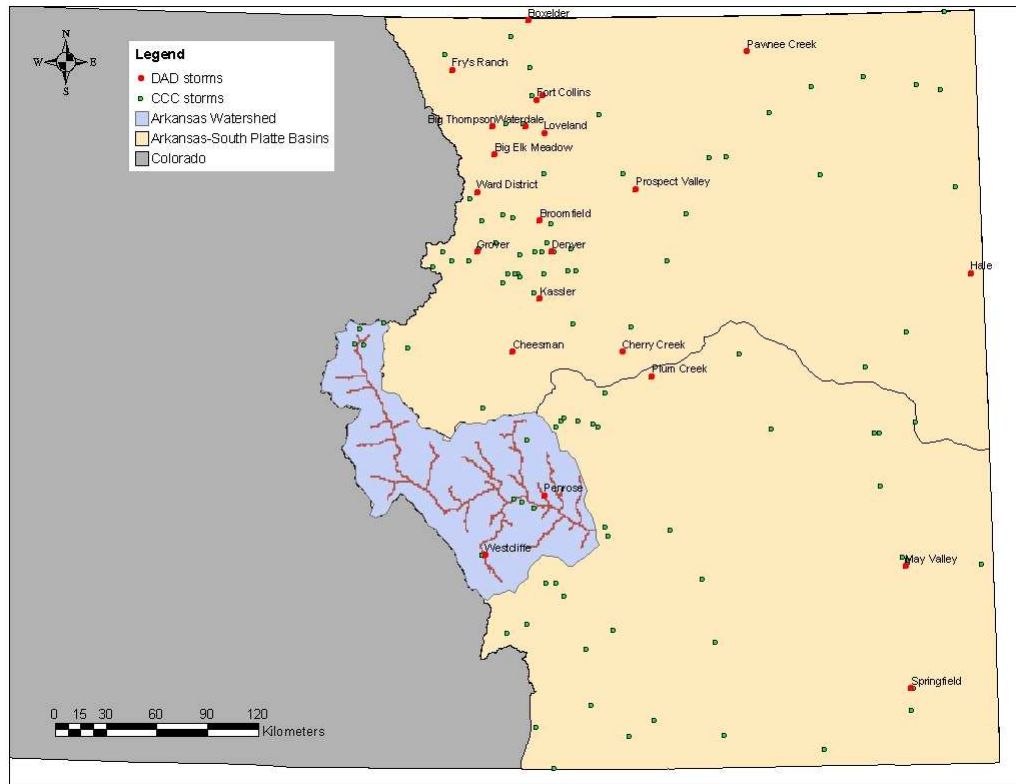
Figure 4.12. Locations of extreme storms near the Arkansas River watershed from the CCC catalog (green dots) and those from the DAD database (labeled red dots).

probability estimation. From the DAD catalog, 77 storms are considered for analysis. These storms were chosen using the Continental Divide to 103rd Meridian (CD-103) geographic region (Hansen et al., 1988) within the United States, and also included the April 1900 Springfield storm, the October 1908 May Valley storm, and the May 1935 Hale storm centered in eastern Colorado. In addition to these 77 storms, 33 supplemental storms located between about the 103rd and 98th meridian are also examined. McKee and Doesken (1997) describe a recommended final list of thirty-six storms for consideration in investigating extreme rainfall potential in the Rocky Mountain region of Colorado. Six of these storms occurred in the Arkansas and South Platte River basins and have available DAD data. A

106

final subset of 40 storms was closely examined and considered for stochastic storm

transposition (Table 4.7).

Table 4.7: Extreme Storms from DAD Catalog Considered for Transposition to Pueblo Watershed

Date	Assignment No.	Location	State	Duration (hours)	Orientation (degrees)	total 10mi^2 depth	max 24hr 10mi^2 depth	areal extent mi^2
05/30/1935	MR 3-28A	Cherry Creek	CO	24	47	22.20	22.20	6,300
09/20/1941	GM 5-19	McColleum Ranch	NM	78	16	21.20	12.10	38,000
05/30/1935	MR 3-28AZoneA	Hale	CO	24	32	21.20	21.20	1,291
05/04/1969	19690504bemCO	Big Elk Meadow	CO	96	14	18.21	11.83	5,000
06/13/1965	SW 3-23	Plum Creek	CO	181	5	18.10	13.20	39,266
09/27/1923	MR 4-23	Savageton	WY	108	46	16.90	9.50	95,000
06/06/1964	NP 2-23	Gibson Dam	MT	36	141	16.40	14.90	12,096
06/17/1921	MR 4-21	Springbrook	MT	108	38	15.10	13.30	52,600
06/09/1972	MR 10-12	Rapid City	SD	12		14.90		2,000
07/29/1997	19970729pawCO	Pawnee Creek	CO	24	65	14.00	12.00	1,070
06/06/1906	MR 5-13	Warrick	MT	54	90	13.30	10.20	40,000
07/21/1905	GM 3-13	Elk	NM	108	80	13.10	5.70	44,000
06/12/1949	R7-2-5	Prospect Valley	CO	36	63	13.00	9.10	360
06/02/1921	SW 1-23	Penrose	CO	114	0	12.00	12.00	1,000
07/27/1997	19970727ftcCO	Fort Collins	CO	32	0	12.00	10.00	1,000
07/31/1976	19760731bgtCO	Big Thompson	CO	4	25	11.70		50
08/30/1938	MR 5-8	Loveland	CO	126	42	10.60	7.00	21,500
06/01/1953	19530601bltMT	Belt	MT	48		10.40	8.60	14,000
05/20/1941	GM 5-18	Prairieview	NM	108	5	10.00	6.50	44,000
10/09/1930	SW 2-6	Porter	NM	60	26	9.90	9.90	27,700
07/19/1915	SW 1-18	Tajique	NM	240	26	9.90	5.20	95,000
04/29/1914	SW 1-16	Clayton	NM	66	22	9.60	9.00	36,500
09/15/1919	GM 5-15B	Meek	NM	54	25	9.50	7.40	75,000
06/17/1947	MR 7-16	Gering	NE	10	156	9.40		220
08/30/1938	R4-1-23	Waterdale	CO	108	35	9.20	8.50	57,000
06/19/1916	R6-1-8	Sun River Canyon	MT	66	106	8.90	6.20	10,000
06/16/1948	19480616dprMT	Dupuyer	MT	48		8.80		2,275
05/29/1894	MR 6-14	Ward District	CO	60	165	8.50	5.60	25,300
08/29/1942	SW 2-29	Rancho Grande	NM	84	12	8.00	7.90	35,600
06/03/1908	MR 5-15	Evans	MT	72	42	8.00	6.50	20,000
06/06/1913	SW 1-14	Fort Union	NM	132	161	7.90	5.10	23,000
09/26/1904	SW 1-6	Rociada	NM	90	29	7.90	6.60	70,000
05/26/1937	GM 5-17	Ragland	NM	84	69	7.80	4.40	37,000
05/30/1948	MR 7-18	Fort Collins	CO	8	73	7.80		83
09/03/1911	MR 5-18	Knobles Ranch	MT	72	36	7.60	3.70	37,000
09/27/1941	SW 3-1	Tularosa	NM	48	49	7.50	5.70	66,700
04/14/1921	MR 4-19	Fry's Ranch	CO	42	167	7.50	7.30	9,200
06/01/1915	MR 5-21	Adel	MT	108	33	6.70	3.60	12,800
08/06/1929	SW 2-27	Valmora	NM	144	37	6.60	4.60	49,000
04/22/1900	MR 5-10	Big Timber	MT	60	0	6.60	3.80	30,000

4.3.2   <u>Radar Data and Flood Zones</u>

Radar data are a good source for understanding and modeling precipitation over large

watersheds in space and time. The NWS WSR 88D radar data from Pueblo (KPUX) were

used by Javier et al. (2004, 2005) to examine space-time storm rainfall properties in the

Arkansas River basin. Here, I utilize their work to document storm rainfall with elevation.

There are several quality issues with ground rainfall estimates in orographic regions within

the western United States from WSR 88D radar data (e.g. NRC, 2005). These typically

include beam blockage, degradation of the signal with distance from the radar, and

calibration of the rainfall-reflectivity (Z-R) relationship. However, the radar data are

extremely valuable for two purposes: estimation of storm rainfall in space (areal extent,

coverage, coherence, spatial correlation); and estimates of rainfall depth with time at all

locations in space. From these data, one can determine nondimensional depth-duration

curves, and the storm spatial structure, regardless of magnitude. It is very difficult to obtain

this information based on raingage networks as the network coverage in the western United

States is fairly sparse, and does not capture orographic effects particularly well. Radar data

from the NWS KPUX radar in Pueblo were processed by Princeton University. Javier et al.

(2004, 2005) described the methods used in developing a radar-based catalog of sixty-six

storms based on data from 1995 through 2003 from the KPUX radar. The radar data were

used to derive 5-minute rain rates at a spatial resolution of 1 km^2 for each event, over a 200

km by 200 km area. The storm events from the radar data are for the warm season during

months June, July and August. Based on aggregate properties of the sixty-six events, storm

activity is high along the Front Range, especially at the base of Pikes Peak, and the area

between Pueblo and Canon City (Figure 4.13). There is very little extreme storm activity in

the watershed upstream of Wellsville, and at higher elevations (Figure 4.14). Accumulated

precipitation from the 66 events also shows a strong decrease with increasing elevation

(Figure 4.15). These results suggest that restrictions should be placed on storm center

location and on storm areal extent in modeling. Stochastic storm transposition and storm

modeling (Chapter 6) incorporate these observations.
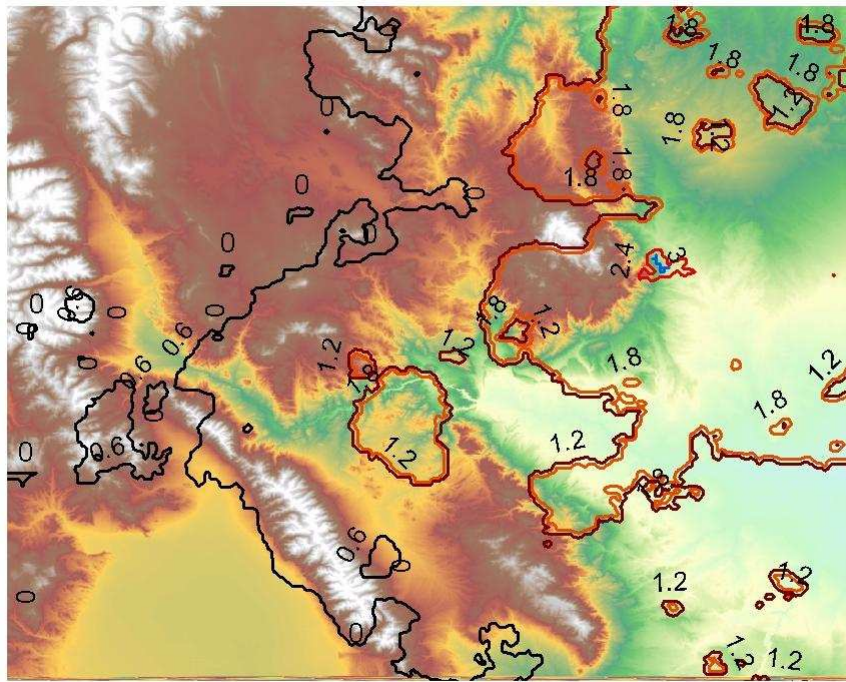
Figure 4.13. Geographical distribution of storm activity (percent) of the sixty-six storms events from 1995-2003 based on KPUX radar (Javier et al., 2005).
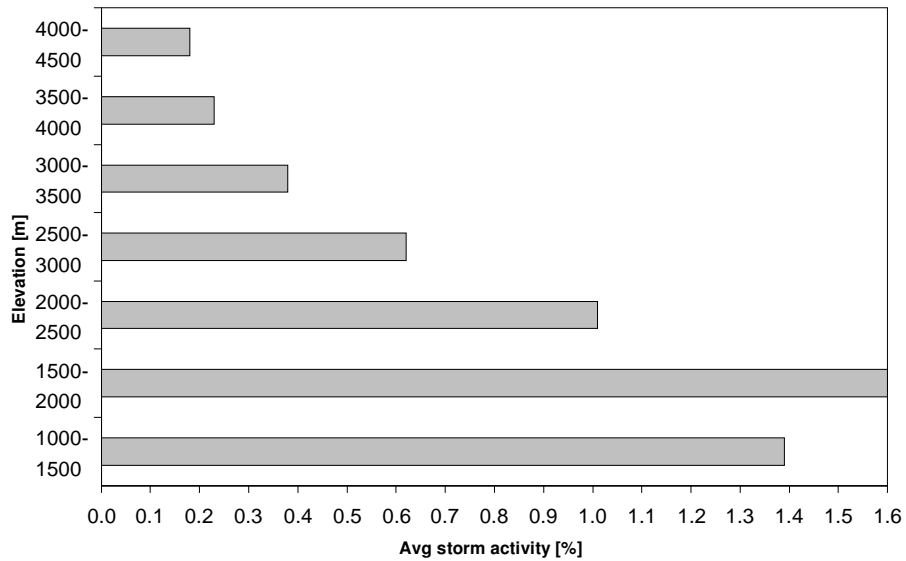
Figure 4.14. Storm activity (percent) as a function of elevation of the sixty-six storms events from 1995-2003 based on KPUX radar (Javier et al., 2005).
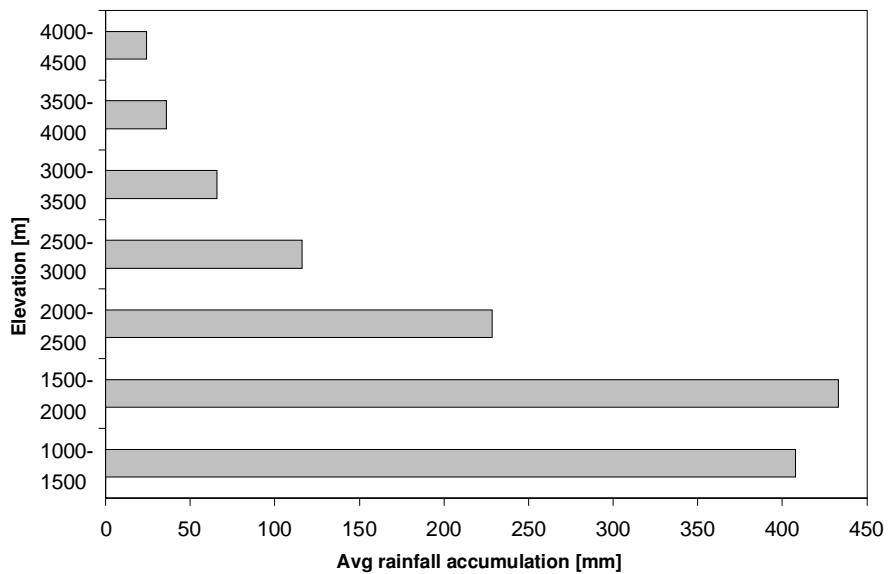
Figure 4.15. Storm accumulations as a function of elevation of the sixty-six storms events from 1995-2003 based on KPUX radar (Javier et al., 2005).

Based on streamflow data analyses, the storm database, and radar data, an estimate of the extreme flood zones for rainfall, transition (rainfall to snowmelt) and snowmelt for the Arkansas River basin is shown in Figure 4.16. The zones integrate the effects of drainage area, river network, elevation, streamflow, storm rainfall and radar information.

110
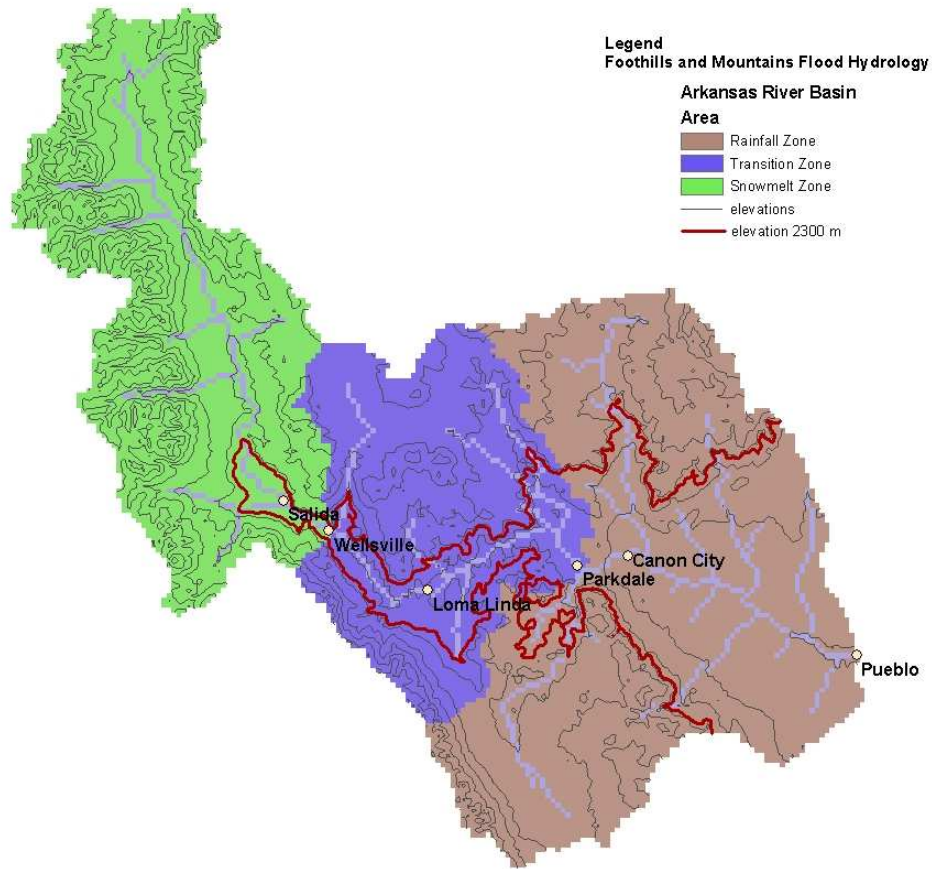
Figure 4.16. Estimated extreme flood zones in the Arkansas River basin.

4.4   SUMMARY

This chapter presented streamflow and storm data within the Arkansas River basin and surrounding region. Analysis of streamflow records revealed several important features that reflect the physical hydrology of this watershed. A database of storm rainfall was developed for modeling extreme storms; it included DAD data and storm properties to implement the elliptical storm model presented in Chapter 3.

The largest peak flows in the region resulted from three extreme storms: June 1921, June 1965 and July 1976. There appears to be a very clear break in scaling relationships

between peak flows and drainage areas at scales larger than about 1,000 mi^2 (Figure 4.4). It

is inferred that this change in relationship is due to partial-area storms in orographic areas.

Extreme storms and radar data suggest the partial-area storm concept is valid. Peak flow,

mean daily flow and hydrograph analyses clearly demonstrate mixed-population rainfall-

runoff and snowmelt runoff areas within the Arkansas River watershed. Peak flow

magnitudes within the basin are dramatically reduced with elevation (Figure 4.5), supporting

Jarrett's (1987, 1993) elevation limit hypothesis.

Streamflow records were analyzed for seasonality and correlations between locations

in the basin. Snowmelt runoff shows a strong spatial coherence, as demonstrated by the

largest snowmelt runoff hydrographs in June 1957 and June 1995. The upper watershed

upstream of Parkdale has maximum peaks and daily flows in May and June. A transition in

monthly peak distributions is observed between Parkdale and Canon City. Upstream of

Parkdale, snowmelt runoff is the dominant streamflow mechanism and the cause of the

largest peaks. Downstream of Parkdale, peaks and maximum mean daily flows are caused

by large rainfall-runoff events, and sometimes snowmelt runoff. The maximum flows

usually occur in June through August (Figure 4.6). Peak-flow and mean daily flow

correlations support the transition between snowmelt runoff upstream of Canon City and

rainfall-caused large floods in the lower portion of the watershed. Peak flows in the upper

snowmelt-dominant basin are highly correlated; peaks in the lower watershed between

Canon City and Pueblo are essentially uncorrelated.

Chapter V

FLOOD FREQUENCY ANALYSIS WITH PALEOFLOOD DATA

This chapter describes peak discharge frequency analysis at sites within the Arkansas

River Basin. A moments-based 3-parameter flood frequency model (Cohn et al., 1997) was

used to conduct at-site peak discharge frequency analysis. This model and methods for

comparing frequency curves in a regional frequency context are briefly presented. Peak

discharge, historical and paleoflood data used in the frequency analysis at each site are

summarized. The frequency analysis results for each site are discussed. Regional frequency

analysis results are then presented. These frequency curves are later used as a basis to

compare frequency curves from the TREX rainfall-runoff model.

Paleoflood investigations and peak discharge probability estimates were made at four

main sites within the Arkansas River basin: the Arkansas River at Pueblo State Park near

Pueblo; the Arkansas River at Parkdale; the Arkansas River at Wellsville (Loma Linda); and

the Arkansas River at Salida (Figure 5.1). Paleoflood peak discharge estimates, and

estimates of paleohydrologic bounds, were combined with available historical information

and peak discharge estimates from gaging stations at these sites. Peak discharge estimates

from several gaging stations were combined, where appropriate, to obtain longer records. At

selected locations, peak discharge estimates from gaging stations were deliberately censored. The peak-flow data and uncertainties used in peak discharge frequency analysis at each site are summarized below. Soils stratigraphy, age estimates, and hydraulic modeling associated with paleofloods and paleohydrologic bounds are described in detail in Klawon et al. (2005).
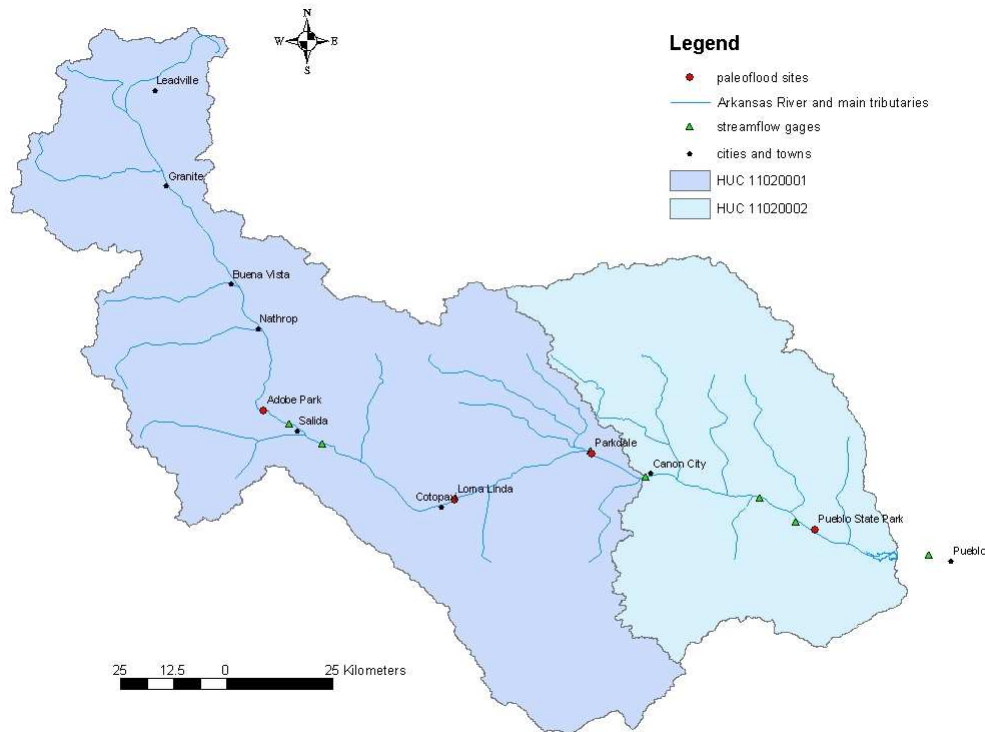
Figure 5.1. Locations of four paleoflood study sites within the Arkansas River basin.

The flood frequency results for each site are presented immediately following the data at each site. The major goal of the flood frequency analysis is to develop probability relationships directly from historical, streamflow gage and paleoflood data. These relationships are then used as a basis for comparing TREX rainfall-runoff model flood frequency curves. In this way, the paleoflood data are used as an independent check on the rainfall-runoff model.

5.1   FLOOD FREQUENCY METHODS

Two flood frequency methods are used in this research: at-site flood frequency and

regional flood frequency.

Peak-flow frequency estimates were made for annual instantaneous peak discharge

estimates. Peak discharge probabilities are estimated directly from the data using Cunnane's

plotting position with the threshold-exceedance formula (Stedinger et al., 1993) that includes

historical and paleoflood data. The data were assumed to follow a log-Pearson Type III (LP-

III) distribution. The method of moments was used to estimate the LP-III parameters for

peak discharge estimates using Expected Moments Algorithm (EMA) techniques (Cohn et

al., 1997; England, 1999). EMA (Cohn et al., 1997, 2001; England et al., 2003a) is a new

moments-based parameter estimation procedure that was designed to incorporate many

different types of systematic, historical, and paleoflood data into flood frequency analysis.

EMA assumes the LP-III distribution is the true distribution for floods. EMA was designed

to handle the four different classes of historical and paleoflood data beyond the applicability

of the Bulletin 17B historical weighting procedure (IAWCD, 1982). As noted by Cohn et al.

(1997, 2001) and England (1998), EMA is philosophically consistent with, and is an

improvement to, the Bulletin 17B method of moments procedure when one has historical or

paleoflood information. EMA is specifically designed to use historical and paleoflood data,

in addition to annual peak flows from gaging stations, in a manner similar to Maximum

Likelihood Estimators (Lane and Cohn, 1996). It is a more logical and efficient way to use

historical and paleoflood data than the current Bulletin 17B historical method, and it is a natural extension to the moments-based framework of Bulletin 17B. Confidence intervals were estimated using the approach in Cohn et al. (2001). Because the record length was long, no regional skew weighting was performed. An at-site estimate of the station skewness coefficient was used in the analysis. EMA has been rigorously peer reviewed in the literature (Cohn et al., 1997, 2001; England et al., 2003a, 2003b) and provides a suitable flood frequency model. EMA has been applied at many sites for peak-flow frequency (England et al., 2003b).

A simplified regional frequency analysis was conducted for the four sites with paleoflood data, using the index flood method (Stedinger et al., 1993; Hosking and Wallis, 1997). The regional frequency analysis was conducted to compare the distributions from each site for "consistency" in a qualitative sense. The goal was to determine if the estimated frequency curve for the Arkansas River immediately upstream of Pueblo was similar to frequency curves from the other three sites. Similarity in the frequency curve at Pueblo, to those from other sites, would provide additional confidence in estimating extreme flood probabilities at Pueblo Dam. Differences between the frequency curves could clearly highlight mixed-population flood effects within the basin. A regional distribution, based on the frequency curves and data from the four sites, was not estimated. Following Smith (1989), the preferred peak discharge frequency curve at each site was non-dimensionalized using the at-site 0.10 exceedance probability (10-year flood). This estimate was made from

the LP-III model frequency curve at each site that included gage data, historical and

paleoflood peak flow estimates.

5.2   PALEOFLOOD DATA IN THE ARKANSAS RIVER BASIN

        A paleoflood study of the Upper Arkansas River Basin was conducted at four detailed

sites to characterize paleofloods and non-exceedance bounds for application to Pueblo Dam

(Klawon et al., 2005). Two types of paleoflood information were investigated: individual

paleofloods and paleohydrologic bounds. A paleohydrologic bound (non-exceedance bound)

is a time interval during which a given discharge has not been exceeded (Levish, 2002). The

sites were strategically selected to provide information about hydrologic conditions at

various locations in the basin. Of most importance was to characterize flood hazards both

upstream and downstream of the Royal Gorge, where there appears to be a transition from

snowmelt-dominated to rainfall-dominated floods. Suitable sites were found and studied in

Adobe Park, the Loma Linda recreation area, Parkdale, and Pueblo State Park. Nine

soil/stratigraphic descriptions and seven radiocarbon dates of key deposits were used in

conjunction with geomorphic mapping and HEC-RAS flow modeling to determine age

estimates of each soil and peak discharges required to inundate the surfaces (Klawon et al.,

2005). Paleofloods and paleohydrologic bound estimates are summarized in Table 5.1. With

the exception of Adobe Park, non-exceedance bounds for similar age surfaces appear to

increase in the downstream direction and change markedly between Loma Linda and Pueblo

State Park from approximately 14,000 ft^3/s to 150,000 ft^3/s for Holocene alluvium between

the ages of 700 and 2000 years. Complete details of the paleoflood data, including soil

stratigraphy, macrofloral analysis, radiocarbon ages, and hydraulic modeling are presented in

Klawon et al. (2005).

Table 5.1: Summary of paleofloods and paleohydrologic bounds, Upper Arkansas River basin

Location	Stratigraphic Site Name	Type of Estimate	Age Range (years BP)	Age Range (years before 2004)	Mean Age	Peak Discharge Range (ft^3/s)	Preferred Peak Discharge (ft^3/s)
Pueblo State Park	AR9	non-exceedance bound	730-840	780-890	840	130,000-160,000	150,000
Parkdale	AR5	paleoflood	historical (ca. 1921 or post 1870)	historical (ca. 1921 or post 1870)		18,000-22,000	20,000
	AR3, AR4	non-exceedance bound	1,100-1,300	1,150-1,350	1250	24,000-34,000	30,000
Loma Linda	AR7	non-exceedance bound	700-2,200	750-2,250	1500	13,000-18,000	14,000
	AR6	non-exceedance bound	10,000-14,000	10,000-14,000	10000	50,000-60,000	50,000
Adobe Park	AR8	non-exceedance bound	400-600	450-650	550	17,000-27,000	20,000

5.3   ARKANSAS RIVER AT PUEBLO STATE PARK

Peak discharge estimates on the Arkansas River at Pueblo State Park are combined

from three gaging stations (Table 5.2). It was assumed that peak discharge estimates from

these gages were unaffected by upstream regulation. The total combined gage record length,

excluding historical data, is 110 years (1895-2004). There are no significant tributaries

between the stations. Although there are slight differences in drainage areas between the

three sites, no adjustments were made to transfer the records to upstream of Pueblo

Reservoir.

Based on reviews of available historical information (Chapter 4), including

Follansbee and Jones (1922), Munn and Savage (1922), and Follansbee and Sawyer (1948)

(among others), there is a substantial amount of historical flood information on the Arkansas

River in Pueblo that was usable for frequency analysis. The historical record was estimated

to begin in 1859, resulting in a 146-year period (1859-2004). The criteria for inclusion of

historical floods in frequency analysis were: the ability to rank the floods relative to the June

1921 event; and to estimate magnitudes for the individual floods. Three historical floods

were included: June 1864, July 1893, and May 1894. The magnitudes of these floods were

large relative to the floods in the gaging record; estimates within a range were based on

Follansbee and Sawyer (1948) and included in the flood frequency analysis. These estimates

in general all have relatively large uncertainties as compared to the smaller floods in the gage

record (Figure 5.2).

Table 5.2: Peak discharge records from the Arkansas River near Pueblo State Park that are used for frequency analysis

USGS Gaging Station No.	Station Name	Drainage Area (mi²)	Period of Record (Water Year)	Records Used for Frequency Analysis (Water Year)	Maximum Discharge (ft³/s) and Date
07097000	Arkansas River at Portland, CO	4,024	1939 - 2002	1975 - 1976	21,100; 06/05/1949
07099200	Arkansas River near Portland, CO	4,280	1965 - 1974	1974	23,900; 08/21/1965
07099500	Arkansas River near Pueblo, CO	4,686	1895 - 1975	1895 - 1973	103,000; 06/03/1921

A paleohydrologic bound of about 840 years was estimated at this site (Table 5.1) for

inclusion in the flood frequency curve. The estimate is based on three soils pits, two

radiocarbon ages, and hydraulic modeling of a 7,500 foot reach (Klawon et al., 2005). No

estimates of individual paleofloods were made at this site, due to the relatively wide channel

geometry and the lack of apparent stratigraphic evidence of large paleofloods during the

limited field study. A time series plot of the peak discharge, historical flood and

paleohydrologic bound data is shown in Figure 5.2.
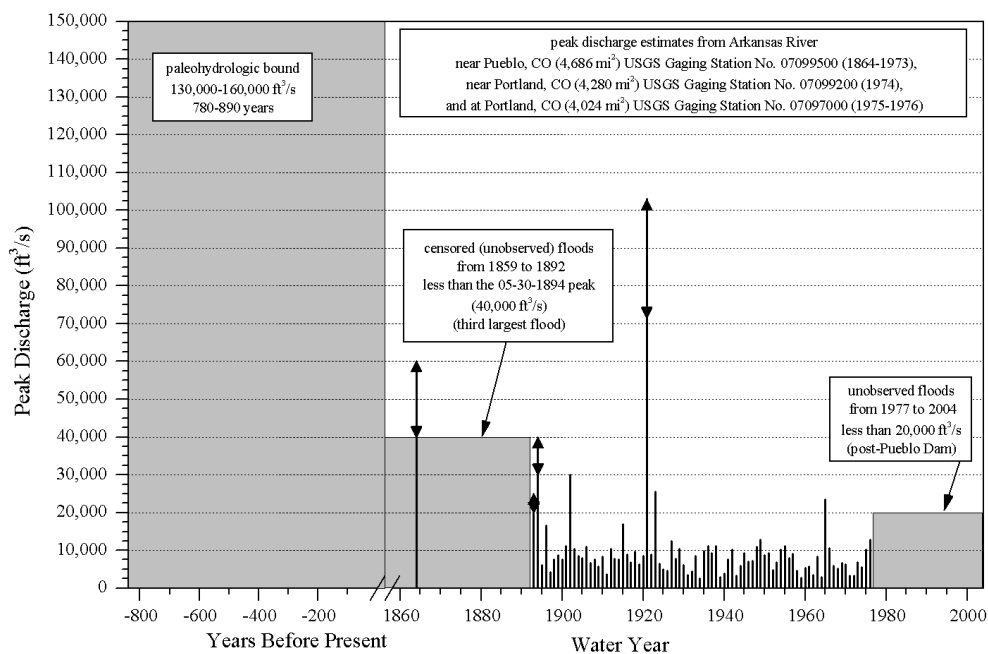
Figure 5.2. Approximate unregulated peak discharge, historical and paleoflood estimates, Arkansas River at Pueblo Dam. A scale break is used to separate the gage and historical data from the longer paleoflood record. Arrows on the 1864, 1893, 1894 and 1921 floods indicate floods in a range.

The flood frequency results are shown in Figure 5.3 and Table 5.3. Peak discharge

estimates from the gage are shown as open squares with estimated data uncertainty for some

of the largest floods that were described in a range. One can observe the large positive skew

(0.8 log space) and relatively steep transition between snowmelt-dominant floods to rainfall

dominant floods greater than about 10,000 ft^3/s. These large rainfall-caused floods are

120

responsible for the shape of the upper portion of the frequency curve. The return period of

the largest flood on record (June 1921) is about 270 years from the exceedance-based

plotting position, and about 1,600 years from the LP-III model.

The results indicate that the LP-III model provides an adequate fit to the gage,

historical and paleohydrologic bound data. The model fits the bulk of the data well,

including most of the large floods, but undershoots the largest flood (June 1921) due to the

addition of paleoflood data. The paleohydrologic bound data at Pueblo State Park increases

the peak discharge record length substantially to about 840 years, and has an effect on the

upper end of the extrapolated frequency curve principally by reducing the skewness

coefficient.

One can estimate design flood probabilities based on significant extrapolation of the

LP-III model and 90 percent confidence interval (Figure 5.3). The spillway design outflow

capacity for Pueblo Dam (191,000 ft^3/s) has an estimated return period of 13,000 years, and a

return period estimate for the volume-critical spillway design inflow peak (270,000 ft^3/s) is

about 42,000 years.
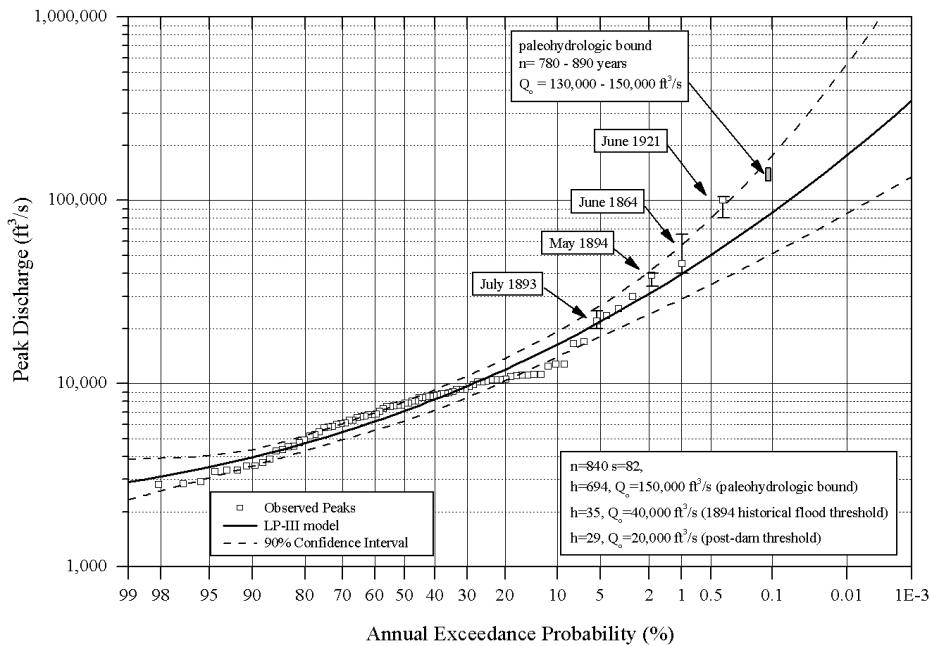
Figure 5.3. Approximate peak discharge frequency curve, Arkansas River at Pueblo State Park, including gage, historical and paleoflood data.

Table 5.3: Arkansas River at Pueblo State Park Peak Discharge Frequency Results

Annual Exceedance Probability (%)	Return Period (years)	Peak Discharge (ft^3/s)		
		Model Estimate*	5% Confidence Limit*	95% Confidence Limit*
10	10	16400	14,100	19,400
4	25	23,800	19,400	29,700
2	50	31,000	23,900	41,000
1	100	39,800	29,000	57,100
0.5	200	50,600	34,800	79,900
0.2	500	68,700	43,700	125,000
0.1	1,000	86,100	51,400	176,000
0.05	*2,000*	*107,000*	*60,100*	*249,000*
0.02	*5,000*	*143,000*	*73,400*	*393,000*
0.01	*10,000*	*177,000*	*85,000*	*556,000*
0.005	*20,000*	*218,000*	*98,100*	*787,000*
*Results shown in italics are extrapolated beyond available data				

5.4   ARKANSAS RIVER AT PARKDALE

Peak discharge estimates on the Arkansas River at Parkdale are based on the Parkdale

gage with historical information, the largest flood from the Canon City gage, and the basin

snowmelt flood of record in June 1957 (Chapter 4). It was assumed that peak discharge

estimates from these gages were unaffected by upstream regulation. The gage record length

at Parkdale, excluding historical data and gaps in the gage record, is 48 years (1946-2004).

Based on reviews of available historical information (Chapter 4), including

Follansbee and Jones (1922) and Follansbee and Sawyer (1948) (among others), there is

some amount of historical flood information on the Arkansas River in Canon City that was

usable for frequency analysis. The historical record was estimated to begin in 1868,

resulting in a 137-year period (1868-2004). It was also clear from the very long streamflow

record at Canon City (Figure 5.4), that the storms causing the largest floods at Pueblo (June

1921 and May 1894) did not cause significantly large peaks at Parkdale or Canon City. The

May 1894 flood at Pueblo was only about 4,400 ft^3/s at Canon City. The rainstorm that

caused the June 1921 flood at Pueblo centered downstream of Canon City. The largest peak

of record at Canon was the August 2, 1921 flood (Figure 5.4).
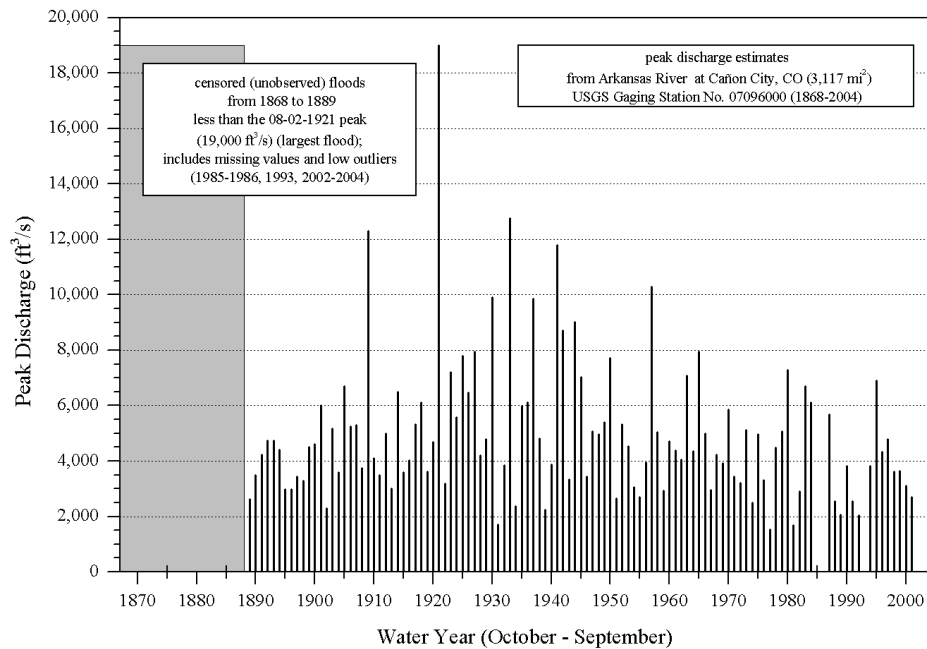
Figure 5.4. Approximate unregulated peak discharge and historical flood estimates, Arkansas River at Canon City. Note the distinct differences in magnitude for the largest floods versus those at Pueblo.

A paleohydrologic bound of about 1,250 years was estimated at Parkdale (Table 5.1) for inclusion in the flood frequency curve. The estimate is based on two soils pits, two radiocarbon ages, and hydraulic modeling of a 2,330 foot reach (Klawon et al., 2005). A historical flood estimate was made based on stratigraphy in a third soils pit. The flood age was estimated to be historical (post 1870). Given the streamflow data at Canon (Figure 5.4) and the correlations between Parkdale and Canon (Chapter 4), it is estimated that this deposit is from the August 1921 flood. A time series plot of the peak discharge, historical flood and paleohydrologic bound data is shown in Figure 5.5.
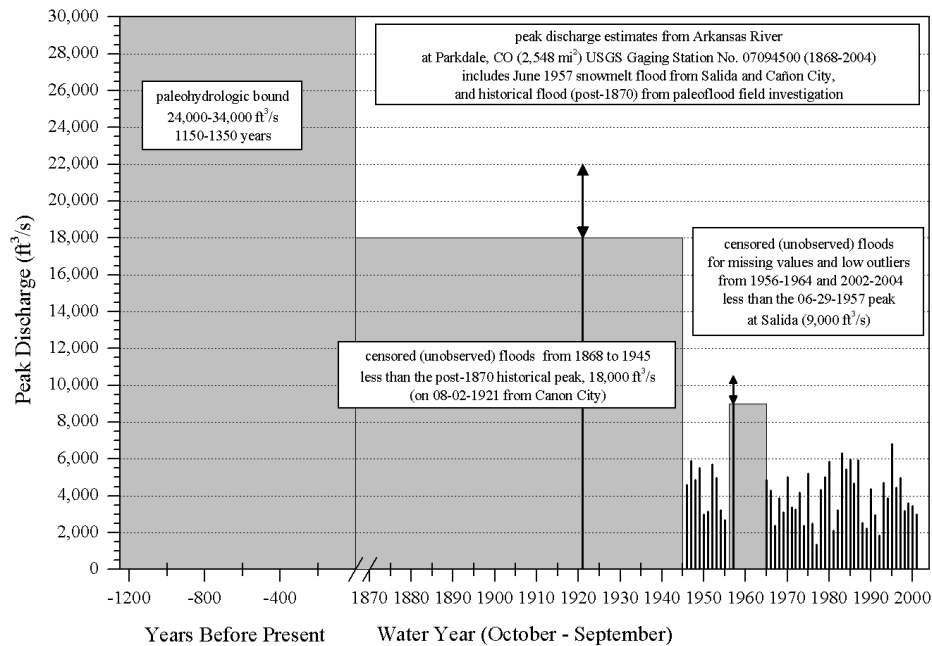
Figure 5.5. Approximate unregulated peak discharge, historical and paleoflood estimates, Arkansas River at Parkdale. A scale break is used to separate the gage and historical data from the longer paleoflood record. Arrows on the 1921 and 1957 floods indicate floods in a range.

The flood frequency results are shown in Figure 5.6 and Table 5.4. Peak discharge estimates from the gage are shown as open squares with estimated data uncertainty for the two largest floods that were described in a range. One can observe that the skewness coefficient (0.3 log space) is positive, but much reduced from downstream at Pueblo. Peak-flow magnitudes are also dramatically less. There is only one observation that exceeds 10,000 ft^3/s (August 1921 rain flood); this flood is partly responsible for the shape of the upper portion of the frequency curve. The majority of the observations, including the second-largest and third-largest floods, are from snowmelt. The return period of the largest flood on record (August 1921) is about 270 years from the exceedance-based plotting position, and about 1,300 years from the LP-III model.

125

The results indicate that the LP-III model provides an adequate fit to the gage, historical and paleohydrologic bound data. The model fits the bulk of the data well, including all of the large floods, except for undershooting the largest flood (August 1921) due to the addition of paleoflood data. The paleohydrologic bound data at Parkdale increase the peak discharge record length substantially to about 1,250 years, and have an effect on the upper end of the extrapolated frequency curve principally by reducing the skewness coefficient for a very large flood in a shorter record. The 90 percent confidence interval encompasses the data, including paleohydrologic bounds.
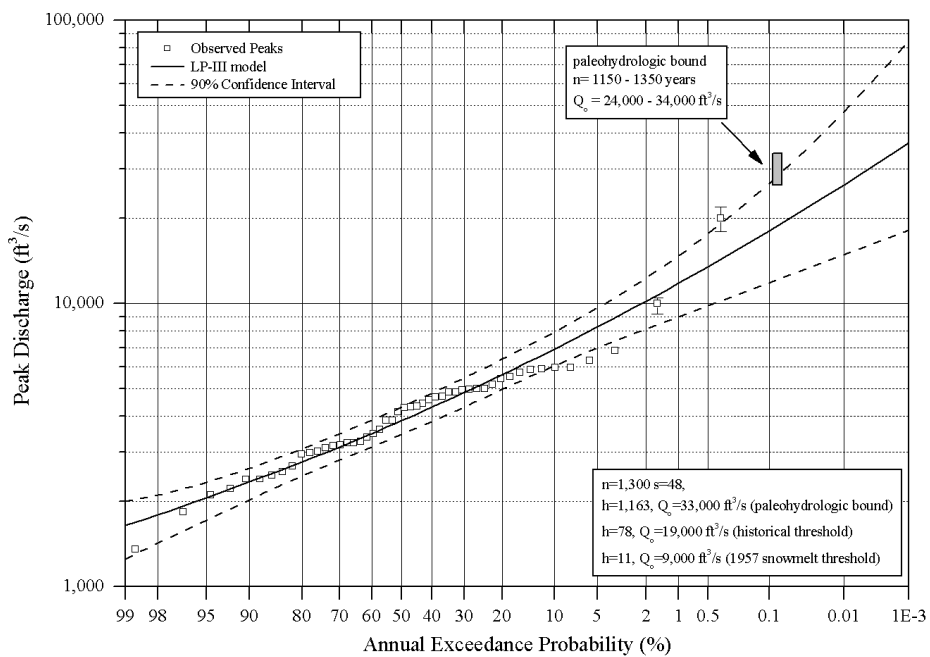
Figure 5.6. Approximate peak discharge frequency curve, Arkansas River at Parkdale, including gage, historical and paleoflood data.

Table 5.4: Arkansas River at Parkdale Peak Discharge Frequency Results

Annual Exceedance Probability (%)	Return Period (years)	Peak Discharge (ft³/s)		
		Model Estimate*	5% Confidence Limit*	95% Confidence Limit*
10	10	6,910	6,030	7,950
4	25	8,730	7,280	10,300
2	50	10,200	8,150	12,300
1	100	11,800	9,000	14,800
0.5	200	13,500	9,840	17,600
0.2	500	16,000	11,000	22,300
0.1	1,000	18,100	11,900	26,600
0.05	*2,000*	*20,400*	*12,800*	*31,800*
0.02	*5,000*	*23,700*	*14,000*	*40,100*
0.01	*10,000*	*26,400*	*14,900*	*47,800*
0.005	*20,000*	*29,400*	*15,900*	*56,900*
*Results shown in italics are extrapolated beyond available data				

5.5   ARKANSAS RIVER AT LOMA LINDA

The Loma Linda site was selected for its intermediate location in the watershed and reflects the upper basin snowmelt hydrology. Peak discharge estimates on the Arkansas River at Loma Linda are based on the Wellsville gage with historical information and the basin snowmelt flood of record in June 1957 (Chapter 4). It was assumed that peak discharge estimates from this gage were unaffected by upstream regulation. The gage record length at Wellsville, excluding historical data and gaps in the gage record, is 41 years (1961-2004).

Based on reviews of available historical information (Chapter 4), including Campbell (1922), Baker and Hafen (1927) and Crowfoot et al. (2004) (among others), there is some limited amount of historical flood information on the Arkansas River at Salida that was

usable for frequency analysis. The historical record was estimated to begin in 1880,

resulting in a 125-year period (1880-2004). It was also clear from the relatively long

streamflow record at Salida (shown below) in conjunction with this site and Parkdale, that

the largest floods are caused by snowmelt. The largest peak of record at Salida and in the

upper Arkansas River watershed was the June 1957 snowmelt flood (Chapter 4).

Two paleohydrologic bounds (Table 5.1) for inclusion in the flood frequency curve

were estimated at Loma Linda: a Holocene bound about 1,500 years; and a Pleistocene

bound about 10,000 years. The estimates are based on two soils pits, two radiocarbon ages,

and hydraulic modeling of a 2,340 foot reach (Klawon et al., 2005). No estimates of

individual paleofloods were made at this site, as there are few deposits of Holocene alluvium

preserved in the reach. A time series plot of the peak discharge, historical flood and

paleohydrologic bound data is shown in Figure 5.7.

The flood frequency results are shown in Figure 5.8 and Table 5.5. Peak discharge

estimates from the gage are shown as open squares with estimated data uncertainty for the

largest flood that was described in a range. One can observe that the skewness coefficient

(-0.2 log space) is negative, and reduced from downstream at Parkdale. Peak-flow

magnitudes are also dramatically less. There is only one observation that exceeds 7,000 ft^3/s

(June 1957 snowmelt flood); this flood fits well with the other snowmelt flood observations.

Figure 5.7. Approximate unregulated peak discharge, historical and paleoflood estimates, Arkansas River at Loma Linda. A scale break is used to separate the gage and historical data from the longer paleoflood record. A second scale break separates the gage/historical and lower paleohydrologic bound from the larger paleohydrologic bound. Arrows indicate the 1957 flood in a range.

Nearly all the observations, including the largest floods, are from snowmelt. The return period of the largest flood on record (June 1957) is about 250 years from the exceedance-based plotting position, and about 450 years from the LP-III model.

The results indicate that the LP-III model provides a very good fit to the gage, historical and paleohydrologic bound data. The model fits the bulk of the data well, including all of the large floods and the Holocene paleohydrologic bound. The paleohydrologic bound data at Loma Linda significantly increase the peak discharge record length to about 10,000 years. The Pleistocene paleohydrologic bound has little to no influence on the frequency curve because of the negative skew and the very large difference in flow magnitude between the Pleistocene and Holocene bounds. The paleohydrologic

129

bounds are consistent with the observed streamflow data; there have been no floods in the

geologic record substantially larger than the snowmelt floods observed from the gage record.

The 90 percent confidence interval encompasses the observed data.
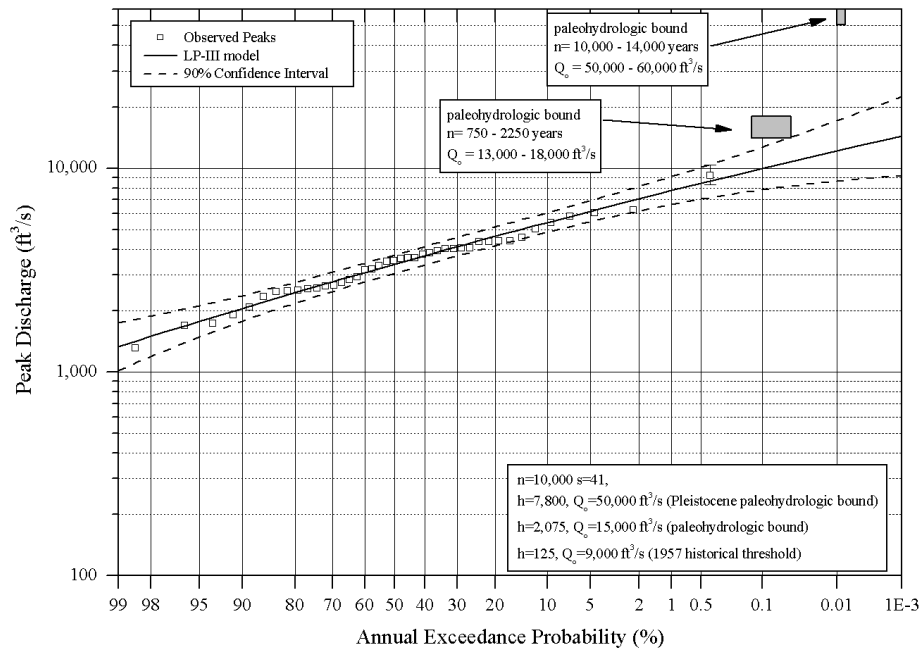
Figure 5.8. Approximate peak discharge frequency curve, Arkansas River at Loma Linda, including gage, historical and paleoflood data.

Table 5.5: Arkansas River at Loma Linda Peak Discharge Frequency Results

Annual Exceedance Probability (%)	Return Period (years)	Peak Discharge (ft^3/s)		
		Model Estimate*	5% Confidence Limit*	95% Confidence Limit*
10	10	5,420	4,850	6,050
4	25	6,380	5,640	7,220
2	50	7,080	6,170	8,130
1	100	7,760	6,630	9,090
0.5	200	8,440	7,040	10,100
0.2	500	9,320	7,520	11,500
0.1	1,000	9,980	7,830	12,700
0.05	2,000	10,600	8,110	13,900
0.02	5,000	11,500	8,440	15,700
0.01	10,000	12,200	8,660	17,100
0.005	*20,000*	*12,800*	*8,850*	*18,600*
Results shown in italics are extrapolated beyond available data				

130

5.6   ARKANSAS RIVER AT ADOBE PARK

The Adobe Park site was selected for its relatively higher location in the watershed to document snowmelt hydrology and potentially limit areal extents of extreme storms. Peak discharge estimates on the Arkansas River at Adobe Park are based on the Salida gage with historical information and the basin snowmelt flood of record in June 1957 (Chapter 4). It was assumed that peak discharge estimates from this gage were unaffected by upstream regulation. The gage record length at Salida, excluding historical data and gaps in the gage record, is 77 years (1895-1979).

Based on reviews of available historical information (Chapter 4), including Campbell (1922), Baker and Hafen (1927) and Crowfoot et al. (2004) (among others), there is some limited amount of historical flood information on the Arkansas River at Salida that was usable for frequency analysis. The historical record was estimated to begin in 1880, resulting in a 125-year period (1880-2004). It was also clear from the relatively long streamflow record at this site that the largest floods are caused by snowmelt. The largest peak of record at Salida and in the upper Arkansas River watershed was the June 1957 snowmelt flood (Chapter 4).

One paleohydrologic bound (Table 5.1) for inclusion in the flood frequency curve was estimated at Adobe Park, a Holocene bound about 550 years. The estimate is based on mapping of two Holocene surfaces, one soils pit, one radiocarbon age, and hydraulic modeling of a 1,870 foot reach (Klawon et al., 2005). No estimates of individual paleofloods

were made at this site, as there are few deposits of younger Holocene alluvium preserved

within Pinedale and Bull Lake outwash terraces. A time series plot of the peak discharge,

historical flood and paleohydrologic bound data is shown in Figure 5.9.
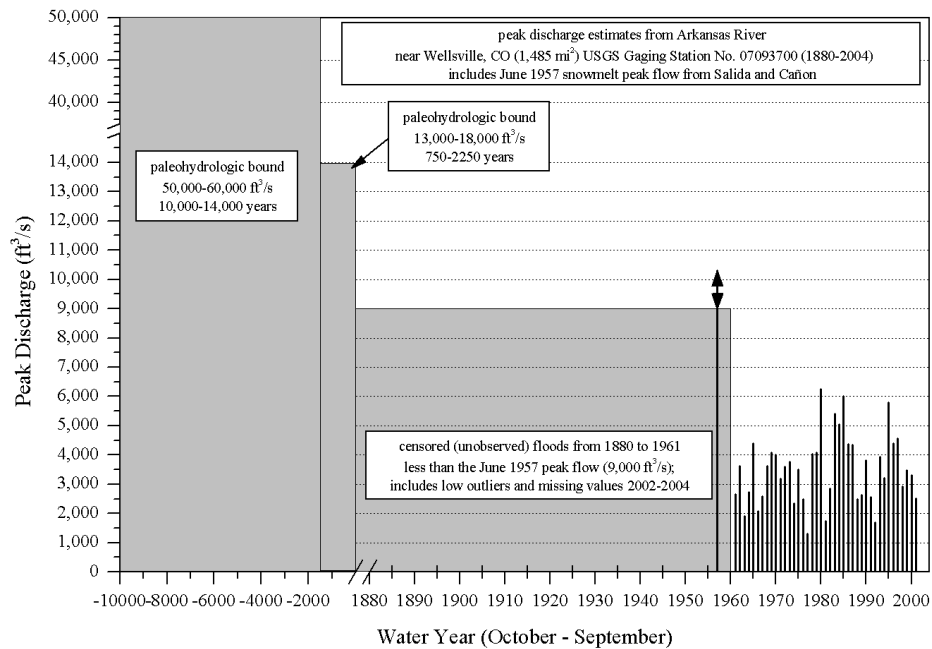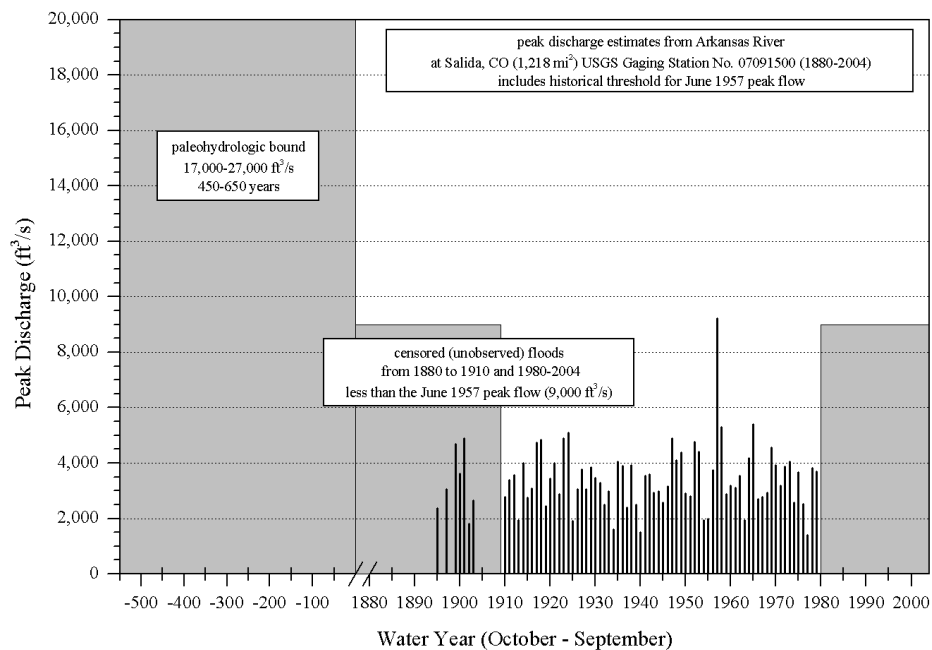

Figure 5.9. Approximate unregulated peak discharge, historical and paleoflood estimates, Arkansas River at Adobe Park. A scale break is used to separate the gage and historical data from the longer paleoflood record.

The flood frequency results are shown in Figure 5.10 and Table 5.6. One can observe

that the skewness coefficient (-0.2 log space) is negative, and identical to that at Loma Linda.

Peak-flow magnitudes are also about the same (slightly less) as Loma Linda, and

dramatically less than at Pueblo. There is only one observation that exceeds 6,000 ft^3/s (June

1957 snowmelt flood); this flood is a bit larger than the other snowmelt flood observations.

Nearly all the observations, including the largest floods, are from snowmelt. The return

period of the largest flood on record (June 1957) is about 250 years from the exceedance-

based plotting position, and about 4,000 years from the LP-III model.

132

The results indicate that the LP-III model provides a very good fit to the gage, historical and paleohydrologic bound data. The model fits the bulk of the data well, but departs slightly from the larger floods in order to attempt to fit the largest flood. The paleohydrologic bound data at Adobe Park increase the peak discharge record length to about 550 years. This Holocene paleohydrologic bound has a small influence on the frequency curve because of the negative skew and the very large difference in flow magnitude between the Holocene bound and the largest flood. The paleohydrologic bound is consistent with the observed streamflow data and suggests that there have been no floods in the geologic record substantially larger than the snowmelt floods observed from the gage record. The 90 percent confidence interval encompasses the observed data.
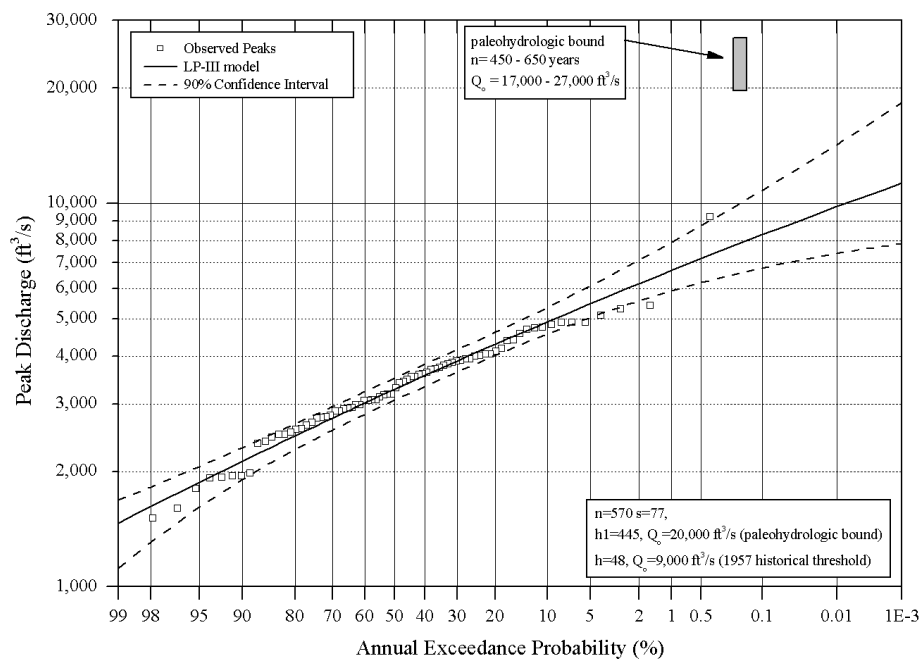
Figure 5.10. Approximate peak discharge frequency curve, Arkansas River at Adobe Park, including gage, historical and paleoflood data.

Table 5.6: Arkansas River at Adobe Park Peak Discharge Frequency Results

Annual Exceedance Probability (%)	Return Period (years)	Peak Discharge (ft³/s)		
		Model Estimate*	5% Confidence Limit*	95% Confidence Limit*
10	10	4,910	4,570	5,360
4	25	5,660	5,180	6,350
2	50	6,180	5,570	7,120
1	100	6,690	5,910	7,920
0.5	200	7,180	6,210	8,750
0.2	500	7,820	6,560	9,900
0.1	*1,000*	*8,290*	*6,790*	*10,800*
0.05	*2,000*	*8,750*	*7,000*	*11,800*
0.02	*5,000*	*9,360*	*7,240*	*13,200*
0.01	*10,000*	*9,820*	*7,410*	*14,300*
0.005	*20,000*	*10,300*	*7,560*	*15,400*
*Results shown in italics are extrapolated beyond available data				

5.6   REGULAR FREQUENCY ANALYSIS

The main purpose of the regional frequency analysis was to compare peak discharge frequency curves from the four sites, and show distinct differences between the locations. In concept, the frequency curves should show clear differences between downstream, large rainfall-runoff events and upstream snowmelt-dominant events. The goal is to demonstrate these mixed-population differences, and document upper and lower basin frequency curve changes with scale, process and elevation. If the frequency curves from the snowmelt-dominant upstream sites were similar, and substantially different from downstream sites, one can use these results to limit areal extent of extreme storms.

Non-dimensional peak discharge frequency curves, based on LP-III models derived from the data set at each site, are shown in Figure 5.11. The at-site 10-year peak discharge was used to non-dimensionalize the flood frequency model results. The lower-basin

134

frequency curves (Pueblo and Parkdale) clearly reflect rainstorms (mixed-population snowmelt and large rainstorms), whereas the upper basin sites (Loma Linda and Adobe Park) are from snowmelt. The frequency curves for the downstream locations are clearly different for the most extreme floods; they have a much steeper shape. The curvature is primarily determined by the LP-III model skewness coefficient. The log-space skew is positive at Pueblo (0.8) and Parkdale (0.3), and negative at Loma Linda (-0.2) and Adobe Park (-0.2). The extreme peak-flow magnitudes at Pueblo are substantially larger than at upstream locations within the same time period, giving a much steeper frequency curve. The shapes and slopes of the Adobe Park and Loma Linda frequency curves are very similar, and are clearly different than the two downstream locations. The streamflow and paleoflood data do not show any evidence of extreme floods substantially larger than that recorded in the gage record for the upper basin snowmelt locations. The Parkdale frequency curve is similar in shape to the upstream curves for flows less than about the 10-year peak. This suggests a separation in flood process in the record; the upper end of the Parkdale frequency curve behaves similarly to Pueblo, but is not as steep. One can infer from this that there is a transition in peak-flow frequency behavior between Pueblo and Loma Linda; storms that affect Pueblo and cause extreme floods do not cause as large peaks at Parkdale. The results show that the use of a partial-area storm concept on the lower part of the basin is warranted.
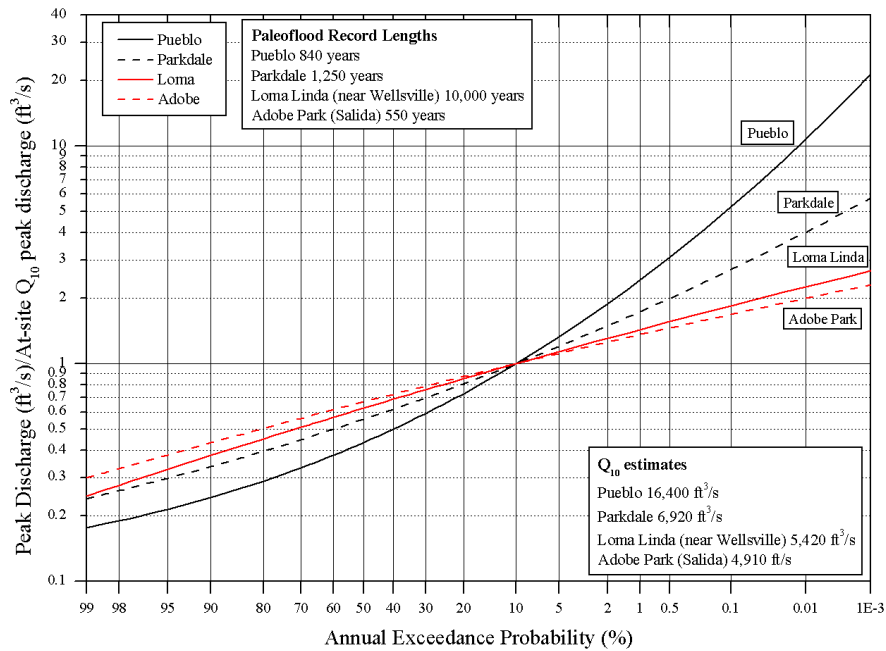
Figure 5.11. Approximate unregulated non-dimensional peak discharge frequency curves for the four sites within the Arkansas River basin. Each curve is non-dimensionalized by its respective at-site 10-year model peak flow.

5.7   SUMMARY

Flood frequency analysis was conducted using peak-flow (gage), historical and

paleoflood data at four locations along the main stem of the Arkansas River upstream from

Pueblo. The Expected Moments Algorithm was used with the LP-III distribution to estimate

flood frequency curves at Pueblo, Parkdale, Loma Linda (Wellsville) and Adobe Park

(Salida). Confidence intervals for each frequency curve were also estimated.

Paleohydrologic bounds spanned 550 to 10,000 years within the watershed and provided

substantially longer record lengths for frequency analysis. Peak flows in the lower

watershed at Pueblo and Parkdale reflected extreme floods from rainfall, and were relatively

much larger than at the two upstream locations. The lower sites had positive log-space

skews. The largest floods at upstream sites were from snowmelt; these locations had

relatively flat frequency curves and negative log-space skews. Using a regional index-flood

approach, it was shown that there is a different population of floods between upstream

snowmelt and downstream rainfall-runoff sites. The frequency curves are later used in

Chapter 7 to contrast flood frequency curves estimated with a rainfall-runoff model.

Chapter VI

EXTREME STORM MODELING

This chapter presents an extreme storm model that predicts basin-average extreme

rainfall depths and probabilities using stochastic storm transposition. The model is applied

for the first time in a mountainous region for an actual watershed; predictions are then used

as input to the TREX runoff model (Chapter 7). A brief sensitivity analysis demonstrates

storm location and areal distribution effects on basin-average rainfall depth predictions.

6.1   STORM TRANSPOSITION OVERVIEW

Extreme storms are considered in two dimensions (x,y) in space, in order to describe

and numerically model them. Cumulative rainfall totals for an extreme storm are shown in

Figure 6.1. Two-dimensional models are able to quantitatively describe the extreme storm

rainfall magnitude at each specified coordinate (x,y) location. The vertical (third) dimension

(z) is ignored in the present work, as we focus on the magnitude of rainfall on the ground in

space (x and y). Operational storm models used for Probable Maximum Precipitation

estimation typically are developed in two dimensions (e.g., Wiesner, 1970). In addition to

the spatial distribution of a storm, the rainfall magnitudes are also described in time *t* at each

(*x,y*) location by either a mass curve (cumulative rainfall depth with time), or a hyetograph

(rainfall intensity versus time). Typical mass curves and hyetographs are described in

standard hydrology textbooks (e.g. Chow et al., 1988). Reclamation has used two

hyetograph patterns for distributing PMP estimates in time (Cudworth, 1989): a "standard"

alternating block pattern arrangement with the maximum at 2/3*t*; and an exponential-like

"front-end loaded" pattern with the maximum at *t*=0. The spatial and temporal storm model

used in this research is described in Section 6.2.
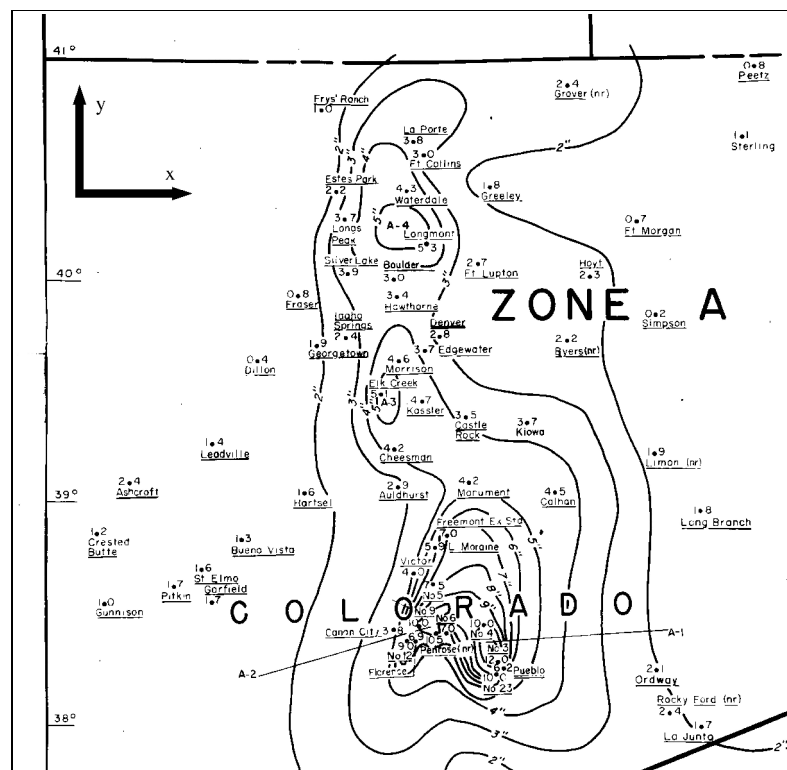
Figure 6.1. Typical extreme storm total rainfall accumulation estimates in space (*x,y*) for the June 2-6, 1921 Penrose, CO storm (114 hours). Isohyets (solid lines) represent total storm rainfall in inches over the area encompassed by the line.

An important concept in hydrology is regionalization, which means studying the

hydrologic properties of a large and homogeneous region with the objective of applying the

results to a watershed within the region (Laurenson and Kuczera, 1998). Within a specific

river valley, there are often inadequate records of extreme storms (Wiesner, 1970).

Frequency analysis is a problem in hydrology because sufficient information is seldom

available at a site to adequately determine the frequency of rare events (Stedinger et al.,

1993). The at-site storm record within a watershed can be extended significantly by using

data from the surrounding region. Using the regional storm data, the hydrologist is

substituting space for time. Space for time substitution is one of the three principles

advocated by NRC (1988) to improve estimates of extreme flood probabilities. The regional

data of given length are effectively equivalent to a much longer record at the watershed of

interest.

Storm transposition is a regionalization concept that involves moving (transposing)

storms within an area to the watershed of interest. Transposition involves relocating

individual storm precipitation within a region considered homogeneous relative to

topographic and meteorologic characteristics deemed significant to that storm (Cudworth,

1989). Transposition greatly increases the available data for evaluating the rainfall potential

for a drainage (Schreiner and Riedel, 1978). Transposition concepts are illustrated in Figure

6.2. Stochastic storm transposition is a generalization of the concept of storm transposition,

which is the basis for estimating PMP in the United States (e.g., Hansen et al., 1988). In the

PMP application, storm transposition is based on the assumption that there exist

meteorologically homogeneous regions such that a major storm occurring somewhere in the

region could occur anywhere else in the region, with the provision that there may be

differences in the averaged depth of rainfall produced based upon differences in moisture

potential (NRC, 1988; Cudworth, 1989). Stochastic storm transposition (SST) extends this

concept by incorporating the probability of occurrence (Fontaine and Potter, 1989).
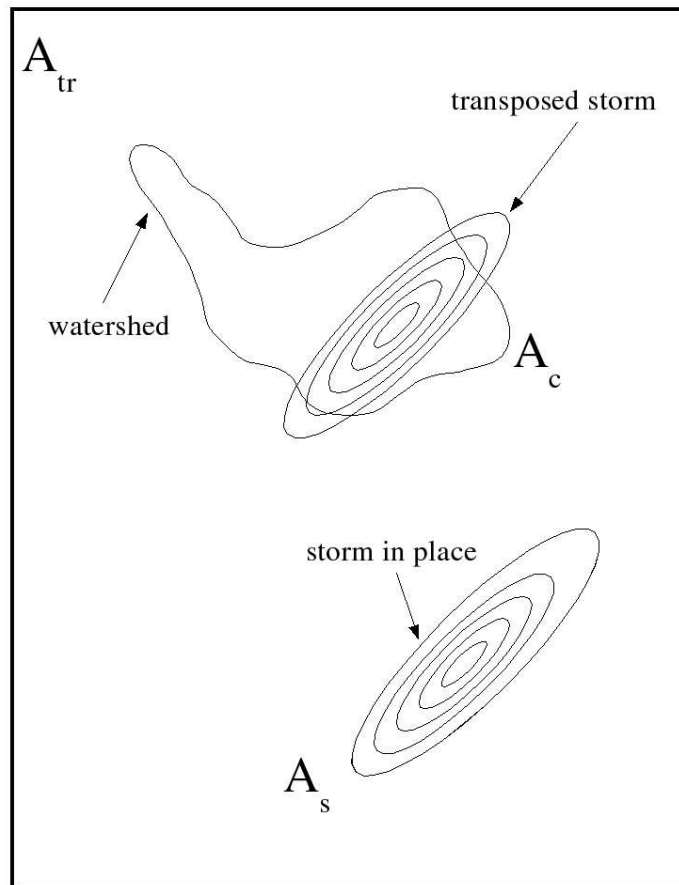
Figure 6.2. Storm transposition concepts, showing transposition area A_{tr}, watershed area A_c, and storm area A_s (modified from Foufoula-Georgiou, 1989).

The storm transposition area A_{tr} is the area within which all the occurred storms can be

transposed anywhere in the region either with the same depths and an adjustment to their

probability of occurrence, or with the same probability of occurrence but with an adjustment

to their depths (Foufoula-Georgiou, 1989).

6.2 STOCHASTIC STORM TRANSPOSITION MODEL

6.2.1 Overview of Probability Concepts

When estimating the frequency of rare floods for a given catchment using storm

rainfall data, a pertinent question is: "What is the probability of a rainfall averaging more

than d inches (in a specified duration) occurring over the catchment in question within a long

period such as the life of a dam (Alexander, 1963)?" The general approach for stochastic

storm transposition consists of two main parts: (1) estimating a basin-average depth of storm

rainfall $\bar{d}_c$ over a particular watershed with area A_c during a time period Δt; and (2)

estimating the cumulative probability distribution function (cdf) of the basin-average depth

$F_{\bar{d}_c(\Delta t)}$ during that time period. The cdf of $\bar{d}_c$ depends on the joint distribution of the

storm properties (described below) and the storm position (x,y). For conceptual

understanding, one can consider this joint distribution in two parts: a "transposition"

probability P_t that represents the probability of a storm center (x,y) falling within or near the

watershed of interest; and a probability of occurrence P_r of a storm with depth that exceeds

some minimum depth or rank in one year (Alexander, 1963). Alexander (1963) suggested

that the probability of occurrence P_c of a transposable storm occurring over the watershed in

any given year is equal to the product P_rP_t. Gupta (1972), YAEC (1984) and Fontaine and

Potter (1989) utilized other alternative definitions of SST probabilities; these are summarized

by Wilson (1989). The SST method described below uses the theoretical analysis framework

of Foufoula-Georgiou (1989) to estimate probabilities.

6.2.2   Stochastic Storm Transposition Theory

The formal theoretical framework for the stochastic storm transposition (SST) model

that is used here is adopted from Foufoula-Georgiou (1989) and Wilson and Foufoula-

Georgiou (1990). The SST model describes the annual exceedance probability of the

maximum basin-average depth over a catchment. The theory and equations to estimate $\bar{d}_c$

and its annual exceedance probability are described below and follow that of Wilson and

Foufoula-Georgiou (1990). The SST model is later coupled with a rainfall-runoff model in

order to estimate extreme flood probabilities.

The maximum areally averaged depth that can occur over a catchment of area A_c

during a time period Δt is estimated via:

$$\bar{d}_c(\Delta t)=\frac{1}{|A_c|}\int\int_{Ac}\left[d(x,y,t_s+\Delta t)-d(x,y,t_s)\right]dxdy \quad (6.1)$$

where $\bar{d}_c$ is the maximum areally-averaged depth, *(x,y)* are spatial coordinates and Δt is a

critical duration of rainfall in terms of flood production. This critical duration may be a fixed

time period such as 6, 12, 24 or 72 hours, up to the total storm duration t_r, and t_s is defined as:

143

$$t_s = \int\int_{Ac} \left[d(x,y,t_s + \Delta t) - d(x,y,t_s) \right] dxdy$$
$$\geq \int\int_{Ac} \left[d(x,y,t + \Delta t) - d(x,y,t) \right] dxdy \ \forall \, t < t_r - \Delta t \qquad (6.2)$$

and we interpret the random variable $\bar{d}_c(\Delta t)$ as the maximum average depth from a storm

over a catchment with area A_c during a time period equal to Δt.

An important step in SST is the storm selection. A storm severity criterion E is used to select

storms (Wilson, 1989):

$$Criterion \ E: \qquad \{ \bar{d}[\Delta t, A] \geq d_{min} \} \quad (6.3)$$

where $\bar{d}[\Delta t, A]$ denotes the average storm depth over an area A accumulated over a period

of time Δt, and d_{min} is some minimum depth value based on Δt and A, such that all storms

having an effect on the exceedance probabilities are included in the sample set.

Let $\mathbf{\Lambda}_s$ represent the random vector of storm characteristics that describe a storm.

These characteristics may be random variables, such as the average depth over an area (e.g.,

10 mi^2 depth), or random functions, such as a function that describes the storm depth at a

position (x,y) and at time t (a stochastic model of the rainfall field). Let $\mathbf{\Lambda}_p$ represent a two-

dimensional vector which describes the position of the storm based on the x,y-coordinates of

the location of its center. The center of the storm can be defined as the location of the

maximum observed total depth, the location of the maximum accumulated depth over a

period of time, or as the center of mass of the storm. It is assumed here that the storm center

is defined as the location of the maximum observed total depth, and is estimated from the

depth-area duration (DAD) catalog.

The cumulative distribution function F of the maximum average total storm depth $\bar{d}_c(\Delta t)$ can be written as:

$$F_{\bar{d}_c(\Delta t)}(d) = pr\left[\bar{d}_c(\Delta t) \leq d\right] \quad (6.4)$$

This cumulative distribution F is now defined in terms of the joint distribution of Λ_s and Λ_p (Wilson and Foufoula-Georgiou, 1990), noting that (λ_s, λ_p) are the lower case variates:

$$F_{\bar{d}_c(\Delta t)}(d) = \int_{[\Lambda_s]} \int_{[\Lambda_p]} pr\left[\bar{d}_c(\Delta t) \leq d | \lambda_s, \lambda_p\right] dF_{\Lambda_s, \Lambda_p}(\lambda_s, \lambda_p) \quad (6.5)$$

and $F_{\Lambda_s, \Lambda_p}(\lambda_s, \lambda_p)$ is the cumulative joint distribution function of the random vectors Λ_s and Λ_p. Wilson (1989) notes that $[\Lambda_s]$ and $[\Lambda_p]$ represent the functional spaces within which the vectors Λ_s and Λ_p vary. One challenge is to estimate this joint distribution of storm characteristics and storm position. Using Bayes' theorem, these distributions can be analyzed as either

$$f(\lambda_s, \lambda_p) = f(\lambda_p | \lambda_s) f(\lambda_s) \quad (6.6)$$

where $f(\lambda_p | \lambda_s)$ denotes the probability that a storm of given characteristics λ_s will occur at a position given by λ_p, or as

$$f(\lambda_s, \lambda_p) = f(\lambda_s | \lambda_p) f(\lambda_p) \quad (6.7)$$

where $f(\lambda_s | \lambda_p)$ denotes the probability that a storm that occurred at a position given by λ_p had the storm properties λ_s. Following Wilson and Foufoula-Georgiou (1990), I consider

implementing the latter version based on storm position (equation 6.7), using a

nonhomogeneous point process model.

One is most interested in estimating the exceedance probability. The exceedance

probability G in terms of F is defined as:

$$G_{\bar{d}_c(\Delta t)}(d)=1-F_{\bar{d}_c(\Delta t)}(d) \quad (6.8)$$

Using the superscript a for the annual probability of a variable, the annual exceedance

probability G^a of the maximum average total storm depth $\bar{d}_c(\Delta t)$ is:

$$G^a_{\bar{d}_c(\Delta t)}(d)=1-F^a_{\bar{d}_c(\Delta t)}(d) \quad (6.9)$$

To determine annual probabilities, let $Z(t)$ represent a counting process of the number of

extreme storms in an interval of t years. One can eliminate $\bar{d}_c(\Delta t)$ subscripts on F and G

and write (Wilson and Foufoula-Georgiou, 1990):

$$G^a(d)=1-\sum_{\nu=0}^{\infty} pr\left[\bar{d}_c(\Delta t)\leq d|Z(1)\right]\cdot pr\left[Z(1)=\nu\right] \quad (6.10)$$

If one assumes that the random number of extreme storms per year $Z(1)$ is independent of

storm depths $\bar{d}_c(\Delta t)$ and that $\bar{d}_c(\Delta t)$ are independent and identically distributed

variables, the annual exceedance probability of the maximum average depth is (Wilson and

Foufoula-Georgiou, 1990):

$$G^a(d)=1-\sum_{\nu=0}^{\infty}\left[F(d)\right]^{\nu}\cdot pr\left[Z(1)=\nu\right] \quad (6.11)$$

One can assume that the $Z(1)$ follows a Poisson distribution with annual occurrence rate λ, as:

$$pr\left[Z(1)=v\right] = \frac{e^{-\lambda}\lambda^{v}}{v!} \quad (6.12)$$

where v is the variate of $Z(t)$ and t is one year. This distribution assumption was shown to be adequate for the midwestern United States (Foufoula-Georgiou and Wilson, 1990; Wilson and Foufoula-Georgiou, 1990), but needs further testing in Colorado. Given this distribution, the annual exceedance probability can be estimated from:

$$G^{a}(d)=1-\exp\left[-\lambda G(d)\right] \quad (6.13)$$

where $G(d)$ is estimated from equation 6.8.

The stochastic storm transposition model is defined by coupling equations 6.5, 6.7, 6.8 and 6.13. However, several additional models are needed to fully define the properties of equation 6.5. In order to develop a complete SST model, one needs to define the contents of the position vector Λ_p and the storm vector Λ_s. In addition to these vectors, one needs to define a model that describes the storm rainfall distribution in space, and a model that describes the storm center occurrence in space. The maximum storm center depth needs to be described with a model. In order to conduct rainfall-runoff simulations, a temporal model that describes the time-varying rainfall depth or rates over the storm duration is also needed (e.g., Franchini et al., 1996). These four models are required to implement the SST approach, but other models and distributions for parameters may also be needed depending

147

on the assumptions made. A distribution model would be needed for storm duration if one wanted to simulate the variation in extreme storm duration rather than assuming that the duration is fixed for all simulated storms (e.g., Foufoula-Georgiou and Wilson, 1990). Similarly, other distribution models could be defined for storm orientation and storm shape. In a more general framework, one could specify a storm occurrence and location model coupled with spatial and temporal models.

6.2.3   Storm Spatial Distribution

There are several approaches to develop a spatial distribution of an extreme storm. The approach that is implemented here is a simple, parsimonious model based on DAD data. It is assumed that the storm is single-centered, and isohyets are geometrically similar in the form of an ellipse (e.g., Hansen et al., 1982). This assumed storm shape describes both within-storm amounts and storm totals, and can be an adequate spatial representation based on the DAD data (Foufoula-Georgiou and Wilson, 1990). Although storm shapes are generally very complex, Hansen et al. (1982) recommended using a standardized elliptical pattern to represent the storm isohyets. The storm spatial pattern that is adopted has geometrically similar ellipses with a major (a) to minor (b) axis ratio c, where $c = a/b$ (Chapter 3).

The spatial model is from Horton (1924) who related the maximum average depth to storm area:

$$\bar{d}(A) = d_o e^{-kA^n} \quad (6.14)$$

where d_o is the maximum observed storm depth for a particular duration, $\bar{d}(A)$ is the

average depth over the area A, and k and n are parameters to be estimated. This model has

been shown to provide an adequate fit to the largest observed 24-hour storms in the Miami

Conservancy District (Horton, 1924), DAD data from the Gulf Coast and Northern, Central

and Southern Plains (Boyer, 1957), and DAD data from the Midwestern United States

(Foufoula-Georgiou and Wilson, 1990), and used with SST (Foufoula-Georgiou, 1989;

Wilson and Foufoula-Georgiou, 1990). In adopting this formula, it is assumed that d_o can be

estimated from the 10 mi^2 depth as point data are unavailable from the DAD summary tables.

Following Wilson and Foufoula-Georgiou (1989), we define a shifted exponential

distribution to represent the frequency of maximum storm center depth D_o for a particular

duration Δt:

$$f_{D_o}(d_o) = \frac{1}{\theta} \exp\left[-\frac{(d_o - d_{min})}{\theta}\right] \quad (6.15)$$

where θ is a parameter to be estimated, and d_{min} is a specified minimum (cutoff) rainfall depth

based on the storm data from the region. The storm duration Δt (or eventually a Δt

distribution) first needs to be determined for the problem under investigation. The parameter

θ and d_{min} can then be estimated from the DAD data.

The parameters k and n in equation (6.14) can be estimated from the DAD tables for a

particular duration. Wilson and Foufoula-Georgiou (1990) assumed a bivariate normal

distribution for *k* and *n*:

$$f_{K',N}(k',n) = \frac{1}{2\pi\,\sigma_{K'}\,\sigma_N\,\sqrt{1-\rho^2}}\ \exp\left[-\frac{1}{2}Q(K',N)\right] \quad (6.16)$$

where

$$Q(k',n) = \frac{1}{1-\rho^2}\left[\left(\frac{k'-\mu_{K'}}{\sigma_{K'}}\right)^2 - 2\rho\left(\frac{k'-\mu_{K'}}{\sigma_{K'}}\right)\left(\frac{n-\mu_N}{\sigma_N}\right) + \left(\frac{n-\mu_N}{\sigma_N}\right)^2\right] \quad (6.17)$$

Foufoula-Georgiou and Wilson (1990) show that *k* and *n* are significantly correlated and that this cross-correlation of parameters should not be ignored in simulation studies.

There are alternative approaches to define the storm spatial distribution including multifractal approaches (e.g., Gupta and Waymire, 1993) and those based on radar data (e.g., Durrans et al., 2002), but using a storm-centered approach (e.g., Dixon and Weiner, 1993) rather than a fixed area method. These ideas are not pursued here, but could potentially be considered as part of future research, and may employ alternative spatial models than those described above. Radar data that have been processed for the Colorado Front Range (Javier et al., 2005) could be useful in parameter estimation for the depth-area relationship (equation 6.14), limits on storm area, and storm area resampling.

6.2.4   Storm Center Distribution

The two general options for SST storm center locations are that storms may occur anywhere within a homogeneous region with differences in average depth, or the depth may be the same throughout the region with differences in probabilities. The approach that is

considered in this work is to vary the average depth in space for a fixed exceedance

probability, duration, and area, using the nonhomogeneous spatial point process model of

Wilson and Foufoula-Georgiou (1990) for depths greater than d_{min}. This model considers the

storm center location (x,y) to be dependent on the storm center depth (d_o) by determining the

conditional pdf $f_{XY|D_o}(x,y|d_o)$ and then the marginal pdf $f_{D_o}(d_o)$. The distribution

function shape is estimated empirically based on the available data. Wilson and Foufoula-

Georgiou (1990) modeled storm spatial occurrences in the Midwest using two functions: (1)

a uniform distribution for $d < d_{min}$; and (2) a transformed bivariate distribution for $d \geq d_{min}$.

The uniform distribution for (x,y) denoted $f^{(1)}_{XY}$ is:

$$f^{(1)}_{XY} \equiv f_{XY|D_o < d_{min}}(x,y|d_o < d_{min}) = \frac{1}{|A_{tr}|} \cdot I(x,y) \quad (6.18)$$

where $I(x,y)$ is an indicator function defined over A_{tr} as

$$I(x,y)=1 \quad if \ (x,y) \in A_{tr} \quad (6.19)$$
$$I(x,y)=0 \quad otherwise$$

The transformed bivariate normal distribution for (x,y) denoted $f^{(2)}_{XY}$ is (Wilson and Foufoula-

Georgiou, 1990):

$$f^{(2)}_{XY} \equiv f_{XY|D_o \geq d_{min}}(x,y|d_o \geq d_{min}) = f^{(2)}_X(x) \cdot f^{(2)}_Y(y) \quad (6.20)$$

where

$$f_X^2(x) = \frac{1}{\sqrt{2\pi}\,\sigma_X} \cdot \exp\left[-\frac{1}{2}\left(\frac{x-\mu_X}{\sigma_X} \right)^2 \right], \quad -\infty < x < \infty \quad (6.21)$$

and

$$f_Y^2(y) = \frac{\sqrt{2}}{\sqrt{\pi}\,\sigma_o} \cdot \exp\left[-\frac{1}{2}\left(\frac{y-\mu_o}{\sigma_o} \right)^2 \right], \quad \mu_o \leq y < \infty \quad (6.22a)$$

$$f_Y^2(y) = 0 \quad for \quad -\infty < y < \mu_o \quad (6.22b)$$

The combined distributions are:

$$f_{XYD_o}(x,y,d_o) = f_{XY}^{(1)}(x,y) \cdot F_{D_o}(d_{min}) + f_{XY}^{(2)}(x,y) \cdot \left[1 - F_{D_o}(d_{min}) \right] \quad (6.23)$$

These distribution shapes need to be investigated based on data for the region and watershed

of interest. In orographic and mountainous regions, transformed bivariate distributions in

both x and y may be necessary. As a first step, one can assume a uniform probability

distribution of storm centers in space (Fontaine and Potter, 1989; Franchini et al., 1996),

within some smaller homogeneous transposition area. These relationships apply to a storm

conceptualized with a single storm center (Chapter 3). This concept may need to modified in

order to incorporate multi-cellular storms such as those typically observed from radar data.

In addition, the distributions depend on the computational grid cell size and area selected to

determine storm center coordinates. For example, Wilson and Foufoula-Georgiou (1990)

used a 1 degree by 1 degree grid to count the number of observations within each block in the

Midwest. They were able to describe these distributions based on an approximate square

area. When one has a topographic boundary to transposition (e.g., the Continental Divide),

the distribution choice and parameters can have a large effect on storm probabilities near the

boundary. A second issue in orographic regions is that there may be potential limits on

storm center locations for larger-area storms. The storm center may be located at lower

elevations, with rainfalls reduced at higher elevations. The distributions postulated above

may need to be modified or different functions selected to handle this phenomenon. These

issues could potentially be investigated as part of future research.

6.2.5   Storm Temporal Distribution

The major theoretical developments of the SST approach by Foufoula-Georgiou

(1989) and Fontaine and Potter (1989) focused on estimating basin-average rainfall depths

for a specified duration. They did not develop or include procedures to include the temporal

distribution of rainfall within the storm. This step is needed for rainfall-runoff modeling and

hydrograph generation. The input to a rainfall-runoff model such as TREX is in the form of

rainfall hyetographs or mass curves. There are several ways of distributing basin-average

storm rainfall depths over time. The method that is used as part of this research is

normalized mass curves (Huff, 1967; Koutsoyiannis and Foufoula-Georgiou, 1993) using

DAD storm data and radar data. Franchini et al. (1996) used mass curves from Huff (1967)

to distribute basin-average depths from SST in the Midwest.

Normalized mass curves are obtained using DAD data by: (1) dividing the cumulative

storm depth d at time t by the total storm depth; and (2) dividing the time t by the total storm

time (e.g., Koutsoyiannis and Foufoula-Georgiou, 1993). Examples of these curves for two Colorado Front Range storms (June 1921 and May 1894) are shown in Figure 6.3. The curves Huff (1967) developed were applicable for heavy storms in Illinois on areas ranging up to 400 mi^2. An average relationship was used for areas of 50 to 400 mi^2. Based on the two storms shown in Figure 6.3, this assumption might be appropriate for these area sizes. However, for larger-area storms and watersheds, the assumption does not hold for storm areas greater than 1,000 mi^2 depending on the individual storm (Figure 6.3a). There are several data-based approaches to correct this problem. One way is to conduct data-based modeling with the database described in Chapter 4 and develop probabilistic relations (e.g., Huff, 1967) for two area sizes (e.g., 10 to 1,000 mi^2 and greater than 1,000 mi^2). A second technique that may be used is by resampling the DAD tables in discrete form from a database at fixed area sizes. A further improvement that could be attempted, depending on the amount of available data, is to segregate by storm type.

Others have presented alternative methods for estimating temporal distributions, such as self-similar (simple scaling) models (e.g., Koutsoyiannis and Foufoula-Georgiou, 1993), random cascades (e.g., Over and Gupta, 1996) and multifractal disaggregation (Lovejoy and Schertzer, 1995; Harris et al., 1996). These methods are not pursued here, but could potentially be investigated as part of future research.
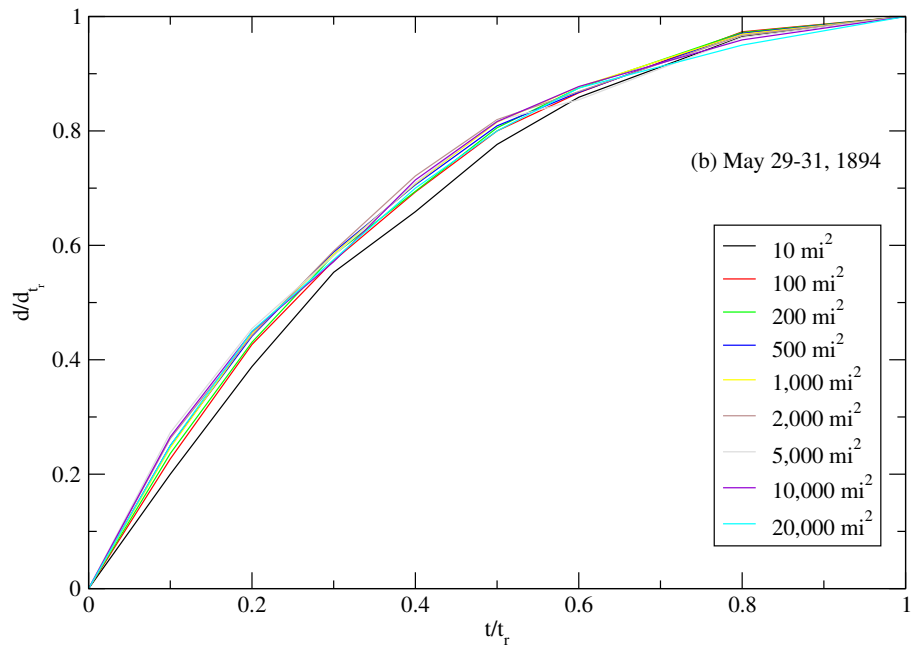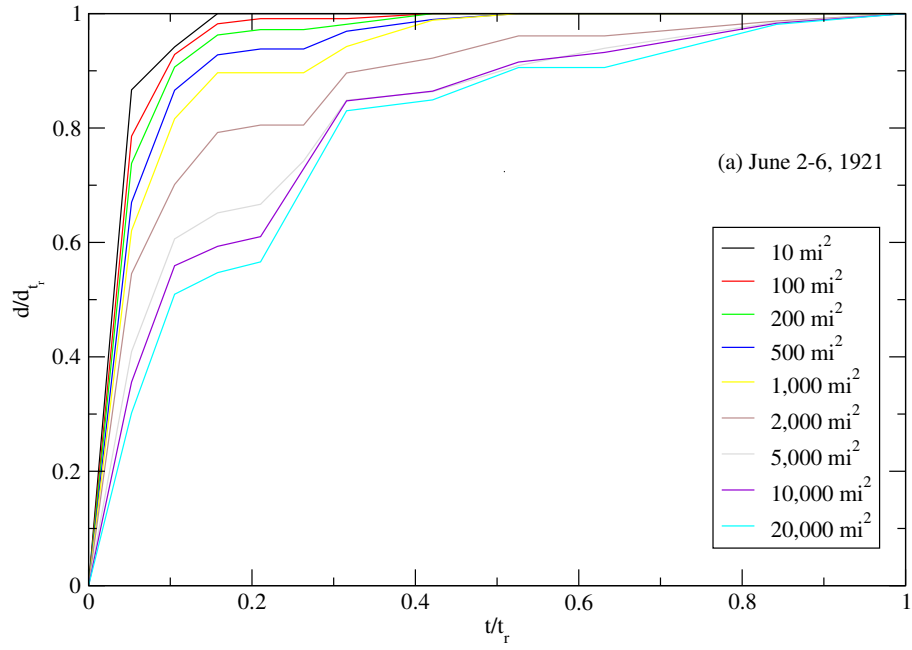
Figure 6.3. Normalized mass curves from DAD data for: (a) June 2-6, 1921 (SW1-23) storm; and (b) May 29-31, 1894 (MR6-3) storm.

6.4   EXTREME STORM MODELING RESULTS AND DISCUSSION

Extreme storm DAD data (Chapter 4) were used to implement the SST model.

Several simplifying assumptions were made in order to demonstrate the main concepts and

estimate extreme storm probabilities for application to the Arkansas River basin. The

criterion for storms to be transposed, using equation (6.3), is:

$$Criterion\ E: \quad \{\bar{d}[\Delta t = t_r,\ A = 10\,mi^2] \geq 11.0\,in.\} \quad (6.24)$$

which means that the storm set is composed of storms that had a maximum observed 10 mi^2

total depth over the whole storm duration (t_r) exceeding 11 inches. Wilson (1989) and

Foufoula-Georgiou (1989) used similar criteria for selecting and transposing storms in the

Midwest. Based on this criterion, fifteen storms are identified and selected from the 77

extreme storms (Chapter 4); these storms are listed with pertinent properties in Table 6.1.

Sensitivity of estimated basin-average depth probabilities to this criterion is discussed below.

A storm transposition region A_{tr} for the Arkansas River basin was selected based the

DAD data (Chapter 4) and hydrometeorological analyses in Hansen et al. (1988), and

encompasses the area between the Continental Divide (CD) and the 103rd meridian (CD-103).

The 397,200 mi^2 region includes parts of eight states, and also includes the Arkansas River

study watershed (Figure 6.4). One important feature of this region is the CD boundary and

the location of the study watershed on the western edge of the region. The basin orography

and CD boundary play a major role in estimating the spatial distributions of extreme storm

centers and storm areas within the region and the watershed. The region also has an irregular

shape, being long and relatively narrow. This geometry can affect the selection of a storm

center location distribution, such as the bivariate spatial model described in Section 6.2.4.

Table 6.1: Fifteen Extreme Storms from DAD Catalog Transposed to Arkansas Watershed

Date	Assignment No.	Location	State	Duration (hours)	Orientation (degrees)	total 10mi^2 depth	max 24hr 10mi^2 depth	areal extent mi^2	Ellipse c
05/30/1935	MR 3-28A	Cherry Creek	CO	24	47	22.20	22.20	6,300	4.0
09/20/1941	GM 5-19	McColleum Ranch	NM	78	16	21.20	12.10	38,000	3.5
05/30/1935	MR 3-28AZoneA	Hale	CO	24	32	21.20	21.20	1,291	2.0
05/04/1969	19690504bemCO	Big Elk Meadow	CO	96	14	18.21	11.83	5,000	2.0
06/13/1965	SW 3-23	Plum Creek	CO	181	5	18.10	13.20	39,266	1.5
09/27/1923	MR 4-23	Savageton	WY	108	46	16.90	9.50	95,000	2.5
06/06/1964	NP 2-23	Gibson Dam	MT	36	141	16.40	14.90	12,096	2.0
06/17/1921	MR 4-21	Springbrook	MT	108	38	15.10	13.30	52,600	1.0
06/09/1972	MR 10-12	Rapid City	SD	12	172	14.90	14.90	2,000	2.0
06/06/1906	MR 5-13	Warrick	MT	54	90	13.30	10.20	40,000	1.2
07/21/1905	GM 3-13	Elk	NM	108	80	13.10	5.70	44,000	1.5
06/12/1949	R7-2-5	Prospect Valley	CO	36	63	13.00	9.10	360	2.0
06/02/1921	SW 1-23	Penrose	CO	114	0	12.00	12.00	1,000	2.5
07/27/1997	19970727ftcCO	Fort Collins	CO	32	0	12.00	10.00	1,000	2.0
07/31/1976	19760731bgtCO	Big Thompson	CO	4	25	11.70	11.70	50	3.5

The spatial occurrence of storm centers was assumed to be a homogeneous Poisson

process. Given the limited number of storms used, and their geographic centers (Figure 6.1),

this assumption means that storm transposition probabilities are equal within A_{tr}, and are

independent of storm properties. The spatial model for all depths then is reduced to that of

equation (6.18), and Λ_p consists of *(x,y)* with uniform probabilities in space. This

simplification was also made by Foufoula-Georgiou (1989) and Franchini et al. (1996), and

is sufficient for providing initial estimates of basin-average rainfall depth probabilities for

subsequent runoff modeling.

The temporal occurrence model of extreme storms was simplified to a Bernoulli

process with a success probability p_s and estimated by:

$$\hat{p}_s = \frac{N_s}{N} \quad (6.24)$$

where N_s is the number of extreme storms, and N is the number of years of record. Based on

the DAD storm data presented in Chapter 4, $\hat{p}_s$ is 0.144 with N_s=15 and N=104 years
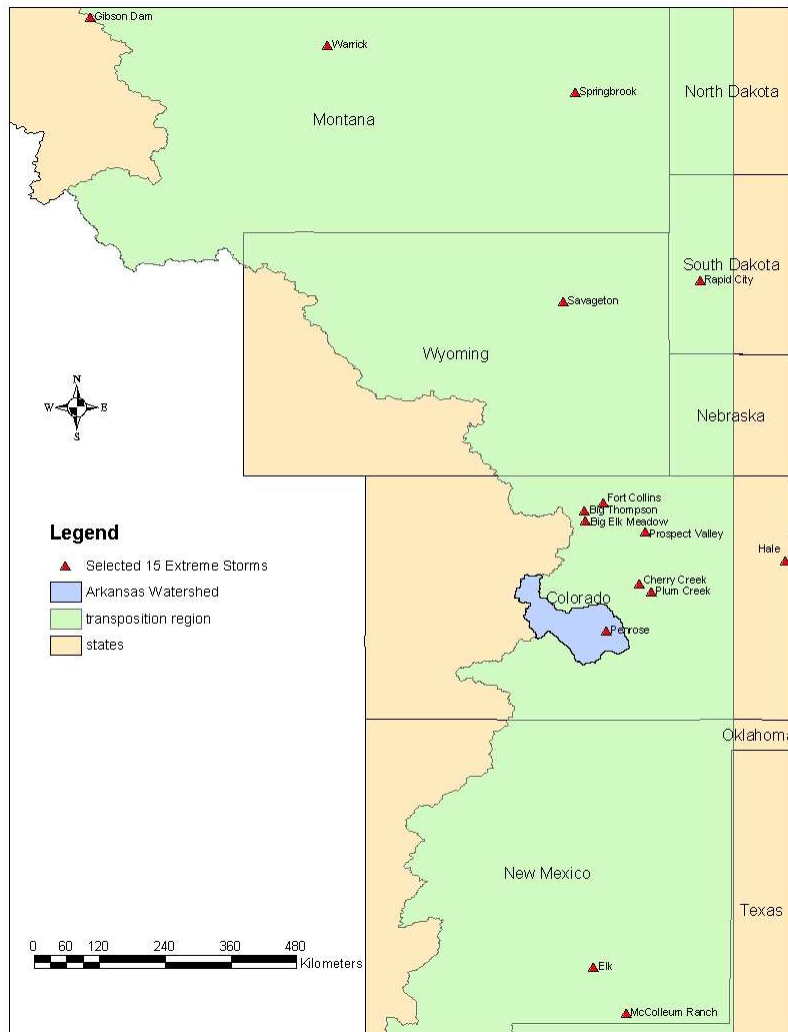
(1894-1997).

Figure 6.4. Storm transposition region and spatial distribution of the 15 selected extreme storms.

The joint estimation of storm properties Λ_s was simplified to a summation over all storms sampled, rather than integration of the pdf over each property. In this way, the stochastic storm transposition was employed using the actual storm properties for duration, orientation, areal extent, and ellipse parameters (Table 6.1). Spatial and temporal properties from each observed storm were used directly in the summation. This assumption results in the following simplification of equation (6.10) for annual exceedance probabilities, following Foufoula-Georgiou (1989):

$$G^a(d) = p_a(\bar{d}_c \geq d) = \hat{p}_s \sum_{j=1}^{N_s} \hat{p}_j \left(\bar{d}_c \geq d \right) \left(\frac{A_{eff,j}}{A_{tr}} \right) \quad (6.25)$$

where $A_{eff,j}$ is the effective area of the jth storm, A_{tr} is the transposition region, and

$p_j(\bar{d}_c \geq d)$ is the probability for the jth storm that the average depth over the catchment is greater than some value d. This probability value is determined by simulating each observed storm j 1,000 times uniformly within the effective area, using a 960m grid cell resolution over the $A_{eff,j}$ domain.

The major factors in (6.25) are the number of storms N_s, $\hat{p}_s$ and $A_{eff,j}$. The effective area is defined as the area within which the storm must be centered and still cover at least one point within the catchment (Wilson and Foufoula-Georgiou, 1990). This is a crucial definition that allows the probability estimation to include extreme rainfall depths for storms centered outside the catchment that partially cover or fully cover the watershed. The storm

effective area changes every time a new storm is simulated over the watershed. Previous

investigators (e.g., Foufoula-Georgiou, 1989; Wilson and Foufoula-Georgiou, 1990) used

simple shapes for storms and catchments, such as circles, ellipses, triangles and rectangles,

and were able to use analytical methods to estimate the catchment-storm interaction. Here, a

new approach was developed using numerical methods to account for the actual basin

geometry and interaction with each storm elliptical pattern. Using the June 1921 storm as an

example, the orientation, areal extent and ellipse parameter c dictate the intersection between

the watershed and the storm (Figure 6.5). By placing the storm footprint at every watershed

cell, one obtains the storm-dependent effective area. This area is a combined image of the
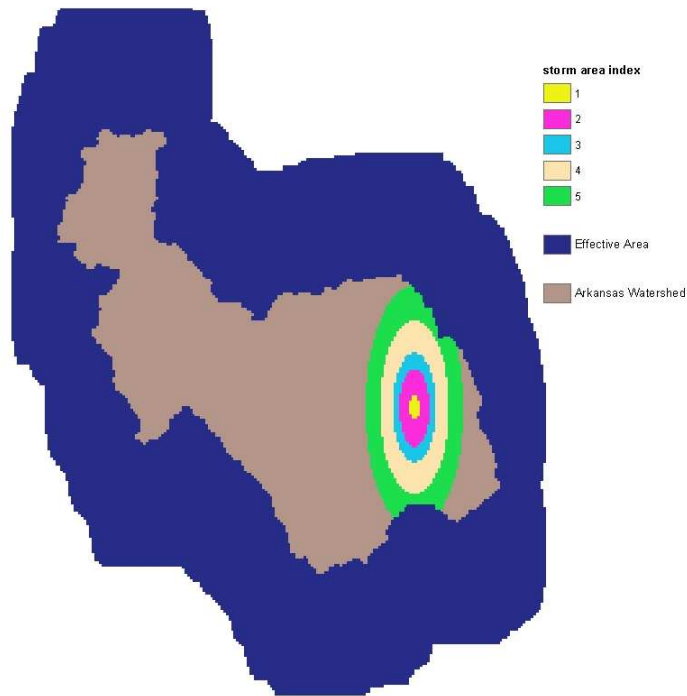
watershed and storm geometries.

Figure 6.5. Example effective storm area determined from the intersection of the June 1921 storm and the Arkansas watershed.

Based on the assumptions stated above, basin-average depth probabilities for the 15 storms are estimated and combined using (6.25). The results of the simulation are shown in Figure 6.6. The shape of the basin-average depth distribution is generally similar to that obtained for 1,000 mi^2 (Foufoula-Georgiou, 1989) and 2,000 mi^2 (Wilson, 1989) hypothetical circular watersheds in the Midwest. The upper tail of the distribution is also similar in shape to Fontaine and Potter (1989) and Wilson and Foufoula-Georgiou (1990). This upper tail shape is due primarily to the limited storm sample, the use of fixed storm parameters, and interactions of the storms with the watershed. The lower part of the distribution appears to give relatively large average depths for this watershed. For a 0.01 annual probability, the basin-average depth is 7.0 inches; this value appears high compared to NOAA Atlas II published point rainfall information. This is a result of the extreme storms used in the analysis. Their extreme space-time characteristics result in large depth estimates for more common probabilities. For subsequent runoff modeling, the rainfall distribution is truncated for AEPs greater than 0.01. The depth distribution does encompass the design basin average rainfall estimate for Pueblo Dam (10.52 inches in 27 hours over 2,000 mi^2), but falls short of the PMP general storm basin average depth estimate (13.71 inches in 72 hours over 4,686 mi^2). An alternative shape for the upper tail is considered below as part of sensitivity.

A sensitivity was performed to demonstrate the effects of the number of storms, number of simulations, storm locations, and storm area sizes. The procedure to estimate A_{eff} was modified to enable limiting storm center locations based on location. The flood runoff

characteristics within the Arkansas River basin indicate that the transition zone between

rainfall-runoff and snowmelt runoff is near Parkdale (Chapter 4). Based on the flood

hydrology, distribution of extreme storm center locations with elevation, and storm radar

investigations (Javier et al., 2005), it is hypothesized that extreme storm centers are restricted

to locations east of Parkdale. This assumption reduces the effective area (Figure 6.7). It is

also hypothesized that there are restrictions to the size of extreme storms that can occur in the

Arkansas watershed. The most extreme storms that have occurred immediately adjacent to

the foothills, such as the June 1921 Penrose storm, the July 1976 Big Thompson storm and

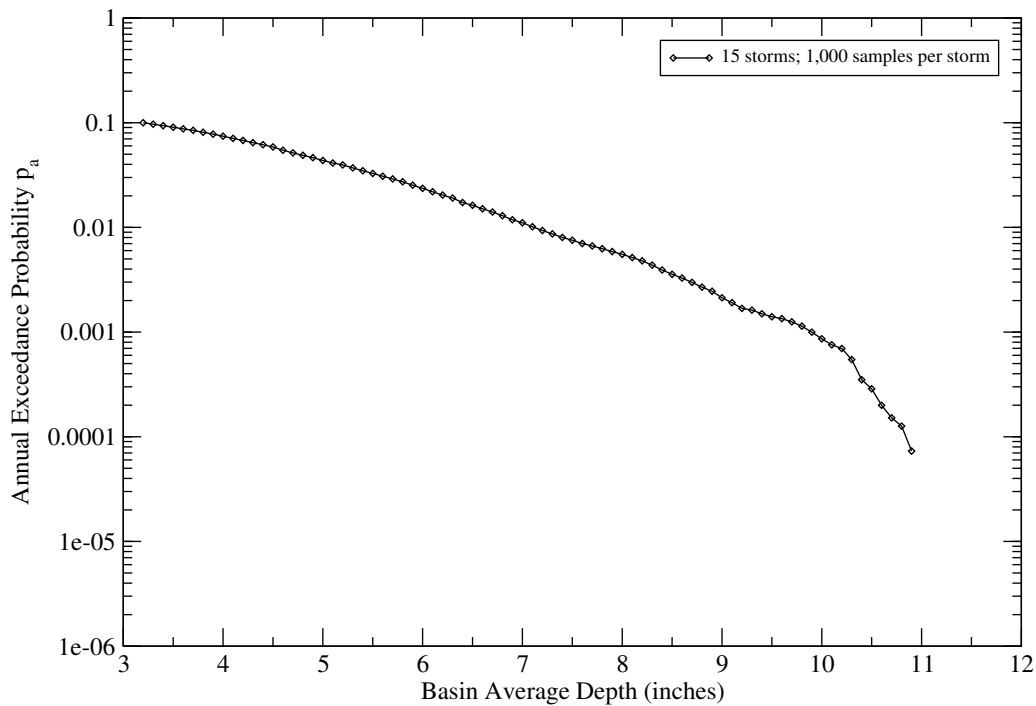the July 1997 Fort Collins storm, occurred over areal extents less than 5,000 mi^2.

Figure 6.6. Annual exceedance probability of the average rainfall depth d_c over the Arkansas River watershed.

The sensitivity of the probability distribution of storm depths was determined for four cases. The first was to increase the number of extreme storms included in the analysis from 15 to 20, and to increase the number of simulations from 1,000 to 10,000. The second case was to restrict the storm centers to locations east of Parkdale. The third and fourth cases were to restrict the storm center locations and to restrict the maximum storm area to 5,000 mi^2 and 2,000 mi^2, respectively. Results of these simulations are shown in Figure 6.8.
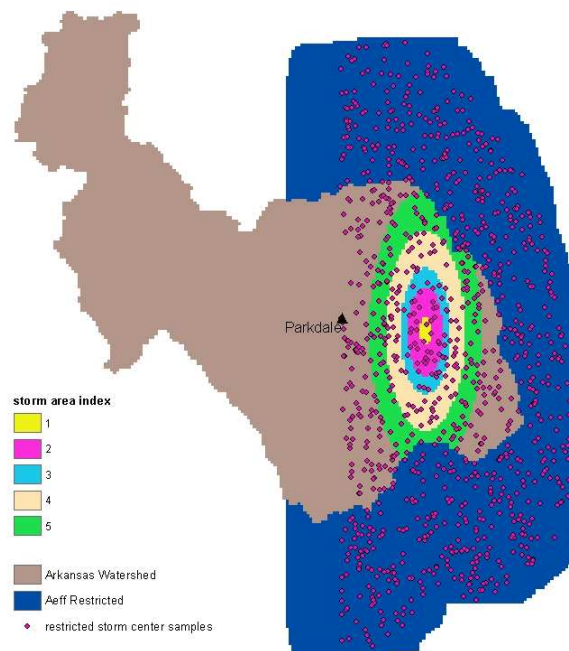
Figure 6.7. Example restricted effective storm area determined from intersecting the June 1921 storm and the Arkansas watershed, and limiting storm centers west of Parkdale; 1,000 simulated centers shown.

Increasing the number of storms from 15 to 20 shifts the distribution to more frequent probabilities for the lower magnitude depths. The results indicate that increasing the number of simulations has little effect; the shape is nearly identical to the base case with 15 storms and 1,000 simulations. The restriction of storm centers results in a shifted frequency

163

distribution to smaller exceedance probabilities, due to a reduction of A_{eff} by about a factor of two (Table 6.2). The extreme tail of the distribution also drops more quickly, but predicted maximum depths are about the same. A restriction on storm areas has the largest effect on the probability distribution. The distributions are shifted much lower, by over an order of magnitude for the 2,000 mi^2 case, and maximum depths are dramatically reduced. The shape of the upper tail for all the simulated cases is approximately similar. This suggests that the simulated distributions are a function of the total depth, duration, orientation, and estimated shape storm characteristics from the actual storms used in the analysis. These factors should be investigated as part of future research.
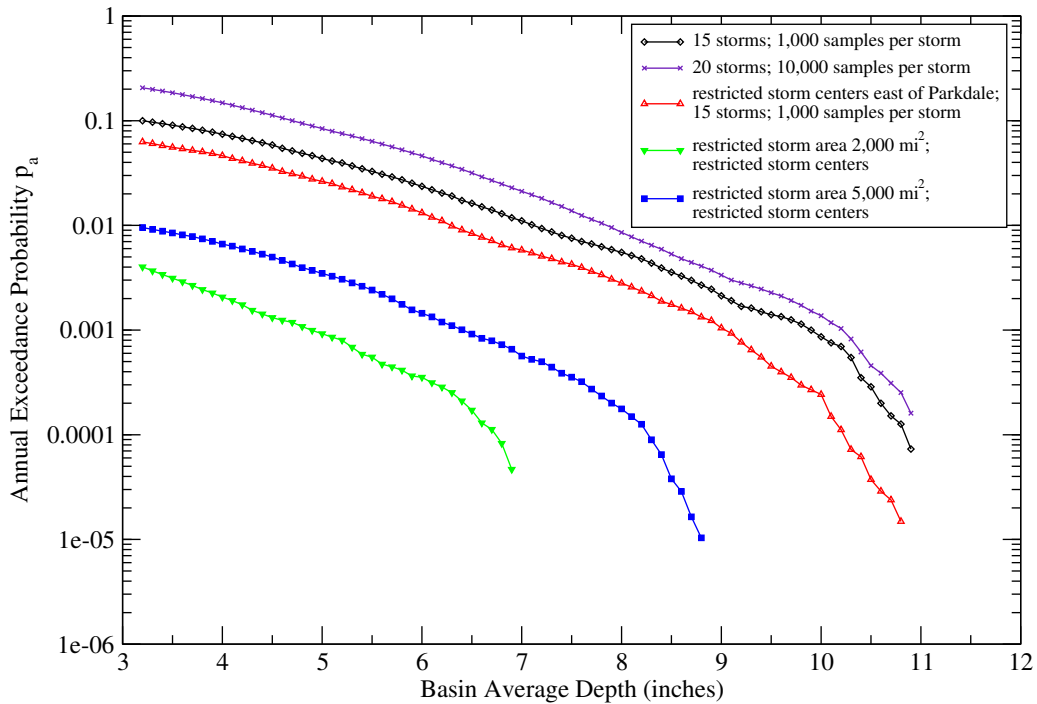

Figure 6.8. Sensitivity of the annual exceedance probability of the average rainfall depth d_c over the Arkansas River watershed due to number of extreme storms, restricted storm center locations, and restricted storm areas.

Table 6.2: Sensitivity of Effective Area Estimates for Restricted Storm Centers and Storm Areas

Assignment No.	Simulated Storms		Restricted Storm Centers West of Parkdale		Restricted Storm Centers West of Parkdale and Storm Areas Limited to 5,000 mi^2		Restricted Storm Centers West of Parkdale and Storm Areas Limited to 2,000 mi^2	
	Aeff (km^2)	Aeff/Atr	Aeff (km^2)	Aeff/Atr	Aeff (km^2)	Aeff/Atr	Aeff (km^2)	Aeff/Atr
MR 3-28A	105,591.4	0.103	56,668.3	0.055	47,833.8	0.046	27,371.5	0.027
MR 3-28AZoneA	40,456.4	0.039	18,221.9	0.018	18,221.9	0.018	18,221.9	0.018
GM 5-19	286,011.2	0.278	191,908.5	0.187	44,387.9	0.043	25,844.4	0.025
19690504bemCO	73,805.4	0.072	39,851.8	0.039	39,851.8	0.039	23,086.1	0.022
SW 3-23	219,303.0	0.213	150,522.2	0.146	34,109.3	0.033	34,109.3	0.033
MR 4-23	537,095.6	0.522	305,152.8	0.297	40,058.3	0.039	23,367.2	0.023
NP 2-23	106,270.6	0.103	64,369.2	0.063	37,176.4	0.036	22,024.4	0.021
MR 4-21	210,591.1	0.205	103,666.2	0.101	25,880.4	0.025	16,810.0	0.016
MR 10-12	45,050.6	0.044	22,843.7	0.022	22,843.7	0.022	22,843.7	0.022
MR 5-13	189,742.7	0.184	116,066.3	0.113	26,818.6	0.026	17,272.6	0.017
GM 3-13	240,497.0	0.234	143,526.3	0.140	30,258.9	0.029	18,677.1	0.018
R7-2-5	25,682.2	0.025	10,281.4	0.010	10,281.4	0.010	10,281.4	0.010
SW 1-23	36,035.5	0.035	16,528.0	0.016	16,528.0	0.016	16,528.0	0.016
19970727ftcCO	36,035.5	0.035	16,528.0	0.016	16,528.0	0.016	16,528.0	0.016
19760731bgtCO	16,624.7	0.016	6,388.5	0.006	6,388.5	0.006	6,388.5	0.006

The SST sensitivity indicates that the critical factors are storm center locations and the distribution of storm areas. Basin average depth and probability estimates for the base case and restricted cases are subsequently used in runoff modeling to explore runoff prediction sensitivity to the depth and probability estimates. Because a limited sample of storms were used, and can potentially affect the upper tail of the rainfall distributions, we briefly explore alternative shapes. The main portions of the rainfall frequency curves appear to be similar to a Normal distribution (Figure 6.9) based on plotting the functions on probability paper. Alternative tail distributions are postulated as straight lines (Figure 6.9); these give much larger AEPs for a specific depth. The sensitivity of the flood peak distributions to these different tails are subsequently examined in Chapter 7.
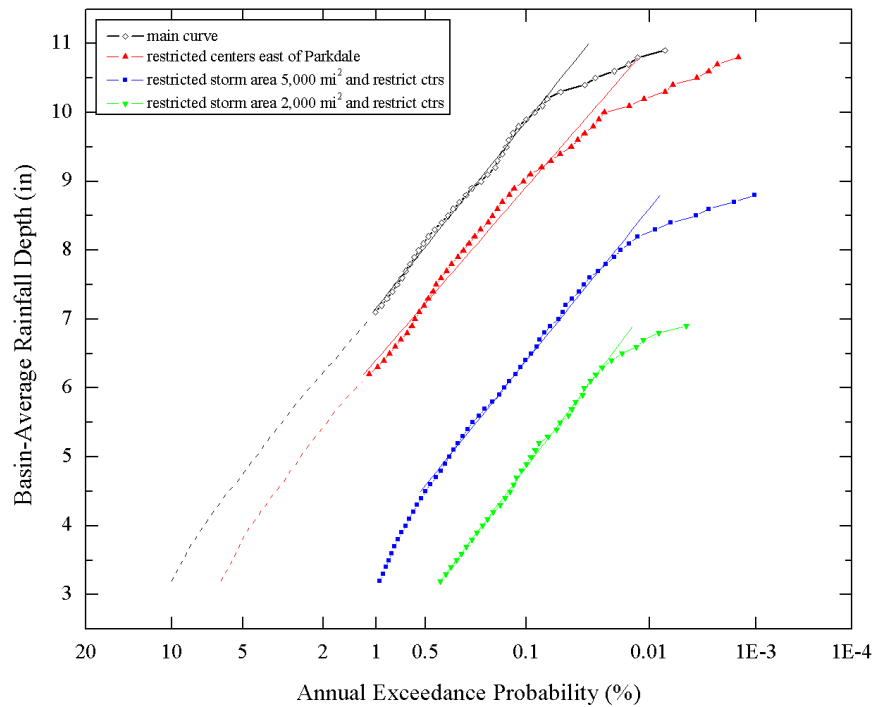
Figure 6.9. Postulated alternative tail (Normal) distributions for basin-average rainfall depth probability curves. Dashed lines represent more frequent, less accurate estimates that are not used in runoff modeling.

6.5   SUMMARY

A stochastic storm transposition model was presented to estimate basin-average rainfall depths and probabilities. The spatial distributions of storms were described as an elliptical pattern with major to minor axis ratio c, orientation θ and storm center (x_s, y_s). Temporal distributions were estimated using mass curves. Two new features were developed and implemented to extend the SST method: a numerical procedure to determine the effective area for an arbitrary-shaped watershed rather than simple geometric shapes (circles); and a restriction on storm center locations to account for basin orography. The SST

166

method was applied for the first time to a large, orographic region and to an actual watershed, rather than a hypothetical one. Actual storms were used in the simulation to estimate extreme basin average rainfall depth probabilities. Fifteen storms were selected and used in the stochastic storm generation based on a criterion that the storm had a maximum observed 10 mi^2 depth exceeding 11 inches in the region. A limited sensitivity analysis demonstrated that the effects of restricting storm centers and storm areas are important on the basin-average depth frequency curve. These factors had not been previously examined by others. Further research efforts in stochastic storm transposition are needed to investigate impacts of storm center, orientation, duration and ellipse parameters of storms, and their interactions with watersheds. The current SST model that was implemented and applied to the Arkansas watershed should eventually be improved by completing further DAD data analysis and simulating storms using Monte Carlo techniques.

Chapter VII

DERIVED FLOOD FREQUENCY WITH TREX

This chapter presents an application of the TREX model to the Arkansas River basin. The focus is a new application of the model to a large watershed and demonstration that the model can be used to provide flood frequency estimates. The input data for the Arkansas watershed are presented. Model calibration and validation results for the two largest flood events are discussed, and the model ability to simulate extreme floods on a large watershed is shown. New model features, including spatial channel properties, and extreme storms, are demonstrated. It is shown that the model can be used to develop a flood frequency curve. Performance of the model for flood frequency estimation and comparisons to a streamflow and paleoflood data-based peak-flow frequency curve are made. A sensitivity analysis of selected hydrologic and hydraulic factors is conducted.

7.1   MODEL INPUTS

As part of this research, TREX has been applied to the Arkansas River above Pueblo, Colorado. The available data within the Arkansas River watershed were presented in Chapter 4. Here, the focus is on TREX model parameter estimation and calibration. An

elevation grid, obtained and processed from the USGS National Elevation Data set (NED), was used as the base for the watershed hydraulic routing. A 960 m grid cell size was used in the modeling to capture spatial variability and for faster model run times (Figure 7.1). The number of active grid cells in the 11,869 km^2 watershed is 12,879. Based on this elevation grid, channels were derived using a 100 cell area threshold for initiation; this resulted in 764 defined channel cells and 69 links.
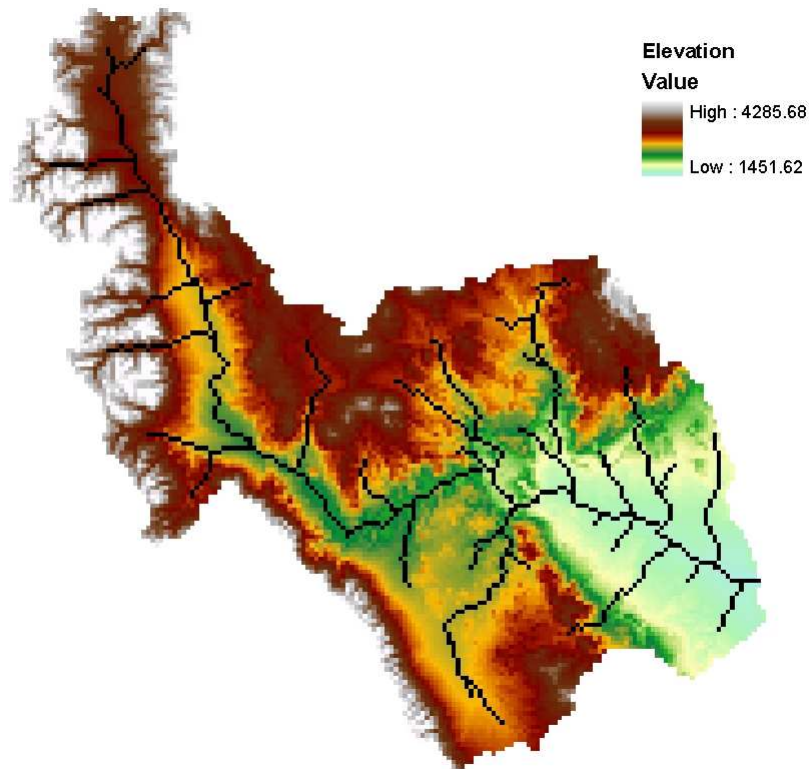

Figure 7.1. Elevation grid (960 m) and channel cells for modeling the Arkansas River basin upstream of Pueblo.

A field reconnaissance was conducted within the Arkansas River basin on July 26-30, 2004 to locate paleoflood study sites and estimate river channel dimensions at select locations. Channel base width and bank height properties were measured at 20 locations

within the watershed (Table 7.1). As in Orlandini and Rosso (1998), and many others, power

functions were fit based on drainage area to estimate channel base width (Figure 7.2) and

bank height (Figure 7.3) in space. Widths ranged from 11 to 57 m; a spatial map is shown in

Chapter 3. Bank heights ranged from 0.9 to 3.1m. A rectangular channel shape (sideslope z

=0) and sinuosity equal to 1.0 were assumed. Manning n was assumed constant throughout

the network.

Table 7.1: Channel Width and Bank Height Measurements in the Arkansas River Basin

| Location	Drainage Area (km^2)	Floodplain Width (m)	Floodplain Bank Height (m)
Cottonwood Creek at Mouth	168.35	12.19	0.82
Chalk Creek near Nathrop (CODWR gage)	251.23	19.81	1.22
Texas Creek at Mouth	372.96	15.54	0.91
South Arkansas River near Salida (CODWR gage at mouth)	538.72	21.03	2.07
Badger Creek at Mouth	546.49	17.37	1.52
Beaver Creek at Mouth	554.26	38.1	1.52
Grape Creek near Westcliffe	828.80	24.38	1.37
Arkansas River at Granite (CODWR gage)	1,105.93	34.44	1.52
Fourmile Creek at Mouth	1,124.06	16.76	1.83
Arkansas River near Howard Lakes	1,437.45	25.6	1.52
Arkansas River at Buena Vista (near former USGS gage)	1,582.49	24.38	3.05
Arkansas River near Nathrop (USGS gage)	2,745.40	27.43	3.66
Arkansas River at Adobe Park	2,991.45	50.29	1.65
Arkansas River at Salida (CODWR gage)	3,154.62	44.5	1.22
Arkansas River at Swissvale (near Wellsville, u/s Badger Creek)	3,846.15	27.25	3.26
Arkansas River at Loma Linda	4,817.40	38.1	1.83
Arkansas River at Texas Creek	5,439.00	70.71	1.68
Arkansas River at Parkdale gage	6,599.32	41.45	3.05
Arkansas River in Royal Gorge upstream from Grape Creek	6,734.00	41.76	2.53
Arkansas River at Pueblo State Park	11,564.35	60.96	3.66
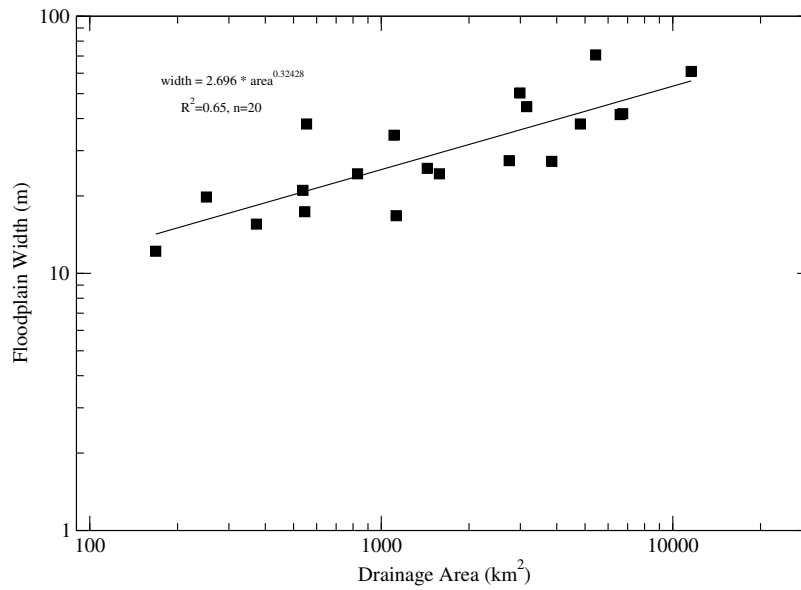
Figure 7.2. Spatial channel width estimation from Arkansas River basin data.
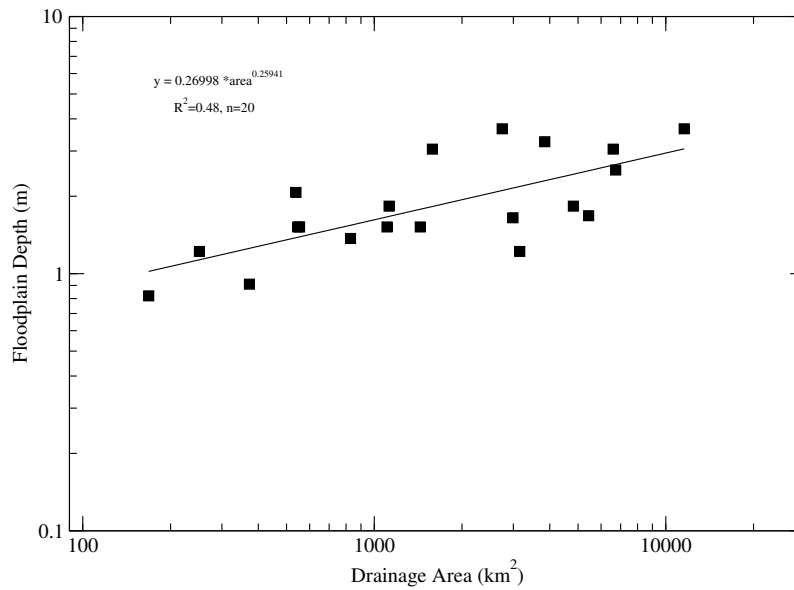

Figure 7.3. Spatial channel bank height estimation from Arkansas River basin data.

The remaining model parameters to be estimated included Manning *n* for overland

flow, and Green-Ampt parameters for effective porosity θ_e, effective suction head ψ,

saturated hydraulic conductivity K_s and effective soil saturation S_e. Overland Manning n

roughness values were estimated by correlation with USGS National Land Cover Data set

(NLCD) land classes based on Engman (1986). Nine land use classes were used (Figure

7.4). Green-Ampt parameters were estimated based on the STATSGO soils database and the

equations presented in Chapter 3. Eighteen soils classes were used (Figure 7.5).
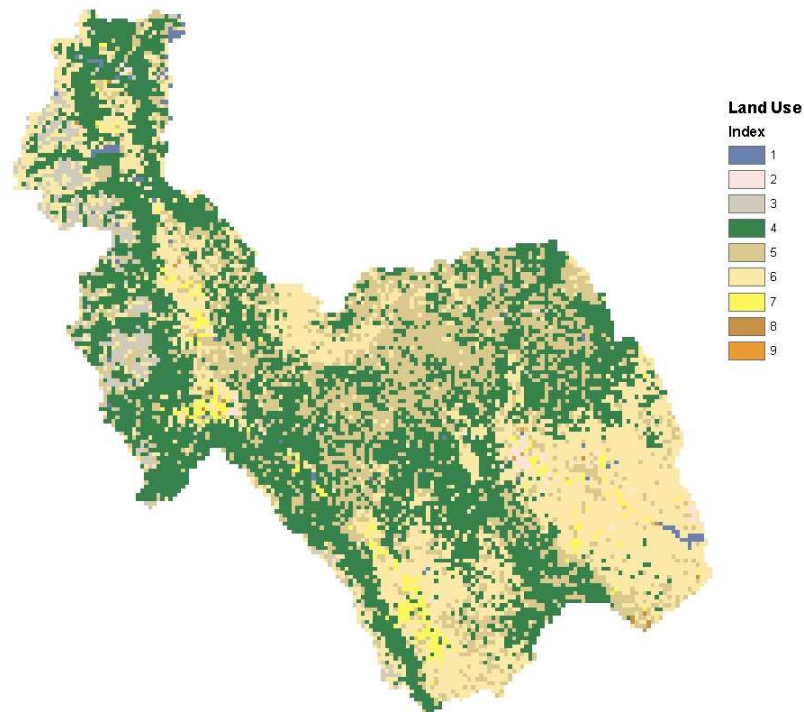
Figure 7.4. Spatial Manning n overland flow index map. Classes are listed in Table 7.3.

The remaining model inputs consisted of time step selection and rainfall. Constant

time steps equal to 2.5 and 5 seconds, depending on rainfall inputs, were used to ensure

computational stability for model simulations. Storm rainfall based on the DAD data for

extreme storms (Chapter 4) was used as rainfall input. These storms usually have rainfall

depths specified in 6-hour increments for various fixed area sizes. The spatial distribution of

each storm was represented with an ellipse (Chapter 3).
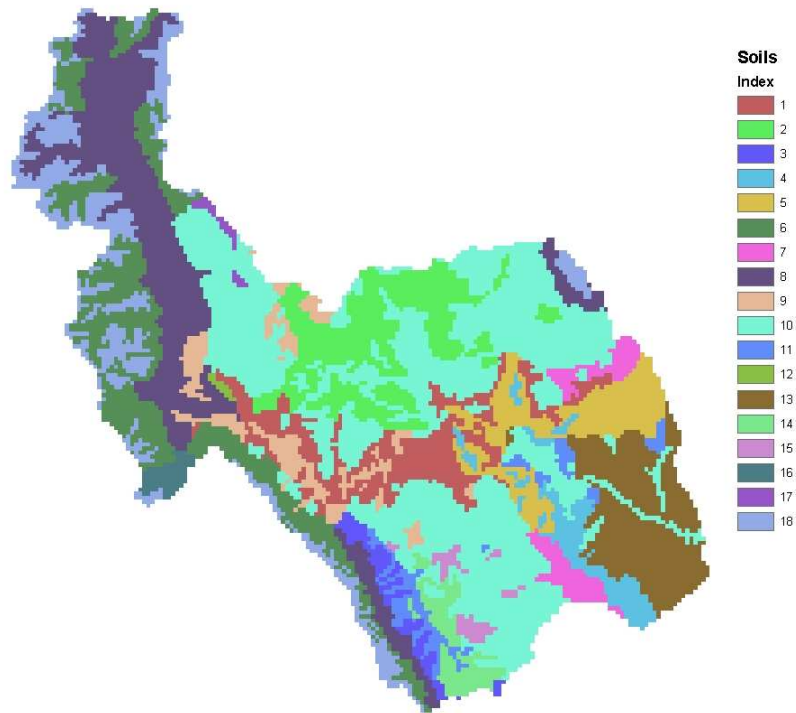
Figure 7.5. Spatial Green-Ampt parameter index map. Classes are listed in Table 7.4.

7.2   CALIBRATION AND VALIDATION TO LARGEST OBSERVED FLOODS

The criteria used for calibration and validation were peak discharge, runoff volume, and time to peak of flood hydrographs. The parameters that were used to calibrate the model were Manning *n* for overland cells and channel segments, saturated hydraulic conductivity, and initial soil moisture.

The June 3-4, 1921 storm was selected for TREX model calibration. This flood is the largest on record in the Arkansas River basin near Pueblo, and resulted in at least 78 deaths (Follansbee and Jones, 1922). The rainfall amounts, hydrometeorology and flood runoff of

this extreme event are principally described in Munn and Savage (1922) and Follansbee and

Jones (1922), and exceeded 12 inches. Rainfall estimates are used from USACE (1945-) and

Hansen et al. (1988). Mass curves for the storm are shown in Figure 7.6; storm total isohyets

are shown in Figure 6.1 of Chapter 6. The peak flow from this flood is estimated to be

between 83,500 ft^3/s and 103,000 ft^3/s, depending on the timing of tributary flow from Dry

Creek (Follansbee and Jones, 1922). It was shown that the peak flow of this flood has a

return period between about 150 and 1,000 years (Chapter 5). The calibration runoff data for

this event are based on a table and descriptions by Munn and Savage (1922, p. 10):

> "The main part of the flood started at 5:00 pm on June 3rd, and totaled more than 78,000 acre-feet in the following 18 hours. At 10:30 am June 4th, the river was still flowing 40,000 second-feet, as estimated by Mr. Hosea. There is, however, no information on which to base an accurate estimate of the volume added after this time. It is probable that fully 20,000 acre-ft was added and that the main part of the flood, starting at 5:00 pm June 3, and ending some time during the night of June 4th, totaled about 100,000 acre-ft."

Their estimated data for the June 3-4 hydrograph are shown in Figure 7.7.
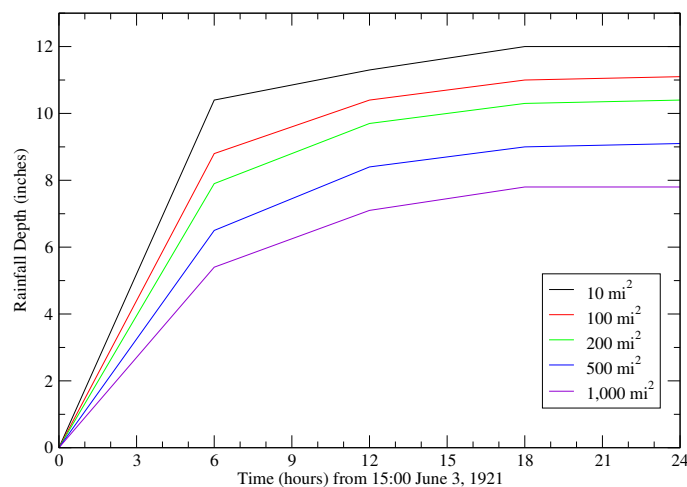
Figure 7.6. Mass curves for the June 1921 storm.

The results of the calibration are shown in Figure 7.7. The model does a good job at matching the peak, volume and time to peak (Table 7.2). The shape of the model hydrograph is considered good given the uncertainty in the data. Model results, consisting of rainfall rate, water depth, and cumulative infiltration, are shown for selected time steps in Figures 7.8 through 7.10. Based on this calibration, the model can successfully be used to simulate extreme floods on large watersheds on the order of 12,000 km^2.
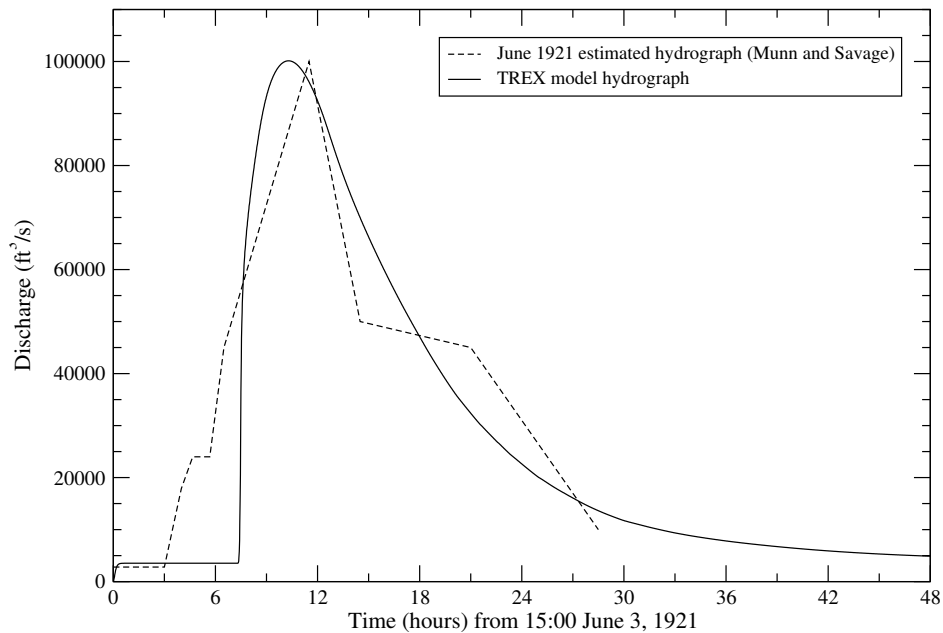
Figure 7.7. June 1921 extreme flood hydrograph and TREX model calibration.

Table 7.2: Calibration Results for the June 1921 Flood

Hydrograph	Peak Discharge (ft^3/s)	Runoff Volume (acre-ft)	Time to Peak (hours)
Observed	100,000	100,000	11.5
TREX Model	100,200	105,600	10.3
Percent Difference	0.2	5.6	-10.5
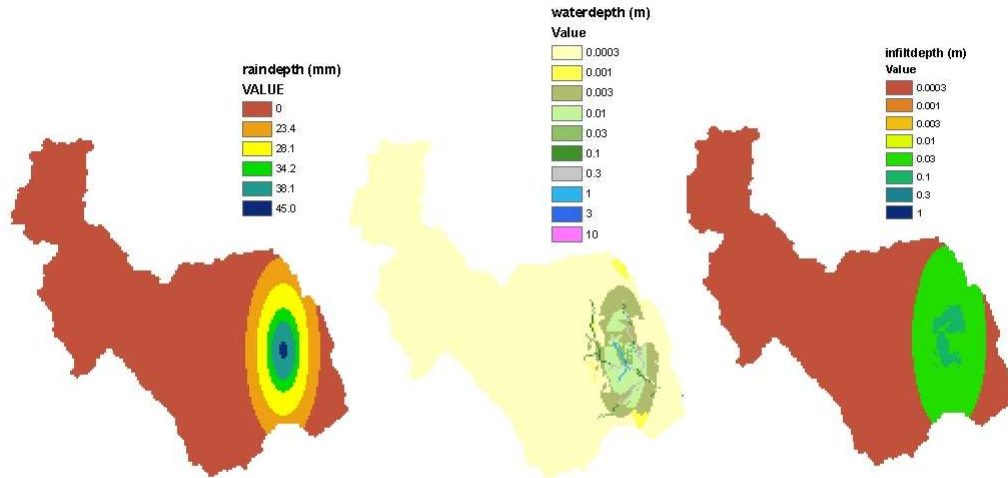
Figure 7.8. Cumulative rainfall, surface depth, and cumulative infiltration results at 3.5 hours.
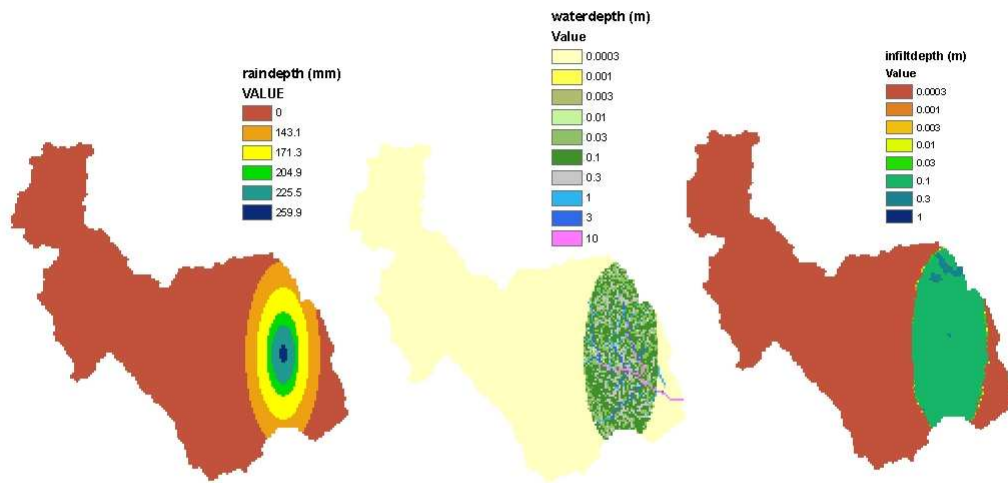
Figure 7.9. Cumulative rainfall, surface depth, and cumulative infiltration results at 10.3 hours (at peak).
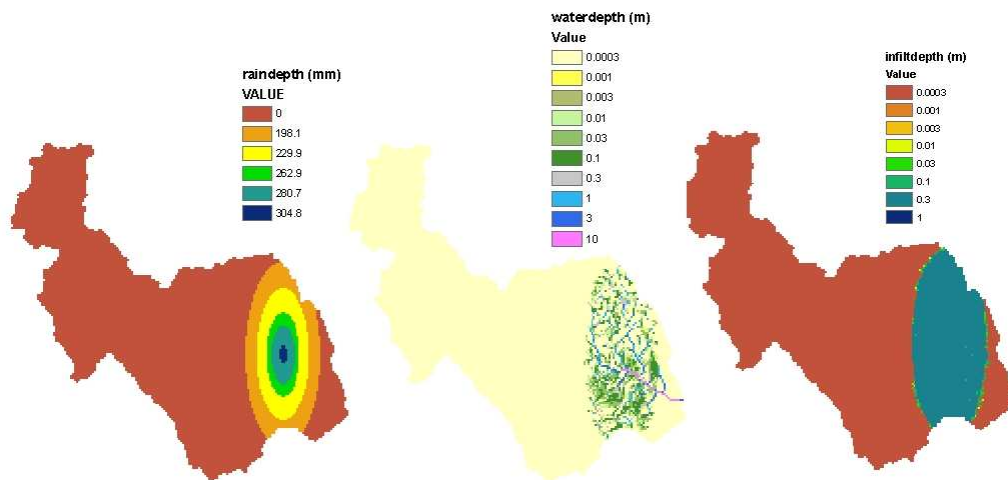
Figure 7.10. Cumulative rainfall, surface depth, and cumulative infiltration results at 24 hours.

Calibrated estimates of spatially varying Manning *n* (Table 7.3) and spatially varying

infiltration parameters (Table 7.4) are within published ranges (Engman, 1986; Rawls et al.,

1983). A calibrated Manning *n* for channels was set equal to 0.050. This value is within the

range of published estimates in Colorado (Jarrett, 1985).

Table 7.3: Calibrated Manning *n* Estimates for Overland Flow Grid Cells

| Map No.	Land Use Class No.	USGS NLCD Land Use Class Name	Calibrated Manning *n*	Percent of Watershed
1	11	Open Water; Perennial Ice/Snow	0.07	0.71
2	21	Low Intensity Residential; High Intensity Residential; Commercial/Industrial/Transportation	0.02	0.60
3	31	Bare Rock/Sand/Clay; Quarries/Strip Mines/Gravel Pits; Transitional	0.03	3.14
4	41	Deciduous Forest; Evergreen Forest; Mixed Forest	0.52	42.07
5	51	Shrubland	0.59	22.85
6	71	Grasslands/Herbaceous	0.20	28.36
7	81	Pasture/Hay	0.46	2.09
8	82	Row Crops; Small Grains; Fallow	0.21	0.15
9	85	Urban/Recreational Grasses	0.33	0.04

The model was validated with rainfall and runoff from the May 31, 1894 flood. This

flood caused the third largest estimated peak flow on the Arkansas River at Pueblo (Chapter

5), and was the most destructive flood in the history of the Arkansas valley prior to June

1921 (Follansbee and Jones, 1922 p. 38). Rainfall data for this event were obtained from

Reclamation files and the U.S. Army Corps of Engineers catalog for storm MR6-14 (Chapter

4). Mass curves of rainfall for the storm are shown in Figure 7.11. This storm was of lower

intensity and longer duration than June 1921. Flood flow for this event is based on estimates

Table 7.4: Calibrated Green-Ampt Infiltration Parameters for Overland Flow Grid Cells

Soils No.	USDA Texture Class from STATSGO Database	Porosity ϕ (cm³/cm³)	Effective Porosity θ_e (cm³/cm³)	Effective Saturation S_e	Effective Suction Head ψ (cm)	Saturated Hydraulic Conductivity K_s (cm/hr)	Percent of Watershed
1	very bouldery sandy loam	0.363	0.455	0.1	27.72	0.3	6.22
2	cobbly loam	0.437	0.450	0.1	20.76	0.48	7.89
3	very cobbly sandy loam	0.321	0.407	0.1	19.03	0.57	1.36
4	clay loam	0.528	0.426	0.1	27.42	0.2	2.61
5	channery loam	0.464	0.418	0.1	22.63	0.4	4.99
6	fine sandy loam	0.465	0.411	0.1	12.58	1.2	9.73
7	gravelly coarse sandy loam	0.377	0.352	0.1	23.75	0.3	2.03
8	gravelly sandy loam	0.446	0.415	0.1	20.24	0.5	12.83
9	very gravelly loam	0.498	0.463	0.1	30.54	0.22	3.40
10	very gravelly sandy loam	0.431	0.400	0.1	29.81	0.21	28.52
11	loam	0.473	0.408	0.1	26.21	0.25	1.98
12	loamy sand	0.472	0.422	0.1	7.44	4.38	0.13
13	silt loam	0.491	0.413	0.1	34.97	0.13	6.97
14	sandy loam	0.528	0.460	0.1	7.75	3.93	1.84
15	stony sandy loam	0.448	0.399	0.1	10.74	1.57	0.75
16	very stony loam	0.165	0.470	0.1	20.64	0.52	0.71
17	very stony sandy loam	0.257	0.418	0.1	16.17	0.91	0.31
18	extremely stony loam and extremely stony sandy loam	0.050	0.408	0.1	31.41	0.18	7.73

published by the USGS at Canon City (staff gage read twice daily), and a peak flow estimate

(39,100 ft³/s) made by the Pueblo city engineer using slope-conveyance with a cross section

just upstream of Pueblo.
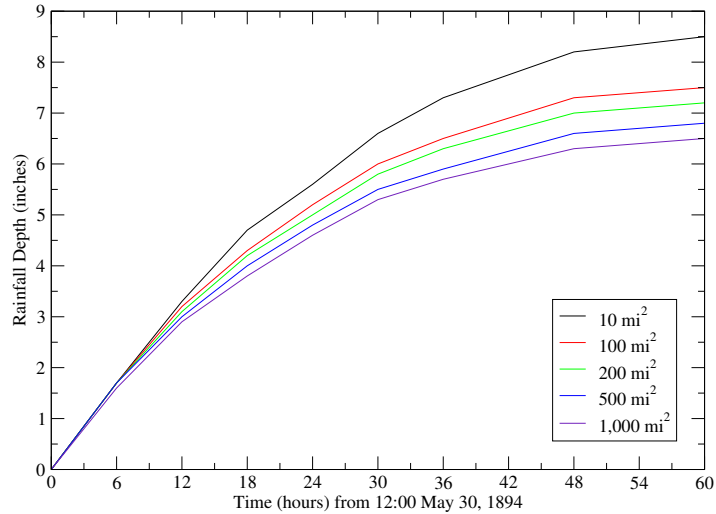
Figure 7.11. Mass curves for the May 1894 storm.

The validation results are shown in Table 7.5 and Figure 7.12. The initial soil

moisture was increased so that the model matched the observed runoff data. All other

parameters retained their calibrated values. The model does a fairly good job at matching the

peak flow, approximate time to peak and total runoff volume (Table 7.5), within the

uncertainty of the data. Given the storm rainfall, the validation run balances matching the

peak flow at Pueblo and the runoff volume at Canon. If the modeled peak flow at Pueblo

were to increase, this would also increase the runoff volume at Canon City. The other factor

in the validation run is the potential errors in rainfall inputs. Fontaine (1995) shows that

errors in precipitation data are the primary source of uncertainty in calibrating rainfall-runoff

models for extreme floods. As the rainfall input data are inexact for this storm, changes in

the rainfall forcing can have an effect on the validation.

Table 7.5: Validation Results for the May 1894 Flood

Variable	Canon City			Pueblo		
	Observed	**Model**	**Percent Difference**	**Observed**	**Model**	**Percent Difference**
Peak Discharge (ft^3/s)				39,100	35,100	-10
60-hour Volume (acre-ft)	18,460	20,300	9.9			
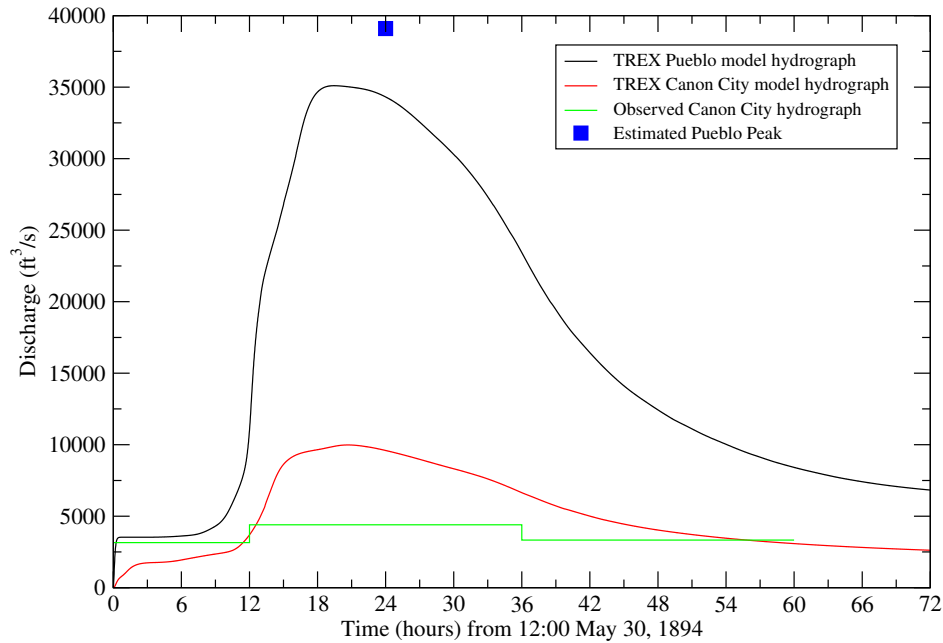
Figure 7.12. May 1894 extreme flood hydrographs and TREX model validation.

7.3   PEAK-FLOW FREQUENCY ESTIMATION WITH EXTREME STORMS

The calibrated and validated model was then used to estimate a flood frequency curve. The inputs to the model were storms used in stochastic storm transposition (Chapter 6). Basin-average depths were selected for specified annual exceedance probabilities in the general range of 0.01 to 0.0001. The lower limit (0.01) was chosen because the SST results suggested that depths at more frequent probabilities were not reliable (Chapter 6). Storms

were then constructed to distribute the basin-average rainfall depths in space and time over

the watershed. Because a simplified SST methodology was implemented to estimate a

rainfall depth frequency curve based on actual storms, an actual storm is used as input to

TREX. The following storm properties are considered fixed: storm center location,

orientation, storm area, ellipse parameter, spatial and temporal distributions. The storm that

contributed the largest depths in the SST (NP2-23, June 1964) was selected as the base

pattern. This storm covers 12,096 mi^2, has an orientation of 141°, $c = 2.0$ and the duration is

36 hours. The center was transposed to just west of Parkdale, and the storm spatial

distribution covers the entire Arkansas River watershed (Figure 7.13). The orientation most

likely optimizes flood runoff production, as the major axis is nearly in line with the river in
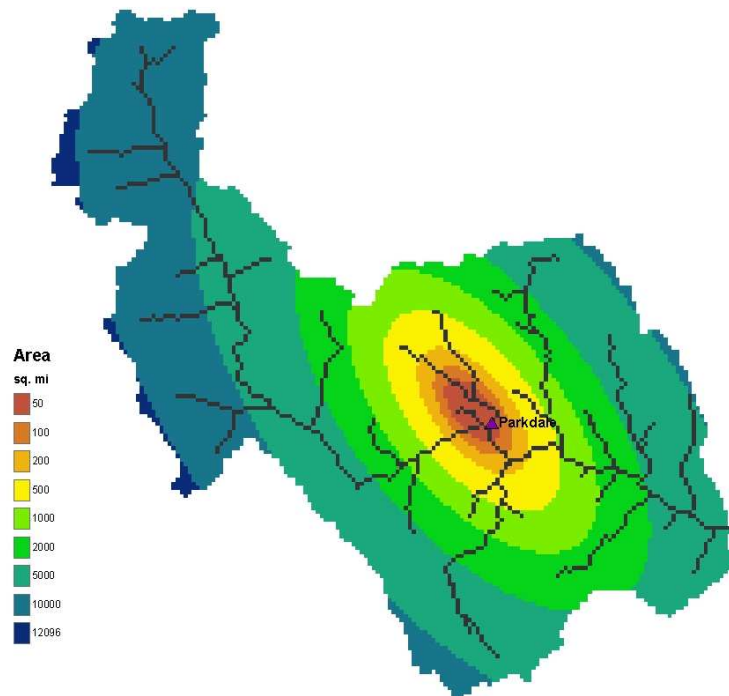
the lower watershed.

Figure 7.13. Spatial storm pattern for TREX model runs and flood frequency.

The input to the TREX model for flood frequency consisted of the storm with area

amounts adjusted to meet the target basin-average depth, and the calibrated model

parameters. The initial soil saturation was set to 0.5 for each run. The flood frequency curve

was then determined by selecting rainfall depths from the basin-average rainfall frequency

curve and running the TREX model for each specified depth. In this way, the peak-flow

probabilities are conditioned on the rainfall depth probabilities, as the inputs are held

constant except for the rainfall depth, so the rainfall term contributes to the peak flow

distribution (equation 3.24 in Chapter 3). The complete rainfall depth frequency curve is

discretized into sixteen points for subsequent runoff modeling. The computer time to

complete 16 TREX model runs for the rainfall depths ranged from five to 16 hours,

depending on model inputs.

A flood frequency curve is estimated based on the model inputs, storm and rainfall

depths. The main basin-average depth rainfall probability distribution (Chapter 6) is used as

the input. The rainfall curve and resulting TREX flood frequency curve are shown in Figure

7.14. The flood frequency curve has the same overall shape as the rainfall frequency curve.

The main portion of each distribution from 1 to 0.1 percent is nearly Normal; the tails of both

distributions flatten. The rainfall tail behavior was discussed in Chapter 6; clearly the

rainfall distribution upper tail affects the shape of the peak-flow frequency curve. Flood

frequency curves at Salida, Wellsville, Parkdale and Pueblo are shown in Figure 7.15. The

reduction in peak flow magnitude from downstream to upstream is readily apparent.
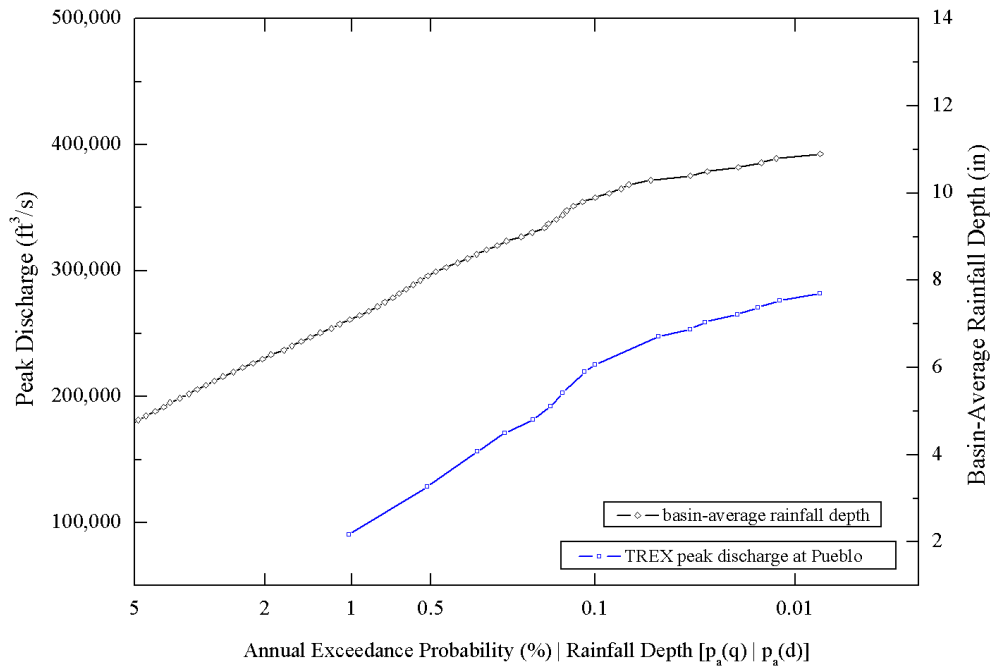
Figure 7.14. Flood frequency curve at Pueblo from TREX with corresponding SST basin-average depth main curve.
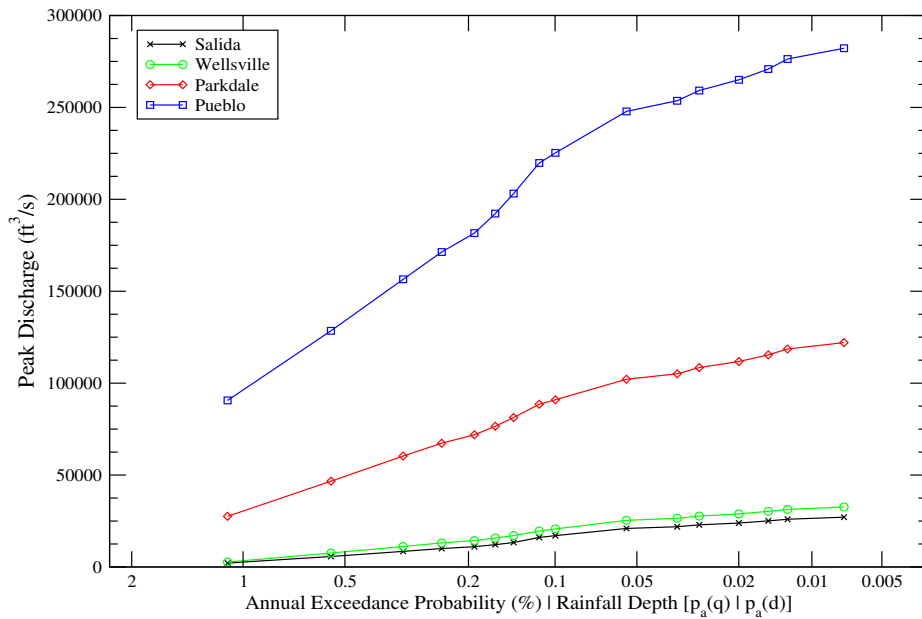
Figure 7.15. Flood frequency curves at Pueblo, Parkdale, Wellsville and Salida from TREX.

183

The spatial rainfall distribution and storm center location are the principal factors in the

relatively dramatic reduction of peak flows from downstream to upstream sites. Runoff

hydrographs for the largest simulated rainfall depth (basin average 10.9 inches) that has an

estimated AEP of 0.00007 are shown in Figure 7.16. The hydrograph shapes indicate that

the model is stable and can simulate extreme floods on watershed of this scale. It has been

demonstrated that the model can be used to estimate a flood frequency curve. Model

predictions can now be compared to data-based flood frequency curves. Sensitivity analysis

is conducted to examine the effects of some factors on model predictions.

Figure 7.16. Runoff hydrographs for the largest simulated rainfall depth at four locations in the watershed.

7.4   MODEL AND PALEOFLOOD DATA-BASED PEAK-FLOW FREQUENCY

COMPARISONS

The TREX model flood frequency curves at four locations (downstream to upstream),

Pueblo, Parkdale, Wellsville and Salida, are compared with LP-III peak-flow frequency

curves based on streamflow, historical and paleoflood data (Chapter 5). Here we are

interested in the differences in flood frequency shapes, if the TREX model-generated
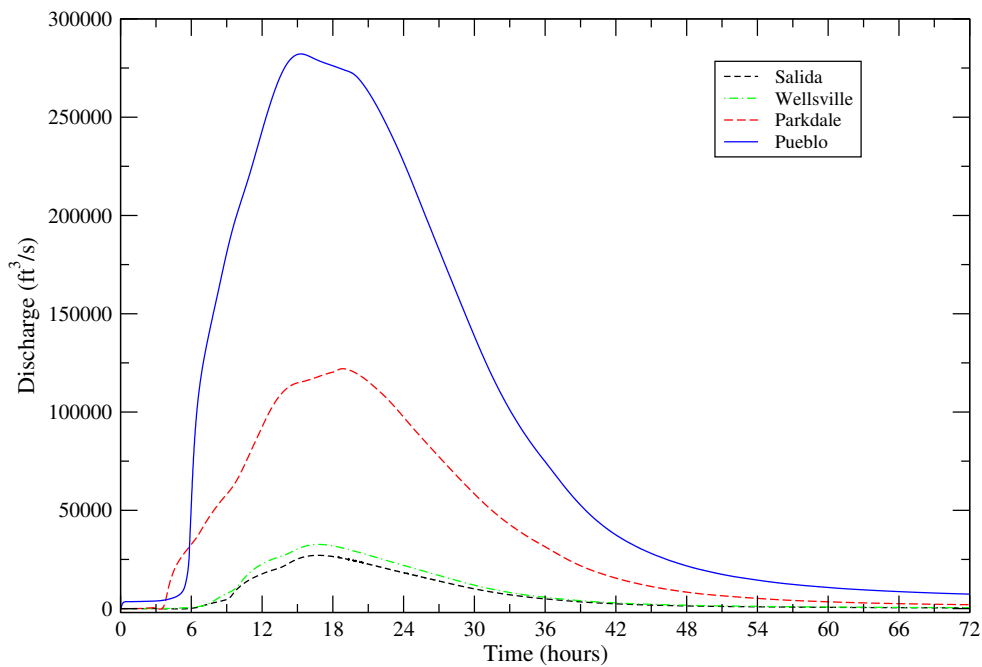
frequency curve matches the LP-III curves, if it falls within the confidence intervals, and if it

matches magnitudes and plotting position estimates of the largest floods and paleofloods.

The basic concept for making the comparisons is that the TREX model flood frequency

curve should be "consistent" with the gage, historical and paleoflood peak flow estimates.

The frequency curves for the four sites are shown in Figure 7.17. LogNormal

probability paper is used for the graphical comparison; the color and symbol for each TREX

frequency curve corresponds to that shown in Figure 7.15. Recall that from Chapters 4 and

5, runoff mechanisms were distinguished between snowmelt (Salida and Wellsville) and

rainfall-runoff (Parkdale and Pueblo). The focus of these comparisons is thus in the lower

watershed at Parkdale and Pueblo as we are simulating runoff from extreme rainfalls.

Nevertheless, TREX flood frequency curves at the upper sites are compared to data-based

snowmelt-dominant frequency curves to see if the rainfall-runoff generated curves are much

larger than the snowmelt curves.

Figure 7.17. TREX model flood frequency and streamflow/paleoflood frequency curves at (a) Pueblo, (b) Parkdale, (c) Wellsville and (d) Salida. Based on SST main curve.

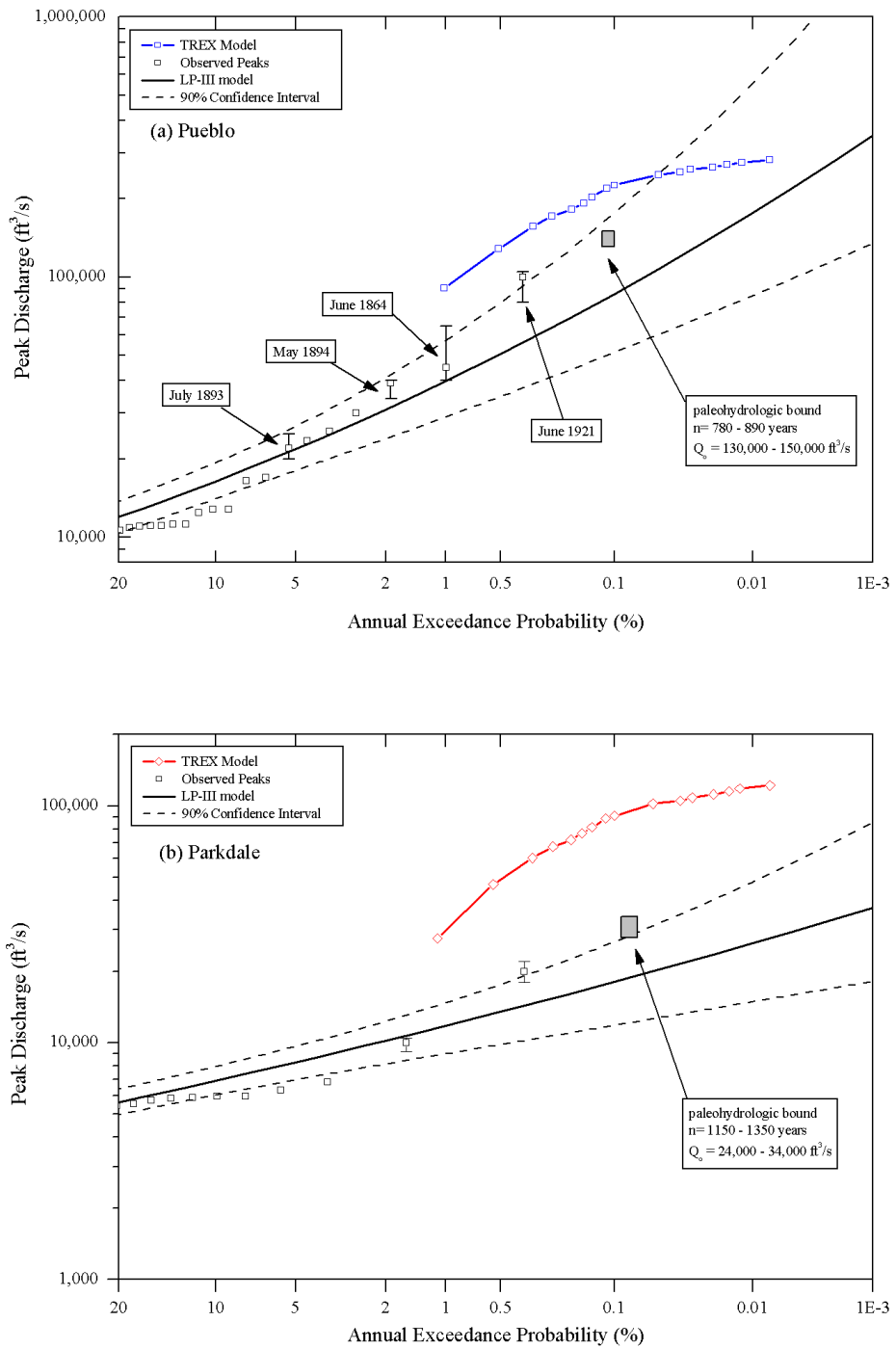**Figure 7.17 (continued).** TREX model flood frequency and streamflow/paleoflood frequency curves at (a) Pueblo, (b) Parkdale, (c) Wellsville and (d) Salida. Based on SST main curve.
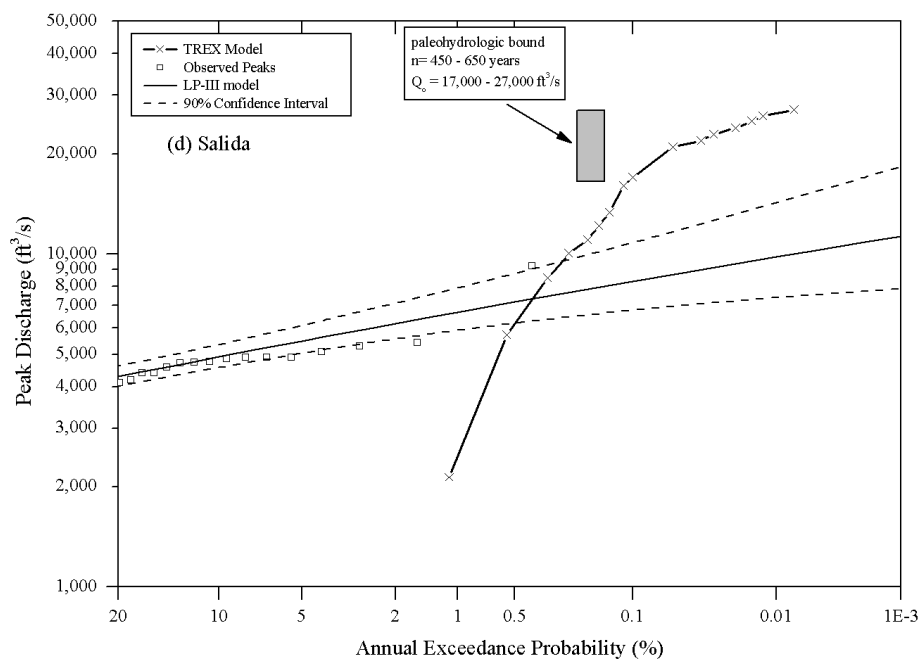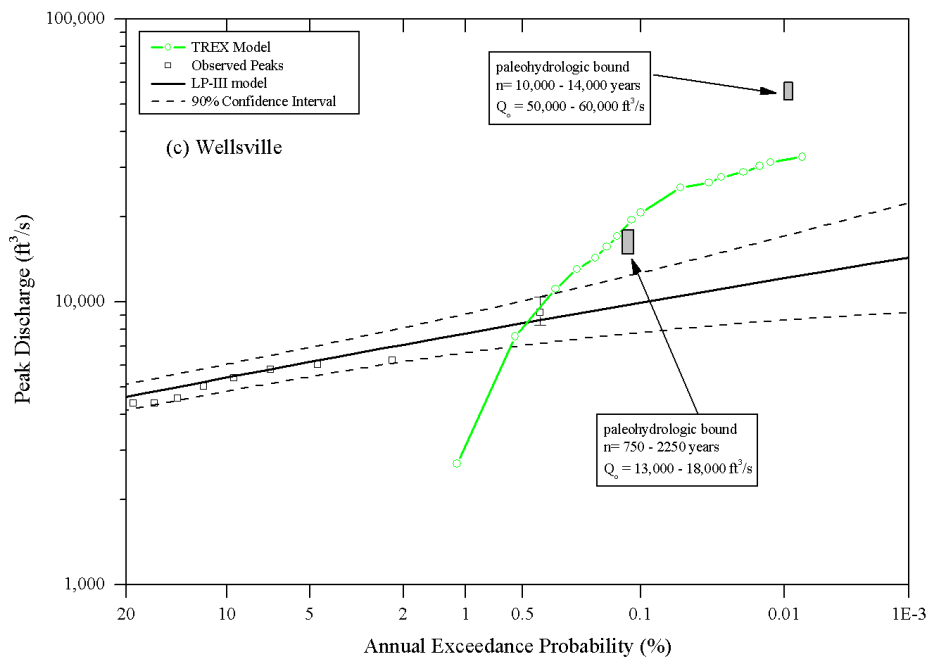
The comparisons indicate that the TREX flood frequency curves are larger than the data-based frequency curves at the four locations. At Pueblo, the upper tail of the TREX frequency curve is within the data-based confidence interval. This upper tail is directly related to the rainfall distribution. The impact of changing the rainfall frequency curve on the resulting flood frequency is conducted below as part of sensitivity analysis. The lower portion of the curve at Pueblo, as well as the entire curve at Parkdale, appears too high compared to the data. This suggests that the rainfall magnitudes and potentially the initial soil moisture might be too high. The shapes of the TREX flood frequency curves are also distinctly different than the positive-skewed data-based LP-III distributions; they have flatter slopes in the main portion of each curve and relatively flat tails. The curves at upstream locations (Wellsville and Salida) also have dramatically different shapes compared to the data-based frequency curves. The lower portions are much steeper, reflecting rainfall-runoff, and the upper portions clearly exceed the streamflow observations, but are consistent with the paleohydrologic bounds. Recall that paleohydrologic bounds are defined as a time interval where a given discharge has not been exceeded (Levish, 2002). At Wellsville, the TREX curve is close to the lower paleohydrologic bound, and is less than the 10,000-year paleohydrologic bound. At Salida, the curve is less than the paleohydrologic bound within the time frame of the bound. However, the curves at the upper sites are still much larger than any observation. This suggests that rainfall amounts in this part of the watershed are too large.

7.5   <u>SENSITIVITY ANALYSIS</u>

A sensitivity analysis was conducted to investigate the impacts of three main factors on the flood frequency curves: initial conditions, spatial distributions of storms, and storm temporal distributions. Frequency curve comparisons to data-based flood frequency curves are then revisited. TREX is then tested using Probable Maximum Precipitation inputs.

7.5.1   <u>Initial Conditions</u>

As discussed in Chapter 2, initial soil moisture conditions play an important role in runoff predictions, and can affect infiltration rate, peak and volume. The role of initial soil moisture in peak flow predictions is explored by changing the initial soil saturation S_e. The value used for the results shown above is 0.5, and represents a 50% saturation level across the watershed. Three saturation levels are chosen for sensitivity: 0.05 (dry), 0.2 (slight saturation) and 0.8 (near saturation). The initial soil moisture amounts were assumed to be uniform in space across the watershed domain.

The soil moisture sensitivity results are shown in Figure 7.18 for the three sensitivity cases as compared to the base case. In all runs, the main SST depth-average rainfall curve was used, and all other parameters were held constant. It is apparent that the soil saturation has a moderate to large effect on the predictions. The curves are shifted from the base run (shown in blue), but the frequency curves do not change shape substantially. The peak discharges and volumes (not shown) can increase by a factor of 1.24 to 1.41 for $S_e = 0.5$ to 0.8, or decrease by about 1.18 to 1.34 for $S_e = 0.5$ to 0.2. As rainfall (peak discharge)

increases, the change in initial soil moisture has less of an effect; larger percent differences are observed for the lower peaks. The slope of the curves change slightly. The amount of change for the largest floods with $S_e = 0.8$ to 0.05 is 1.58, and for the more frequent floods the ration with $S_e = 0.8$ to 0.05 is 2.15. Thus, the initial soil moisture does play a major role in flood peak predictions from TREX.
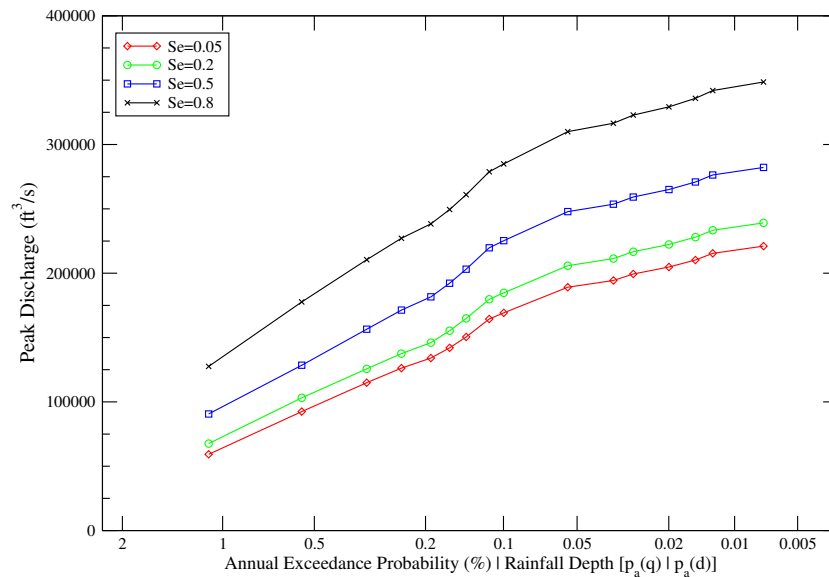
Figure 7.18. TREX model flood frequency curves at Pueblo with varying initial soil saturation *Se*.

7.5.2   Spatial Distributions of Storm Rainfall

The sensitivity of runoff peak flows to the spatial distribution of storm rainfall was explored by placing restrictions on the storm location, storm area, and storm pattern. Three experiments were performed. The first was to restrict the storm center (*x,y*) locations such that storm centers were allowed east of Parkdale. This restriction mimics what has been seen

in the historical record, where storms have centered near Penrose in the lower watershed.

The second experiment was to restrict storm centers to east of Parkdale and restrict storm

areas to 5,000 mi^2 or less. The third experiment was to restrict storm centers to east of

Parkdale, restrict storm areas to 2,000 mi^2 or less, and use a different extreme storm with

different properties (location, duration, orientation, and ellipse ratio). These experiments

correspond to the variations in SST rainfall depth frequency curves shown in Chapter 6, and

reflect conditions for some of the extreme storms in the database and the radar data (Chapter

4).

The results of the spatial distribution changes are shown in Figure 7.19. Each

frequency curve corresponds to an experiment; the base case is shown in black diamonds and

the curve colors and symbols match those in Figures 6.8 and 6.9 (Chapter 6). It is evident

that a restriction in the storm spatial distribution can significantly affect the peak flow

frequency curve shape. As the storm location within the watershed is restricted, and storm

areas reduced, the peak flow frequency curves shift to the right so that a given peak

discharge is less frequent. There is variability in frequency curve shape due to the shifts in

basin-average depth probabilities. The effective storm area reduction (described in Chapter

6) causes a reduction in flood probabilities; the tails of the distributions are extended. The

frequency curve for restricting storm areas to less than 5,000 mi^2 steepens (blue curve with

squares) because for a fixed basin-average rainfall, the depth is distributed over a smaller

area. The outer two ellipses of the storm pattern (Figure 7.13) are eliminated. The largest

reduction in flood peaks is due to restricting the storm area to 2,000 mi^2 and utilizing a

different storm pattern, as shown by the green line with inverted triangles (Figure 7.19. In

this case, the SW3-23 June 1965 storm was used as the rainfall pattern. The longer storm

duration (181 hours versus 36 hours for the main case) and areal reduction cause the

dramatic shift and reduction in flood peak discharge. These flood frequency curves mimic

the shapes of the rainfall frequency curves (Figure 6.8 in Chapter 6).
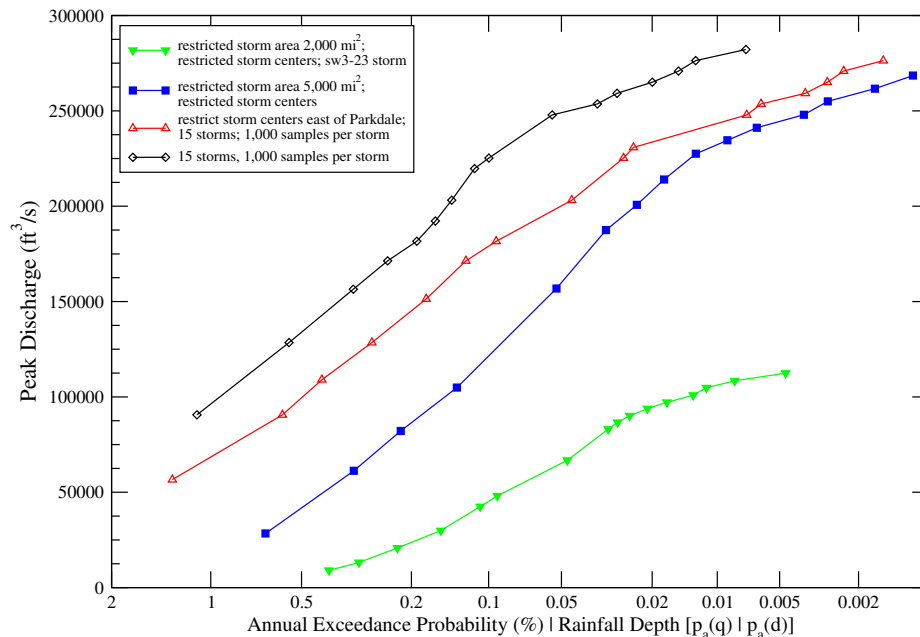
Figure 7.19. TREX model flood frequency curve at Pueblo with varying basin-average depth rainfall frequency.

7.5.3 Storm Duration and Temporal Distribution

In order to show effects of storm duration on the flood frequency curve, two

experiments are conducted with the 36-hour NP2-23 storm. The first experiment is to stretch

the existing storm from 36 hours to 48 hours, a factor of 1.33. In this way, each of the 6-hour rainfall amounts in the mass curves are extended by this factor. The second experiment is to change the within-storm temporal distribution. The existing storm temporal distributions for the nine area sizes are shown in Figure 7.20. All curves are very similar, and follow a "first quartile" distribution (Huff, 1967). This curve is then flipped to follow a "fourth quartile" storm. These two quartiles span the range of temporal distributions of large storms.
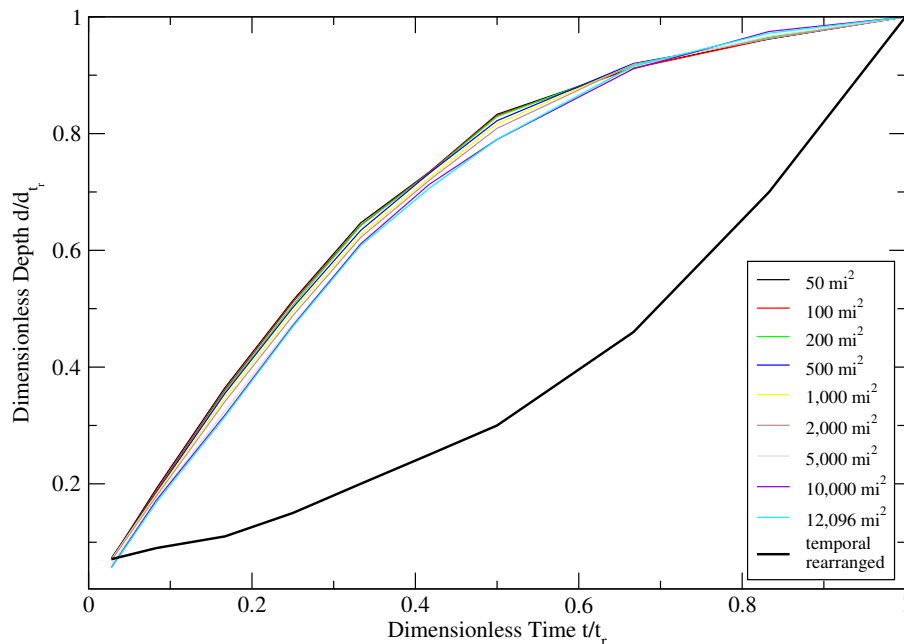
Figure 7.20. Rearranged temporal distribution of the 36-hour NP2-23 storm of June 1964.

The results of the two temporal distribution experiments are shown in Figure 7.21 with the base run (black line with diamonds). Given this storm, the rearrangement of the temporal distribution results in a minor decrease (7 to 9 percent) in peak flows; the curve

shifts slightly lower. The increase in storm duration has a much larger effect. Peak flows

decrease by factors between 1.46 and 1.66, and the slope of the frequency curve flattens,

especially at the upper tail.
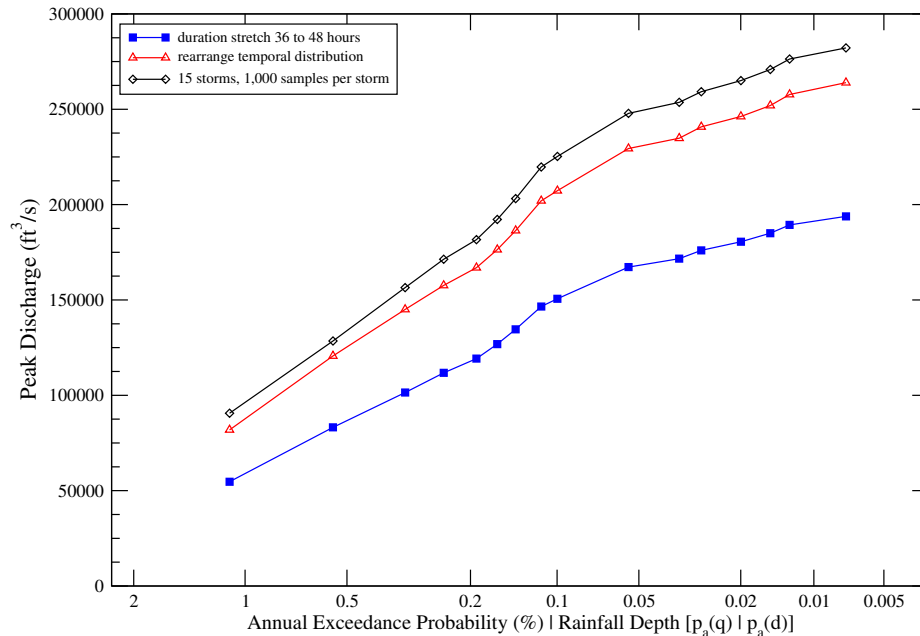
Figure 7.21. TREX model flood frequency curves at Pueblo with rearranged temporal distributions and stretched durations.

7.5.4   Model and Peak Flow Frequency Revisited

Based on the sensitivity analysis, we now revisit the comparisons between TREX and

data-based flood frequency curves. It was shown earlier that model flood frequency curves

are larger than the data and data-based flood frequency curves. The storm spatial distribution

(via changes in basin-average depth frequency), initial soil moisture, and storm duration all

can affect the model frequency curve shape and peak-flow magnitudes. Considering only the

restriction on the storm location to east of Parkdale and storm area less than 5,000 mi^2

(Figure 7.22), we compare model frequency curves with data-based ones at the four

locations. The SST basin-average rainfall curve that is used is shown in Figure 6.9 (blue

with filled squares). A Normal distribution upper tail for the rainfall distribution is also

considered. By limiting the comparisons to the rainfall curve, we can isolate the effect on the

resulting flood frequency curves.
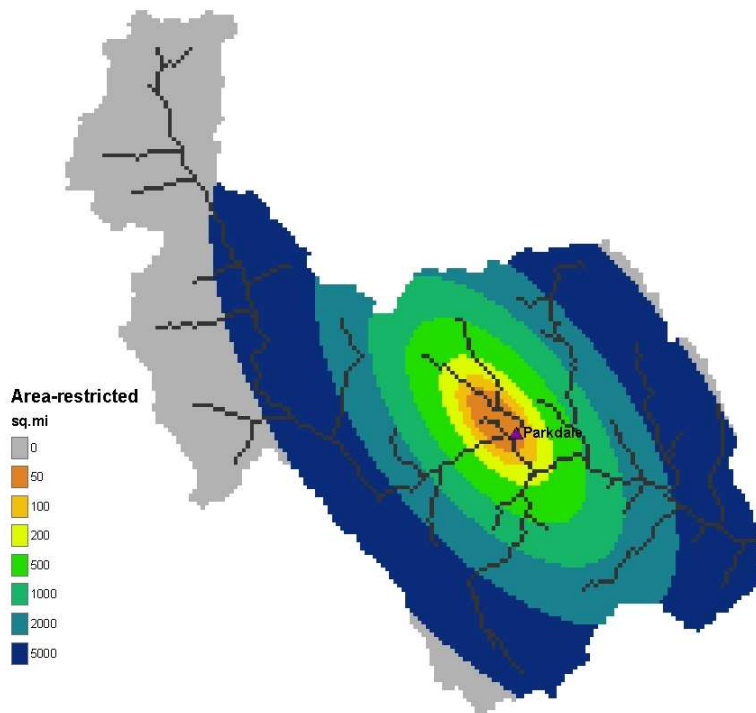
Figure 7.22. Restricted spatial storm pattern for TREX model runs and flood frequency.

The model flood frequency curves at the four sites, using the restricted storm center

and 5,000 mi^2 restricted area, are shown in Figure 7.23. The TREX model frequency curves

at the four locations changed fairly substantially from the base case results (Figure 7.17).

The lower basin curves at Pueblo and Parkdale have shifted down and have steepened slopes.
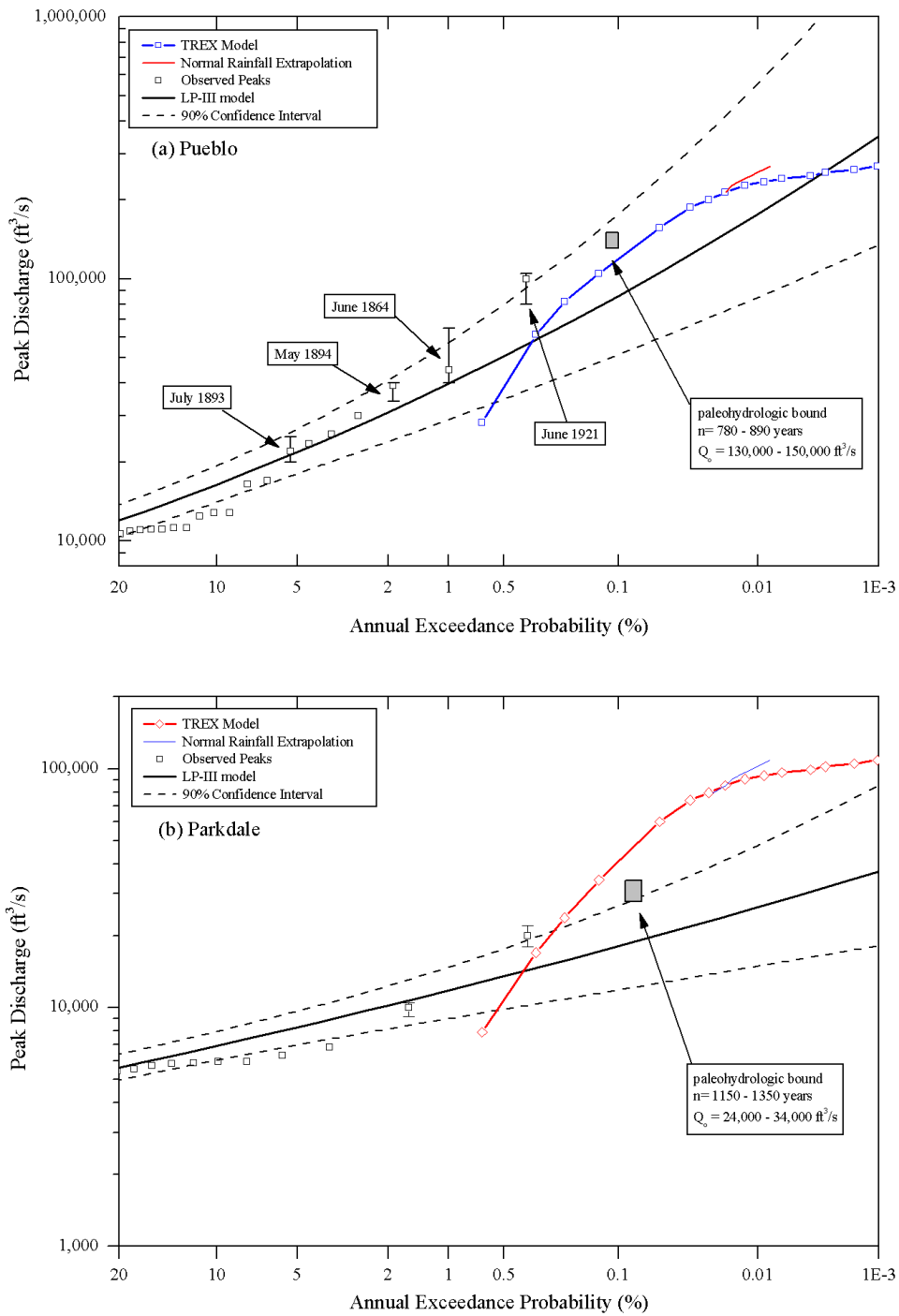
Figure 7.23. TREX model flood frequency and streamflow/paleoflood frequency curves at (a) Pueblo, (b) Parkdale, (c) Wellsville and (d) Salida. Based on SST curve with restricted storm centers and maximum 5,000 mi² storm area. Short solid line represents peak probabilities based on alternative Normal distribution rainfall extrapolation.
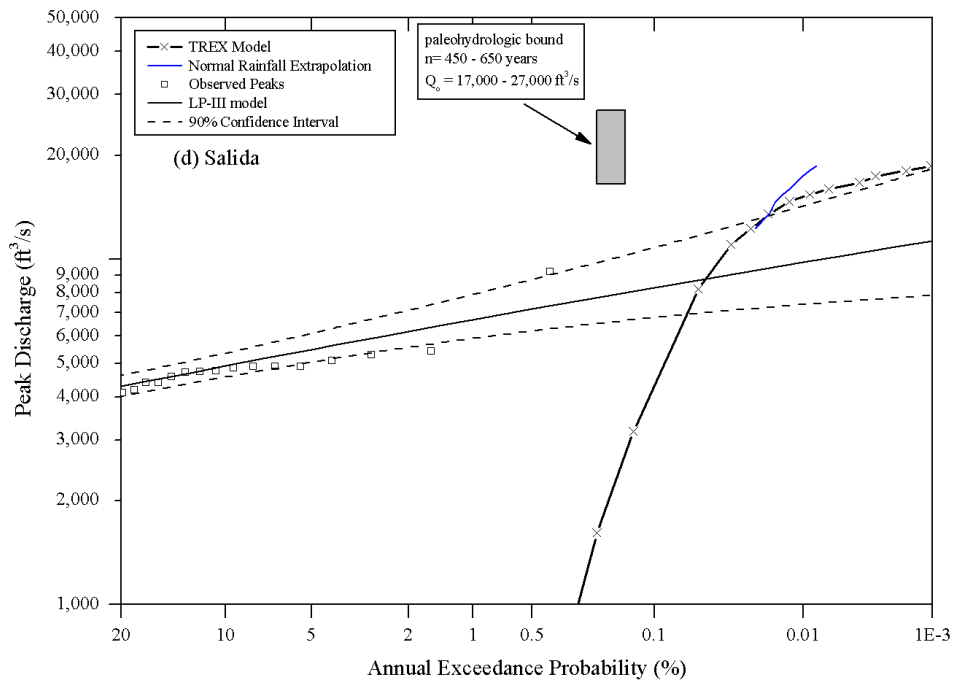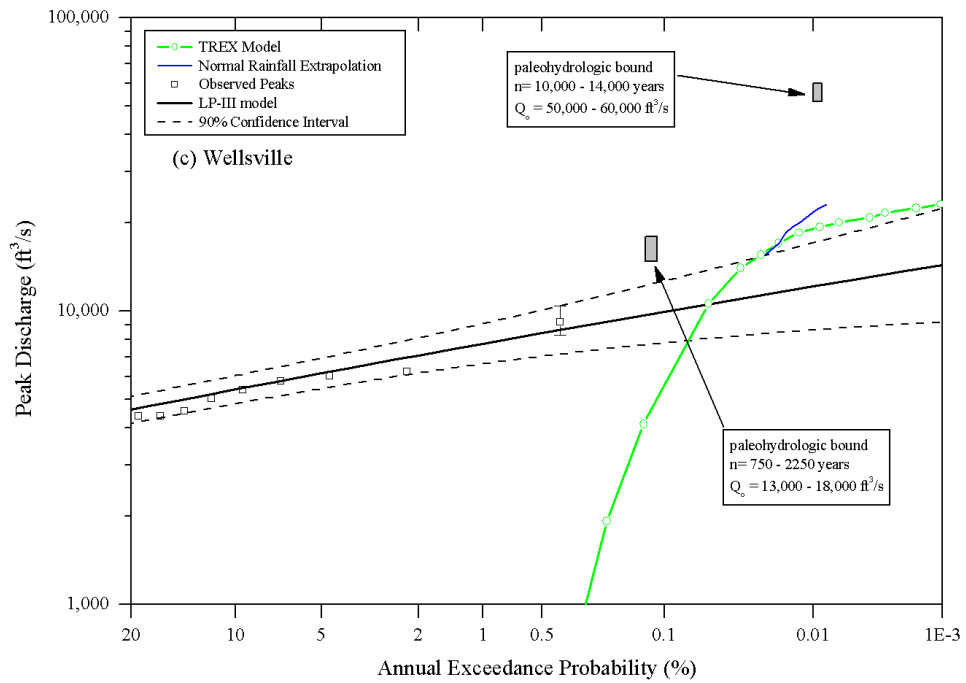
Figure 7.23 (continued). TREX model flood frequency and streamflow/paleoflood frequency curves at (a) Pueblo, (b) Parkdale, (c) Wellsville and (d) Salida. Based on SST curve with restricted storm centers and maximum 5,000 mi^2 storm area. Short solid line represents peak probabilities based on alternative Normal distribution rainfall extrapolation.

197

The curve at Pueblo is well within the LP-III confidence intervals, but the shape has a strong

negative skew with a very flat upper tail. The Normal distribution tail approximation on the

rainfall curve results in a curve that is closer to the data slope. The curve at Parkdale is close

to the data in the lower tail, but still appears to be much higher than the data in the upper tail

and inconsistent with the paleohydrologic bound. These two curves have different shapes

than the data-based curves clearly because of the rainfall frequency distribution. As this

rainfall distribution is based on storm transposition, there is no reason why the model and

data-based flood distributions should necessarily be the same, as storms transposed into the

watershed are not part of the observed flood records. The data-based flood frequency curve

is based in-part on the June 1921 and May 1894 storms; these events were used in

calibration/validation as well as in SST. The comparisons suggest that storms should be

further limited in areal distribution, location, and/or intensity to reduce the peaks at Parkdale.

In the upper watershed, the curves have shifted substantially downward and

steepened due to the limited rainfall extent (partial area) for the storm (Figure 7.22). The

upper tails are consistent with the confidence intervals from the snowmelt-dominant

frequency curves. Normal distribution rainfall extensions appear to be too steep in this area

of the watershed. Because the data-based frequency curves represent snowmelt, further

reductions in rainfall amounts may be warranted in this part of the watershed.

Based on the sensitivity analysis that is presented, there are several areas in which

future research could be conducted to gain increased understanding of extreme floods and

probabilities on watersheds such as the Arkansas River. One main avenue that should be

explored is further experiments with rainfall forcing, as the flood frequency curve shape is

dominated by the rainfall frequency distribution. As noted in Chapter 6, it is unknown how

much of a role the catchment shape plays in the shape of the rainfall and flood frequency

tails, but this could be explored by examining other sites within the storm transposition

region. A second main area that should be explored is developing distributions for runoff

model input parameters and conducting a full Monte-Carlo analysis and performing the full

integration of equation (3.29) in Chapter 3. One would gain in obtaining unconditional peak-

flow probabilities and possibly uncertainty of predictions. However, the computational

demands of TREX are still a bit high, and would require substantial effort to determine

whether a full Monte-Carlo simulation were feasible.

7.5.5   Probable Maximum Precipitation Runs

Because the Bureau of Reclamation, Corps of Engineers, and others rely on the

Probable Maximum Precipitation (PMP) and Probable Maximum Flood (PMF) as the

standard to assess dam safety, the use of PMP as an input to TREX is explored. The storm

rainfall input to TREX is the 72-hour general storm PMP for Pueblo (Bullard and Leverson,

1991). This storm was computed using HMR 55A procedures (Hansen et al., 1988), and is

shown in Figure 7.24. The rainfall mass curves used Reclamation's standard temporal

distribution with the maximum rainfall at the 2/3 point (48 hours) of the 72-hour storm

(Cudworth, 1989). These mass curves are applied at six subareas (Figure 3.2 in Chapter 3).
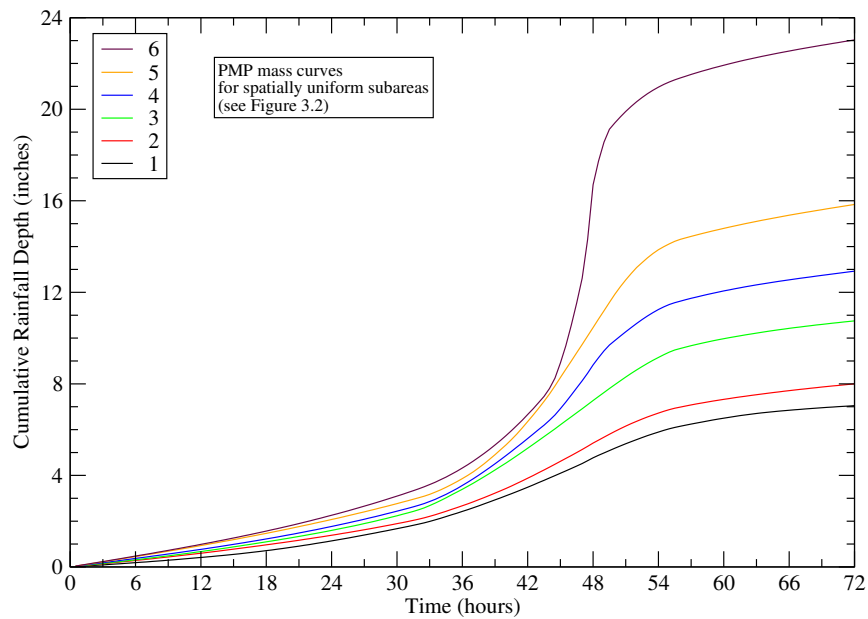
Figure 7.24. PMP rainfall mass curves for the Arkansas River basin above Pueblo Dam.

The TREX model was run with the PMP mass curves and the calibrated TREX

parameters, with S_e equal to 0.1. Two additional TREX runs were made to examine the

effects of initial soil moisture with $S_e = 0.5$ (flood frequency base case) and $S_e = 0.8$

(watershed near saturation). The PMP input hydrograph results at Pueblo are shown in

Figure 7.25, and demonstrate that TREX can be used to estimate extreme floods up to and

including those based on PMP. PMP is the most extreme rainfall that is considered in

hydrologic engineering for dam safety. The hydrographs have very smooth shapes and show

that TREX is stable for these extreme rainfall inputs. The TREX model results with $S_e = 0.8$

are compared with the Pueblo PMF hydrograph (Bullard and Leverson, 1991), with the PMF

snowmelt contribution removed, in Figure 7.26.
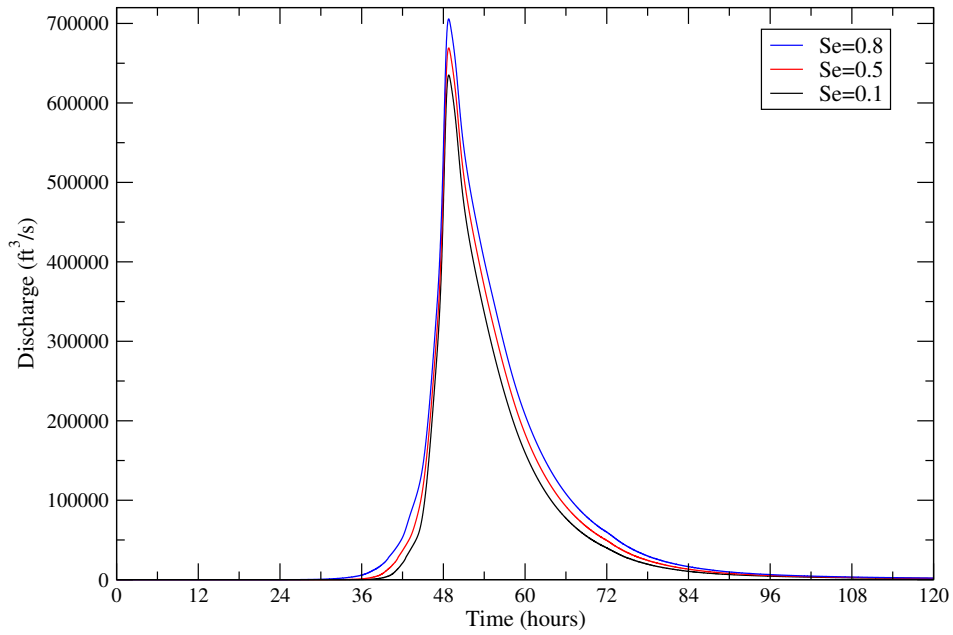
Figure 7.25. TREX PMP-based hydrographs with varying initial soil moisture.
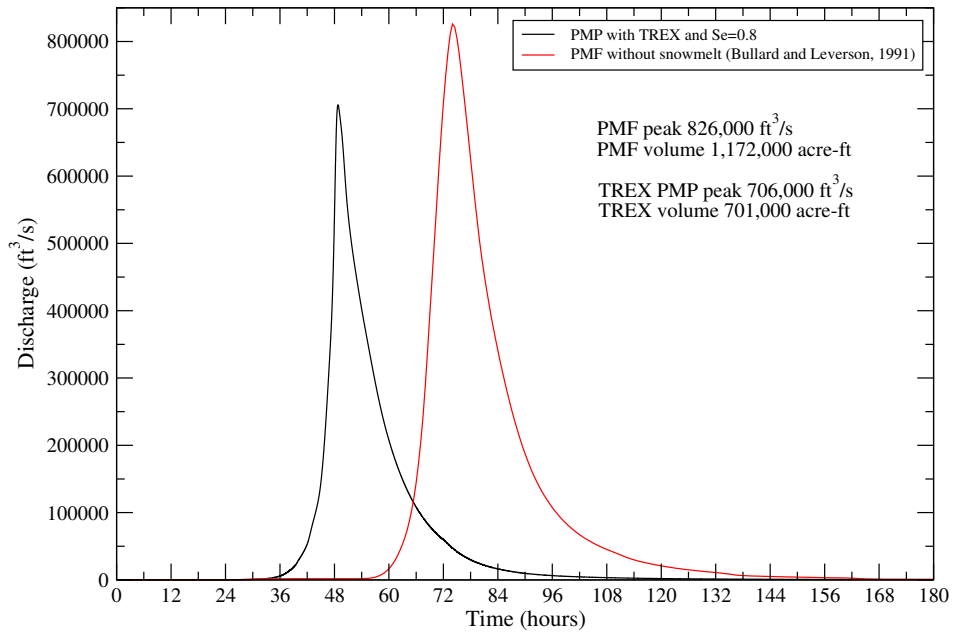
Figure 7.26. TREX PMP-based hydrograph and Reclamation PMF hydrograph.

201

The TREX runs based on PMP indicated that initial soil moisture was less sensitive a

factor on model peak flows for this extreme rainstorm. Peaks increased 11 percent from $S_e =$

0.1 to $S_e = 0.8$. Soil moisture did have a somewhat larger effect on runoff volumes; the total

hydrograph volume increased 27 percent from $S_e = 0.1$ to $S_e = 0.8$. Given PMP rainfall input,

the TREX model with $S_e = 0.8$ has a very similar shape to the unit hydrograph-based PMF

(Figure 7.26). The PMF peak flow is about 17 percent larger than the TREX prediction, and

the PMF volume is about 67 percent larger. The much larger PMF volume is due to

dramatically lower infiltration rates and differing model infiltration methods.

7.6   SUMMARY

The TREX model was applied to the Arkansas River basin upstream of Pueblo,

Colorado. The inputs for estimating model parameters were described. The model was

successfully calibrated to the June 1921 flood, the largest flood on record in the basin. The

model was validated with the May 1894 flood, the third largest flood on record. It was

shown that the model can successfully be applied to a large watershed of this scale (12,000

km^2) and simulate extreme floods.

The calibrated model was used to estimate flood frequency curves. Basin-average

rainfall depths and probabilities were obtained from a stochastic storm transposition model

that was applied to the watershed (Chapter 6). It was demonstrated that the model can be

used to develop a flood frequency curve. TREX model frequency curves at four sites within

the watershed were compared with data-based peak-flow frequency curves with paleoflood data. The comparison showed that peak flows from the rainfall-runoff model were generally larger than the data-based flood frequency curves. The shapes of the rainfall frequency curves dictated the shapes of the flood frequency curves. Rainfall frequency and flood frequency curve extreme upper tails were relatively flat compared to LP-III curves.

A series of sensitivity analysis experiments were performed to illustrate the effects of initial soil moisture, rainfall distribution, storm location and area, and storm duration and temporal distribution on flood frequency predictions. A particular factor was changed and others were held constant. Initial soil moisture was found to be important and could affect peak flows by a factor of 1.18 to 2.15 for the four cases considered. The spatial distribution of storms effect was simulated by restricting storm locations and areas for three cases, and was an important factor. Frequency curves generally became stretched out (less frequent probabilities for a fixed discharge), and in some cases steeper as storm areas were reduced and centers restricted to the lower watershed. A change in rainfall temporal distribution had less of an effect than extending the storm duration. Based on the sensitivity analysis, a better match between model frequency curves and data-based frequency curves was obtained at some locations by restricting storm area and storm center locations. It was shown that TREX can be used to estimate an extreme flood based on the PMP. TREX results based on the PMP were generally comparable in terms of peak flow to a published PMF hydrograph at Pueblo, but runoff volumes were lower.

Chapter VIII

CONCLUSIONS AND RECOMMENDATIONS

This chapter presents major conclusions that are drawn from this research and some

recommendations for further investigation.

8.1   <u>CONCLUSIONS</u>

There were four research objectives on extreme floods and flood frequency on a large

watershed with a two-dimensional rainfall runoff model. Overall, it was shown that the

TREX model can be successfully used to simulate extreme floods and estimate flood

frequency curves on a large watershed. This model provides a unique physically-based

method for determining flood frequency curves under varied scenarios of antecedent

moisture conditions, space and time variability of rainfall and watershed characteristics, and

storm center locations. Specific conclusions are summarized below.

1. A new channel mesh generator was developed to provide spatially-distributed

    channel geometry inputs to TREX. It was tested using power functions for bank

    heights and channel widths based on field data collected at 20 sites within the

    Arkansas River basin, Colorado. An improved channel topology algorithm was

implemented. It allows channels to be connected in eight directions; TREX can be applied on large watersheds with an improved representation of channels and their connectivity in the watershed network.

2. The TREX model was applied to the 12,000 km^2 Arkansas River basin above Pueblo, Colorado. It was shown that the model can be applied to a large watershed of this scale. The model was successfully calibrated to the June 1921 flood of record on the watershed. This flood had an approximate peak of 103,000 ft^3/s and a return period greater than 200 years. The calibrated peak discharge, volume and hydrograph shape were appropriate. The model was validated with the May 1894 flood. Based on the calibration and validation, the model performance indicated it is suitable for simulating extreme floods on large watersheds.

3. A spatial storm rainfall model was implemented within TREX and demonstrated on the Arkansas River basin. The storm model uses an elliptical pattern, depth-area duration data, and storm center, orientation and major-to-minor axis ratio parameters. The initial soil moisture was reparameterized using a saturation fraction for explicit initial condition for TREX. Following general concepts in NRC (1988), TREX was coupled with stochastic storm transposition (SST) techniques to develop a flood frequency curve. This pairing is a new application for the TREX model. A SST model using data from 15 of the most extreme storms in a large region was used to estimate basin-average depths and storm probabilities, and to subsequently derive a

flood frequency curve. Model-generated peak flows at Pueblo for annual exceedance probabilities 0.01 to 0.0001 were from 90,000 to 282,000 ft^3/s. It was successfully demonstrated that the TREX model can be used to develop a flood frequency curve at this scale. Model-generated frequency curves were generally higher than peak flow and paleoflood data-based frequency curves. Model upper tails were relatively flat.

4. Sensitivity analysis experiments were performed to illustrate the effects of initial soil moisture, rainfall distribution, storm location and area, and storm duration and temporal distribution on flood frequency predictions. Initial soil moisture was found to be important and could affect peak flows by a factor of 1.18 to 2.15 for the four cases considered. The sensitivity of the flood frequency curves due to changes in the basin-average rainfall depth frequency revealed several interesting features. Flood frequency curves generally had very similar shapes to the rainfall frequency curves. Rainfall frequency curves had very flat tails due to the interaction of storms with the watershed and the extreme storm characteristics. A restriction of storm centers resulted in a flood frequency distribution with smaller exceedance probabilities. A restriction on storm areas reduced the peak flows of the flood frequency curve. Frequency curves generally became stretched out (less frequent probabilities for a fixed discharge), and in some cases steeper as storm areas were reduced and centers restricted to the lower watershed. The temporal distribution of rainstorms did not significantly affect flood frequency curves. An improved match between model

frequency curves and streamflow/paleoflood data-based frequency curves was

obtained by restricting storm area and storm center locations.

8.2   RECOMMENDATIONS FOR FUTURE STUDY

Based on the research conducted for this dissertation, three areas for future research

are identified.

1. An uncertainty analysis of TREX model parameters should be conducted. The use of
   a priori parameter estimation procedures (e.g., Leavesley et al., 2003) to define model
   parameter uncertainty should be explored.

2. The current SST model that was implemented and applied to the Arkansas watershed
   should eventually be improved by completing further DAD data analysis,
   determining distributions for all model parameters, and simulating storms using full
   monte carlo simulation techniques. The difficulties of developing a spatial point
   process model for storm centers in orographic areas and near basin boundaries (such
   as the Continental Divide) need to be addressed.

3. Further research efforts in stochastic storm transposition are needed to investigate
   impacts of: storm center, orientation, duration and ellipse parameters of storms and
   their interactions with watersheds. Radar data should be investigated to be directly
   coupled with SST to provide an alternate space-time extreme storm model that
   captures spatial variability in orographic regions.

REFERENCES

Agho, K., Kuczera, G., Green, J., Weinmann, E., and Laurenson, E. (2000) Estimation of rainfall exceedance probabilities: nondimensional stochastic storm transposition. Proc. Hydro2000, Perth, Institution of Engineers, Aust., 6 p.

Alexander, G.N. (1963) Using the probability of storm transposition for estimating the frequency of rare floods. J. Hydrol., 1, p. 46-57.

Anderson, J.R., Hardy, E.E., Roach, J.T. and Witmer, R.E (1976) A land use and land cover classification system for use with remote sensor data. U.S. Geological Survey Professional Paper 964, 28 p.

Andrieu, H., Creutin, J.D., Delrieu, G. and Faure, D. (1997) Use of a weather radar for the hydrology of a mountainous area. Part I: radar measurement interpretation. J. Hydrol., 193, pp. 1-25.

Andrieu, H., French, M.N., Krajewski, W.F., and Georgakakos, K.P. (2003) Stochastic-dynamical rainfall simulation based on weather radar volume scan data. Adv. Water Res., 26, pp. 581-593.

Ang, A.H.S. and Tang, W.H. (1975) Probability concepts in Engineering Planning and Design, Vol. 1. Basic Principles, John Wiley, New York, 409 p.

Archer, D.R. (1989) Flood wave attenuation due to channel and floodplain storage and effects on flood frequency. Chapter 3 in Floods: Hydrological, Sedimentological and Geomorphological Implications, Beven, K. and Carling, P. (eds.), John Wiley & Sons, Chichester, pp. 37-46.

Arnaud, P. and Lavabre, J. (2002) Coupled rainfall model and discharge model for flood frequency estimation. Water Resour. Res. 38(6), doi:10.1029/2001WR00474, pp. 11-1 – 11-11.

Ashby, C.T. (2001) Impact of soil moisture initialization on a simulated flash flood. M.S. Thesis, Department of Atmospheric Science, Paper No. 702, Colorado State University, Fort Collins, CO, 177 p.

Atkinson, S.E., Sivapalan, M., Woods, R.A., and Viney, N.R. (2003) Dominant physical controls on hourly streamflow predictions and the role of spatial variability: Mahurangi catchment, New Zealand. Adv. Water Res., 26, pp. 219-235.

Australian Rainfall and Runoff (ARR) (2001) Volume One: A Guide to Flood Estimation (in eight books). The Institution of Engineers, Australia.

Baker, V.R. (1987) Paleoflood hydrology and extraordinary flood events. J. Hydrology, 96, nos. 1-4, pp. 79-99.

Baker, J.H. and Hafen, L.R. (1927) History of Colorado, Volume II. Linderman Co., Denver, pp. 429-867.

Bandaragoda, C, Tarboton, D.G., and Woods, R.A. (2004) Application of TOPNET in the distributed model intercomparison project. J. Hydrol., 298 (1-4), pp. 178-201.

Beven, K.J. (1989) Changing ideas in hydrology – the case of physically-based models. J. Hydrol., 105, pp. 157-172.

Beven, K.J. (2000) Uniqueness of place and process representations in hydrological modelling. Hydrol. Earth Sys. Sci., 4(2), pp. 203-213.

Beven, K.J. (2001) Rainfall-Runoff Modeling, The Primer. John Wiley and Sons, Chichester, 360 p.

Beven, K.J. (2002) A perceptual model of runoff generation in semi-arid areas. In Bull, L.J and Kirkby, M.J. (eds.) Dryland Rivers: Hydrology and Geomorphology of Semi-arid Channels, John Wiley and Sons, Ltd., pp. 57-105.

Blazkova, S. and Beven, K.J. (2002) Flood frequency estimation by continuous simulation for a catchment treated as ungaged (with uncertainty). Water Resour. Res., 38(8), doi:10.1029/2001WR000500, pp. 14-1 – 14- 14.

Blazkova, S. and Beven, K.J. (2004) Flood frequency estimation by continuous simulation of subcatchment rainfalls and discharges with the aim of improving dam safety assessment in

a large basin in the Czech Republic. J. Hydrol., 292, pp. 153-172.

Blöschl, G. (2001) Scaling in hydrology. Hydrol. Process. 15, pp. 709-711.

Blöschl, G. and Sivapalan, M. (1995) Scale issues in hydrological modelling: A review. Hydrol. Process. 9, pp. 251-290.

Bocchiola, D., De Michele, C. and Rosso, R. (2003) Review of recent advances in index flood estimation. Hydrol. Earth Sys. Sci., 7(3), pp. 283-296.

Borga M. (2002) Accuracy of radar rainfall estimates for streamflow simulation. J. Hydrol., 267, pp. 26-39.

Borga M., Anagnostou E.T., and Frank, E. (2000) On the use of real-time radar rainfall estimates for flood prediction in mountainous basins. J. Geophys. Res. Atmos., 105, pp. 2269-2280.

Borga, M., Tonelli, F., Moore, R.J. and Adrieu, H. (2002) Long-term assessment of bias adjustment in radar rainfall estimation. Water Resour. Res. 38(11), doi: 10.1029/2001WR000555 pp. 8-1 – 8-10.

Boston, T., Xia, J. and Zhu, Y. (2004) Pre-processing rainfall data from multiple gages to improve TOPMODEL simulation results in a large semi-arid region. Hydrol. Process. 18, pp. 2313-2325.

Boyer, M.C. (1957) A correlation of the characteristics of great storms. Trans. Amer. Geophys. Union, 38(2), pp. 233-238.

Bradley, A.A. and Potter, K.W. (1992) Flood Frequency Analysis of Simulated Flows. Water Resour. Res., 28(9), pp. 2375-2385.

Bras, R.L. (1990) Hydrology, An Introduction to Hydrologic Science. Addison-Wesley, Reading, MA, 643 p.

Bullard, K.L. and Leverson, V. (1991) Pueblo Dam, Fryingpan-Arkansas Project Probable Maximum Flood (PMF) Study. Flood Section, Bureau of Reclamation, Denver, CO, dated June, 1991, 23 p. and enclosures.

Burges, S.J. (1998) Streamflow prediction: Capabilities, opportunities and challenges. In

Hydrologic Sciences: Taking Stock and Looking Ahead, National Research Council, Washington, D.C., pp. 101-134.

Burnash, R.J.C. (1995) The NWS river forecast system – catchment modeling. Chapter 10 in Singh, V.P. (ed.) Computer Models of Watershed Hydrology, Water Resources Publications, Highlands Ranch, CO, pp. 311-366.

Cadavid, L., Obeysekera, J.T.B., and Shen, H.W. (1991) Flood-frequency derivation from kinematic wave. J. Hydraul. Eng., ASCE, 117(4), 489-509.

Calver, A. and Lamb, R. (1996) Flood frequency estimation using continuous rainfall-runoff modeling. Phys. Chem. Earth, 20, pp. 479-483.

Cameron, D.S., Beven, K.J., Tawn, J., Blazkova, S., and Naden, P. (1999) Flood frequency estimation by continuous simulation for a gaged upland catchment (with uncertainty). J. Hydrol., 219, pp. 169-187.

Cameron, D.S., Beven, K.J., Tawn, J., Blazkova, S., and Naden, P. (2000) Flood frequency estimation by continuous simulation (with likelihood based uncertainty estimation). Hydrol. Earth Sys. Sci., 4(1), pp. 23-34.

Campbell, M.R. (1922) Guidebook of the Western United States, Part E. The Denver and Rio Grande Western Route. U.S. Geological Survey Bulletin 707, 266 p.

Carrigan, P.H. (1971) A flood-frequency relation based on regional record maxima. U.S. Geological Survey Professional Paper 434-F, 22 p.

Castillo, V.M., Gomez-Plaza, A., and Martinez-Mena, M. (2003) The role of antecedent soil water content in the runoff response of semiarid catchments: a simulation approach. J. Hydrol., 284, pp. 114-130.

Cecilio, C.B., Kraeger, B.A., and Yucel, V. (1974) Spillway design for series of reservoirs. J. Hydraul. Eng., ASCE, 100(HY10), 1329-1342.

Chow, V.T., Maidment, D.R. and Mays, L.W. (1988) Applied Hydrology: McGraw-Hill, New York, 572 p.

Cohn, T.A., Lane, W.L, and Baier, W.G. (1997) An algorithm for computing moments-based flood quantile estimates when historical information is available. Water Resour. Res. 33(9),

pp. 2089-2096.

Cohn, T.A., Lane, W.L., and Stedinger, J.R. (2001) Confidence intervals for EMA flood quantile estimates. Water Resour. Res. 37(6), pp. 1695-1706.

Colorado State Engineer (1885) Report of the State Engineer to the Governor of Colorado for the years 1883 and 1884, Denver, Colorado.

Cordova, J.R. and Rodriguez-Iturbe, I. (1983) Geomorphoclimatic estimation of extreme flow probabilities. J. Hydrol., 65, pp. 159-173.

Crawford, N.H. and Linsley, R.K. (1966) Digital simulation in hydrology, Stanford Watershed Model IV. Tech. Rep. 39, Department of Civil Engineering, Stanford University, Palo Alto, CA., 210 p.

Creagher, W.P., Justin, J.D. and Hinds, J. (1945) Engineering for Dams. Volume I. General Design. John Wiley and Sons, New York, pp. 99-140.

Creutin, J.D., Andrieu, H., and Faure, D. (1997) Use of a weather radar for the hydrology of a mountainous area. Part II: radar measurement validation. J. Hydrol., 193, pp. 26-44.

Creutin, J.D. and Borga, M. (2003) Radar hydrology modifies the monitoring of flash-flood hazard. Hydrol. Process. 17, pp. 1453-1456.

Crippen, J.R. (1982) Envelope curves for extreme flood events. J. Hydraul. Engr., ASCE, 108(HY10), pp. 1208-1212.

Crippen, J.R. and Bue, C.D. (1977) Maximum floodflows in the Conterminous United States. U.S. Geological Survey Water-Supply Paper 1887, 52 p.

Crowfoot, R.M., Payne, W.F. and O'Neill, G.B. (2004) Water Resources Data, Colorado, Water Year 2003, Volume 1. Missouri River Basin, Arkansas River Basin, and Rio Grande Basin. U.S. Geological Survey Water-Data Report CO 03 1, 577 p.

Cudworth, A.G. Jr. (1989) Flood Hydrology Manual. A Water Resources Technical Publication, U.S. Department of Interior, Bureau of Reclamation, Denver, Colorado, 243 p.

Dalrymple, T. (1964) Hydrology of Flood Control, Part I. Flood Characteristics and Flow Determination. In Handbook of Hydrology, Chow, V.T. (ed.), McGraw-Hill, New York,

Section 25-I, pp. 25-1 – 25-33.

de Lima, J.L.M.P. and Singh, V.P. (2002) The influence of the pattern of moving rainstorms on overland flow. Adv. Water Res., 25, pp. 817-828.

De Michele, C. and Salvadori, G. (2002) On the derived flood frequency distribution: analytical formulation and the influence of antecedent soil moisture condition. J. Hydrol., 262, pp. 245-258.

Diaz-Granados, M.A., Valdez, J.B. and Bras, R.L. (1984) A physically based flood frequency distribution. Water Resour. Res., 20(7), pp. 995-1002.

Dixon, M. and Weiner, G. (1993) TITAN: Thunderstorm Identification tracking, analysis and nowcasting - A radar-based methodology. J. Atmos. Ocean Technol., 10(6), pp. 785-797.

Doe III, W.W., Saghafian, B. and Julien, P.Y. (1996) Land-use impact on watershed response: the integration of two-dimensional hydrologic modelling and Geographic Information Systems. Hydrol. Process. 10, pp. 1503-1511.

D'Odorico, P. and Rignon, R. (2003) Hillslope and channel contributions to the hydrologic response. Water Resour. Res., 39(5), 1113, doi:10.1029/2002WR001708, pp. SWC 1-1 – SWC 1-9.

Doesken, N.J. (1991) General Climatology in Colorado, in National Water Summary 1988-89-Hydrologic Events and Floods and Droughts, R.W. Paulson, E.B. Chase, R.S. Roberts, and D.W. Moody (compilers), U.S. Geological Survey Water-Supply Paper 2375, pp. 207-208.

Doesken, N.J. (1998) A post-evaluation of rainfall reports associated with the Pawnee Creek flood of July 29-30, 1997 in eastern Weld and western Logan counties in northeast Colorado, Climatology Report #98-3, Department of Atmospheric Science, Colorado State University, Fort Collins, Colorado, 33 p.

Doesken, N.J. and McKee, T.B. (1998) An Analysis of Rainfall for the July 28, 1997 Flood in Fort Collins, Colorado, Climatology Report #98-1, Department of Atmospheric Science, Colorado State University, Fort Collins, Colorado, 55 p.

Dooge, J.C.I. (1986) Looking for hydrologic laws. Water Resour. Res. 22(9), supplem., pp. 46S-58S.

Downer, C.W. and Ogden, F.L. (2003) Prediction of runoff and soil moistures at the watershed scale: Effects of model complexity and parameter assignment. Water Resour. Res., 39(3), 1045, doi:10.1029/2002WR001439, pp. SWC 1-1 – SWC 1-13.

Downer, C.W. and Ogden, F.L. (2004) GSSHA: A model for simulating diverse stream flow producing processes, J. Hydrol. Engr., ASCE, 9(3), pp.161-174.

Downer, C.W., Ogden, F.L., Martin, W.D., and Harmon, R.S. (2002) Theory, development, and applicability of the surface water hydrologic model CASC2D, Hydrol. Process., 16, pp 255-275.

Dunne, T. (1998) Wolman Lecture: Hydrologic Science ... in Landscapes ... on a Planet ... In the Future. In Hydrologic Sciences: Taking Stock and Looking Ahead, National Research Council, Washington, D.C., pp. 10-43.

Durrans, S.R., Julian, L.T., and Yekta, M. (2002) Estimation of depth-area relationships using radar-rainfall data. J. Hydrol. Eng., ASCE, 7(5), pp. 356-367.

Eagleson, P.S. (1972) Dynamics of Flood Frequency. Water. Resour. Res. 8(4), pp. 878-898.

Elliott, J.G., Jarrett, R.D., and Ebling, J.L. (1982) Annual snowmelt and rainfall peak-flow data on selected foothills region streams, South Platte River, Arkansas River, and Colorado River Basins, Colorado. U.S. Geological Survey Open-File Report 82-426, 86 p.

England, J.F. Jr. (1996) Compilation of an Extreme Streamflow Data Base as Part of an Extreme Precipitation Data Study. Prepared for the Colorado Climate Center, Colorado State University, dated May 1, 1996, 32 p., 1 figure, 28 tables, and 2 appendices.

England, J.F. Jr. (1998) Assessment of Historical and Paleohydrologic Information in Flood Frequency Analysis. Unpublished M.S. Thesis, Department of Civil Engineering, Colorado State Univ., Fort Collins, Colorado, 292 p.

England, J.F. Jr. (1999) Draft User's manual for program EMA, At-Site Flood Frequency Analysis with Historical/Paleohydrologic Data. Flood Hydrology Group, Bureau of Reclamation, Denver, CO, 52 p.

England, J.F. Jr. (2004) Review of Selected Large Flood Estimates in the United States for the U.S. Geological Survey. Bureau of Reclamation, Denver, CO, August, 14 p. and appendices.

England, J.F. Jr., Salas, J.D., and Jarrett, R.D. (2003a) Comparisons of two moments-based estimators that utilize historical and paleoflood data for the log-Pearson Type III distribution, Water Resour. Res. 39(9), pp. 5-1 – 5-16, doi:10.1029/2002WR001791.

England, J.F. Jr., Jarrett, R.D., and Salas, J.D. (2003b) Data-based comparisons of moments estimators that use historical and paleoflood data. J. Hydrol., 278(1-4), pp. 170-194.

Engman, E.T. (1986) Roughness coefficients for routing surface runoff. J. Irrig. Drain. Engr., ASCE, 112(1), pp. 39-53.

Entekhabi, D. and Rodriguez-Iturbe, I. (1994) Analytical framework for the characterization of the space-time variability of soil moisture. Adv. Water Res., 17, pp. 35-45.

Environmental Systems Research Institute (ESRI) (2003) ArcGIS/ArcInfo 8.3. ESRI, Redlands, CA.

Fellows, A.L. (1902) Water Resources of the State of Colorado. U.S. Geological Survey Water-Supply and Irrigation Paper No. 74, 151 p.

Ferraris, L., Rudari, R. and Siccardi, F. (2002) The uncertainty in the prediction of flash floods in the Northern Mediterranean environment. J. Hydrometeor., 3, pp. 714-727.

Feyen, L., Vasquez, R., Christiaens, K., Sels, O. and Feyen, J. (2000) Application of a distributed physically-based hydrological model to a medium size catchment. Hydrol. Earth Sys. Sci., 4(1), pp. 47-63.

Fiorento, M. and Iacobellis, V. (2001) New insights about the climatic and geologic control on the probability distribution of floods. Water Resour. Res., 37(3), pp. 721-730.

Follansbee, R. and Jones, E.E. (1922) Arkansas River flood of June 3-5, 1921. U.S. Geological Survey Water-Supply Paper 487, 44 p.

Follansbee, R. and Hodges, P.V. (1925) Some floods in the Rocky Mountain region. U.S. Geological Survey Water-Supply Paper 520-G, pp. 105-125.

Follansbee, R. and Sawyer, L.R. (1948) Floods in Colorado. U.S. Geological Survey Water-Supply Paper 997, 151 p.

Fontaine, T.A. (1989) Estimating the exceedance probabilities of extreme floods using

stochastic storm transposition and rainfall-runoff modeling. Ph.D. Dissertation, University of Wisconsin-Madison, 152 p.

Fontaine, T.A. (1995) Rainfall-runoff model accuracy for an extreme flood. J. Hydraul. Engr., ASCE, 121(4), pp. 365-374.

Fontaine, T.A. and Potter, K.W. (1989) Estimating probabilities of extreme rainfalls. J. Hydraul. Engr., ASCE, 115(11), pp. 1562-1575.

Fontaine, T.A. and Potter, K.W. (1993) Estimating exceedance probabilities of extreme floods. In Kuo, C.Y. (ed.) Engineering Hydrology-Proceedings of the symposium sponsored by the Hydraulics Division, ASCE, July 25-30, 1993, San Francisco, CA, pp. 635-640.

Foster, E.E. (1948) Rainfall and Runoff. Macmillan, New York, 487 p.

Foufoula-Georgiou, E. (1989) A probabilistic storm transposition approach for estimating exceedance probabilities of extreme precipitation depths. Water Resour. Res., 25(5), pp. 799-815.

Foufoula-Georgiou, E. and Wilson, L.L. (1990) In search of regularities in extreme rainstorms. J. Geophys. Res., 95(D3), pp. 2061-2072.

Franchini, M., Helmlinger, K.R., Foufoula-Georgiou, E., and Todini, E. (1996) Stochastic storm transposition coupled with rainfall-runoff modeling for estimation of exceedance probabilities of design floods. J. Hydrol., (175)1-4, pp. 511-532.

Franz, D.D., Kraeger, B.A. and Linsley, R.K. (1989) A system for generating long streamflow records for study of floods of long return period. NRC Report Phase II, contract NRC-04-85-143, Nuclear Regulatory Commission, Washington, D.C., 220 p.

Franz, D.D., Kraeger, B.A. and Linsley, R.K. (1991) Estimating the frequency of extreme flood events. EOS, Trans. AGU, 72(26), pp. 276-277.

Frazier, A.H and Heckler, W. (1972) Embudo, New Mexico, Birthplace of Systematic Stream Gaging. U.S. Geological Survey Professional Paper 778, 23 p.

Frenette, M. and Julien, P.Y. (1987) Computer modeling of soil erosion and sediment yield from large watersheds. Intl. J. Sed. Res., 1, pp. 39-68.

Fuller, W.E. (1914) Flood flows. Trans. Am. Soc. Civ. Eng., Paper No. 1293, vol. 77, pp. 564-617, with discussion pp. 618-694.

Garbrecht, J. (1984) The physical basis of stream flow hydrology with emphasis on drainage network morphology. Ph.D. Dissertation, Department of Civil Engineering, Colorado State Univ., Fort Collins, Colorado, 289 p.

Garbrecht, J. and Shen, H.W. (1988) The physical framework of the dependence between channel flow hydrographs and drainage network morphometry. Hydrol. Process. 2, pp. 337-355.

Gaume, E., Livet, M., Desbordes, M. and Villeneuve, J.-P. (2004) Hydrological analysis of the river Aude, France, flash flood on 12 and 13 November 1999. J. Hydrol., 286, pp. 135-154.

Gerard, R. and Karpuk, E.W. (1979) Probability analysis of historical flood data. J. Hydraulics Div. ASCE, 105(HY9), pp. 1153-1165.

Giannoni, F., Smith, J.A., Zhang, Y. and Roth, G. (2003) Hydrologic modeling of extreme floods using radar rainfall estimates. Adv. Water Res., 26(2), pp. 195-203.

Goel, N.K., Kurothe, R.S., Mathur, B.S., and Vogel, R.M. (2000) A derived flood frequency distribution for correlated rainfall intensity and duration. J. Hydrol., 228, pp. 56-67.

Goldman, D.M. (1987) Estimating runoff prediction uncertainty using a physically-based stochastic watershed model. Ph.D. Dissertation, University of California-Davis, 373 p.

Goldman, D.M., Mariño, M.A. and Feldman, A.D (1990) Runoff prediction uncertainty for ungaged agricultural watersheds. J. Irrig. Drain. Engr., ASCE, 116(6), pp. 752-767.

Goodrich, D.C., Schmugge, T.J., Jackson, T.J., Unkrich, C.L., Keefer, T.O., Parry, R., Bach, L.B., and Amer, S.A. (1994) Runoff simulation sensitivity to remotely sensed initial soil water content. Water Resour. Res. 30(5), pp. 1393-1405.

Goodrich, D.C., Lane, L.J., Shillito, R.M., Miller, S.N., Syed, K.H. and Woolhiser, D.A. (1997) Linearity of basin response as a function of scale in a semiarid watershed. Water Resour. Res. 33(12), pp. 2951-2965.

Gottschalk, L. and Weingartner, R. (1998) Distribution of peak flow derived from a

distribution of rainfall volume and runoff coefficient, and a unit hydrograph. J. Hydrol., 208, pp. 148-162.

Grayson, R. and Blöschl, G. (2000) Spatial Patterns in Catchment Hydrology: Observations and Modelling. Cambridge University Press, London, 416 p.

Green, W.H. and Ampt, G.A. (1911) Studies on soil physics. Part 1. The flow of air and water through soils. J Agric. Sci. 4, pp. 1-24.

Grossman, S.I. (1984) Calculus. Third Edition. Academic Press, Orlando, FL, 1178 p.

Guntner, A. and Bronstert, A. (2004) Representation of landscape variability and lateral redistribution processes for large-scale hydrological modelling in semi-arid areas. J. Hydrol., 297, pp. 136-161.

Gupta, V.K. (1972) Transposition of storms for estimating flood probability distributions. Hydrology Paper 59, Colorado State Univ., Fort Collins, Colorado, 35 p.

Gupta, V.K. and Waymire, E. (1993) A statistical analysis of mesoscale rainfall as a random cascade. J. Appl. Meteorol., 32, pp. 251–267.

Hafen, L.R. (1948) Colorado and Its People. A Narrative and Topical History of the Centennial State, Volume I. Lewis Historical Publishing, New York, 644 p.

Hansen, E.M., Schreiner, L.C., and Miller, J.F. (1982) Application of Probable Maximum Precipitation Estimates-United States East of the 105th Meridian. Hydrometeorological Report No. 52, National Weather Service, National Oceanic and Atmospheric Administration, U.S. Department of Commerce, Washington, DC, 168 p.

Hansen, E.M., Fenn, D.D., Schreiner, L.C., Stodt, R.W., and Miller, J.F. (1988) Probable Maximum Precipitation Estimates-United States between the Continental Divide and the 103rd Meridian. Hydrometeorological Report No. 55A, National Weather Service, National Oceanic and Atmospheric Administration, U.S. Department of Commerce, Silver Spring, MD, 242 p.

Harris, D., Menabde, M., Seed, A. and Austin, G. (1996) Multifractal characterization of rain fields with a strong orographic influence. J. Geophys. Res. (Atmos.), 101(D21, pp. 26,405-26,414.

Hashemi, A.M., Franchini, M., and O'Connell, P.E. (2000) Climate and basin factors affecting the flood frequency curve: PART I – A simple sensitivity analysis based on the continuous simulation approach. Hydrol. Earth Sys. Sci., 4(3), pp. 463-482.

Hazen, A.M. (1914) Discussion of Flood flows by W.E. Fuller. Trans. Am. Soc. Civ. Eng., Paper No. 1293, vol. 77, pp. 626-632.

Hebson, C. and Wood, E.F. (1982) A derived flood frequency distribution using Horton order ratios. Water Resour. Res., 18(5), pp. 1509-1518.

Heggen, R.J. (2001) Normalized antecedent precipitation index. J. Hydrol. Eng., ASCE, 6(5), pp. 377-381.

Hirschboeck, K.K. (1987) Catastrophic flooding and atmospheric circulation anomalies. Chapter 2 in Catastrophic Flooding, Mayer, L. and Nash, D. (eds.), Allen and Unwin, Boston, pp. 23-56.

Hirschboeck, K.K. (1991) Climate and Floods, in National Water Summary 1988-89-Hydrologic Events and Floods and Droughts, R.W. Paulson, E.B. Chase, R.S. Roberts, and D.W. Moody (compilers), U.S. Geological Survey Water-Supply Paper 2375, pp. 67-88.

Hornberger, G.M and Boyer, E.W. (1995) Recent advances in watershed modeling. U.S. National Report to IUGG, 1991-1994, Rev. Geophys., vol. 33, Supplem., pp. 949-957.

Horton, R.E. (1924) Discussion of The distribution of intense rainfall and some other factors in the design of storm-water drains flows. Proc. Am. Soc. Civ. Eng., 50, pp. 564-617, with discussion pp. 660-667.

Horton, R.E. (1933) The role of infiltration in the hydrologic cycle. Trans. Am. Geophys. Union, 14, 446-460.

Horton, R.E. (1936) Natural stream channel storage. Trans. Am. Geophys. Union, 17, 406-415.

Horton, R.E. (1937a) Determination of infiltration-capacity for large drainage-basins. Trans. Am. Geophys. Union, 18(2), 371-385.

Horton, R.E. (1937b) Natural stream channel storage (second paper). Trans. Am. Geophys. Union, 18, 820-835.

Horton, R.E. (1941) Flood-crest reduction by channel-storage. Trans. Am. Geophys. Union, 22, 440-456.

Hosking, J.R.M. and Wallis, J.R. (1997) Regional Frequency Analysis - An Approach based on L-Moments. Cambridge University Press, 224 p.

Hoyt, W.G. and Langbein, W.B. (1955) Floods. Princeton University Press, Princeton, NJ, 469 p.

Huff, F.A. (1967) Time distribution of rainfall in heavy storms. Water Resour. Res. 3(4), pp. 1007-1019.

Hydrologic Engineering Center (HEC) (1998) HEC-1 Flood Hydrograph Package, User's Manual, CPD-1A, version 4.1. U.S. Army Corps of Engineers, Davis, CA, 434 p.

Iacobellis, V. and Fiorento, M. (2000) Derived distribution of floods based on the concept of partial area coverage with a climatic appeal. Water Resour. Res., 36(2), pp. 469-482.

Institute of Hydrology (IH) (1999) Flood Estimation Handbook (FEH) - Procedures for Flood Frequency Estimation (in five volumes). Institute of Hydrology, Wallingford, Oxfordshire, United Kingdom.

Interagency Committee on Water Data (IACWD) (1982) Guidelines for determining flood flow frequency: Bulletin 17-B. Hydrology Subcommittee, March 1982 (revised and corrected), 28 p. and appendices.

Iseri, K.T. and Langbein, W.B (1974) Large Rivers of the United States. U.S. Geological Survey Circular 686, 10 p.

Ivanov, V.Y., Vivioni, E.R., Bras, R.L., and Entekhabi, D. (2004) Preserving high-resolution surface and rainfall data in operational-scale basin hydrology: a fully distributed physically-based approach. J. Hydrol., 298 (1-4), pp. 80-111.

Jarrett, R.D. (1985) Determination of roughness coefficients for streams in Colorado. U.S. Geological Survey Water-Resources Investigations Report 85-4004, 54 p.

Jarrett, R.D. (1987) Flood Hydrology of Foothill and Mountain Streams in Colorado. Ph.D. Dissertation, Department of Civil Engineering, Colorado State Univ., Fort Collins, Colorado, 239 p.

Jarrett, R.D. (1990) Paleohydrologic techniques used to define the spatial occurrence of floods. Geomorphology, 3, pp. 181-195.

Jarrett, R.D. (1993) Flood elevation limits in the Rocky Mountains. In Kuo, C.Y. (ed.) Engineering Hydrology-Proceedings of the symposium sponsored by the Hydraulics Division, ASCE, July 25-30, 1993, San Francisco, CA, pp. 180-185.

Jarrett, R.D. and Costa, J.E. (1988) Evaluation of the flood hydrology in the Colorado Front Range using precipitation, streamflow, and paleoflood data for the Big Thompson River Basin. U.S. Geological Survey Water-Resources Investigations Report 87-4117, 37 p.

Jarrett, R.D. and Tomlinson, E.M. (2000) Regional interdisciplinary paleoflood approach to assess extreme flood potential. Water Resour. Res. 36(10), pp. 2957-2984.

Jarvis, C.S. and others (1936) Floods in the United States, Magnitude and Frequency. U.S. Geological Survey Water-Supply Paper 771, 497 p.

Javier, J.R., Smith, J.A., England, J.F., and Baeck, M.L. (2004) A Radar Climatology of Extreme Rainfall in the Front Range of the Rocky Mountains. Eos Trans. AGU, 85(47), Fall Meet. Suppl., Abstract H11F-0376.

Javier, J.R., Smith, J.A., Baeck, M.L., and Steiner, M. (2005) A Radar Climatology of Extreme Rainfall in the Colorado Front Range of the Rocky Mountains. Draft report submitted to Bureau of Reclamation. Department of Civil and Environmental Engineering, Princeton University, Princeton, NJ, 48 p.

Johnson, B.E., Julien, P.Y., Molnar, D.K., and Watson, C.C. (2000) The two-dimensional upland erosion model CASC2D-SED. J. Amer. Water Resour. Assoc., AWRA, 36(1), pp. 31-42.

Jorgeson, J.J. (1999) Peak flow analysis using a two-dimensional watershed model with radar precipitation data. Ph.D. Dissertation, Department of Civil Engineering, Colorado State Univ., Fort Collins, Colorado, 194 p.

Jothityangkoon, C. and Sivapalan, M. (2001) Temporal scales of rainfall-runoff processes and spatial scaling of flood peaks: space-time connection through catchment water balance. Adv. Water Res., 24, pp. 1015-1036.

Jothityangkoon, C. and Sivapalan, M. (2003) Towards estimation of extreme floods:

examination of the roles of runoff process changes and floodplain flows. J. Hydrol., 281, pp. 206-229.

Julien, P.Y. (2002) River Mechanics. Cambridge University Press, Cambridge, UK, 434 p.

Julien, P.Y. and Rojas, R. (2002) Upland erosion modeling with CASC2D-SED. Intl. J. Sed. Research, 17(4), pp. 265-274.

Julien, P. Y. and Saghafian, B. (1991) CASC2D users manual - A two dimensional watershed rainfall-runoff model. Civil Eng. Report CER90-91PYJ-BS-12, Colorado State University, Fort Collins, Fort Collins, CO, 66 p.

Julien, P.Y., Molnar, D.K., Johnson, B.E. and Combs, P.G. (1998) Flood forecasting reaches new potential, EOS, Trans. AGU, 79(14) April 7, 1998 and electronic file at http://www.agu.org/eos_elec/9727le.html.

Julien, P. Y., Saghafian, B., and Ogden, F. L. (1995) Raster-Based hydrologic modeling of spatially-varied surface runoff. Water Resources Bulletin, AWRA, 31(3), pp. 523-536.

Kandel, D.D., Western, A.W., Grayson, R.B., and Turral, H.N. (2004) Process parameterization and temporal scaling in surface runoff and erosion modelling. Hydrol. Process. 18, pp. 1423-1446.

Kircher, J.E., Choquette, A.F. and Richter, B.D. (1985) Estimation of Natural Streamflow Characteristics in Western Colorado. U.S. Geological Survey Water-Resources Investigations Report 85-4086, 28 p.

Klawon, J.E., Klinger, R.E. and Bauer, T.R. (2005) Paleoflood Hydrology for Flood Hazard Study, Pueblo Dam, Colorado. Draft Report, Bureau of Reclamation, Denver, CO, 37 p.

Klemeš, V. (1990) The modelling of mountain hydrology: the ultimate challenge. In Molnár, L. (ed.) Hydrology of Mountainous Areas. IAHS Publ. No. 190, pp. 29-43.

Kouwen, N. and Mousavi, S.-F. (2002) WATFLOOD/SPL9 hydrological model & flood forecasting system. In Singh, V.P. and Frevert, D. (eds.) Mathematical Models of Large Watershed Hydrology, Ch. 15, Water Resources Publications, Littleton, CO, pp. 649-685.

Koutsoyiannis, D. and Foufoula-Georgiou, E. (1993) A scaling model of a storm hyetograph. Water Resour. Res., 29(7), pp. 2345-2361.

Kraeger, B.A. and Franz, D.D. (1992) Determining the frequency of extreme flood events. Hydro Review, July, pp. 60-67.

Krajewski, W.F. and Smith, J.A. (2002) Radar hydrology: rainfall estimation. Adv. Water Res., 25, pp. 1387-1394.

Lamb, R. (1999) Calibration of a conceptual rainfall-runoff model for flood frequency estimation by continuous simulation. Water Resour. Res. 35(10), pp. 3103-3114.

Lane, W.L., and Cohn, T.A. (1996) Expected moments algorithm for flood frequency analysis, in N. Am. Water and Environ. Cong. 1996, edited by C.T. Bathala, Amer. Soc. Civ. Eng., Anaheim, California.

Lange, J., Leibundgut, C., Greenbaum, N. and Schick, A.P. (1999) A noncalibrated rainfall-runoff model for large, arid catchments. Water Resour. Res., 35(7), pp. 2161-2172.

Laurenson, E.M. and Kuczera, G.A. (1998) Annual Exceedance Probability (AEP) of the Probable Maximum Precipitation (PMP) – Report on a review and recommendations for practice. Prepared for NSW Department of Land and Water Conservation and the Snowy Mountains Hydro-Electric Authority, 63 p.

Laurenson, E.M. and Mein, R.G. (1995) RORB: Hydrograph Synthesis by runoff routing. Chapter 5 in Singh, V.P. (ed.) Computer Models of Watershed Hydrology, Water Resources Publications, Highlands Ranch, CO, pp. 151-164.

Leavesley, G.H., Lichty, R.W., Troutman, B.M., and Saindon, L.G. (1983) Precipitation-runoff modeling system - User's Manual. U.S. Geological Survey Water Resource-Investigations Report 83-4238.

Leavesley, G.H., Hay, L.E., Viger, R.J. and Markstrom, S.L. (2003) Use of a priori parameter-estimation methods to constrain calibration of distributed-parameter models. In Calibration of Watershed Models, Q. Duan, H.V. Gupta, S. Sorooshian, A.N. Rousseau and R. Turcotte (eds.), American Geophysical Union Water Science and Application Series vol. 6, pp. 255-266.

Levish, D.R. (2002) Paleohydrologic bounds: Non-exceedance information for flood hazard assessment. In Ancient Floods, Modern Hazards: Principles and Applications of Paleoflood Hydrology, P.K. House, R.H. Webb, V.R. Baker and D.R. Levish (eds.), American Geophysical Union Water Science and Application Series vol. 5, pp. 175-190.

Li, R. M., Stevens, M. A., and Simons, D. B. (1976) Solutions to Green-Ampt infiltration equations. J. Irrig. Drain. Eng., ASCE, 102(IR2), pp. 239-248.

Lichty, R.W. and Liscum, F. (1978) A rainfall-runoff modeling procedure for improving estimates of T-year (annual) floods for small drainage basins. U.S. Geological Survey Water-Resources Investigations Report 78-7, 44 p.

Linsley, R.K. (1986) Flood estimates: How good are they? Water Resour. Res. 22(9), supplem., pp. 159S-164S.

Liu, Y.B., Gebremeskel, S., De Smedt, F., Hoffmann, L. and Pfister, L. (2003) A diffusive transport approach for flow routing in GIS-based flood modeling. J. Hydrol., 283, pp. 91-106.

Loague, K. and VanderKwaak, J.E. (2004) Physics-based hydrologic response simulation: platinum bridge, 1958 Edsel, or useful tool. Hydrol. Process. 18, pp. 2949-2956.

Loukas, A. (2002) Flood frequency estimation by a derived distribution procedure. J. Hydrol., 255, pp. 69-89.

Loukas, A., Vasiliades, L., and Dalezios, N.R. (2000) Flood producing mechanisms identification in southern British Columbia, Canada. J. Hydrology, 227, pp. 218-235.

Lovejoy, S, Schertzer, D. (1995) Multifractals and rain. In New Uncertainty Concepts in Hydrology and Hydrological Modeling, Kundzewicz, Z.W. (ed.), Cambridge University Press, New York, pp. 61–103.

Maddox, R.A., Canova, F., and Hoxit, L.R. (1980) Meteorological characteristics of flash flood events over the Western United States. Mon. Weath. Rev. 108(11), pp. 1866-1877.

Marco, J.B. and Valdés, J.B. (1995) Hydrologic implications of partial storm coverage. In Morel-Seytoux (ed.), Proceedings of the AGU 15th Annual Hydrology Days, Fort Collins, CO, pp. 149-162.

Marco, J.B. and Valdés, J.B. (1998) Partial area coverage distribution for flood frequency analysis in arid regions. Water Resour. Res., 34(9), pp. 2309-2317.

Matthai, H.F. (1968) Magnitude and frequency of floods in the United States – Part 6-B, Missouri River Basin below Sioux City, Iowa. U.S. Geological Survey Water-Supply Paper

1680, 491 p.

Matthai, H.F. (1969) Floods of June 1965 in South Platte River Basin, Colorado. U.S. Geological Survey Water-Supply Paper 1850-B, 64 p.

Matthai, H.F. (1990) Floods. In M.G. Wolman and H.C. Riggs (eds.) Surface Water Hydrology, Geol. Soc. America, the Geology of North America, 0-1, pp. 97-120.

Matthes, G.H. (1922) Floods on small streams caused by rainfall of the cloudburst type. Trans. Am. Soc. Civ. Eng., Paper No. 1505 (symposium), vol. 85, pp. 1388-1399.

McCain, J.F. and Ebling, J.L. (1979) A plan for the study of flood hydrology of foothill streams in Colorado. U.S. Geological Survey Open-File Report 79-1276, 29 p.

McCain, J.F. and Jarrett, R.D. (1976) Manual for estimating flood characteristics of natural-flow streams in Colorado. Colorado Water Conservation Board Technical Manual 1, 68 p.

McCain, J.F., Hoxit, L.R., Maddox, R.A., Chappel, C.F. and Caracena, F. (1979) Storm and flood of July 31-August 1, 1976 in the Big Thompson and Cache la Poudre River Basins, Larimer and Weld Counties, Colorado, Part A. Meteorology and Hydrology in the Big Thompson River and Cache la Poudre River Basins. U.S. Geological Survey Professional Paper 1115, pp. 1-85.

McKee, T.B. and Doesken, N.J. (1997) Colorado Extreme Storm Precipitation Data Study, Climatology Report #97-1, Department of Atmospheric Science, Colorado State University, Fort Collins, Colorado, 34 p. and appendices.

Menabde, M. and Sivapalan, M. (2001) Linking space-time variability of river runoff and rainfall fields: a dynamical approach. Adv. Water Res., 24, pp. 1001-1014.

Merz, R. and Blöschl, G. (2003) A process typology of regional floods. Water Resour. Res. 39(12), 1340, doi:10.1029/2002WR001952, pp. SWC 5-1 – SWC 5-20.

Meyer, A.F. (1917) Elements of Hydrology. John Wiley and Sons, New York, 487 p.

MGS Engineering Consultants, Inc. (MGS) (2001) General Storm Stochastic Event Flood Model (SEFM) - Technical Support Manual. Prepared for the United States Department of the Interior Bureau of Reclamation, Flood Hydrology Group, March 2001, various paging.

Molnar, D. K. (1997) Grid size selection for 2-D hydrologic modeling of large watersheds. Ph.D. Dissertation, Department of Civil Engineering, Colorado State Univ., Fort Collins, Colorado, 201 p.

Molnar, D.K. and Julien, P.Y. (1998) Estimation of upland erosion using GIS. Comp. Geosci., 24(2), pp. 183-192.

Molnar, D.K. and Julien, P.Y. (2000) Grid size effects on surface runoff modeling. J. Hydrol. Eng., ASCE, 5(1), pp. 8-16.

Montaldo, N., Mancini, M. and Rosso, R. (2004) Flood hydrograph attenuation induced by a reservoir system: analysis with a distributed rainfall-runoff model. Hydrol. Process. 18, pp. 545-563.

Moon, J., Kim, J.-H., and Yoo, C. (2004) Storm-coverage effect on dynamic flood frequency analysis: empirical data analysis. Hydrol. Process. 18, pp. 159-178.

Munn, J. and Savage, J.L. (1922) The Flood of June 1921 in the Arkansas River, at Pueblo, Colorado. Trans. Am. Soc. Civ. Eng., Paper No. 1480, vol. 85, pp. 1-35, with discussion pp. 36-65.

Murphy, E.C. and others (1906) Destructive Floods in the United States in 1905, with a discussion of flood frequency and an index to flood literature. U.S. Geological Survey Water-Supply Paper 162, 105 p.

Nathan, R.J. and Weinmann, P.E. (1999) Estimation of Large to Extreme Floods: Book VI in Australian Rainfall and Runoff, A Guide to Flood Estimation. the Institution of Engineers, Australia.

National Research Council (NRC) (1988) Estimating Probabilities of Extreme Floods: Methods and recommended research. National Academy Press, Washington, D.C., 141 p.

National Research Council (NRC) (1994) Estimating Bounds on Extreme Precipitation Events: A brief assessment. National Academy Press, Washington, D.C., 29 p.

National Research Council (NRC) (1999) Hydrologic hazards science at the U.S. Geological Survey. National Academy Press, Washington, D.C., 79 p.

National Research Council (NRC) (2002) Report of a workshop on predictability and limits-

to-prediction in hydrologic systems. National Academy Press, Washington, D.C., 118 p.

National Research Council (NRC) (2005) Flash Flood Forecasting over Complex Terrain, With an Assessment of the Sulphur Mountain NEXRAD in Southern California. National Academy Press, Washington, D.C., 191 p.

Natural Resources Conservation Service (NRCS) (1994) State Soil Geographic (STATSGO) Data Base, Data Use Information. Misc. Publ. 142, U.S. Department of Agriculture, Natural Resources Conservation Service, National Soil Survey, Washington, DC, 35p. and appendices.

Neary, V.S., Habib, E. and Fleming, M. (2004) Hydrologic modeling with NEXRAD precipitation in middle Tennessee. J. Hydrol. Eng., ASCE, 9(5), pp. 339-349.

Obled, Ch., Wendling, J. and Beven, K. (1994) The sensitivity of hydrological models to spatial rainfall patterns: an evaluation using observed data. J. Hydrol., 159, pp. 305-333.

O'Connor, J.E. and Costa, J.E. (2004) Spatial distribution of the largest rainfall-runoff floods from basins between 2.6 and 26,000 km^2 in the United States and Puerto Rico. Water Resour. Res. 40, W01107, doi:10.1029/2003WR002247, 11 p.

Ogden, F.L. (1992) Two-dimensional runoff modeling with weather radar data. Ph.D. Dissertation, Department of Civil Engineering, Colorado State Univ., Fort Collins, Colorado, 211 p.

Ogden, F.L. and Julien, P.Y. (1993) Runoff sensitivity to temporal and spatial rainfall variability at runoff plane and small basin scales. Water Resour. Res., 29(8), pp. 2589-2597.

Ogden, F.L. and Julien, P.Y. (1994) Runoff model sensitivity to radar rainfall resolution. J. Hydrol., 158, pp. 1-18.

Ogden, F.L. and Julien, P.Y. (2002) CASC2D: A Two-Dimensional, Physically-Based, Hortonian Hydrologic Model. In Singh, V.P. and Frevert, D. (eds.) Mathematical Models of Small Watershed Hydrology and Applications, Ch. 4, Water Resources Publications, Littleton, CO, pp. 69-112.

Ogden, F.L., Richardson, J.R., and Julien, P.Y. (1995) Similarity in catchment response 2. Moving rainstorms. Water Resour. Res., 31(6), pp. 1543-1547.

Ogden, F.L., Saghafian, B. and Krajewski, W.F. (1994) GIS-Based channel extraction and smoothing algorithm for distributed hydrologic modeling. In Cotroneo, G.V. and Rumer, R.R. (eds.) Proceedings, Hydraulic Engineering '94, American Society of Civil Engineers, Buffalo, NY, Aug. 1-5, pp. 237-241.

Ogden, F.L., Sharif, H.O., Senarath, S.U.S., Smith, J.A., Baeck, M.L. and Richardson, J.R. (2000) Hydrologic analysis of the Fort Collins, Colorado, flash flood of 1997. J. Hydrol., 228, pp. 82-100.

Orlandini, S. and Rosso, R. (1998) Parameterization of stream channel geometry in the distributed modeling of catchment dynamics. Water. Resour. Res. 34(8), pp. 1971-1985.

Osterkamp, W.R. and Friedman, J.M. (2000) The disparity between extreme rainfall events and rare floods – with emphasis on the semi-arid American West. Hydrol. Process. 14, pp. 2817-2829.

Osterwald, D.B. (2003) Rails Thru the Gorge. A mile-by-mile guide for the Royal Gorge Route. Western Guideways, Ltd., Hugo, CO, 167 p.

Ott, R.F. (1971) Streamflow frequency using stochastically generated rainfall. Tech. Rep. 151, Department of Civil Engineering, Stanford University, Palo Alto, CA, 111 p.

Ott, R.F. and Linsley, R.K. (1972) Streamflow frequency using stochastically generated hourly rainfall. Proceedings of the International Symposium on Uncertainties in Hydrologic and Water Resource Systems, Vol. 1, Dec. 11-14, University of Arizona, Tucson, pp. 230-244.

Over, T.M. and Gupta, V.K. (1996) A space-time theory of mesoscale rainfall using random cascades. J. Geophys. Res. (Atmos.), 101(D21, pp. 26,319-26,331.

Paik, K. and Kumar, P. (2004) Hydraulic geometry and the nonlinearity of the network instantaneous response. Water Resour. Res. 40, W03602, doi:10.1029/2003WR002821, 7 p.

Pan, F., Peters-Lidard, C.D., Sale, M.J. and King, A.W. (2004) A comparison of geographic information systems-based algorithms for computing the TOPMODEL topographic index. Water. Resour. Res. 40, W06303, doi:10.1029/2004WR003069 11 p.

Patterson, J.L. (1964) Magnitude and frequency of floods in the United States – Part 7, Lower Mississippi River Basin. U.S. Geological Survey Water-Supply Paper 1681, 636 p.

Pielke, R.A. Jr. (1999) Nine fallacies of floods. Climatic Change, 42, pp. 413-438.

Pilgrim, D.H., Chapman, T.G. and Doran, D.G. (1988) Problems of rainfall-runoff modeling in arid and semiarid regions. Hydrol. Sci. J., 33(4), pp. 379-400.

Pilgrim, D.H., and Cordery , I. (1993) Flood Runoff. In Handbook of Hydrology, Maidment, D.R. (ed.), McGraw-Hill, New York, Ch. 9, pp. 9.1-9.42.

Ponce, V.M. (1989) Engineering Hydrology, Principles and Practices. Prentice-Hall, NJ, 640 p.

Rahman, A., Weinmann, E., and Mein, R.G. (2002) The use of probability-distributed initial losses in design flood estimation. Aust. J. Water Res., 6(1), pp. 17-29.

Rahman, A., Weinmann, E., Hoang, T.M.T., and Laurenson, E.M. (2002) Monte carlo simulation of flood frequency curves from rainfall. J. Hydrol., 256, pp. 196-210.

Ramirez, J.A. (2000) Derived Distribution Approach – Summary Notes, CE522 Engineering Hydrology. Department of Civil Engineering, Colorado State University, Fort Collins, CO.

Ramirez, J.A., Salas, J.D. and Rosso, R. (1994) Determination of flood characteristics by physically-based methods. Chapter 6 in Coping With Floods, Rossi, G. Harmancioglu, N. and Yevjevich, V. (eds.), Kluwer Academic Publishers, Dordrecht, pp. 77-110.

Rawls, W.J., Ahuja, L.R., Brakensiek, D.L., and Shirmohammadi, A. (1993) Infiltration and soil water movement. In Handbook of Hydrology, Maidment, D.R. (ed.), McGraw-Hill, New York, Ch. 5, pp. 5.1-5.51.

Rawls, W.J. and Brakensiek, D.L. (1985) Prediction of soil water properties for hydrologic modeling. In Jones, E.B. and Ward, T.J. (eds.) Watershed Management in the Eighties, American Society of Civil Engineers, New York, pp. 293-299.

Reed, S.M., Koren, V.I., Smith, M.B, Zhang, Z., Moreda, F., Seo, D.-J., and DMIP Participants (2004) Overall distributed model intercomparison project results. J. Hydrol., 298 (1-4), pp. 27-60.

Robinson, J.S. and Sivapalan, M. (1997a) An investigation into the physical causes of scaling and heterogeneity of regional flood frequency. Water Resour. Res. 33(5), pp. 1045-1059.

Robinson, J.S. and Sivapalan, M. (1997b) Temporal scales and hydrological regimes: Implications for flood frequency scaling. Water Resour. Res. 33(12), pp. 2981-2999.

Rojas-Sanchez, R. (2002) GIS-based upland erosion modeling, geovisualization and grid size effects on erosion simulations with CASC2D-SED. Ph.D. Dissertation, Department of Civil Engineering, Colorado State Univ., Fort Collins, Colorado, 140 p.

Rulli, M.C. and Rosso, R. (2002) An integrated simulation method for flash-flood risk assessment: 1. Frequency predictions in the Bisagno River by combining stochastic and deterministic methods. Hydrol. Earth Sys. Sci., 6(2), pp. 267-283.

Saco, P.M. and Kumar, P. (2002a) Kinematic dispersion in stream networks 1. Coupling hydraulic and network geometry. Water Resour. Res. 38(11), 1244, doi:10.1029/2001WR000695, pp. 26-1 – 26-14.

Saco, P.M. and Kumar, P. (2002b) Kinematic dispersion in stream networks 2. Scale issues and self-similar network organization. Water Resour. Res. 38(11), 1245, doi:10.1029/2001WR000694, pp. 27-1 – 27-15.

Saco, P.M. and Kumar, P. (2004) Kinematic dispersion effects on hillslopes. Water Resour. Res. 40, W01301, doi:10.1029/2003WR002024, 12 p.

Saghafian, B. (1992) Hydrologic analysis of watershed response to spatially varied infiltration. Ph.D. Dissertation, Department of Civil Engineering, Colorado State Univ., Fort Collins, Colorado, 215 p.

Saghafian, B. and Julien, P.Y. (1995) Time to equilibrium for spatially variable watersheds. J. Hydrol., 172, pp. 231-245.

Saghafian, B., Julien, P.Y. and Ogden, F.L. (1995) Similarity in catchment response 1. Stationary rainstorms. Water Resour. Res., 31(6), pp. 1533-1541.

Salas, J.D., Smith, R.A., Tabios, G.Q. and Heo, J-H. (2002) Statistical Computer Techniques in Water Resources and Environmental Engineering. Draft of book, Department of Civil Engineering, Colorado State Univ., Fort Collins, Colorado.

Schaefer, M. and Barker, B. (2002) Stochastic Event Flood Model. In Singh, V.P. and Frevert, D. (eds.) Mathematical Models of Small Watershed Hydrology and Applications, Ch. 20, Water Resources Publications, Littleton, CO, pp. 707-748.

Schreiner, L.C. and Riedel, J.T. (1978) Probable Maximum Precipitation Estimates, United States East of the 105th Meridian. Hydrometeorological Report No. 51, National Weather Service, National Oceanic and Atmospheric Administration, U.S. Department of Commerce, Silver Spring, MD, 87 p.

Seaber, P.R., Kapinos, F.P., and Knapp, G.L. (1987) Hydrologic Unit Maps. U.S. Geological Survey Water-Supply Paper 2294, 63 p.

Senarath, S.U.S., Ogden, F.L., Downer, C.W., and Sharif, H. O. (2000) On the calibration and verification of two-dimensional, distributed, Hortonian, continuous watershed models. Water Resour. Res., 36(6), pp.1495-1510.

Seo, D.-J. and Smith, J.A. (1996) Characterization of the climatological variability of mean areal rainfall through fractional coverage. Water Resour. Res., 32(7), pp. 2087-2095.

Seyfried, M.S. and Wilcox, B.P. (1995) Scale and the nature of spatial variability: Field examples having implications for hydrologic modeling. Water Resour. Res., 31(1), pp. 173-184.

Sharif, H.O., Ogden, F.L., Krajewski, W.F., and Xue, M. (2002) Numerical simulations of radar rainfall error propagation. Water Resour. Res. 38(8), doi: 10.1029/2001WR000525 pp. 15-1 – 15-14.

Shen, H.W., Koch, G.J., and Obeysekera, J.T.B. (1990) Physically based flood features and frequencies. J. Hydraul. Eng., ASCE, 116(4), 494-514.

Simanton, J.R. and Osborn, H.B. (1980) Reciprocal-distance estimate of point rainfall. J. Hydraul. Eng., ASCE, 106(HY7), pp. 1242-1246.

Singh, P. and Singh, V.P. (2001) Snow and Glacier Hydrology. Water Science and Technology Library Vol. 37, Kluwer Academic Publishers, Boston, 742 p.

Singh, V.P. (1995) Computer Models of Watershed Hydrology. Water Resources Publications, Littleton, CO, 1130 p.

Singh, V.P. (1997) Effect of spatial and temporal variability in rainfall and watershed characteristics on stream flow hydrograph. Hydrol. Process. 11, pp. 1649-1669.

Singh, V.P. (2002) Effect of the duration and direction of storm movement on infiltrating

planar flow with full areal coverage. Hydrol. Process. 16(7), pp. 1479-1511.

Singh, V.P. (in press) Effects of storm direction and duration on infiltrating planar flow with partial area coverage. Hydrol. Process. in press, DOI: 10.1002/hyp.5554, 24 p.

Singh, V.P. and Frevert, D.K. (2002) Computer Models of Large Watershed Hydrology. Water Resources Publications, Littleton, CO, 891 p.

Singh, V.P. and Woolhiser, D.A. (2002) Mathematical modeling of watershed hydrology. J. Hydrol. Eng., ASCE, 7(4), pp. 270-292.

Sivakumar, B. (2004) Dominant processes in hydrology: moving forward. Hydrol. Process. 18, pp. 2349-2353.

Sivapalan, M. (2003) Process complexity at the hillslope scale, process simplicity at the watershed scale: is there a connection? Hydrol. Process. 17, pp. 1037-1041.

Sivapalan, M., Wood, E.F., and Beven, K.J. (1990) On hydrologic similarity: 3. A dimensionless flood frequency model using a generalized geomorphologic unit hydrograph and partial area runoff generation. Water Resour. Res., 26(1), pp. 43-58.

Skøien, J.O., Blöschl, G. and Western, G. (2003) Characteristic space scales and timescales in hydrology. Water Resour. Res. 39(10), 1304, doi:10.1029/2002WR001736, pp. 11-1 – 11-19.

Sloan, W.T., Ewen, J., Kilsby, C.G., Fallows, C.S. and O'Connell, P.E. (1997) A physically based model for large river basins. In English, M. and Szollosi-Nagy, A. (eds.) Managing Water: Coping with Scarcity and Abundance-Proceedings of theme A, Water for A Changing Global Community, 27th Congress of the IAHR, sponsored by the Water Resource Engineering Division, ASCE, August 10-15, 1997, San Francisco, CA, pp. 853-858.

Smith, J.A. (1989) Regional flood frequency analysis using extreme order statistics of the annual peak record. Water Resour. Res., 25(2), pp. 311-317.

Smith, J.A., Baeck, M.L., Steiner, M. and Miller, A.J. (1996) Catastrophic rainfall from an upslope thunderstorm in the Central Appalachians: the Rapidan storm of June 27, 1997. Water Resour. Res., 32(10), pp. 3099-3113.

Smith, J.A., Baeck, M.L., Morrison, J.E. and Sturdevant-Rees, P. (2000) Catastrophic rainfall and flooding in Texas. J. Hydrometeor., 1, pp. 5-25.

Smith, J.A., Baeck, M.L., Morrison, J.E., Sturdevant-Rees, P., Turner-Gillespie, D.F., and Bates , P.D. (2002) The regional hydrology and hydrometeorology of extreme floods in an urbanizing drainage basin. J. Hydrometeor., 3, pp. 267-282.

Smith, M.B, Seo, D.-J., Koren, V.I., Reed, S.M., Zhang, Z., Duan, Q., Moreda, F., and Cong S. (2004) The distributed model intercomparison project (DMIP): motivation and experiment design. J. Hydrol., 298 (1-4), pp. 4-26.

Smith, R.E. (2002) Infiltration theory for hydrologic applications. Water Resources Monograph 15, Am. Geophys. Union, Washington, D.C., 212 p.

Spah, J. A. (2000) Rainfall runoff and the effects of initial soil moisture associated with the Little Washita River Watershed, Oklahoma. M.S. Thesis, Department of Civil Engineering, Colorado State Univ., Fort Collins, Colorado, 140 p.

Steel, M.E., Black, A.R., Werrity, A., and Littlewood, I.G. (1999) Reassessment of flood risk for Scottish rivers using synthetic runoff data. In Hydrological Extremes: Understanding, Predicting, Mitigating. IAHS Publ. No. 255, pp. 209-215.

Stedinger, J.R., Vogel, R.M., and Foufoula-Georgiou, E. (1993) Frequency analysis of extreme events. In Handbook of Hydrology, Maidment, D.R. (ed.), McGraw-Hill, New York, Ch. 18, pp. 18.1-18.66.

Sturdevant-Rees, P., Smith, J.A., Baeck, M.L., and Morrison, J.E. (2001) Tropical storms and the flood hydrology of the Central Appalachians. Water Resour. Res., 37(8), pp. 2143-2168.

Swain, R.E., England, J.F. Jr., Bullard, K.L. and Raff, D.A. (2004) Hydrologic hazard curve estimating procedures. Dam Safety Research Program Research Report DSO-04-08, U.S. Department of Interior, Bureau of Reclamation, Denver, Colorado, 79 p.

Tabios, G.Q. and Salas, J.D. (1985) A comparative analysis of techniques for spatial interpolation of precipitation. Water Resour. Bull., AWRA, 21(3), pp. 365-380.

Tarboton, D.G. (1997) A new method for the determination of flow directions and upslope areas in grid digital elevation models. Water Resour. Res. 33(2), pp. 309-319.

Tarboton, D.G. (2002) TauDEM: Terrain Analysis Using Digital Elevation Models. Utah State University, Department of Civil and Environmental Engineering, http://moose.cee.usu.edu/taudem/taudem.html, October 2002.

Thomson, M.T., Gannon, W.B., Thomas, M.P., and Hayes, G.S. (1964) Historical floods in New England. U.S. Geological Survey Water-Supply Paper 1779-M, 105 p.

Todini, E. (2002) The ARNO model. In Singh, V.P. and Frevert, D. (eds.) Mathematical Models of Large Watershed Hydrology, Ch. 16, Water Resources Publications, Littleton, CO, pp. 687-716.

Todini, E. and Ciarapica, L. (2002) The TOPKAPI model. In Singh, V.P. and Frevert, D. (eds.) Mathematical Models of Large Watershed Hydrology, Ch. 12, Water Resources Publications, Littleton, CO, pp. 471-506.

Troch, P.A., Smith, J.A., Wood, E.F., and de Troch, F.P. (1994) Hydrologic controls of large floods in a small basin: central Appalachian case study. J. Hydrol., 156, pp. 285-309.

Troutman, B.M. and Karlinger, M.R. (2003) Regional flood probabilities. Water Resour. Res. 39(4), 1095, doi:10.1029/2001WR001140, pp. SWC 4-1 – SWC 4-15.

Turner-Gillespie, D.F., Smith, J.A. and Bates, P.D. (2003) Attenuating reaches and the regional flood response of an urbanizing drainage basin. Adv. Water Res., 26, pp. 673-684.

U.S. Army Corps of Engineers (USACE) (1945 -) Storm Rainfall in the United States (ongoing publication). Washington, D.C.

U.S. Army Corps of Engineers (USACE) (1998) Runoff from Snowmelt. Engineer Manual EM 1110-2-1406, Department of the Army, U.S. Army Corps of Engineers, Washington, D.C.

U.S. Department of Interior, Bureau of Reclamation (Reclamation) (1990) Flood Hydrograph and Routing System (FHAR) Computer Model version 4.14, Technical Service Center, Denver, CO.

U.S. Department of Interior, Bureau of Reclamation (Reclamation) (1999) Dam Safety Risk Analysis Methodology (version 3.3). Bureau of Reclamation, Denver, September 1999, 48 p.

U.S. Department of Interior, Bureau of Reclamation (Reclamation) (2003) Guidelines for achieving public protection in dam safety decisionmaking. Bureau of Reclamation, Denver, Colorado, 19 p.

U.S. Geological Survey (USGS) (1923) Surface water supply of the United States, 1921, Part 7, Lower Mississippi River Basin. U.S. Geological Survey Water-Supply Paper 527, 39 p.

U.S. Geological Survey (USGS) (1955) Compilation of records of surface waters of the United States through September 1950, Part 7, Lower Mississippi River Basin. U.S. Geological Survey Water-Supply Paper 1311, 606 p.

U.S. Geological Survey (USGS) (1964) Compilation of records of surface waters of the United States, October 1950 to September 1960, Part 7, Lower Mississippi River Basin. U.S. Geological Survey Water-Supply Paper 1731, 552 p.

U.S. Geological Survey (USGS) (1969) Surface water supply of the United States, 1961-65, Part 7, Lower Mississippi River Basin, Volume 2, Arkansas River Basin. U.S. Geological Survey Water-Supply Paper 1921, 878 p.

Vaill, J.E. (2000) Analysis of the Magnitude and Frequency of Floods in Colorado. U.S. Geological Survey Water-Resources Investigations Report 99-4190, 35 p.

Velleux, M. L. (2005) Spatially distributed model to assess watershed contaminant transport and fate. Ph.D. Dissertation, Department of Civil Engineering, Colorado State Univ., Fort Collins, Colorado, 261 p.

Verbunt, M., Gurtz, J., Jasper, K., Lang, H., Warmerdam, P. and Zappa, M. (2003) The hydrological role of snow and glaciers in alpine river basins and their distributed modeling. J. Hydrol. 282, pp. 36-55.

Vieux, B.E., Cui, Z., and Gaur, A. (2004) Evaluation of a physics-based distributed hydrologic model for flood forecasting. J. Hydrol., 298 (1-4), pp. 155-177.

Vogel, R.M., Zafirakou-Koulouris, A. and Matalas, N.C. (2001) Frequency of record-breaking floods in the United States. Water Resour. Res. 37(6), pp. 1723-1731.

Wahl, K.L. (1982) Simulation of regional flood-frequency curves based on peaks of record. In: Biswas, M.R. and Biswas, A.K., eds., Alternative strategies for desert development and management, vol.3, Pergamon Press, New York, pp. 760-769.

Weiler, M. and McDonnell, J. (2004) Virtual experiments: an new approach for improving process conceptualization in hillslope hydrology. J. Hydrol.*,* 285, pp. 3-18.

Weingartner, R., Barben, M. and Spreafico, M. (2003) Floods in mountainous areas – an overview based on examples from Switzerland. J. Hydrol.*,* 282, pp. 10-24.

White, A.B., Kumar, O., Saco, P.M., Rhoads, B.L., and Yen, B.C. (2004) Hydrodynamic and geomorphologic dispersion: scale effects in the Illinois River Basin. J. Hydrol.*,* 288, pp. 237-257.

Wiesner, C.J. (1970) Hydrometeorology. Chapman and Hall, London, 232 p.

Wilson, L.L. (1989) Assessment of the exceedance probability of extreme rainfalls in the Midwest by stochastic storm transposition. M.S. Thesis, Iowa State University, Ames, IA, 127 p.

Wilson, L.L. and Foufoula-Georgiou, E. (1990) Regional rainfall frequency analysis via stochastic storm transposition. J. Hydraul. Engr., ASCE, 116(7), pp. 859-880.

Wolff, C.G. and Burges, S.J. (1994) An analysis of the influence of river channel properties on flood frequency. J. Hydrol.*,* 153, pp. 317-337.

Wolock, D.M. and McCabe, G.J. (1995) Comparison of single and multiple flow direction algorithms for computing topographic parameters in TOPMODEL. Water. Resour. Res. 31 (5), pp. 1315-1324.

Woltemade, C.J. and Potter, K.W. (1994) A watershed modeling analysis of fluvial geomorphologic influences on flood peak attenuation. Water Resour. Res. 30(6), pp. 1933-1942.

Wood, E.F., Sivapalan, M., Beven, K. and Band, L. (1988) Effects of spatial variability and scale with implications to hydrologic modeling. J. Hydrol.*,* 102, pp. 29-47.

Wood, E.F., Sivapalan, M., and Beven, K. (1990) Similarity and scale in catchment storm response. Rev. Geophys.*,* 28(1), pp. 1-18.

Woods, R. and Sivapalan, M. (1999) A synthesis of space-time variability in storm response: Rainfall, runoff generation, and routing. Water Resour. Res. 35(8), pp. 2469-2485.

Woolhiser, D. A. (1996) Search for physically based runoff model - A hydrologic El Dorado? J. Hydraul. Eng., ASCE, 122(3), 122-129.

Woolhiser, D.A., Smith, R.E. and Goodrich, D.C. (1990) KINEROS, a kinematic runoff and erosion model: documentation and user manual. U.S. Department of Agriculture, Agricultural Research Service, ARS-77, 130 p.

Woolhiser, D.A., Smith, R.E. and Giraldez, J.-V. (1996) Effects of spatial variability of saturated hydraulic conductivity on Hortonian overland flow. Water Resour. Res. 32(3), pp. 671-678.

Yankee Atomic Energy Company (YAEC) (1984) Probability of extreme rainfalls and the effect on the Harriman Dam. Yankee Atomic Energy Company, Framingham, MA, 16 p. and four appendices.

Yates, D., Warner, T.T., Brandes, E.A., Leavesley, G.H., Sun, J. and Mueller, C.K. (2001) Evaluation of flash-flood discharge forecasts in complex terrain using precipitation. J. Hydrol. Eng., ASCE, 6(4), pp. 265-274.

Yu, Z. (2002) A storm simulation in large watersheds with a hydrologic model system and a mesoscale meteorological model. In Singh, V.P. and Frevert, D. (eds.) Mathematical Models of Large Watershed Hydrology, Ch. 10, Water Resources Publications, Littleton, CO, pp. 385-432.

Zehe, E. and Blöschl, G. (2004) Predictability of hydrologic response at the plot and catchment scales: Role of initial conditions. Water Resour. Res., 40, W10202, doi:10.1029/2003WR002869, 21 p.

Zhang, Y., Smith, J.A. and Baeck, M.L. (2001) The hydrology and hydrometeorology of extreme floods in the Great Plains of Eastern Nebraska. Adv. Water Res., 24, pp. 1037-1049.

Zhang, Z., Koren, V., Smith, M., Reed, S. and Wang, D. (2004) Use of next generation weather radar data and basin disaggregation to improve continuous hydrograph simulations. J. Hydrol. Eng., ASCE, 9(2), pp. 103-115.